Technische Universität München
TUM School of Life Sciences

Monitoring climate change impacts on vegetation canopies in Central Europe with passive remote sensing techniques: new insights and perspectives

Simon Michael Kloos

Vollständiger Abdruck der von der TUM School of Life Sciences der Technischen Universität München zur Erlangung eines

Doktors der Naturwissenschaften (Dr. rer. nat.)

genehmigten Dissertation.

Vorsitz: Prof. Dr. Axel Göttlein

Prüfende der Dissertation:

1. Prof. Dr. Annette Menzel
2. Prof. Dr. Lukas Lehnert

Die Dissertation wurde am 28.05.2024 bei der Technischen Universität München eingereicht und durch die TUM School of Life Sciences am 07.11.2024 angenommen.

Acknowledgments

For me, the submission of this dissertation not only marks the end of a major chapter in my life to date but also a brief pause on a journey. A journey that began over 12 years ago with a seminar paper on climate change in Munich, continued with my studies in geography, finally led me to a doctorate in ecoclimatology and was accompanied during all this time by an enduring curiosity and interest in the nature and environment of our planet. Especially in the last years in my doctorate, I was able to learn a lot of new knowledge, both professionally and methodologically, broaden my horizons and develop personally. I am very grateful for this, and I associate this gratitude with some very specific people.

First, I would like to thank Prof. Dr. Annette Menzel for the intensive and professional supervision of this doctorate, for the confidence in my abilities from the very beginning, and for introducing me to areas of environmental science that were previously unknown to me. Prof. Dr. Lukas Lehnert for the examination of this thesis and his valuable feedback regarding this doctorate. Dr. Florian Zabel for his mentorship and all co-authors for their productive collaboration on the individual publications on which this dissertation is based. Special thanks also go to Nicole for always having an open office door, a sympathetic ear, and well-meant advice. Thanks also go to Marvin for countless hours spent together in Weltwald Freising and on excursions, and especially for the insight into the world of measurement technology. Thanks also to Ye and Wael for guiding me in my first steps in scientific data analysis and to Brigitte and Sabine for their help in the university bureaucracy. Thanks also to Yahya, Caryl, Fanxiang, Mingzheng, Haiyin, and Nik for enriching my lunch breaks and having a refreshing conversation in the hallway. I would also like to take this opportunity to thank Lars, Johanna, and Alissa, who have been particularly close to me over the past three years and have enriched my life both at university and in my private life.

Finally, I would like to thank my friends and family, who always give me cheerfulness and confidence. Especially, I would like to mention my parents, Sylvia and Dieter, who have given me every freedom for personal development and have always supported me unconditionally on my journey.

Danksagungen

Die Einreichung dieser Dissertation stellt für mich nicht nur den Abschluss eines großen Kapitels in meinem bisherigen Leben dar, sondern auch das kurze Innehalten auf einer Reise. Eine Reise, die vor über 12 Jahren mit einer Seminararbeit über den Klimawandel in München begann, die sich mit dem Studium der Geographie fortsetzte, mich schließlich zur Promotion in der Ökoklimatologie führte und während all dieser Zeit von einer dauerhaften Neugier und einem nicht abreißenden Interesse an der Natur und Umwelt unserer Erde begleitet wurde. Vor allem in den letzten Jahren der Promotion durfte ich sowohl fachlich als auch methodisch eine Menge neues Wissen erlernen, meinen Horizont vergrößern und mich persönlich weiterentwickeln. Dafür bin ich sehr dankbar und ich verbinde diese Dankbarkeit mit einigen Personen ganz konkret.

Zuallererst will ich Prof. Dr. Annette Menzel für die intensive und fachliche Betreuung dieser Promotion danken, für das von Anfang an vorhandene Vertrauen in meine Fähigkeiten und für die Einführung in für mich vorher unbekannte Bereiche der Umweltwissenschaften. Prof. Dr. Lukas Lehnert für die Prüfung dieser Arbeit und sein wertvolles Feedback bezüglich dieser Promotion. Dr. Florian Zabel für die Mentorenschaft sowie allen Co-Autoren für die produktive Zusammenarbeit bei den einzelnen Publikationen, auf welche diese Dissertation basiert. Ein besonderer Dank gilt auch Nicole für eine immer offenstehende Bürotür, ein offenes Ohr und einen immer wohlgemeinten Ratschlag. Ebenso geht ein großer Dank an Marvin für unzählige gemeinsame Stunden im Weltwald Freising und auf Exkursion und insbesondere für den Einblick in die Welt der Messtechnik. Dank gebührt auch Ye und Wael beim Begleiten meiner ersten Schritte in der wissenschaftlichen Datenanalyse sowie Brigitte und Sabine für ihre Hilfe in der universitären Bürokratie. Danke auch an Yahya, Caryl, Fanxiang, Mingzheng, Haiyin und Nik für die Bereicherung meiner Mittagspausen oder einer erfrischenden Unterhaltung auf dem Flur. Ganz besonders danken will ich an dieser Stelle auch Lars, Johanna und Alissa, die mich in den letzten drei Jahren besonders nahe begleitet und mein Leben sowohl in der Universität als auch privat bereichert haben.

Zuletzt gilt mein großer Dank meinen Freunden und meiner Familie, die mir immer Frohsinn und Zuversicht schenken. Abschließend will ich hier meine Eltern, Sylvia und Dieter, hervorheben, die mir jegliche Freiheit zur persönlichen Entfaltung gegeben und mich immer bedingungslos auf meiner Reise unterstützt haben.

Abstract

Global warming increases the mean temperature and leads to more heat and drought events in Central Europe. This fundamentally affects the physiology and phenology of vegetation and changes its interaction with the atmosphere. In this context, it is essential to know where and when plant growth is water-limited in Central Europe and how these changing climatic conditions might alter the autumn senescence of deciduous forests. Furthermore, it is important to understand the growth strategies of different temperate deciduous tree species to better assess the future suitability of these species in the context of climate change. This thesis analyzed various aspects of these questions using passive remote sensing methodology in three Central European study areas. A second focus was on assessing the extent to which passive remote sensing data can capture agricultural drought and plant phenology. In Central Europe, areas below 800 m above sea level, particularly agricultural areas and grassland, are at risk of drought in the summer months of July and August. Dry and warm growing seasons tend to prolong the leaf senescence of a Central European deciduous forest. However, there are still substantial differences between the tree species regarding trends and drivers. This also applies to the onset of spring and autumn phenology under almost identical environmental conditions, resulting in species-specific differences in the length of the growing season of up to two months. Plant functional traits can partly explain the growth strategy of tree species. In addition, both agricultural drought and plant phenology can be recorded with passive sensors from various remote sensing platforms. While water limitation is an important monitoring condition for drought, the spatial resolution and the phenological phase to be observed must be specified for phenology to obtain robust results. In the future, this monitoring methodology, in combination with other data sets, promises a deeper understanding of the physiology and phenology of vegetation in the context of global warming.

Zusammenfassung

Die globale Erwärmung erhöht die Mitteltemperatur und führt zu mehr Hitze- und Dürreereignissen in Zentraleuropa. Dies beeinflusst die Vegetation in ihrer Physiologie und Phänologie erheblich und verändert deren Interaktion mit der Atmosphäre. In diesem Zusammenhang ist es essenziell zu wissen, wo und wann Pflanzenwachstum in Zentraleuropa wasser-limitiert ist und wie diese veränderten klimatischen Bedingungen die Herbstseneszenz von Laubwäldern verändern könnten. Darüber hinaus ist es von großer Bedeutung, Wachstumsstrategien verschiedener Laubbaumarten der gemäßigten Breiten zu verstehen, um die zukünftige Eignung dieser Baumarten im Kontext des Klimawandels besser einschätzen zu können. Diese Arbeit untersuchte mittels der Methodik der passiven Fernerkundung in drei zentraleuropäischen Untersuchungsgebieten verschiedene Aspekte dieser Fragestellungen. Ein zweiter Fokus lag auf der Einschätzung, inwieweit passive Fernerkundungsdaten landwirtschaftliche Dürre und Pflanzenphänologie erfassen können. In Zentraleuropa sind demnach vor allem Flächen unterhalb 800 m ü. NN, und hier insbesondere landwirtschaftliche Flächen und Grasland, in den Sommermonaten Juli und August dürregefährdet. Trockene und warme Wachstumsperioden verlängern tendenziell die Blattseneszenz eines mitteleuropäischen Laubwalds. Hinsichtlich der Trends und Treiber existieren zwischen den Baumarten dennoch substanzielle Unterschiede. Dies gilt auch für den Eintrittszeitpunkt der Frühlings- und Herbstphänologie unter nahezu identischen Umweltbedingungen, wodurch sich baumartenspezifische Unterschiede bei der Länge der Wachstumsperiode von bis zu zwei Monaten ergeben. Pflanzenfunktionelle Merkmale können dabei teilweise die Wachstumsstrategie vom Baumarten erklären. Darüber hinaus können sowohl landwirtschaftliche Dürre als auch Pflanzenphänologie mit passiven Sensoren verschiedener Fernerkundungsplattformen erfasst werden. Während bei der Dürre vor allem die Wasserlimitation eine wichtige Monitoringbedingung darstellt, muss bei der Phänologie je nach Fragestellung die räumliche Auflösung sowie die zu beobachtende phänologische Phase präzisiert werden, um robuste Ergebnisse zu erhalten. Perspektivisch verspricht diese Monitoring-Methodik in der Kombination mit weiteren Datensätzen ein tieferes Verständnis von Physiologie und Phänologie von Vegetation im Kontext der globalen Erwärmung.

Content

List of Figures

List of Tables

1. Introduction

Besides the ocean, the atmosphere and biosphere are two main components of the Earth's climate system and are closely related to each other. The atmosphere is defined at its lower boundary above the Earth's surface. It merges upwards into interplanetary space, whereby only the lower 10-50 km are usually relevant for weather and climate processes. The vast majority of the Earth's atmosphere is gaseous, which additionally contains hydrometeors and aerosols (Schönwiese, 2020). The dominant gases are nitrogen (N_2) and oxygen (O_2), with anthropogenic greenhouse gases such as carbon dioxide (CO_2), methane (CH_4), and nitrous oxide (N_2O) also making up a small proportion (Häckel, 2016; Schönwiese, 2020). The lowest layer of the atmosphere (troposphere) is the site of the Earth's weather events, and the atmosphere's composition significantly influences the Earth's radiation and energy balance (Brönnimann, 2018).

The Earth's biosphere can be divided into vegetation, animals, and humans. A large part of the global land surface is covered by vegetation and can be again roughly classified into natural and cultivated plants (Schönwiese, 2020). Weather patterns, climate, and site-specific conditions significantly influence the function and composition of vegetation, allowing a further global subdivision into zonal plant formations from the polar desert to the tropical rainforest (Schultz, 2016). On the other hand, vegetation influences several climatically and meteorologically relevant processes within the atmosphere, which means that the interactions between the atmosphere and vegetation play an essential role in the Earth's climate system (Bonan, 2008; Chapin et al., 2008; Jia et al., 2019).

1.1. Atmosphere-vegetation interactions

The atmosphere influences the global vegetation in many ways, but only the most important aspects will be briefly mentioned here. Temperature and precipitation (or soil moisture) are two essential factors for plant growth and the distribution of different plant species. They form the hygrothermal growth conditions of the individual ecozones and significantly determine the occurrence of certain plant formations (Kadereit et al., 2021; Schultz, 2016). In addition, extremes in the form of frost or drought, for example, are life-threatening to varying degrees depending on the plant species, while specific temperature and moisture ranges mean optimum productivity for the respective plant (Augspurger, 2013; Glaser et al., 2010; Huang et al., 2019; Schönwiese, 2020). Air humidity regulates vegetation's transpiration and photosynthesis processes (Glaser et al., 2010; Kaiser et al., 2015). Wind, in turn, has a significant influence on air humidity and, thus, transpiration (Grace, 1988; Häckel, 2016) and, in extreme forms, can also cause massive (breakage) damage to vegetation (Peterson, 2000; Schönwiese, 2020) and favor certain growth forms (Glaser et al., 2010).

Photosynthesis is influenced directly by sunlight and the atmosphere's composition: Short-wave solar radiation is the primary energy source for the global biomass balance and enables the life of all autotrophic plants (Glaser et al., 2010). This radiation is subject to absorption, scattering, and reflection in the atmosphere, which in turn is strongly dependent on the atmosphere's composition (Häckel, 2016; Schönwiese, 2020). In addition, the composition of the atmosphere in the form of specific gas concentrations (e.g., CO_2) also has a direct influence on the photosynthesis and respiration processes of vegetation (Gonzalez-Meler et al., 2004; Kadereit et al., 2021; Reddy et al., 2010). Finally, extreme weather events such as hurricanes, heat waves, or hailstorms should

also be mentioned in this context, which can have long-term and large-scale effects on various vegetation types (Houston, 1999; Hu & Smith, 2018; Yuan et al., 2016).

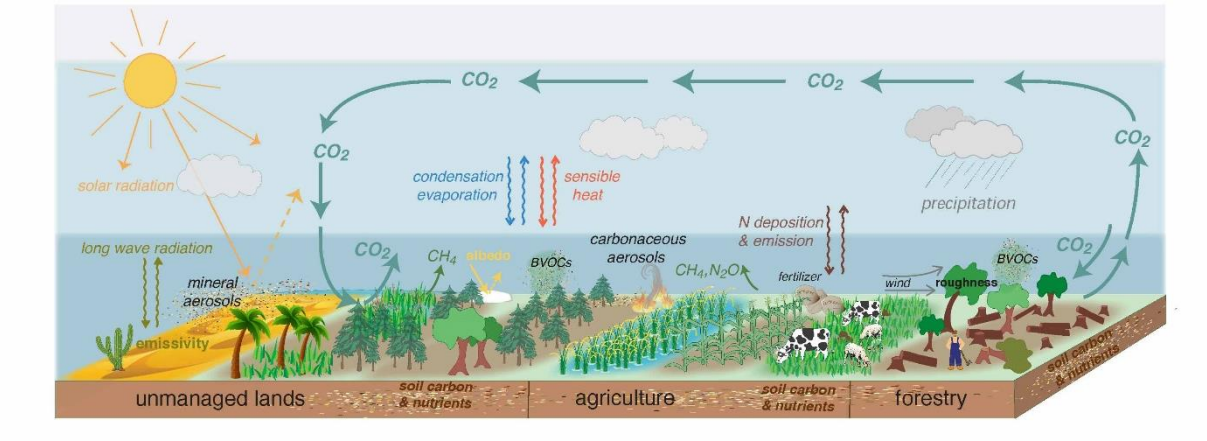

Figure 1: The structure and functioning of managed and unmanaged ecosystems that affect local, regional and global climate (figure and caption are taken from Jia et al., 2019; Box 2.1, Figure 1).

On the other hand, the Earth's vegetation interacts strongly with the atmosphere, with feedback processes influencing the climate and, thus, the vegetation again (see Figure 1). A distinction is made here between biophysical and biogeochemical interactions (Jia et al., 2019). One of the most important biophysical interactions is the albedo, i.e., the proportion of reflected energy compared to irradiated solar energy (Schönwiese, 2020). The albedo is strongly dependent on the land cover, which means that vegetation is a significant influencing factor here: Forest areas in high latitudes (and especially in winter), for example, have a lower albedo than other biomes and, therefore, absorb more short-wave radiation (Bonan, 2008; Ellison et al., 2017; Li et al., 2015). Compared to arable land or grassland, this leads to a warming of the earth's surface (Anderson et al., 2011). In addition, evapotranspiration processes are also of great importance in this context, whereby the transpiration of vegetation cools via latent heat flux and feedback with cloud formation and precipitation, especially for forest areas (Bonan, 2016; Ellison et al., 2017; Shen et al., 2015; Strengers et al., 2010). Finally, the vegetation also influences the surface roughness and thus the aerodynamics of the earth's surface through its height: large trees can cause more turbulence and thus higher sensible and latent heat fluxes, which has a cooling effect on the earth's surface (Bonan, 2016; Jia et al., 2019).

The biogeochemical perspective primarily considers the influence on the composition of the atmosphere. One of the most important interactions directly related to vegetation is carbon dioxide exchange via photosynthesis and plant respiration (Jia et al., 2019). Vegetation currently acts under natural conditions as a carbon sink, which leads to a reduction in the CO_2 content of the atmosphere and thus to a reduced greenhouse effect and cooling of the Earth's surface (Bonan, 2016; Fang et al., 2007; Friedlingstein et al., 2023). In addition, the burning of biomass and the resulting black carbon and aerosols in the atmosphere also play a role in this context, which have different influences on the Earth's radiation and energy balance (Bonan, 2016; Bond et al., 2013; Jia et al., 2019; Ramanathan & Carmichael, 2008). Finally, trees also emit biogenic volatile organic compounds (BVOCs), especially isoprenes and monoterpenes (Bonan, 2016; Guenther et al., 2012). BVOCs affect the oxidant concentrations in the atmosphere and are an important precursor

of secondary organic aerosols (SOA), which influence cloud reflectivity or aerosol scattering (Jia et al., 2019).

All these components and processes constantly interact and can differ remarkably depending on the geographical area (Anderson et al., 2011; Bonan, 2016). Another important factor in this complex is the human being: On the one hand, human activities have massively changed the biophysical and biogeochemical properties of the Earth's surface over the past millennia (Goldewijk, 2001; Hurtt et al., 2020). On the other hand, human emissions of greenhouse gases have caused a global warming, which has increased the Earth's surface temperature by around 1.1°C from 2011 to 2020 compared to 1850 to 1900 (IPCC, 2023). These climatic changes impact the biosphere, especially vegetation, in several ways and vary depending on the geographical region. In the following, the text sections refer mainly to Central Europe.

1.2. Climate change impacts on vegetation in Central Europe

As a result of anthropogenic global warming, average temperatures in Central Europe have risen remarkably in the recent past, for example, in Germany (1881-1910 to 2011-2020), Austria (1880 to 2011), and Switzerland (1864 to 2019) by 2°C, which is substantially higher than the global average (APCC, 2014; BAFU, 2020; DWD, 2021d). In addition, a change in various extreme weather events in this region is observed in this context, for example, an increase in heat and drought events and a decrease in cold events (BAFU, 2020; DWD, 2023; IPCC, 2023). These changes, both average and extreme, have a variety of effects on vegetation in Central Europe, be it in the change of distribution areas (Feehan et al., 2009; Vitasse et al., 2021), the shift in phenological phases (Menzel et al., 2020; Vitasse et al., 2021) or the functional influence of heat or drought events on vegetation (Gazol & Camarero, 2022; Lindner et al., 2014; Riedel & Weber, 2020). Two central aspects of atmosphere-vegetation interaction influenced by climate change in this region are agricultural drought and plant phenology.

1.2.1. Agricultural drought

Drought is a complex phenomenon primarily caused by a precipitation deficit (Heim, 2002; Zargar et al., 2011). In general, droughts are classified into different categories depending on the field of application, the most important being meteorological drought (precipitation deficit), agricultural drought (soil moisture deficit), hydrological drought (runoff and water storage deficit) and socio-economic drought (water supply and demand; Dai, 2011; Wilhite & Glantz, 1985). These types of drought typically occur in chronological order and are interdependent: initially, there is a precipitation deficit, which after a certain period leads (in combination with increased evapotranspiration) to a soil moisture deficit and, due to low soil runoff to water deficits in rivers and lakes (see Figure 2; Zargar et al., 2011). Agricultural drought, in particular, is defined slightly differently depending on the perspective, but in general, the soil moisture deficit reaches a level at which the plant's water requirements are no longer met or the growth of the (agricultural) plant is affected by the soil moisture deficit (Liu et al., 2016c; Sepulcre-Canto et al., 2012; Wilhite & Glantz, 1985).

The effects of agricultural drought on plants are diverse and can be described both directly and indirectly. In general, the main direct effects are reduced plant growth, reduced transpiration, limited nutrient uptake, reduced photosynthesis, and a reduction in the yield of agricultural plants

(Bréda et al., 2006; Farooq et al., 2009; Gupta et al., 2020). In addition, extreme drought events can also trigger or amplify increased mortality rates (Allen et al., 2010; Bréda et al., 2006; Wang et al., 2012). These effects, in turn, imply indirect impacts, such as changes in the radiation balance or the carbon or water cycle (see section 1.1.). Droughts also have a remarkable economic impact; for example, the economic damage caused by the extreme drought in Europe in 2003 is estimated at 8.7 billion euros, and in Germany, the damage costs in agriculture in the 2018 drought year amounted to 770 million euros (BMEL, 2022; EEA, 2010).

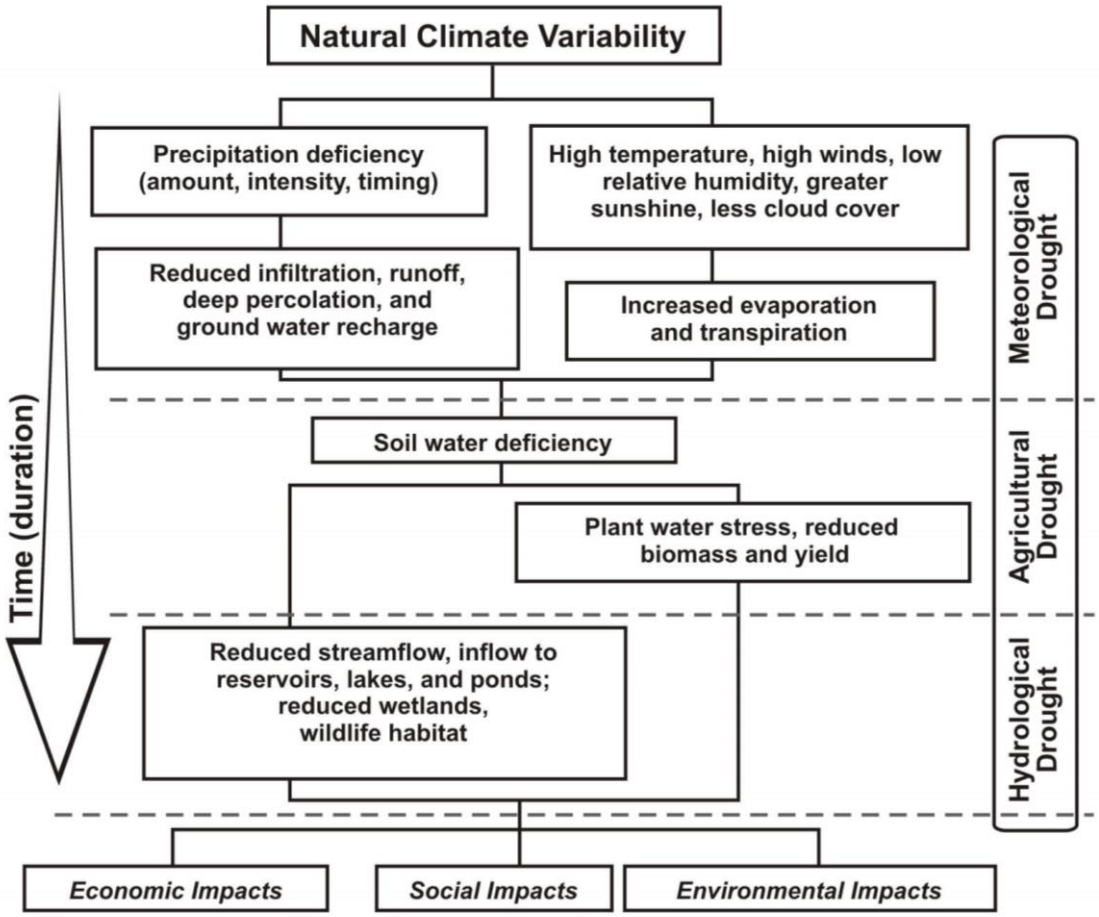

Figure 2: Sequence of drought occurrence and impacts for commonly accepted drought types. All droughts originate from a deficiency of precipitation or meteorological drought but other types of drought and impacts cascade from this deficiency (figure and caption are taken from NDMC, 2024).

In the last 20 years, Central Europe has repeatedly experienced severe drought events, for example, in 2003 (Schär et al., 2004), 2015 (Ionita et al., 2017) and 2018-2020 (Bakke et al., 2020; Hari et al., 2020; Rakovec et al., 2022). Despite the supposed accumulation of these events, no clear significant trends regarding the frequency or severity of droughts have been found in the past for this region (Hänsel et al., 2019; IPCC, 2023; Spinoni et al., 2017; Stagge et al., 2017). In the future, however, an increase is projected for Central Europe as a result of global warming, whereby the severity and frequency will vary depending on the warming scenario (Grillakis, 2019; Ruosteenoja et al., 2018; Spinoni et al., 2018). This also applies to consecutive drought events (Hari et al., 2020).

1.2.2. Plant phenology

Phenology, in general, is "the study of the timing of recurring biological events, the causes of their timing with regard to biotic and abiotic forces, and the interrelation among phases of the same or different species" (Lieth, 1974, p. 4). Plant phenology logically refers to vegetation, with typical phenological phases being leaf unfolding, flowering, fruit ripening, leaf coloring, or leaf fall.

Vegetation phenology interacts closely with the Earth's climate system and the associated atmosphere (see Figure 3). On the one hand, the onset dates of the phenological phases are strongly influenced by weather conditions and climate: In spring, phenology (in addition to the photoperiod) is strongly influenced by temperature via the processes of chilling and forcing and is an essential driver of bud burst and leaf unfolding (Ettinger et al., 2020; Flynn & Wolkovich, 2018; Menzel et al., 2006; Piao et al., 2019).

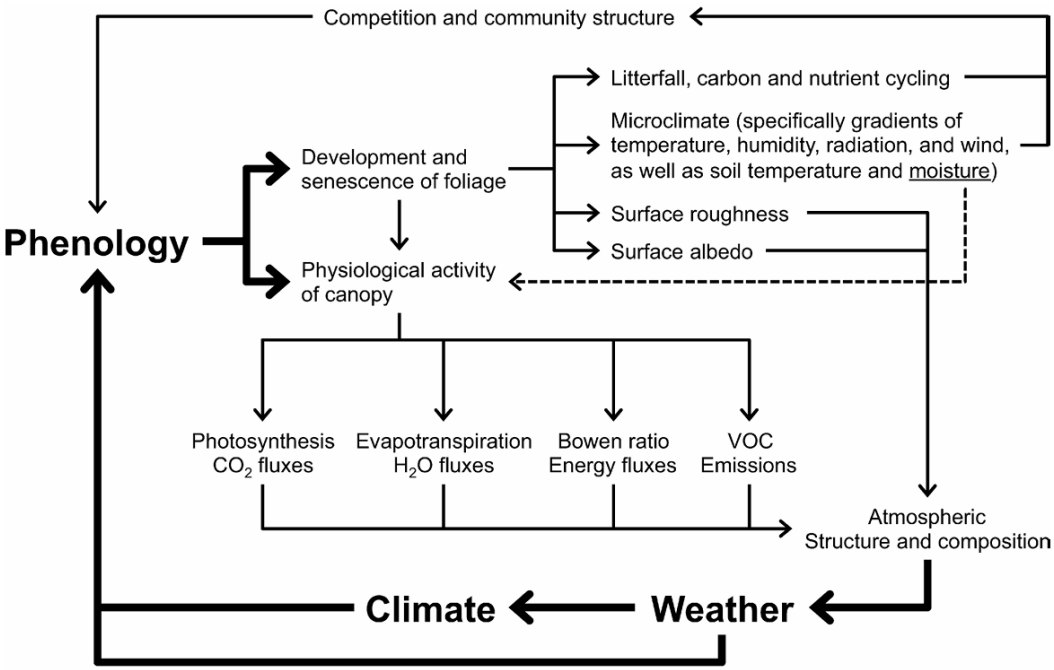

Figure 3: Conceptual model illustrating the primary feedbacks between vegetation and the climate system that are influenced by vegetation phenology (figure and caption taken from figure 2 in Richardson et al., 2013)

Autumn phenology, i.e., leaf coloring and leaf fall, is less well understood in this context, although temperature is also a key driver here (Gallinat et al., 2015; Gill et al., 2015). In addition, however, water availability (Bigler & Vitasse, 2021; Gill et al., 2015; Grossiord et al., 2022; Xie et al., 2018) and insolation (Liu et al., 2016a; Liu et al., 2016b) as well as photoperiod (Gill et al., 2015; Lang et al., 2019), nutrient availability (Fu et al., 2019), spring phenology (Fu et al., 2019; Keenan & Richardson, 2015; Liu et al., 2016b) and photosynthetic activity (Lu & Keenan, 2022; Zani et al., 2020; Zohner et al., 2023) are also considered influencing factors beyond meteorology.

On the other hand, plant phenology influences the atmosphere and, thus, the Earth's weather and climate through biogeochemical and biophysical interactions (see Figure 3). Thus, leaf development and senescence strongly determine the photosynthetic activity and transpiration of the vegetation and, depending on the leaf cover, influence the albedo and surface roughness, which

in turn impacts both the global and local climate in feedback (Gaertner et al., 2019; Keenan et al., 2014; Peñuelas et al., 2009; Richardson et al., 2013).

Similar to the drivers of phenology, a clearer picture emerges in Central Europe also for the trends of phenology in spring than in autumn: Spring phenological phases (leaf unfolding and flowering) have mainly advanced in the last decades due to global warming and the resulting higher spring temperatures. In autumn (leaf coloring), on the other hand, a slight delay in the trend can be seen, whereby, depending on the species and time series, opposing developments can also be observed (Menzel et al., 2020; Piao et al., 2019; Vitasse et al., 2022). Due to the insufficient understanding of physiological processes driving phenology and the resulting inadequate performance of phenological prediction models, future projections regarding various phenological phases do not currently allow any robust statements to be made (Chuine & Régnière, 2017; Piao et al., 2019; Richardson et al., 2013; Tang et al., 2016).

When analyzing plant phenological drivers and trends, the inter- and intraspecific variability of phenological onset dates is also of great importance. In both spring and autumn, phenological phases, such as leaf unfolding or senescence, can differ by several weeks at the same location, depending on the species and individual (Cole & Sheldon, 2017; Marchand et al., 2020; Panchen et al., 2014; Richardson & O'Keefe, 2009). These differences are usually explained by different growth strategies based on plant-functional traits (e.g., plant height, leaf area, seed mass, etc.) or microclimatic differences (Delpierre et al., 2017; Osada & Hiura, 2019; Panchen et al., 2014; Sporbert et al., 2022).

Both plant phenology and agricultural drought are two key aspects influenced by climate change in Central Europe. Continuous vegetation monitoring is essential to better understand this influence in the past and future. This allows trends to be recorded, individual events to be put in relation to each other, and connections with other spheres of the Earth's climate system to be understood (Lovett et al., 2007). In this context, passive remote sensing is a crucial instrument for monitoring vegetation. In the following section, this methodology and the current state of research will be explained in terms of agricultural drought and plant phenology.

1.3. Monitoring vegetation with passive remote sensing

"Remote sensing is the acquisition of information about an object or phenomenon from distance" (Weiss et al., 2020, p. 2). In passive remote sensing, a passive sensor is attached to a platform (e.g., satellite, UAV, ground-based platform, etc.) which measures the reflected or emitted electromagnetic radiation of an observed object (Ghassemian, 2016; Sishodia et al., 2020; Weiss et al., 2020).

From a historical perspective, the first photographs in 1839, the first photographs from an airplane in 1909, and the beginning of color photography in the 1930s are among the milestones in the technological development of this monitoring method. In 1956, Colwell's first experiments in aerial photography followed about the classification of damaged vegetation and different vegetation types, while the first Landsat satellites were launched in the 1970s (Elachi & van Zyl, 2021). This was followed by several other satellite-based systems, such as Terra/Aqua MODIS (1999 and 2002) and Sentinel (2014; Sishodia et al., 2020). In addition, the widespread scientific use of digital repeat photography in the 2000s and UAV-supported systems in the 2010s in the form of alternative sensor platforms also represents an important aspect in this context (Aasen et al., 2018; Burton et al., 2015; Richardson et al., 2007).

The fundament of passive remote sensing monitoring vegetation is the leaf's special reflectance behavior compared to other surfaces, such as open soil (see Figure 4). In the visible wavelength range (VIS, 400-700 nm), reflectance is generally very low and is determined by the strong absorption of the leaf pigments (carotenoids, xanthophylls, and chlorophylls, especially in the non-green range). In the near-infrared (NIR) range, the reflectance increases sharply ("red edge") and remains constantly high in the NIR (700-1300 nm) due to the mesophyll of the vegetation, whereby the reflectance varies depending on the leaf cell structure and turgor. In the short-wave infrared (SWIR, 1300-2500 nm), the reflectance then decreases due to the absorption of water and the lignin, protein, and cellulose content of the vegetation (Huete, 2012; Zeng et al., 2022).

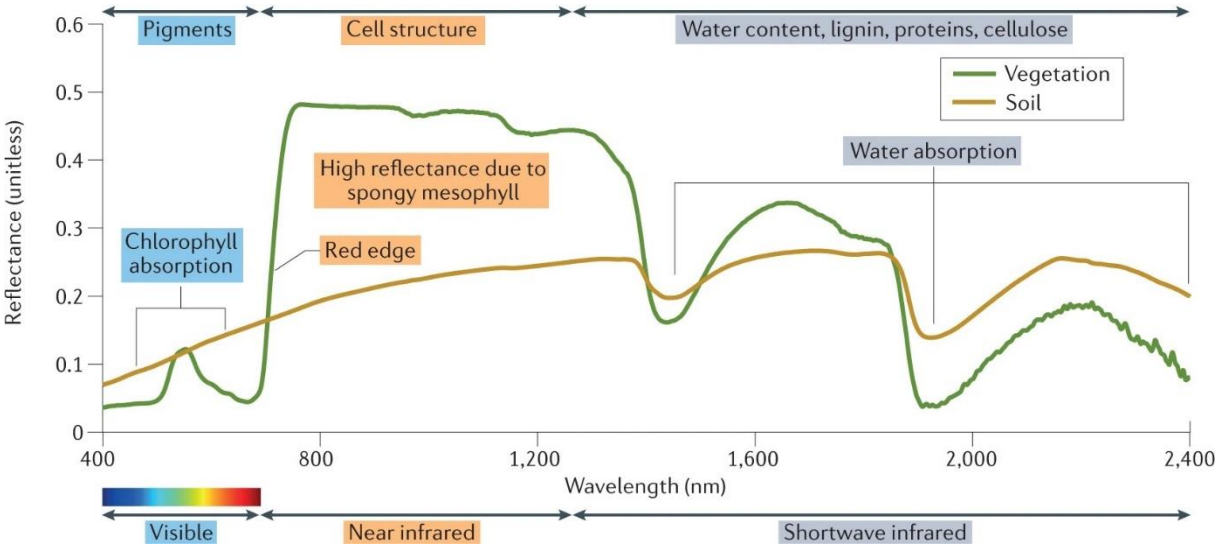

Figure 4: Reflectance of vegetation and soil. These spectral features of vegetation and soil are the foundation of the rationale of vegetation indices and support the design of various vegetation indices (figure and caption taken from figure 2 in Zeng et al., 2022).

These unique spectral properties can be used to obtain a wide range of information within vegetation and in comparison to other objects and land surfaces. Information is usually obtained and analyzed using spectral indices. In connection with vegetation-related questions, different wavelength ranges are combined in the indices, for example, Red-NIR, VIS-NIR, VIS, Red-edge NIR, or NIR-SWIR (Zeng et al., 2022). A selection of the most common spectral indices in passive remote sensing of vegetation can be found in Table 1.

Table 1: Selection of frequently used spectral indices for vegetation analysis in passive remote sensing. Listed is the name of the index and the corresponding abbreviation, equation, and reference (NIR = near infrared; RE = red-edge). The subscripted NDWI values represent the wavelength ranges in nm. The table is an excerpt from Zeng et al. (2022).

Index	Abbreviation	Equation	Reference
Normalized difference vegetation index	NDVI	$\frac{NIR - Red}{NIR + Red}$	Rouse et al. (1974); Tucker (1979)

Enhanced vegetation index	EVI	$\frac{2.5 * (NIR - Red)}{(NIR + 6 * Red - 7.5 * Blue + 1)}$	Huete et al. (2002)
Green chromatic coordinate	GCC	$\frac{Green}{Red + Green + Blue}$	Woebbecke et al. (1995)
Red-edge chlorophyll index	CIred-edge	$\frac{NIR}{RE - 1}$	Gitelson et al. (2005)
Normalized difference water index	NDWI	$\frac{NIR_{860} - SWIR_{1240}}{NIR_{860} + SWIR_{1240}}$	Gao (1996)

Using the indices makes obtaining information on a wide range of vegetation issues possible. For example, statements can be made about the productivity, health, or biodiversity of plants (Kooistra et al., 2024; Lausch et al., 2016; Wang & Gamon, 2019). Two specifically important application areas in Central Europe are agricultural drought and plant phenology, which will be explained in more detail below.

1.3.1. Agricultural drought

Agricultural drought is usually defined in relation to vegetation in such a way that the plant's ability to function is restricted by a soil moisture deficit and the resulting water stress (Liu et al., 2016c; Sepulcre-Canto et al., 2012; Wilhite & Glantz, 1985). Drought stress affects both the bio-physical and chemical properties of the vegetation (and soil) and changes spectral properties, which can be measured by spectral indices (Hazaymeh & Hassan, 2016). In passive remote sensing, optical and thermal remote sensing are primarily used in this context. Passive microwave sensors should not be described further in this context because they mainly focus on soil moisture (West et al., 2019).

In optical remote sensing, the red wavelength range, as well as the NIR and SWIR, are particularly important for detecting drought in vegetation. Directly, a low water content means mostly a higher reflectance, especially in the SWIR (Qin et al., 2021; Thomas et al., 1971). Indirectly, statements about drought stress can also be made via plant physiology: Healthy vegetation has a higher absorption in the red wavelength range and a higher reflectance in the NIR than unhealthy or sparse vegetation (Hazaymeh & Hassan, 2016; Peñuelas & Filella, 1998). Indirect detection represents a large part of this monitoring methodology, with the NDVI (see Table 1) being the most used index in this context (West et al., 2019). Other (partly still young) monitoring approaches include drought detection via solar-induced chlorophyll fluorescence and light and water use efficiency (Qin et al., 2021; West et al., 2019). In thermal remote sensing, the land surface temperature (LST) of vegetation is primarily used as a drought indicator: Under water stress, evapotranspiration generally decreases due to stomatal closure, causing a higher LST than under moist growing conditions (Anderson & Kustas, 2008; Gutman, 1990).

In the vegetation-based monitoring of agricultural drought in Central Europe, satellite-based passive systems represent the main part of existing monitoring approaches. Thereby, one research approach is to understand the relationship with other forms of drought: In connection with meteorological drought, vegetation indices (VIs) react to precipitation deficits with a remarkable

time lag, but this can vary greatly depending on the type of vegetation and the observed region (Afshar et al., 2021; Bachmair et al., 2018; Peled et al., 2010). A temporal offset to soil moisture deficits can also be observed (albeit shorter; Buitink et al., 2020), although the correlation varies depending on the climatic region and season (Peled et al., 2010; van Hateren et al., 2021).

Furthermore, applications of satellite-based VIs in this context include monitoring agricultural yields (Bachmair et al., 2018; Möllmann et al., 2019) and quantifying the impact of extreme drought events on vegetation in Central Europe (Buras et al., 2020). In addition, satellite-based remote sensing is also used to develop combined drought monitoring systems (Sepulcre-Canto et al., 2012; Trnka et al., 2020) or to identify areas and periods in which water is the primary limiting growth factor for vegetation (Karnieli et al., 2019). Research questions that require high spatial resolution and focus on a small study area are also increasingly being analyzed using UAV-based systems, whereby, for example, crop (Ekinzog et al., 2022; Hoffmann et al., 2016) or tree water stress can be detected (Buras et al., 2018; D'Odorico et al., 2021).

1.3.2. Plant phenology

In passive remote sensing of plant phenology, VIs (see Table 1) are usually calculated for each image over the year, whereby these values are corrected if necessary (e.g., with running average or best index slope extraction; Lange & Doktor, 2017; Viovy et al., 1992; Zeng et al., 2020). Subsequently, a phenological curve is fitted using a mathematical function (e.g., Logistic function-fitting or High-Order Annual Splines), which usually contains the typical phenological course of the year with the greening and senescence of the vegetation (Dronova & Taddeo, 2022; Zeng et al., 2020). Finally, a phenological metric is extracted, whereby a methodological distinction is made between threshold-based methods and change detection (Zeng et al., 2020). The phenological metrics such as start of season (SOS) or end of season (EOS) are standard variables, but it is also possible to extract particular phenological phases, for example, from agriculture, or to determine VI magnitude values (Dronova & Taddeo, 2022; Zeng et al., 2020).

As with agricultural drought, satellite-based systems represent the majority of research approaches in passive remote sensing of plant phenology. In general, satellite phenology produces robust results in comparison with in-situ measurements, with autumn phenology, in particular, appearing more complex to determine (Berra & Gaulton, 2021). Especially in Central Europe, this picture is confirmed in the validation of satellite phenology with ground observations (Kowalski et al., 2020; Rodriguez-Galiano et al., 2015b; Verger et al., 2016) or eddy covariance-based phenology (Balzarolo et al., 2016). Due to this fact, the large-scale spatial coverage and the recently advanced observation periods allow statements to be made about the characteristics of European land surface phenology (LSP; Han, 2013; Rodriguez-Galiano et al., 2015a) as well as its trends (Garonna et al., 2014; Zhao et al., 2015) and (climatic) drivers (Bórnez et al., 2021; Jin et al., 2019; Xie et al., 2021).

In recent years, UAV-supported systems have also played an increasingly important role in plant phenology research. In forest areas, the high spatial resolution of drone images makes it possible to record the phenology of individual trees with little personnel effort, with initial approaches in Central Europe also providing promising results in validation with ground observations (Ciocîrlan et al., 2022; Kleinsmann et al., 2023). UAV images can also be used in the field of agriculture to track the phenological development of crops and determine individual phenotypic traits (Burkart et al., 2018; Ganeva et al., 2022), whereby the information could be used to predict agricultural yields (Prey et al., 2022). In addition, fine-scale phenological drone data can also be used in habitat management (Neumann et al., 2020).

A third common approach in passive remote sensing of plant phenology is the observation using fixed installed near-surface cameras, often called "phenocam" (Richardson, 2023). The use of these has increased massively over the last 15 years and is also used in Central Europe for various issues. One of the main applications of the camera data is the validation of other phenological derivation methods, for example, from satellite remote sensing or eddy covariance data (Bórnez et al., 2020; Soudani et al., 2021; Tian et al., 2021). In addition, also other research questions are analyzed, such as the influence of extreme weather on phenology (Cremonese et al., 2017), the relationship between phenology and plant productivity (Liu & Wu, 2020) or the interaction between under- and overstory phenology (Uphus et al., 2021).

1.4. Objectives

Passive remote sensing of vegetation in the context of climate change has become increasingly important in recent decades due to rapid technological development, the growth in platform types, and the progressive increase in observation periods and reference data sets. High spatial and temporal coverage with comparatively low personnel and time expenditure and, in some cases, ready-to-analyze products and rapid data availability are important advantages when monitoring vegetation. Climate change has a remarkable impact on vegetation in Central Europe, and many research questions are still unanswered, particularly concerning the (climatic) influence on the physiology and phenology of vegetation.

Based on the current state of science and respective research gaps described above, this work uses the methodology of passive remote sensing to analyze various questions in this context using exemplary study areas: On the one hand, this thesis aims to answer – in a high spatial as well as temporal resolution – where and when water is the limiting factor for vegetation growth and to what extent land cover and altitude characterize this influence. On the other hand, it will be determined to what extent their respective functional traits can explain the spring and autumn phenological variability of different deciduous tree species and which factors influence the autumn phenology of a deciduous forest.

From a methodological point of view, despite the technological development and the undisputed quality of remote sensing data, there is always the uncertainty of indirect measurement when monitoring vegetation. This uncertainty can be divided into two sub-aspects: First, there is the question of what (vegetation) information is recorded by passive remote sensing and how this information corresponds with data measured directly (on the ground). Second, it is questionable to what extent different remote sensing systems generate different results due to different spatial and temporal resolutions and how these differences can be explained.

A second focus of this work is therefore on answering these methodological questions in climate (change) impacts on vegetation: On the one hand, it will be answered to what extent agricultural drought in Central Europe can be recorded by the remote sensing indices Temperature Condition Index (TCI), Vegetation Condition Index (VCI) and Vegetation Health Index (VHI) in comparison to soil moisture and yield data. On the other hand, it is shown to what extent different passive remote sensing systems capture the spring and autumn phenology of deciduous trees compared to in-situ data and how the differently generated phenological data affect predictor analyses of autumn phenology.

2. Materials and methods

The research questions formulated in section 1.4. of this thesis were answered by analyzing vegetation-related remote sensing data in three different study areas. In study area 1 (Bavaria), it was analyzed when and where vegetation growth is water-limited and whether the remote sensing indices VCI, TCI, and VHI can detect agricultural drought in these regions. In study area 2 (National Park Hainich), the spring and autumn phenology of different data sources were compared, and subsequently, the effect of differently derived phenology on a predictor analysis of autumn phenology was investigated. In study area 3 (Weltwald Freising), intra- and interspecific phenological variability was determined for 74 tree species using in-situ validated UAV data, and differences between species were related to plant functional traits. In the following, the individual study areas (2.1.), the data used in this context (2.2.), the methodology applied (2.3.), and the software used (2.4.) will be described in detail.

2.1. Study sites

The study areas considered in this thesis are all located in Central Europe and in German territory (see Figure 5). One large-scale study area (Federal State of Bavaria, 47°-50.5°N, 9°-14°E) and two small-scale study areas (Hainich National Park with flux tower, 51.079407°N, 10.452089°E, 440 m a.s.l.; Weltwald Freising, 48.4142757°N, 11.6666912°E; 462 to 508 m a.s.l.) are analyzed (Knohl et al., 2003; LDBF, 2023).

According to the Köppen-Geiger classification (1991-2020), all three study areas are located in temperate (Cfb) or cold (Dfb) climate zones without a dry season and with a warm summer (Beck et al., 2018). In Bavaria, the mean annual temperature (MAT; 1991-2020) ranges from -3.3 to 11 °C, with the main part of the area recording values between 8 and 10 °C. The mean annual precipitation sum (MAP) over the same period is 515 to 3184 mm, with the south of the region having more precipitation than the north (DWD, 2021b, 2021c; Kloos et al., 2021). In the two smaller study areas, these key figures (Hainich: 2000-2020; Freising: 2001-2020) are in a similar value range with a MAT of 8.6 °C (Hainich) and 9.4 °C (Freising) and a MAP of 716 mm and 736 mm (DWD, 2024; Kloos et al., 2024; Knohl et al., 2022). In the analyzed year 2022, the average annual temperature in Weltwald Freising was 9.6 °C and the annual precipitation sum was 829 mm (Kloos et al., in review; data provided by the Bavarian State Institute of Forestry).

The analyzed federal state of Bavaria is mainly covered by agricultural area (mainly in NW and SE) and forest (mainly in E and towards the Alps). Grassland represents only a small part of the land area and is mainly present in the Alpine regions and foothills (EEA, 2019; Kloos et al., 2021). The Hainich National Park was developed in 1997 as a 7500-ha beech conservation area and consists mainly of European beech (*Fagus sylvatica* L., 64 %) and European ash (*Fraxinus excelsior* L., 28 %). It has been a UNESCO World Heritage Site since 2011 and contains some trees that are over 270 years old (Tamrakar et al., 2018; Thiel et al., 2020). The Weltwald Freising covers an area of 100 hectares with 400 different tree and shrub species from the northern hemisphere planted since 1987 (Rudolf, 2023). The species are planted in plots with a few individuals up to 200 specimens, whereby the plots are divided according to the continental origin of the respective species: Europe, North America, and Asia (Kloos et al., in review).

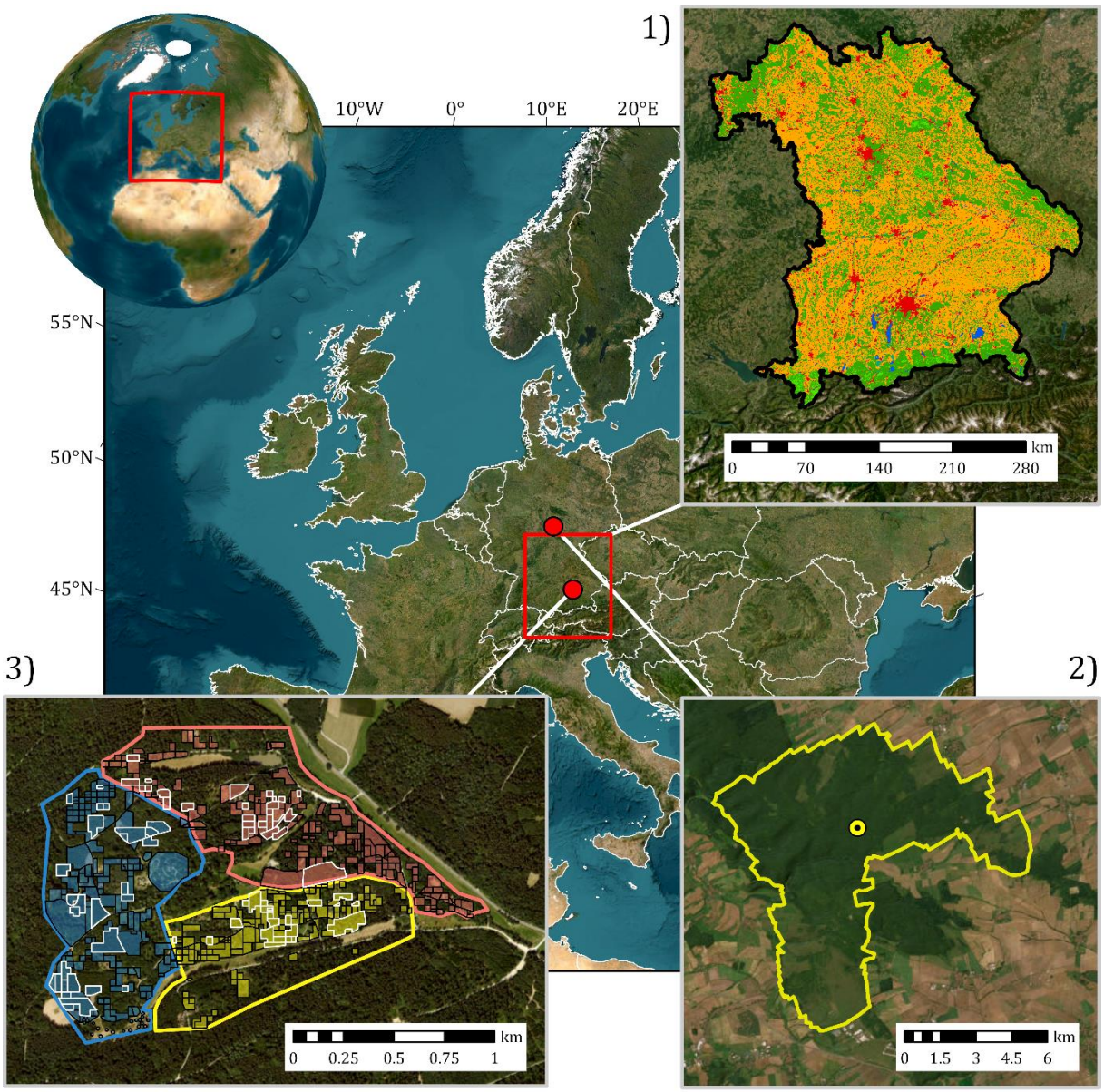

Figure 5: Overview map of the three study areas considered in this thesis (1: Bavaria; 2: Hainich National Park; 3: Weltwald Freising; Kloos et al., 2021; Kloos et al., 2024; Kloos et al., in review) and their location in Europe (middle map) and worldwide (top left). The legend for the respective detailed map of the study areas is shown below the figures (data sources: Esri, Maxar, Earthstar Geographics, and the GIS User Community (top left); EEA (2019), GeoBasis-DE / BKG (2024), Earthstar Geographics (1); TLUBN (2024), GDI-Th, Earthstar Geographics (2); BaySF (2022), BVV – geodaten.bayern.de, Maxar, Microsoft (3); eurostat (2020), Earthstar Geographics (middle map)).

2.2. Data sets overview

Within the three study areas, vegetation data sets from satellite remote sensing (see section 2.2.1.), near-surface remote sensing (see section 2.2.2.), and in-situ observations (see section 2.2.3.) were

analyzed. In addition to the primary analysis of these data sets, they were contextualized and validated in a second step with additional data, which are described in section 2.2.4.

2.2.1. Satellite remote sensing

Only data products from the Moderate-resolution Imaging Spectroradiometer (MODIS) were used to analyze the vegetation using satellite data: MOD13Q1, MOD11A2, MCD12Q1 (all 2001 to 2020) and MCD12Q2 (2001 to 2019; see Table 2). In the pre-processing stage, the LST and land cover data were resampled to a spatial resolution of 250 m (like the NDVI data), and the NDVI data were linearly interpolated to an 8-day temporal resolution (like the LST data). In addition, an annual vegetation mask was applied to both the LST and NDVI data using the land cover data (Kloos et al., 2021).

Table 2: MODIS satellite data products used in this work with the overall description of the product, the individually used layer, as well as the respective spatial and temporal resolution, and the reference of the data set.

MODIS product	Description	Used layer	Spatial resolution	Temporal resolution	Reference
MOD13Q1	Vegetation Indices	NDVI	250 m	16 days	Didan (2015)
MOD11A2	LST and Emissivity	Daytime LST (K)	1 km	8 days	Wan et al. (2015)
MCD12Q1	Global land cover types	Land Cover Type 1: Annual International Geosphere-Biosphere Programme (IGBP) classification	500 m	Annual	Friedl and Sulla-Menashe (2019)
MCD12Q2	Global land surface phenology metrics	Greenup, MidGreenup, Senescence, Dormancy	500 m	Annual	Friedl et al. (2019)

Before the phenological data sets were analyzed, a quality assurance layer was applied to remove low-quality data from the data set. The layer classifies each pixel on a four-level quality scale, which is based on various criteria of the phenology calculation (fraction of missing or filled EVI data in the cycle, spline goodness-of-fit). Only pixels with the highest quality level (value = 0) were included in the analysis (Kloos et al., 2024).

2.2.2. Near-surface remote sensing

Regarding near-surface remote sensing data of vegetation, camera data from tree canopies was analyzed. The camera used in this thesis is mounted on the flux tower top in the Hainich National

Park (see Figure 5) and has been taking images of the canopies of the national park every day at 12:00 noon since 2001 (since August 2020 even every 30 minutes; Dept. Bioclimatology & Knohl, 2024). In this thesis, due to changing camera perspectives and existing data gaps, three bioclimatologists used this data to manually determine the phenology of the tree crowns (Kloos et al., 2024). Each person determined annually two phenological phases according to the BBCH code (Biologische Bundesanstalt für Land- und Forstwirtschaft, Bundessortenamt und CHemische Industrie; Meier, 2018):

1. SOS: BBCH 11 (first leaves unfold)
2. EOS: BBCH 95 (50% of the leaves have fallen/discolored)

Each year, an individual region of interest was defined for the camera images through the changing camera perspectives. The phenological onset dates were determined for two tree species in the national park: *Fagus sylvatica* L. and *Fraxinus excelsior* L. The final results were then averaged and thus represented the final onset dates of the respective phenological phase and species (Kloos et al., 2024).

In addition, UAV data collected in 2022 in Weltwald Freising (see Figure 5) was used: A total of 27 flights with a Phantom 4 multispectral UAV (DJI, Nanshan, Shenzhen, China) were carried out around noon from March to December on days with low wind speed and clear sky/overcast conditions. At an altitude of 100 m above ground level and with a ground sampling distance of 5-8 cm, an image was taken once per second in the red wavelength range (650 nm ± 16 nm), in the NIR (840 nm ± 26 nm) and with an RGB camera (2 MP resolution, NADIR position; Kloos et al., in review).

The UAV used an integrated dual-band high-precision Real Time Kinematic (RTK) GPS with a Networked Transport of RTCM via Internet Protocol (NTRIP) network service. In addition, five measured ground control points were placed for each flight and the flight grid was set up with a frontal and lateral overlap of 85%. The grid orientation was set automatically by the flight software. Before each flight, an image of the calibration reflectance panel (AgEagle Aerial Systems Inc., Wichita, Kansas, USA) was taken to ensure further image processing using PIX4d mapper version 4.75 (Pix4D, Prilly, Switzerland). Finally, several products were generated from the UAV images (Kloos et al., in review):

- RGB orthomosaics (10 cm resolution)
- NDVI maps (10 cm)
- digital terrain model (DTM, 1 m)
- digital surface model (DSM, 10 cm)

2.2.3. In-situ observations

In-situ observations of the vegetation were also used as a starting data set for further analyses. On the one hand, phenological observations from the German Meteorological Service (DWD) were used. In-situ observations of annual onset dates of different phenological phases are interpolated to a Germany-wide grid dataset (1x1 km) using multiple linear regression with respect to altitude, latitude, and longitude (DWD, 2022; Yuan et al., 2021). In this thesis, three phenological phases were specifically analyzed for the Hainich National Park from 2000 to 2020:

- RBUBO: European beech - beginning of unfolding of leaves
- RBUBV: European beech - autumn leaf coloring
- RBUBF: European beech - autumn leaf fall

In addition, flux tower data from the Hainich National Park, which are part of the Integrated Carbon Observation System (ICOS) network, were also analyzed in this context. Specifically, the following variables were used for the period 2000-2020 in daily resolution (Knohl et al., 2022):

- Net ecosystem exchange (NEE) (g C m^{-2} day^{-1})
- Gross primary production, from daytime partitioning method (GPP:DT; Lasslop et al., 2010) (g C m^{-2} day^{-1})
- Gross primary production, from nighttime partitioning method (GPP:NT; Reichstein et al., 2005) (g C m^{-2} day^{-1})

Spring (start of season, SOS) and autumn (end of season, EOS) phenology were then derived from this data. Therefore, the NEE data were converted to net ecosystem production (NEP) values (NEP = -NEE) in order to obtain uniformly positive values with the GPP values for CO_2 uptake (Kloos et al., 2024). The SOS and EOS were then calculated using the smoothed threshold method (central moving-window mean, five days; Barnard et al., 2018). The threshold value was defined as 0 g C m^{-2} day^{-1} for NEP and the 10% value of the respective mean annual GPP maximum from 2000 to 2020 for GPP (Kloos et al., 2024; Zhou et al., 2016; Zhou et al., 2017). The date for the SOS was determined when the threshold value was exceeded for the first time in the year and for the EOS when it was undershot for the first time after the SOS in his year. As an additional criterion, the exceedance or undershoot of the threshold value had to be constant for 20 days for NEP and SOS < 30 and EOS > 330 were excluded for GPP phenology (Kloos et al., 2024).

2.2.4. Explanatory and validating data sets

To place the primarily analyzed vegetation data in a larger context, they were explained and validated with the help of additional data sets. The Corine Land Cover (CLC) 2018 product (100 m resolution; EEA, 2019) and the European Digital Elevation Model (EU-DEM) v1.1 (25 m; EEA, 2021) were used as explanatory datasets. The DEM was scaled up to a resolution of 100 m in pre-processing using the arithmetic mean (Kloos et al., 2021).

Predictors of autumn phenology

To better understand the drivers of autumn phenology in the Hainich National Park, measured meteorological and CO_2 exchange-related data from the flux tower were used (Knohl et al., 2022). Besides the three variables from section 2.2.3., additionally, four meteorological variables were implemented (Kloos et al., 2024):

- Air temperature (°C)
- Precipitation (mm)
- Vapor pressure deficit (VPD) (hPa)
- Soil water content (16 cm depth) (%)

Following literature, especially Zani et al. (2020), 20 different predictor variables were calculated from the seven measured variables for every year between 2000 and 2020 (see Table 3 and Table 1 in Kloos et al. (2024) for further information). The so-called "Dryness-Wetness-Index" (DWI) was developed and calculated in order to adequately represent the complexity of the water availability (Wilhite & Glantz, 1985) of the respective year. This is made up of the following variables (Kloos et al., 2024):

- Growing season precipitation: Precipitation sum from March to October (mm)
- Summer precipitation: Precipitation sum in June, July, and August (mm)

- Growing season VPD: VPD sum from March to October (hPa)
- Summer VPD: VPD sum in June, July, and August (hPa)
- Growing season soil water content: Mean soil water content (16 cm depth) from March to October (%)
- Summer soil water content: Mean soil water content (16 cm depth) in June, July, and August (%)

Table 3: Overview of the 20 predictor variables generated for explaining autumn phenology in the Hainich National Park. Additionally, for each variable, the corresponding abbreviation is given (see Table 1 in Kloos et al. (2024) for further information).

Variable	Abbr.	Variable	Abbr.
Start of season	SOS	**Dryness-Wetness-Index**	DWI
Summer temperature	T_{SU}	**Growing season NEP**	N_T
Autumn temperature	T_{AU}	**Growing season GPP:DT**	GD_T
Extreme heat events	T_{EX}	**Growing season GPP:NT**	GN_T
Frost days	F_{HY}	**Growing season first half NEP**	N_1
Frost days in spring	F_{SP}	**Growing season second half NEP**	N_2
Annual precipitation	P_{HY}	**Growing season first half GPP:DT**	GD_1
Summer precipitation	P_{SU}	**Growing season second half GPP:DT**	GD_2
Heavy rain days	P_{EX}	**Growing season first half GPP:NT**	GN_1
Growing season vapor pressure deficit	VPD	**Growing season second half GPP:NT**	GN_2

The following index was calculated annually from 2000 to 2020 for the precipitation and soil moisture variables:

$$Index = \frac{x_i - x_{min}}{x_{max} - x_{min}} \quad (1)$$

Another index was calculated in parallel for the VPD variables:

$$Index = \frac{x_{max} - x_i}{x_{max} - x_{min}} \quad (2)$$

x_i represents the value for the respective year, and x_{max} and x_{min} are the highest and lowest annual values in the observation period. Each index thus ranges from comparatively dry (0) to wet (1) years. Finally, all six calculated indices were summed up to form the DWI (0 = “very dry” to 6 = “very wet”; Kloos et al., 2024).

Functional traits

To better understand the interspecific phenological variability in Weltwald Freising, 13 functional traits (see Table 4 and Table 1 in Kloos et al. (in review) for further information) and the continent of origin (Europe, Asia, North America) were determined for each observed tree species (except *Alnus rugosa* L., *Carya tomentosa* Nutt., *Populus trichocarpa* Torr. & Gray and *Pterocarya fraxinifolia* Lam.). The age of the trees was defined from BaySF data (BaySF, 2022) and the number of chromosomes was determined for each species using the CCBD (Chromosome Counts Database) medians (Rice et al., 2015), while all other traits were derived from the TRY plant trait database (Kattge et al., 2020). In a first step, a trait matrix was created with all measurements from the database for all traits and existing species. The data set was converted into a normal distribution and z-transformed and the data gaps were then filled with the Bayesian hierarchical probabilistic matrix factorization (BHPMF) gap-filling algorithm (Schrodt et al., 2015). The data were then back-transformed and outliers were removed using the z-transformation. For 70 tree species of the Weltwald Freising, a mean value was then calculated for each trait across all matrix values and assigned to the corresponding species (Kloos et al., in review). The "stable species hierarchy" hypothesis allows this assignment even without having measured the traits directly on site, as a general hierarchical arrangement of the values between the species is assumed (e.g., Cordlandwehr et al., 2013; Kazakou et al., 2014; Violle et al., 2015).

Table 4: Functional traits to analyze the interspecific variability of phenology in Weltwald Freising and its associated units (see Table 1 in Kloos et al. (in review) for further information).

Plant trait	Unit	Plant trait	Unit
Tree (plant) height	m	**Leaf C content per leaf dry mass**	mg g^{-1}
Leaf area	mm^2	**Leaf P content per leaf dry mass**	mg g^{-1}
Leaf thickness	mm	**Root rooting depth**	m
Leaf area per leaf dry mass (SLA)	mm^2 mg^{-1}	**Stem conduit diameter**	µm
Leaf dry mass per leaf fresh mass (LDMC)	g g^{-1}	**Chromosome number**	n
Seed dry mass	mg	**Fine root length per fine root dry mass (specific root length, SRL)**	cm g^{-1}
Leaf N content per leaf dry mass	mg g^{-1}		

Climate distances

In addition to the functional traits, so-called climate distances for the tree species observed in Weltwald Freising were also used. These are Manhattan distances of a 30-year climatology (1961-1990), with 11 climate variables implemented (Buras & Menzel, 2019) and are made up of monthly temperature (CRU TS v4.01; Harris et al., 2020) and precipitation (GPCC; Schneider et al., 2011) data with a spatial resolution of 0.5°. The climate distances were then calculated globally pixel by pixel for the central coordinate: 48.25° N, 11.25° E (Buras & Menzel, 2019). To assign a climate distance to each tree species, the respective distribution areas were defined. For European

species, chorological maps (Caudullo et al., 2017) and relative probability of presence (RPP; de Rigo et al., 2016) data were used, whereby synanthropic and isolated occurrences were excluded from the calculation. For North American and Asian species, the distribution areas were derived from GBIF (GBIF, 2021) data, whereby only observations after 1900 and species with an occurrence in more than 1000 grid cells (0.5° x 0.5°) were included in the analysis. This resulted in final climate distances for 60 species, which represent the median of the respective lower 20% quantile of all assigned climate distance values (Kloos et al., in review).

Validation of drought indices

To validate calculated drought indices (see section 2.3.1.), soil moisture index (SMI) data of the upper soil layer (0-25 cm) were used for Bavaria from 2001 to 2020. These are available monthly, originally have a spatial resolution of 4 km and were downscaled to 250 m using bilinear resampling (Kloos et al., 2021; UFZ, 2021; Zink et al., 2016). For further validation, agricultural crop yield data (annual mean yield per ha, dt ha^{-1}) from 2001 to 2019 were also used at Bavarian county level (Statistical Offices of the Federation and the States, 2021). To support this validation, land use data from agricultural holdings (also at county level, 2016; LfStat, 2018) and annual harvest dates of the respective field crop (phase ID 24 - "Ernte") were used (DWD, 2021a).

Validation of UAV phenology

To validate the UAV-derived phenology of Weltwald Freising (see section 2.3.2.), the spring and autumn phenology for 45 and 27 tree species (see Table S3 in Kloos et al. (in review) for further information), respectively, was observed from the ground in 2022. In spring, the following phenological phases were determined plot-wise twice a week from the end of March to the end of May, whereby only phase 3 was used in the final validation (Vitasse et al., 2013):

- 0: buds closed (no bud activity)
- 1: budburst (buds are open and leaves are partially visible)
- 2: leaf emergence (leaves fully emerged from the buds but are still folded, crinkled, or pendant)
- 3: leaf unfolding (for each tree at least one leaf is fully unfolded)

In autumn, leaf discoloration (including leaves lying on the ground) and leaf fall were estimated in 10% increments twice a week from mid-September to early December. In a second step, the data were interpolated to a daily resolution and the day on which the 50% leaf discoloration mark was reached or exceeded for the first time was included for validation (Kloos et al., in review).

2.3. Methods overview

To answer the research questions posed at the beginning of this thesis (see section 1.4.), the described data sets were analyzed using different methods. In terms of content, these are subdivided below into the detection of water limitation and vegetation drought (see section 2.3.1.), derivation of UAV tree canopy phenology (see section 2.3.2.), data validation (see section 2.3.3.) and specific statistical analysis methods used (see section 2.3.4.).

2.3.1. Detection of water limitation and vegetation drought

A correlation analysis between the MODIS NDVI and LST data was carried out for the Bavarian study area (see Figure 5). The NDVI is used here as a proxy for vegetation health (Norman et al., 2016; Zhang et al., 2013), while the LST provides information on vegetation water stress (see section 1.3.1.; Anderson & Kustas, 2008). When correlating both variables, growth limiters for vegetation are determined: A negative correlation indicates water and a positive correlation indicates energy as the primary limiting factor for plant growth (Karnieli et al., 2010; Karnieli et al., 2019).

Table 5: Monthly subdivision of MODIS data for the correlation analysis between NDVI and LST (Kloos et al., 2021).

Month	MODIS Day Numbers	Month	MODIS Day Numbers
March	065-089	**July**	185-209
April	097-113	**August**	217-241
May	121-145	**September**	249-273
June	153-177	**October**	281-297

Specifically, the NDVI-LST correlation was calculated monthly from March to October (see Table 5) for the period 2001 to 2020 using the method of Abdi et al. (2016). The NDVI-LST correlation maps were then intersected with CLC and EU-DEM data individually and in combination for further differentiation (see Table 6). For this purpose, the NDVI-LST data were resampled to a spatial resolution of 100 m (Kloos et al., 2021).

Table 6: Classification of CLC (Kloos et al., 2021) and EU-DEM data (BaySF, 2018; Hübl et al., 2007; Walentowski et al., 2001; Walentowski & Kopp, 2006) for intersection with the NDVI-LST correlation maps.

ID	Land cover classes (CLC 2018)	ID	Altitude classes (EU-DEM)
NAL	Non-irrigated arable land	**AL1**	< 300 m
PAS	Pastures	**AL2**	300-500 m
BLF	Broad-leaved forest	**AL3**	500-800 m
CFF	Coniferous forest	**AL4**	800-1200 m
MXF	Mixed forest	**AL5**	> 1200 m
NGL	Natural grasslands		

In the second step, three drought indices were calculated for the Bavarian study area every eight days from March to October in the period 2001 to 2020: the VCI, the TCI, and the VHI. The VCI is calculated as follows (Kogan, 1995):

$$VCI = 100 * \frac{(NDVI - NDVI_{min})}{(NDVI_{max} - NDVI_{min})} \quad (3)$$

The NDVI represents the smoothed 8-day NDVI, $NDVI_{min}$ and $NDVI_{max}$ the lowest and highest corresponding NDVI value for the observation period. The TCI is defined as follows (Kogan, 1995):

$$TCI = 100 * \frac{(T_{max} - T)}{(T_{max} - T_{min})} \quad (4)$$

T (LST) represents the smoothed 8-day temperature, T_{min} and T_{max} the lowest and highest corresponding temperature value for the observation period. Both indices thus reach a scale of 0-100, with high values indicating a comparatively high NDVI and a low temperature value. The combination of both indices forms the VHI, which weights both indices equally in this study (α = 0.5; Kogan et al., 2016; Kogan, 1997):

$$VHI = \alpha * \text{VCI} + (1 - \alpha) * \text{TCI} \quad (5)$$

The VHI includes the assumption that there is a negative correlation between NDVI and LST during a vegetation drought, i.e., a comparatively low NDVI with a comparatively high LST due to reduced evapotranspiration (Karnieli et al., 2010). Due to this assumption, the index was only analyzed in areas where the correlation between NDVI and LST was ≤ -0.1 (Kloos et al., 2021).

2.3.2. Derivation of UAV tree canopy phenology

The UAV data recorded in Weltwald Freising were used to derive spring and autumn phenology for individual tree crowns. In a first step, the tree canopy was identified, whereby a canopy height model (CHM) was developed. This was formed from the difference between a digital surface model (DSM, recorded at the end of July with full leaf development) and a digital terrain model (DTM, recorded at the end of March with full ground visibility; Kloos et al., in review). In a second step, the individual treetops were then determined based on the CHM using a variable window filter (Popescu & Wynne, 2004). A height-dependent, iteratively determined function for the window size was applied:

- 3 m to 8 m: constant value of 1
- 8 m to 35 m: $height * 0.06 + 0.52$
- > 35 m: constant value of 2.62

All treetops were then checked manually and removed from the analysis if they were < 5 m in height (Kloos et al., in review). The crowns of the trees were then determined based on the treetops using the algorithm by Dalponte and Coomes (2016). The height threshold was 5 m, growing threshold 1 was 0.35 and 2 was 0.55, and the maximum crown diameter was 90 pixels. All crowns with a crown area < 3 m^2 were excluded from the analysis and crowns with an unrealistic ("non-circular") shape were removed manually. In addition, only trees within the defined plots (derived from BaySF, 2022) were included in the analysis and tree species with n < 5 were removed. Finally, only deciduous tree species were analyzed, with a 10 cm reverse buffer applied around each tree crown to avoid overlaps. This resulted in the phenological analysis of 74 tree species (see Table S3 in Kloos et al. (in review) regarding the analyzed species) and 3099 individuals (Kloos et al., in review).

To extract the phenology of each tree crown, a raster stack was created from all NDVI raster of the 27 UAV flights. Subsequently, the respective 27 median NDVI values were determined for each crown and a double logistic function (Fischer, 1994) was fitted based on these values. The SOS and EOS were then determined using a percentage threshold between the lowest, early-season, and highest NDVI value (SOS) and the highest and lowest, late-season, NDVI value (EOS). The day on which these thresholds were exceeded or undershot was then defined as SOS/EOS. During a pre-validation with the observed phenology (see Section 2.2.4.), the threshold value was set at 0.5 (SOS) and 0.7 (EOS). Finally, the length of season (LOS) was also defined based on the difference between EOS and SOS (Kloos et al., in review).

2.3.3. Data validation

The drought indices determined in Bavaria (see Section 2.3.1.) were validated with the SMI and agricultural yield data (see Section 2.2.4.). For this purpose, a monthly arithmetic drought index mean was formed for the SMI (see Table 5) and a Bravais-Pearson correlation analysis was then calculated both monthly and for the entire vegetation period (March to October). For the crops winter wheat, winter rye, summer barley, oat, sugar beet, winter rapeseed, and silage corn, the relative annual yield anomaly was compared with the respective mean drought index at county level. The mean drought index was calculated from May to July (for sugar beet and silage corn until September) and correlated with the yield data at county level as well as for the entire study area using Bravais-Pearson correlation coefficients. Crops with an area share of the total area of the seven selected crops < 3 % for a county were removed from the analysis (Kloos et al., 2021).

For a more general validation, a weighted relative yield anomaly and a weighted drought index were also calculated at county level. For this purpose, the respective area share was determined for each crop and each county, weighted with the respective yield anomalies, and summed up. Years with data gaps were removed from the analysis. Mean annual drought indices were also weighted according to the area ratios of the crops, summed up, and finally compared with a Bravais-Pearson correlation at county level and for the entire study area (Kloos et al., 2021).

To validate the UAV-derived phenology in Weltwald Freising, a simple linear regression between UAV and observed phenology (see Section 2.2.4.) of the individual species was calculated and the coefficient of determination and p-value were retrieved. In addition, the mean difference and the percentage of species with a difference of < 5 days between the respective onset dates were also used as validation indicators (Kloos et al., in review).

2.3.4. Statistical analyses

To compare the spring and autumn phenology determined from the different data sources in the Hainich National Park, the individual data sets were correlated with each other (Bravais-Pearson). In addition, a trend analysis was carried out using simple linear regression with year as a predictor. To determine the influence of the predictors (see section 2.2.4.) on the EOS, a Spearman-rank correlation was calculated between the EOS and the individual predictor variables. In addition, a multiple linear regression was calculated with the EOS as the dependent variable. The predictors were T_{AU}, T_{SU}, P_{HY} and the individual NEP variables, whereby SOS-dependent variables were averaged across all data sources. There was no multicollinearity within the predictors ($r < 0.7$, p-value > 0.05). Finally, various 2- and 3-variable combinations of the regression model were calculated with the predictor variables (Kloos et al., 2024).

To test the hypothesis of Zohner et al. (2023), which identifies vegetation activity before the solstice and autumn temperature as two essential predictors of autumn phenology, a multiple linear regression was also calculated. The EOS was again the dependent variable, N_1 and T_{AU} the predictors. The regression lines were analyzed here, with a respective predictor median and dynamic predictor always forming the models. In a final step, the 21 observation years in the national park were divided into four 5-year classes: years with low T_{AU} and N_1 (scenario 1), high T_{AU} and N_1 (scenario 2), low T_{AU} and high N_1 (scenario 3), and high T_{AU} and low N_1 (scenario 4). For each of these four classes, the mean EOS for the respective 5-year period was then calculated for the respective data source (Kloos et al., 2024).

To explain the interspecific phenological variability in Weltwald Freising, three Boosted Regression Trees (BRT; see Elith et al., 2008 and Sporbert et al., 2022 for further information) analyses were carried out, with the dependent variable being defined by the SOS/EOS/LOS

median. The 13 functional traits (see section 2.2.4.), the continent of origin, and the climate distance formed the predictors. The BRTs were set up with a Gaussian error distribution, a tree complexity of 1, a learning rate of 0.003, and a bag fraction of 0.5. Partial dependency plots and the relative importance (%) of the predictors formed the results. The model evaluation was carried out using a cross-validation correlation and predicted vs. observed SOS/EOS/LOS plots (Kloos et al., in review).

2.4. Software

For the spatial representation of the data, ArcGIS Pro (Esri, 2024) and R (R Core Team, 2024) or RStudio (RStudio Team, 2024) was applied. The data analysis was carried out in R or RStudio, whereby the following packages were mainly used: *corrplot* (Wei et al., 2021), *data.table* (Barrett et al., 2024), *dismo* (Hijmans et al., 2023a), *dplyr* (Wickham et al., 2023), *ForestTools* (Plowright & Roussel, 2023), *ggplot2* (Wickham, 2016), *lidR* (Roussel et al., 2024), *MODISTsp* (Busetto & Ranghetti, 2016), *phenex* (Lange & Doktor, 2017), *plyr* (Wickham, 2023), *raster* (Hijmans et al., 2023b), *rasterVis* (Lamigueiro et al., 2023), *reshape2* (Wickham, 2020), *terra* (Hijmans et al., 2024), *tidyr* (Wickham et al., 2024), *tidyverse* (Wickham et al., 2019), and *zoo* (Zeileis et al., 2023).

3. Publication abstracts and contributions

This thesis is based on the content of the following three publications:

1. Kloos, S., Yuan, Y., Castelli, M., & Menzel, A. (2021). Agricultural Drought Detection with MODIS Based Vegetation Health Indices in Southeast Germany. *Remote Sensing*, 13(19), 3907.

2. Kloos, S., Klosterhalfen, A., Knohl, A., & Menzel, A. (2024). Decoding autumn phenology: Unraveling the link between observation methods and detected environmental cues. *Global Change Biology*, 30(3), e17231.

3. Kloos, S., Lüpke, M., Estrella, N., Ghada, W., Kattge, J., Bucher, S. F., Buras, A., & Menzel, A. (in review). The linkage between functional traits and drone-derived phenology of 74 Northern Hemisphere tree species. *Science of the Total Environment*.

The following sub-chapters provide a brief summary of the content and a list of the authors' contributions to the individual publications. The authors are abbreviated with the first letter of their first name and surname (e.g., S.K. for Simon Kloos). The complete publications are appended at the end of the thesis.

3.1. Agricultural Drought Detection with MODIS Based Vegetation Health Indices in Southeast Germany

Kloos, S., Yuan, Y., Castelli, M., & Menzel, A. (2021). Agricultural Drought Detection with MODIS Based Vegetation Health Indices in Southeast Germany. *Remote Sensing*, 13(19), 3907.

Abstract

Droughts during the growing season are projected to increase in frequency and severity in Central Europe in the future. Thus, area-wide monitoring of agricultural drought in this region is becoming more and more important. In this context, it is essential to know where and when vegetation growth is primarily water-limited and whether remote sensing-based drought indices can detect agricultural drought in these areas. To answer these questions, we conducted a correlation analysis between the Normalized Difference Vegetation Index (NDVI) and Land Surface Temperature (LST) within the growing season from 2001 to 2020 in Bavaria (Germany) and investigated the relationship with land cover and altitude. In the second step, we applied the drought indices Temperature Condition Index (TCI), Vegetation Condition Index (VCI), and Vegetation Health Index (VHI) to primarily water-limited areas and evaluated them with soil moisture and agricultural yield anomalies. We found that, especially in the summer months (July and August), on agricultural land and grassland and below 800 m, NDVI and LST are negatively correlated and thus, water is the primary limiting factor for vegetation growth here. Within these areas and periods, the TCI and VHI correlate strongly with soil moisture and agricultural yield anomalies, suggesting that both indices have the potential to detect agricultural drought in Bavaria.

Contributions

S.K., A.M., and M.C. designed the research idea. S.K. acquired, processed, and analyzed the data. S.K., Y.Y., and A.M. developed the data visualization. S.K. wrote the first draft, and all authors reviewed and edited it. A.M. supervised the work.

3.2. Decoding autumn phenology: Unraveling the link between observation methods and detected environmental cues

Kloos, S., Klosterhalfen, A., Knohl, A., & Menzel, A. (2024). Decoding autumn phenology: Unraveling the link between observation methods and detected environmental cues. *Global Change Biology*, 30(3), e17231.

Abstract

Leaf coloring and fall mark the end of the growing season (EOS), playing essential roles in nutrient cycling, resource allocation, ecological interactions, and as climate change indicators. However, understanding future changes in autumn phenology is challenging due to the multitude of likely environmental cues and substantial variations in timing caused by different derivation methods. Yet, it remains unclear whether these two factors are independent or if methodological uncertainties influence the environmental cues determined. We derived start of growing season (SOS) and EOS at a mixed beech forest in Central Germany for the period 2000–2020 based on four different derivation methods using a unique long-term data set of in-situ data, canopy imagery, eddy covariance measurements, and satellite remote sensing data and determined their influence on a predictor analysis of leaf senescence. Both SOS and EOS exhibited substantial ranges in mean onset dates (39.5 and 28.6 days, respectively) across the different methods, although inter-annual variations and advancing SOS trends were similar across methods. Depending on the data, EOS trends were advanced or delayed, but inter-annual patterns correlated well (mean $r = 0.46$). Overall, warm, dry, and less photosynthetically productive growing seasons were more likely to be associated with a delayed EOS, while colder, wetter, and more photosynthetically productive vegetation periods resulted in an earlier EOS. In addition, contrary to recent results, no clear influence of pre-solstice vegetation activity on the timing of senescence was detected. However, most notable were the large differences in sign and strength of potential drivers both in the univariate and multivariate analyses when comparing derivation methodologies. The results suggest that an ensemble analysis of all available phenological data sources and derivation methods is needed for general statements on autumn phenology and its influencing variables and correct implementation of the senescence process in ecosystem models.

Contributions

S.K. and A.M. designed the research idea. S.K., A.Kl., and A.Kn. acquired the data. S.K. processed and analyzed the data. S.K. and A.M. developed the data visualization. S.K. wrote the first draft, and all authors reviewed and edited it. A.M. supervised the work.

3.3. The linkage between functional traits and drone-derived phenology of 74 Northern Hemisphere tree species

Kloos, S., Lüpke, M., Estrella, N., Ghada, W., Kattge, J., Bucher, S. F., Buras, A., & Menzel, A. (in review). The linkage between functional traits and drone-derived phenology of 74 Northern Hemisphere tree species. *Science of the Total Environment*.

Abstract

Tree phenology is a major component of the global carbon and water cycle, serving as a fingerprint of climate change, and exhibiting significant variability both within and between species. In the emerging field of drone monitoring, it remains unclear whether this phenological variability can be effectively captured across numerous tree species. Additionally, the drivers behind interspecific variations in the phenology of deciduous trees are poorly understood, although they may be linked to plant functional traits. In this study, we derived the start of season (SOS), end of season (EOS), and length of season (LOS) for 3,099 individuals from 74 deciduous tree species of the Northern Hemisphere at a unique study site in southeast Germany using drone imagery. We validated these phenological metrics with in-situ data and analyzed the interspecific variability in terms of plant functional traits. The drone-derived SOS and EOS showed high agreement with ground observations of leaf unfolding (R^2 = 0.49) and leaf discoloration (R^2 = 0.79), indicating that this methodology robustly captures phenology at the individual level with low temporal and human effort. Both intra- and interspecific phenological variability were high in spring and autumn, leading to differences in the LOS of up to two months under almost identical environmental conditions. Functional traits such as seed dry mass, chromosome number, and continent of origin played significant roles in explaining interspecific phenological differences in SOS, EOS, and LOS, respectively. In total, 55 %, 39%, and 45 % of interspecific variation in SOS, EOS, and LOS could be explained by the Boosted Regression Tree (BRT) models based on functional traits. Our findings encourage new research avenues in tree phenology and advance our understanding of the growth strategies of key tree species in the Northern Hemisphere.

Contributions

S.K., M.L., and A.M. designed the research idea. S.K., M.L., W.G., J.K., and A.B. acquired the data. S.K. and M.L. processed the data. S.K. analyzed the data. S.K., N.E., and A.M. developed the data visualization. S.K. and M.L. wrote the first draft, and all authors reviewed and edited it. A.M. supervised the work.

4. Discussion

In this thesis, the impacts of climate change on vegetation canopies in Central Europe were analyzed in various aspects using passive remote sensing. In the following, these results will be discussed in terms of content (4.1.) and methodology (4.2.) and placed in the context of previous research.

4.1. Differentiation of climate change impacts on vegetation

Over the last 150 years, anthropogenic global warming has led to an increase in the average annual temperature in Central Europe of around 2 °C and an increase in extreme heat and drought events, particularly in the summer months (APCC, 2014; BAFU, 2020; DWD, 2021d, 2023; IPCC, 2023). The global warming trends are expected to continue, although the projections vary depending on the emissions scenario (IPCC, 2023). These developments naturally impact the vegetation growing there and its associated physiology and phenology. Generally, it is assumed that vegetation in Central Europe will be more affected by drought in the future (Grillakis, 2019; Hari et al., 2020). In addition, due to higher temperatures, the phenological phases of spring are currently advancing, while the phenological autumn tends to begin later (Menzel et al., 2020; Piao et al., 2019; Vitasse et al., 2022). Due to its high spatial and temporal coverage and objective measurement series, remote sensing has a high potential to differentiate these general statements and thus provide new insights into understanding climate change impacts on vegetation.

The results of this thesis have shown that the relationship between NDVI and LST in Central Europe depends on the observed period and location as well as on land use and altitude. If these variables are negatively correlated, plant growth is primarily water-limited (Karnieli et al., 2010; Karnieli et al., 2019), and thus, the risk of drought stress for the vegetation is remarkably higher. As mentioned in Kloos et al. (2021), this is mainly the case in July and August, which can also be confirmed by other studies in these latitudes - albeit not at such a high temporal and spatial resolution (Karnieli et al., 2010; Karnieli et al., 2019; Sun & Kafatos, 2007).

Looking at land use, agricultural areas and grassland, in particular, are characterized by a negative NDVI-LST correlation and are, therefore, primarily at risk of drought stress. Forest areas show mostly no negative correlation values and, thus, (on average) a higher drought resilience in this region (Kloos et al., 2021), which is also consistent with other studies (Karnieli et al., 2010; Karnieli et al., 2006). Regarding altitude, negative NDVI-LST correlations in the study area are mainly found below 800 m a.s.l., whereas montane and alpine areas are primarily energy-limited. A general increase in the NDVI-LST correlation coefficient with increasing altitude can also be observed in other parts of the world, which further confirms the results of this thesis (Karnieli et al., 2010; Karnieli et al., 2006; Karnieli et al., 2019).

At first sight, these results are not surprising and appear logical. Nevertheless, the methodology of remote sensing with holistic spatial coverage can be used to show which type of vegetation in which period of the year could be particularly affected by (climate change-induced) droughts in the future. Of course, extreme drought events in Central Europe affect significantly more areas and vegetation types (Rakovec et al., 2022; Schuldt et al., 2020), as this is only a mean analysis over 20 years. Nevertheless, the results show a differentiated view of the regions and periods at risk of drought stress, which is helpful for various stakeholders of society. In this way, particularly affected areas can be identified quickly and efficiently, and adaptation measures such as adapted monitoring, alternative planting, or irrigation strategies can be discussed.

The results of this thesis also generated a differentiated picture of deciduous forest phenology. From a climatological perspective, it could be shown in a mixed beech-ash forest that leaf discoloration and leaf fall tend to occur later in dry years with warm autumn temperatures than in humid years with lower autumn temperatures (Kloos et al., 2024). While the results of the autumn temperature confirm the current study situation (e.g., Gill et al., 2015; Lu & Keenan, 2022; Zohner et al., 2023), the influence of water availability on autumn phenology varies depending on the study design (Bigler & Vitasse, 2021; Zani et al., 2020), which is mainly due to the different definitions of water availability. According to the results of this thesis, climate change should lead to a delay in autumn phenology in mid-latitude deciduous forests due to rising temperatures and lower water availability in the growing season. However, in other studies, heat and drought stress initiate advanced senescence (Bigler & Vitasse, 2021; Schuldt et al., 2020; Xie et al., 2018), which is why a linear trend in this relationship is debatable and a projection of autumn phenology in climate change is associated with great uncertainty.

Furthermore, not only the drivers but also the respective species play a decisive role in the phenological context. While the autumn phenology of beech trees in the Hainich National Park shows some strong correlations with temperature and precipitation variables, these are much less pronounced in ash trees. This species-specific differentiation can also be found in the phenological trend analysis of both species: Within the spring phenology, the leaf-out of beech trees advances during the observation period - in contrast to the phenology of ash trees, which is significantly delayed at the same time. In autumn, contrasting developments can also be observed - albeit not as strongly - with a prolonged vegetation period for beech trees and a shortening growth period for ash trees (Kloos et al., 2024).

On the one hand, these different developments can be attributed to a species-specific climatological sensitivity to individual phenological phases, as has already been established in other studies (e.g., Grossiord et al., 2022; Vitasse et al., 2009). In this specific case, however, the influence of the pathogenic fungus *Hymenoscyphus pseudoalbidus*, which has recently infesting ash trees in Europe (Kowalski & Holdenrieder, 2009; Queloz et al., 2011), is also suspected. This delays leaf emergence (McKinney et al., 2011; Stener, 2013) and could also be a reason for the observed premature leaf senescence in ash trees (Kloos et al., 2024). Therefore, non-climatic factors can also remarkably influence the phenology of individual tree species, and general statements on phenological development in the context of climate change should be made with caution.

Additionally, in terms of global warming, not only is the temporal development of phenological onset dates and their drivers relevant, but so is phenological variability. The results of this thesis showed that within a species, the time of leaf emergence can differ over 20 days, and the time of leaf discoloration can differ over 30 days (Kloos et al., in review), which is also shown in previous studies (Delpierre et al., 2017; Marchand et al., 2020). Climate change could increase the risk of late frost in Central Europe (Lamichhane, 2021; Qiang Liu et al., 2018; Zohner et al., 2020), which is why the intraspecific variability of spring phenology could become more important in this context. As with the drivers and trends of phenology, intraspecific variability is also, as shown in this thesis, highly species-dependent. Species with high variability (in this case, for example, *Fraxinus pennsylvanica* Marsh., *Betula costata* Trautv., and *Quercus alba* L.) could, therefore, be more resilient to such meteorological extremes than those with only a small "phenological window" (Diez et al., 2012).

In addition to the intraspecific variability, this work also revealed major phenological differences between individual tree species: In spring, the onset date of leaf unfolding can differ by more than 40 days depending on the species, and in autumn, the onset date of leaf discoloration can differ by more than 50 days. This results in a difference of up to two months in the growth period under quite similar environmental conditions (Kloos et al., in review). These value ranges match with

previous study results (Archetti et al., 2013; Panchen et al., 2014; Richardson & O'Keefe, 2009). Nevertheless, plant-functional traits and the continental origin of the species haven't been related to phenological variability in deciduous trees yet.

In spring, the continent of origin of the species is one of the most important explanatory factors: As mentioned in Kloos et al. (in review), on average, North American species sprout significantly later than European and Asian species, which can be explained by a higher variability of North American spring temperatures and an associated risk avoidance strategy regarding late frost (Zohner & Renner, 2017). In addition, the strategy of late frost avoidance also explains the later leaf-out of species with heavier seeds, larger stem conduit diameter, and thinner leaves. These invest more energy in reproduction (Kloos et al., in review), are more susceptible to embolism due to freeze-thaw events in the stem (Lechowicz, 1984; Panchen et al., 2014), and have more sensitive leaves to late frost damage (Bucher et al., 2019; Bucher & Rosbakh, 2021).

In autumn, however, an important explanatory factor is the number of chromosomes: the more chromosomes a deciduous tree species has, the earlier it goes into senescence. This is a new finding in phenology and can be interpreted to mean that species that grow in drought-prone areas tend to have lower chromosome numbers and are therefore better able to cope with later senescence (Kloos et al., in review). Plants with a high chromosome number, on the other hand, tend to occur in more stable habitats and thus tend to favor earlier senescence (Carta et al., 2018). Furthermore, species with a lower SRL tend to enter senescence later, which can be explained by better water-use efficiency (Bucher & Römermann, 2021). Finally, autumn phenology occurs later in species with a higher stem conduit diameter, which can be explained by compensation for later carbon sequestration in spring (Kloos et al., in review). Overall, this means species with European origin and a low seed dry mass and SRL have a more extended growth period in the study region (Kloos et al., in review).

The explanation of the onset dates for spring and autumn phenology and the resulting length of the vegetation period via functional traits and the continental origin leads to the different growth strategies of tree species: While early sprouting and late senescence species with a long growing season tend to aim at maximizing carbon sequestration or use seasonally limited resources (Lee & Ibáñez, 2021; Richardson & O'Keefe, 2009), late sprouting species in spring mainly want to avoid late frost damage (Bennie et al., 2010; Vitasse et al., 2014). In the context of climate change projections for Central Europe, species with the longest possible growing season could be at an advantage in the future: As heat and drought stress could often limit photosynthetic activity and thus tree growth in the summer months (Bréda et al., 2006; Farooq et al., 2009; Gupta et al., 2020), the growth-relevant periods in spring and autumn are becoming increasingly important. Thus, from a trait perspective, species with a low chromosome number and SRL, which tend to grow in drought-prone regions and have better water-use efficiency, may have an advantage with prolonged senescence. On the other hand, early sprouting tree species are more likely to be affected by late frost events but – as shown in this thesis with thicker leaves and lower stem conduit diameter – also tend to be more frost resistant (Muffler et al., 2016; Vitra et al., 2017).

4.2. Assessment of remote sensing monitoring approaches of vegetation

The monitoring methodology of passive remote sensing primarily used in this work generates indirect information about vegetation. This creates uncertainty in many research questions and requires a comparison with variables measured on the ground, especially when applied over a study area for the first time. Therefore, validation with in-situ data minimizes the uncertainty and, at the same time, defines the meaning of remote sensing data in the respective context.

In this thesis, the three drought indices TCI, VCI, and VHI, were calculated for the Bavarian study area and compared with soil moisture data. The TCI correlated the highest, the VCI the lowest and the VHI, as a combination index of both indices, was positioned between these two values. This corresponds to the results of previous studies (Chang et al., 2017; Le Du et al., 2018; Zhao et al., 2017) and allows the conclusion that the surface temperature generally correlates more highly with soil moisture values than the state of the vegetation and therefore reacts more quickly to changes in soil moisture. In addition, higher correlations with soil moisture were found for all three indices in summer than in spring and autumn. The correlation of soil moisture with both surface temperature and vegetation condition is, therefore, strongly seasonal. This can be explained by the fact that, on the one hand, the topsoil dries out more easily in summer, which is directly linked to an increase in surface temperature. On the other hand, as described in this thesis, a large proportion of the areas are primarily water-limited for plant growth in summer, which means that fluctuations in soil moisture have a more direct effect on the state of the vegetation at this time of year (Kloos et al., 2021).

Comparing the drought indices with agricultural yield data, all three indices showed high correlations. This means that all indices can provide valid information on annual crop yields, which is also in line with studies in other parts of the world (Dabrowska-Zielinska et al., 2002; García-León et al., 2019; Kogan et al., 2016). Interestingly, the VCI does not achieve higher correlations than the TCI despite the more direct link to the state of the vegetation. This can be attributed to the fact that agricultural yields are largely dependent on the soil moisture status in the topsoil and, therefore, also show a strong correlation with surface temperature. This is a good example of the extent to which fluctuations in vegetation indices (e.g., the VCI) can be explained more specifically by the addition of further remote sensing data sets. Furthermore, the crop yield data for sugar beet and silage corn show higher correlations than other crops due to their late harvest time and the associated longer analysis period in summer. In addition, higher correlations were also found in the more water-limited north of the study area compared to the south of Bavaria (Kloos et al., 2021).

For the application of the drought indices used in this work, this means that there must be a primary water limitation in location and time so that these indices can generate robust statements about agricultural drought. At the beginning and towards the end of the growing season, the drought indices have little in common with soil moisture and yield anomalies and, therefore, should primarily be used in the summer months in Central Europe. The focus of the application should be on the VHI, which can both make direct statements about the state of vegetation and explain possible deficits using surface temperature as a drought indicator. In addition, it seems reasonable to generate statements over a longer observation period due to the lower dynamics of the vegetation condition.

While the vegetation drought in this work was analyzed from the perspective of remote sensing only with satellite data, the plant phenology was also recorded with near-surface cameras and UAV data. Passive remote sensing usually shows medium to high agreement in the determination of phenological onset dates in comparison with data measured on the ground (visual observation, CO_2 fluxes, etc.; Berra & Gaulton, 2021), which is also reflected in the results of this work. Both the phenology derived from satellite (MODIS) and from camera or UAV data correlated moderately to strongly with data measured on the ground and are thus able to reflect temporal as well as species-specific variability of phenological onset dates. The absolute difference between the individual derived onset dates also moved on average in similar temporal ranges for data sources with similar phenological phase definitions (Kloos et al., 2024).

In addition to the generally high level of agreement between the data sets, individual aspects are nevertheless worth mentioning. On the one hand, there were different results in the remote

sensing/in-situ comparison of phenology depending on the (tree) species. This can firstly be explained by differences in the spatial resolution of the observation methods to be compared. For example, the camera data can record species-specific phenology, while CO_2 flux measurements on the ground detect the entire vegetation phenology, which means that the derived phenology is only comparable to a limited extent. Conversely, this mismatch of spatial resolutions is also a known problem in phenological validation when comparing coarse-resolution satellite data with the phenology of individual plants observed on the ground (Fisher & Mustard, 2007; White et al., 2009).

Nevertheless, if the same species is considered in the validation (as in the comparison of the UAV data with the phenology observed on the ground), there may still be differences between the objects considered, i.e., the tree individuals: If the UAV captures all trees within a species plot, the observer only averages the data from a certain viewing angle and thus cannot capture all individuals within a larger area - depending on the species plot (Kloos et al., in review). As mentioned in Kloos et al. (2024), differences between the autumn phenology of beech trees observed with the camera and on the ground in the Hainich National Park can also be attributed to the aspect of intraspecific variability (see, e.g., Marchand et al., 2020 or Capdevielle-Vargas et al., 2015). Finally, if it is possible to observe the same plant both remotely and in situ, there may still be residual differences in the species-specific phenology derived from the phenological variability within a plant (especially in trees) due to the different viewing angles or the subjective estimation of the observer.

A second aspect worth noting are validation differences in the respective phenological phase. The results of this work show that the correlations between the remote sensing data and the phenology measured on the ground tend to be lower in spring than in autumn. This can be explained by the fact that remote sensing data from the perspective of looking down from above (satellite and UAV) also capture the phenology of the understory in spring when the treetops are not yet covered with leaves. Since the understory usually sprouts earlier than the overstory of the forest (Augspurger & Bartlett, 2003; Richardson & O'Keefe, 2009; Vitasse, 2013), this results in an earlier detection of the spring phenology in the remote sensing data (Kloos et al., 2024). In autumn, on the other hand, the understory only becomes visible when the leaves of the tree crowns have already changed color and fallen off, which means that no false detections can occur here. This is a well-known phenomenon in remote sensing of phenology (Filippa et al., 2018; Ryu et al., 2014) and must be considered, especially in spring.

In addition to the comparison of remote sensing data and variables measured on the ground, which is essential for a quality statement about the remote sensing data, the comparison of different remote sensing data sets is also a noteworthy aspect. In this work, large differences were identified between the satellite and camera phenology regarding the determined onset dates, which was also reflected in the correlations of the data. On the one hand, this is due to the difference in spatial resolution described above. On the other hand, there is also a clear difference in the definition of the individual phenological phases considered within the remote sensing phenology detected (which is also a problem in comparison with in-situ data). The satellite data record the degree of greening and discoloration of the tree crowns in spring and autumn with different threshold values, while the camera observes the first leaf unfolding and the average discoloration of the tree crown. In general, there are many different definitions for spring and autumn phenology (Berra & Gaulton, 2021; Caparros-Santiago et al., 2021; Meier, 2018; Zeng et al., 2020), which often means that a comparison of the data is only possible to a limited extent.

However, the various phenological data sources are not only used for the calculation of descriptive statistics or for trend analyses but are often also combined with other data sets, for example, to identify drivers of phenological developments. In this work, it was found that the phenology of

different data sources has a remarkable impact on a predictor analysis of autumn phenology: Depending on the derivation method used, striking differences were found in the univariate or multivariate analysis of the relationship with climatological or CO_2-flux variables, although general trends within individual variables were recognizable between the data sources. These findings are important, as many studies in this field are usually based on only one phenological data source. From these results, it can be deduced that depending on the study area, a comprehensive analysis of all available phenological data sources is useful to be able to make general statements about trends and drivers of phenology (Kloos et al., 2024).

In the context of the findings generated from this work, monitoring phenology using passive remote sensing - as confirmed in many other studies (e.g., Berra & Gaulton, 2021 or Caparros-Santiago et al., 2021) - is generally useful and offers several advantages over ground-based measurements (e.g., spatial coverage, fast data availability, objective measurement, etc.). Nevertheless, differentiation is necessary if the derived phenology is to be robust in its informative value. Firstly, it must be clear from the research question which form of vegetation (total vegetation, plant species, individual) and secondly, which specific phenological phase (e.g., SOS: first leaf emergence or 50% crown foliage; EOS: 50% leaf discoloration or leaf fall) is to be analyzed in detail. This fine adjustment then results in the appropriate comparative data set on the ground, which, on the one hand, specifies which phenology the remote sensing indirectly records and, on the other hand, prevents systematic measurement errors.

In conclusion, it should be noted that remote sensing monitoring of vegetation always goes hand in hand with the indirect measurement of the vegetation canopy. However, a clear difference in the monitoring of drought and phenology is the variable to be recorded or evaluated. Despite existing definitions, agricultural drought is a diffuse complex and can be measured using a wide range of information relating to the soil water balance and, above all, the state of the vegetation. In phenology, on the other hand, a specific day of the year is derived for a specific phenological phase in most research questions. This is also reflected in the validation of these aspects, as drought indices determined from remote sensing data can be compared with more in-situ data sets than phenological onset dates derived from remote sensing. Accordingly, "the same thing" is more likely to be measured in phenology, which also tends to be reflected in higher correlations in the in-situ comparison.

5. Conclusion

Global warming impacts the physiology and phenology of vegetation in Central Europe. Using the methodology of passive remote sensing, this thesis was able to show that in Central Europe, areas below 800 m a.s.l., especially grassland and agricultural areas, are most at risk of drought in the summer months of July and August. Dry and warm growing seasons also prolong the autumn phenology of a deciduous forest, but trends and drivers of phenology differ remarkably depending on the species considered. Under almost identical environmental conditions, a high inter- and intraspecific variability in the phenology of tree species was also found, whereby functional traits could partly explain the respective growth strategy. In the context of climate change, species with high intraspecific phenological variability and a long growing season could be at a growth advantage regarding a projected increase in late frost and drought events in Central Europe.

Since passive remote sensing only takes indirect vegetation measurements, a comparison with data measured on the ground is essential to minimize uncertainty about what is being measured by remote sensing and how this relates to in-situ data. In this work, the drought indices TCI, VCI, and VHI were able to capture agricultural drought well, especially in water-limited regions and time periods, which is why it makes sense to use them for drought detection, especially in the Central European summer. The VHI best captures different aspects of agricultural drought. The phenology of vegetation can also be detected well with remote sensing data. For robust results, a detailed examination of the spatial resolution and the phenological phase to be observed is of great importance. For general statements on trends and drivers of plant phenology, an evaluation of various phenological data sources is essential.

In addition, future research could build on some of the results of this work: for example, it would be of great interest to see how the water limitation (NDVI-LST relationship) behaves in Central Europe in extreme hydrological years and how this relationship is linked to various climatological variables. A combination of a more detailed vegetation classification and a spatially higher-resolution satellite product (e.g., Sentinel data) could also generate added scientific value. The drought indices could, in turn, be compared with other in-situ data on soil water balance and plant vitality to further understand both the indices and the occurrence of agricultural drought. This understanding could be incorporated into a replication of the study design from the drone survey of Weltwald Freising, whereby as many real traits as possible measured on-site would generate great added value to understand the growth strategies of the different tree species even better and more robustly. Regarding future growth conditions, a combined focus could be placed on determining these tree species' frost and heat/drought resistance. Combining this with the phenological sensitivity of each tree species to changes in temperature and water availability would provide an important basis for deciding on the future suitability of tree species in Central Europe in the context of global warming.

References

Aasen, H., Honkavaara, E., Lucieer, A., & Zarco-Tejada, P. (2018). Quantitative Remote Sensing at Ultra-High Resolution with UAV Spectroscopy: A Review of Sensor Technology, Measurement Procedures, and Data Correction Workflows. *Remote Sensing*, *10*(7), 1091. https://doi.org/10.3390/rs10071091

Abdi, A. M., Vrieling, A., Yengoh, G. T., Anyamba, A., Seaquist, J. W., Ummenhofer, C. C., & Ardö, J. (2016). The El Niño – La Niña cycle and recent trends in supply and demand of net primary productivity in African drylands. *Climatic Change*, *138*(1-2), 111–125. https://doi.org/10.1007/s10584-016-1730-1

Afshar, M. H., Al-Yaari, A., & Yilmaz, M. T. (2021). Comparative Evaluation of Microwave L-Band VOD and Optical NDVI for Agriculture Drought Detection over Central Europe. *Remote Sensing*, *13*(7), 1251. https://doi.org/10.3390/rs13071251

Allen, C. D., Macalady, A. K., Chenchouni, H., Bachelet, D., McDowell, N., Vennetier, M., Kitzberger, T., Rigling, A., Breshears, D. D., Hogg, E. H., Gonzalez, P., Fensham, R., Zhang, Z., Castro, J., Demidova, N., Lim, J.-H., Allard, G., Running, S. W., Semerci, A., & Cobb, N. (2010). A global overview of drought and heat-induced tree mortality reveals emerging climate change risks for forests. *Forest Ecology and Management*, *259*(4), 660–684. https://doi.org/10.1016/j.foreco.2009.09.001

Anderson, M., & Kustas, W. (2008). Thermal Remote Sensing of Drought and Evapotranspiration. *Eos, Transactions American Geophysical Union*, *89*(26), 233–234. https://doi.org/10.1029/2008EO260001

Anderson, R. G., Canadell, J. G., Randerson, J. T., Jackson, R. B., Hungate, B. A., Baldocchi, D., Ban-Weiss, G. A., Bonan, G. B., Caldeira, K., Cao, L., Diffenbaugh, N. S., Gurney, K. R., Kueppers, L. M., Law, B. E., Luyssaert, S., & O'Halloran, T. L. (2011). Biophysical considerations in forestry for climate protection. *Frontiers in Ecology and the Environment*, *9*(3), 174–182. https://doi.org/10.1890/090179

APCC. (2014). *Österreichischer Sachstandsbericht Klimawandel 2014 (AAR14)*. Austrian Panel on Climate Change (APCC), Verlag der Österreichischen Akademie der Wissenschaften.

Archetti, M., Richardson, A. D., O'Keefe, J., & Delpierre, N. (2013). Predicting climate change impacts on the amount and duration of autumn colors in a New England forest. *PloS One*, *8*(3), e57373. https://doi.org/10.1371/journal.pone.0057373

Augspurger, C. K. (2013). Reconstructing patterns of temperature, phenology, and frost damage over 124 years: Spring damage risk is increasing. *Ecology*, *94*(1), 41–50. https://doi.org/10.1890/12-0200.1

Augspurger, C. K., & Bartlett, E. A. (2003). Differences in leaf phenology between juvenile and adult trees in a temperate deciduous forest. *Tree Physiology*, *23*(8), 517–525. https://doi.org/10.1093/treephys/23.8.517

Bachmair, S., Tanguy, M., Hannaford, J., & Stahl, K. (2018). How well do meteorological indicators represent agricultural and forest drought across Europe? *Environmental Research Letters*, *13*(3), 34042. https://doi.org/10.1088/1748-9326/aaafda

BAFU. (2020). *Klimawandel in der Schweiz. Indikatoren zu Ursachen, Auswirkungen, Massnahmen.* Umwelt-Zustand Nr. 2013.

Bakke, S. J., Ionita, M., & Tallaksen, L. M. (2020). The 2018 northern European hydrological drought and its drivers in a historical perspective. *Hydrology and Earth System Sciences*, *24*(11), 5621–5653. https://doi.org/10.5194/hess-24-5621-2020

Balzarolo, M., Vicca, S., Nguy-Robertson, A. L., Bonal, D., Elbers, J. A., Fu, Y. H., Grünwald, T., Horemans, J. A., Papale, D., Peñuelas, J., Suyker, A., & Veroustraete, F. (2016). Matching the phenology of Net Ecosystem Exchange and vegetation indices estimated with MODIS and FLUXNET in-situ observations. *Remote Sensing of Environment*, *174*, 290–300. https://doi.org/10.1016/j.rse.2015.12.017

Barnard, D. M., Knowles, J. F., Barnard, H. R., Goulden, M. L., Hu, J., Litvak, M. E., & Molotch, N. P. (2018). Reevaluating growing season length controls on net ecosystem production in evergreen conifer forests. *Scientific Reports*, *8*(1), 17973. https://doi.org/10.1038/s41598-018-36065-0

Barrett, T., Dowle, M., Srinivasan, A., Gorecki, J., Chirico, M., Hocking, T., Stetsenko, P., Short, T., Lianoglou, S., Antonyan, E., Bonsch, M., Parsonage, H., Ritchie, S., Ren, K., Tan, X., Saporta, R., Seiskari, O., Dong, X., Lang, M., . . . Czekanski, M. (2024). *data.table: Extension of 'data.frame'*. https://cran.r-project.org/web/packages/data.table/index.html (accessed 25 March 2024)

BaySF. (2018). *Waldbauhandbuch Bayerische Staatsforsten: Richtlinie für die Waldbewirtschaftung im Hochgebirge*. https://www.baysf.de/fileadmin/user_upload/04-wald_verstehen/Publikationen/WNJF-RL-006_Bergwaldrichtlinie.pdf (accessed 15 April 2021)

BaySF. (2022). *(C) Geodata*. https://services1.arcgis.com/dzpA3ZtAF0zx03DV/ArcGIS/rest/services/Weltwald_Update_05_2022/FeatureServer/1 (accessed 10 January 2024)

Beck, H. E., Zimmermann, N. E., McVicar, T. R., Vergopolan, N., Berg, A., & Wood, E. F. (2018). Present and future Köppen-Geiger climate classification maps at 1-km resolution. *Scientific Data*, *5*, 180214. https://doi.org/10.1038/sdata.2018.214

Bennie, J., Kubin, E., Wiltshire, A., Huntley, B., & Baxter, R. (2010). Predicting spatial and temporal patterns of bud-burst and spring frost risk in north-west Europe: the implications of local adaptation to climate. *Global Change Biology*, *16*(5), 1503–1514. https://doi.org/10.1111/j.1365-2486.2009.02095.x

Berra, E. F., & Gaulton, R. (2021). Remote sensing of temperate and boreal forest phenology: A review of progress, challenges and opportunities in the intercomparison of in-situ and satellite phenological metrics. *Forest Ecology and Management*, *480*, 118663. https://doi.org/10.1016/j.foreco.2020.118663

Bigler, C., & Vitasse, Y. (2021). Premature leaf discoloration of European deciduous trees is caused by drought and heat in late spring and cold spells in early fall. *Agricultural and Forest Meteorology*, *307*, 108492. https://doi.org/10.1016/j.agrformet.2021.108492

BMEL. (2022). *Trockenheit und Dürre im Jahr 2018: Überblick über getroffene Maßnahmen*. https://www.bmel.de/DE/themen/landwirtschaft/klimaschutz/duerre-2018.html (accessed 14 February 2024)

Bonan, G. B. (2008). Forests and climate change: Forcings, feedbacks, and the climate benefits of forests. *Science (New York, N.Y.)*, *320*(5882), 1444–1449. https://doi.org/10.1126/science.1155121

Bonan, G. B. (2016). Forests, Climate, and Public Policy: A 500-Year Interdisciplinary Odyssey. *Annual Review of Ecology, Evolution, and Systematics*, *47*(1), 97–121. https://doi.org/10.1146/annurev-ecolsys-121415-032359

Bond, T. C., Doherty, S. J., Fahey, D. W., Forster, P. M., Berntsen, T., DeAngelo, B. J., Flanner, M. G., Ghan, S., Kärcher, B., Koch, D., Kinne, S., Kondo, Y., Quinn, P. K., Sarofim, M. C., Schultz, M. G., Schulz, M., Venkataraman, C., Zhang, H., Zhang, S., . . . Zender, C. S. (2013). Bounding the role of black carbon in the climate system: A scientific assessment. *Journal of Geophysical Research: Atmospheres*, *118*(11), 5380–5552. https://doi.org/10.1002/jgrd.50171

Bórnez, K., Richardson, A. D., Verger, A., Descals, A., & Peñuelas, J. (2020). Evaluation of VEGETATION and PROBA-V Phenology Using PhenoCam and Eddy Covariance Data. *Remote Sensing*, *12*(18), 3077. https://doi.org/10.3390/rs12183077

Bórnez, K., Verger, A., Descals, A., & Peñuelas, J. (2021). Monitoring the Responses of Deciduous Forest Phenology to 2000–2018 Climatic Anomalies in the Northern Hemisphere. *Remote Sensing*, *13*(14), 2806. https://doi.org/10.3390/rs13142806

Bréda, N., Huc, R., Granier, A., & Dreyer, E. (2006). Temperate forest trees and stands under severe drought: a review of ecophysiological responses, adaptation processes and long-term consequences. *Annals of Forest Science*, *63*(6), 625–644. https://doi.org/10.1051/forest:2006042

Brönnimann, S. (2018). *Klimatologie* (1. Auflage). *utb basics: Vol. 4819*. Haupt Verlag.

Bucher, S. F., Feiler, R., Buchner, O., Neuner, G., Rosbakh, S., Leiterer, M., & Römermann, C. (2019). Temporal and spatial trade-offs between resistance and performance traits in herbaceous plant species. *Environmental and Experimental Botany*, *157*, 187–196. https://doi.org/10.1016/j.envexpbot.2018.10.015

Bucher, S. F., & Römermann, C. (2021). The timing of leaf senescence relates to flowering phenology and functional traits in 17 herbaceous species along elevational gradients. *Journal of Ecology*, *109*(3), 1537–1548. https://doi.org/10.1111/1365-2745.13577

Bucher, S. F., & Rosbakh, S. (2021). Foliar summer frost resistance measured via electrolyte leakage approach as related to plant distribution, community composition and plant traits. *Functional Ecology*, *35*(3), 590–600. https://doi.org/10.1111/1365-2435.13740

Buitink, J., Swank, A. M., van der Ploeg, M., Smith, N. E., Benninga, H.-J. F., van der Bolt, F., Carranza, C. D. U., Koren, G., van der Velde, R., & Teuling, A. J. (2020). Anatomy of the 2018 agricultural drought in the Netherlands using in situ soil moisture and satellite vegetation indices. *Hydrology and Earth System Sciences*, *24*(12), 6021–6031. https://doi.org/10.5194/hess-24-6021-2020

Buras, A., & Menzel, A. (2019). Projecting Tree Species Composition Changes of European Forests for 2061-2090 Under RCP 4.5 and RCP 8.5 Scenarios. *Frontiers in Plant Science*, *9*, 1986. https://doi.org/10.3389/fpls.2018.01986

Buras, A., Rammig, A., & Zang, C. S. (2020). Quantifying impacts of the 2018 drought on European ecosystems in comparison to 2003. *Biogeosciences*, *17*(6), 1655–1672. https://doi.org/10.5194/bg-17-1655-2020

Buras, A., Schunk, C., Zeiträg, C., Herrmann, C., Kaiser, L., Lemme, H., Straub, C., Taeger, S., Gößwein, S., Klemmt, H.-J., & Menzel, A. (2018). Are Scots pine forest edges particularly prone to drought-induced mortality? *Environmental Research Letters*, *13*(2), 25001. https://doi.org/10.1088/1748-9326/aaa0b4

Burkart, A., Hecht, V. L., Kraska, T., & Rascher, U. (2018). Phenological analysis of unmanned aerial vehicle based time series of barley imagery with high temporal resolution. *Precision Agriculture*, *19*(1), 134–146. https://doi.org/10.1007/s11119-017-9504-y

Burton, A. C., Neilson, E., Moreira, D., Ladle, A., Steenweg, R., Fisher, J. T., Bayne, E., & Boutin, S. (2015). REVIEW: Wildlife camera trapping: a review and recommendations for linking surveys to ecological processes. *Journal of Applied Ecology*, *52*(3), 675–685. https://doi.org/10.1111/1365-2664.12432

Busetto, L., & Ranghetti, L. (2016). MODIStsp : An R package for automatic preprocessing of MODIS Land Products time series. *Computers & Geosciences*, *97*, 40–48. https://doi.org/10.1016/j.cageo.2016.08.020

Caparros-Santiago, J. A., Rodriguez-Galiano, V., & Dash, J. (2021). Land surface phenology as indicator of global terrestrial ecosystem dynamics: A systematic review. *ISPRS Journal of Photogrammetry and Remote Sensing*, *171*, 330–347. https://doi.org/10.1016/j.isprsjprs.2020.11.019

Capdevielle-Vargas, R., Estrella, N., & Menzel, A. (2015). Multiple-year assessment of phenological plasticity within a beech (Fagus sylvatica L.) stand in southern Germany. *Agricultural and Forest Meteorology*, *211-212*, 13–22. https://doi.org/10.1016/j.agrformet.2015.03.019

Carta, A., Bedini, G., & Peruzzi, L. (2018). Unscrambling phylogenetic effects and ecological determinants of chromosome number in major angiosperm clades. *Scientific Reports*, *8*(1), 14258. https://doi.org/10.1038/s41598-018-32515-x

Caudullo, G., Welk, E., & San-Miguel-Ayanz, J. (2017). Chorological maps for the main European woody species. *Data in Brief*, *12*, 662–666. https://doi.org/10.1016/j.dib.2017.05.007

Chang, S., Wu, B., Yan, N., Davdai, B., & Nasanbat, E. (2017). Suitability Assessment of Satellite-Derived Drought Indices for Mongolian Grassland. *Remote Sensing*, *9*(7), 650. https://doi.org/10.3390/rs9070650

Chapin, F. S., Randerson, J. T., McGuire, A. D., Foley, J. A., & Field, C. B. (2008). Changing feedbacks in the climate–biosphere system. *Frontiers in Ecology and the Environment*, *6*(6), 313–320. https://doi.org/10.1890/080005

Chuine, I., & Régnière, J. (2017). Process-Based Models of Phenology for Plants and Animals. *Annual Review of Ecology, Evolution, and Systematics*, *48*(1), 159–182. https://doi.org/10.1146/annurev-ecolsys-110316-022706

Ciocîrlan, M. I. C., Curtu, A. L., & Radu, G. R. (2022). Predicting Leaf Phenology in Forest Tree Species Using UAVs and Satellite Images: A Case Study for European Beech (Fagus sylvatica L.). *Remote Sensing*, *14*(24), 6198. https://doi.org/10.3390/rs14246198

Cole, E. F., & Sheldon, B. C. (2017). The shifting phenological landscape: Within- and between-species variation in leaf emergence in a mixed-deciduous woodland. *Ecology and Evolution*, *7*(4), 1135–1147. https://doi.org/10.1002/ece3.2718

Cordlandwehr, V., Meredith, R. L., Ozinga, W. A., Bekker, R. M., van Groenendael, J. M., & Bakker, J. P. (2013). Do plant traits retrieved from a database accurately predict on-site measurements? *Journal of Ecology*, *101*(3), 662–670. https://doi.org/10.1111/1365-2745.12091

Cremonese, E., Filippa, G., Galvagno, M., Siniscalco, C., Oddi, L., Di Morra Cella, U., & Migliavacca, M. (2017). Heat wave hinders green wave: The impact of climate extreme on the phenology of a mountain grassland. *Agricultural and Forest Meteorology*, *247*, 320–330. https://doi.org/10.1016/j.agrformet.2017.08.016

Dabrowska-Zielinska, K., Kogan, F., Ciolkosz, A., Gruszczynska, M., & Kowalik, W. (2002). Modelling of crop growth conditions and crop yield in Poland using AVHRR-based indices. *International Journal of Remote Sensing*, *23*(6), 1109–1123. https://doi.org/10.1080/01431160110070744

Dai, A. (2011). Drought under global warming: a review. *WIREs Climate Change*, *2*(1), 45–65. https://doi.org/10.1002/wcc.81

Dalponte, M., & Coomes, D. A. (2016). Tree-centric mapping of forest carbon density from airborne laser scanning and hyperspectral data. *Methods in Ecology and Evolution*, *7*(10), 1236–1245. https://doi.org/10.1111/2041-210X.12575

Delpierre, N., Guillemot, J., Dufrêne, E., Cecchini, S., & Nicolas, M. (2017). Tree phenological ranks repeat from year to year and correlate with growth in temperate deciduous forests. *Agricultural and Forest Meteorology*, *234-235*, 1–10. https://doi.org/10.1016/j.agrformet.2016.12.008

Dept. Bioclimatology, & Knohl, A. (2024). *Hainich Tower Camera - Canopy and Phenology Photos.* https://doi.org/10.25625/6IWFIY

Didan, K. (2015). *MOD13Q1 MODIS/Terra Vegetation Indices 16-Day L3 Global 250m SIN Grid V006.* https://doi.org/10.5067/MODIS/MOD13Q1.006

Diez, J. M., Ibáñez, I., Miller-Rushing, A. J., Mazer, S. J., Crimmins, T. M., Crimmins, M. A., Bertelsen, C. D., & Inouye, D. W. (2012). Forecasting phenology: From species variability to community patterns. *Ecology Letters*, *15*(6), 545–553. https://doi.org/10.1111/j.1461-0248.2012.01765.x

D'Odorico, P., Schönbeck, L., Vitali, V., Meusburger, K., Schaub, M., Ginzler, C., Zweifel, R., Velasco, V. M. E., Gisler, J., Gessler, A., & Ensminger, I. (2021). Drone-based physiological index reveals long-term acclimation and drought stress responses in trees. *Plant, Cell & Environment*, *44*(11), 3552–3570. https://doi.org/10.1111/pce.14177

Dronova, I., & Taddeo, S. (2022). Remote sensing of phenology: Towards the comprehensive indicators of plant community dynamics from species to regional scales. *Journal of Ecology*, *110*(7), 1460–1484. https://doi.org/10.1111/1365-2745.13897

DWD. (2021a). *Phenological observations of crops from sowing to harvest (annual reporters, historical)*. https://opendata.dwd.de/climate_environment/CDC/observations_germany/phenology/annual_reporters/crops/historical/ (accessed 20 April 2021)

DWD. (2021b). *Vieljährige mittlere Raster der Lufttemperatur (2m) für Deutschland 1991-2020*. https://opendata.dwd.de/climate_environment/CDC/grids_germany/multi_annual/air_temperature_mean/ (accessed 15 March 2024)

DWD. (2021c). *Vieljähriges Mittel der Raster der Niederschlagshöhe für Deutschland 1991-2020*. https://opendata.dwd.de/climate_environment/CDC/grids_germany/multi_annual/precipitation/ (accessed 15 March 2024)

DWD. (2021d). *Was wir heute übers Klima wissen: Basisfakten zum Klimawandel, die in der Wissenschaft unumstritten sind*. https://www.dwd.de/DE/klimaumwelt/aktuelle_meldungen/210609/Faktenpapier-zum-Klimawandel_062021.html?nn=634854 (accessed 01 February 2024)

DWD. (2022). *Annual grids of several phenological plant stages in Germany*. https://opendata.dwd.de/climate_environment/CDC/grids_germany/annual/phenology/ (accessed 19 March 2024)

DWD. (2023). *Was wir 2023 über das Extremwetter in Deutschland wissen: Stand der Wissenschaft zu extremen Wetterphänomenen im Klimawandel in Deutschland*. https://www.dwd.de/DE/Home/_functions/aktuelles/2023/20230927_faktenpapier_extremwetter.html (accessed 07 February 2024)

DWD. (2024). *Historische tägliche Stationsbeobachtungen (Temperatur, Druck, Niederschlag, Sonnenscheindauer, etc.) für Deutschland, Version v23.3: München-Flughafen*. https://opendata.dwd.de/climate_environment/CDC/observations_germany/climate/daily/kl/historical/ (accessed 13 February 2024)

EEA. (2010). *Mapping the impacts of natural hazards and technological accidents in Europe: An overview of the last decade*. Publications Office. https://doi.org/10.2800/62638

EEA. (2019). *Corine Land Cover 2018 (raster 100 m), Europe, 6-yearly - version 2020_20u1, May 2020.* https://doi.org/10.2909/960998c1-1870-4e82-8051-6485205ebbac (accessed 13 April 2021)

EEA. (2021). *EU-DEM v1.1 (raster 25 m), Europe*. https://land.copernicus.eu/imagery-in-situ/eu-dem/eu-dem-v1.1?tab=metadata (accessed 13 April 2021)

Ekinzog, E. K., Schlerf, M., Kraft, M., Werner, F., Riedel, A., Rock, G., & Mallick, K. (2022). Revisiting crop water stress index based on potato field experiments in Northern Germany. *Agricultural Water Management*, *269*, 107664. https://doi.org/10.1016/j.agwat.2022.107664

Elachi, C., & van Zyl, J. (2021). *Introduction to the physics and techniques of remote sensing* (Third edition). *Wiley series in remote sensing and image processing*. Wiley.

Elith, J., Leathwick, J. R., & Hastie, T. (2008). A working guide to boosted regression trees. *The Journal of Animal Ecology*, *77*(4), 802–813. https://doi.org/10.1111/j.1365-2656.2008.01390.x

Ellison, D., Morris, C. E., Locatelli, B., Sheil, D., Cohen, J., Murdiyarso, D., Gutierrez, V., van Noordwijk, M., Creed, I. F., Pokorny, J., Gaveau, D., Spracklen, D. V., Tobella, A. B., Ilstedt, U., Teuling, A. J., Gebrehiwot, S. G., Sands, D. C., Muys, B., Verbist, B., . . . Sullivan, C. A. (2017). Trees, forests and water: Cool insights for a hot world. *Global Environmental Change*, *43*, 51–61. https://doi.org/10.1016/j.gloenvcha.2017.01.002

Esri. (2024). *ArcGIS Pro*. https://www.esri.com/en-us/arcgis/products/arcgis-pro/overview (accessed 25 March 2024)

Ettinger, A. K., Chamberlain, C. J., Morales-Castilla, I., Buonaiuto, D. M., Flynn, D. F. B., Savas, T., Samaha, J. A., & Wolkovich, E. M. (2020). Winter temperatures predominate in spring phenological responses to warming. *Nature Climate Change*, *10*(12), 1137–1142. https://doi.org/10.1038/s41558-020-00917-3

eurostat. (2020). *Administrative Units / Statistical Units: Countries 2020*. https://ec.europa.eu/eurostat/web/gisco/geodata/reference-data/administrative-units-statistical-units/countries (accessed 14 March 2024)

Fang, J., Guo, Z., Piao, S., & Chen, A. (2007). Terrestrial vegetation carbon sinks in China, 1981–2000. *Science in China Series D: Earth Sciences*, *50*(9), 1341–1350. https://doi.org/10.1007/s11430-007-0049-1

Farooq, M., Wahid, A., Kobayashi, N., Fujita, D., & Basra, S. M. A. (2009). Plant Drought Stress: Effects, Mechanisms and Management. In E. Lichtfouse, M. Navarrete, P. Debaeke, S. Véronique, & C. Alberola (Eds.), *Sustainable agriculture* (pp. 153–188). Springer. https://doi.org/10.1007/978-90-481-2666-8_12

Feehan, J., Harley, M., & Minnen, J. (2009). Climate change in Europe. 1. Impact on terrestrial ecosystems and biodiversity. A review. *Agronomy for Sustainable Development*, *29*(3), 409–421. https://doi.org/10.1051/agro:2008066

Filippa, G., Cremonese, E., Migliavacca, M., Galvagno, M., Sonnentag, O., Humphreys, E., Hufkens, K., Ryu, Y., Verfaillie, J., Di Morra Cella, U., & Richardson, A. D. (2018). NDVI derived from near-infrared-enabled digital cameras: Applicability across different plant functional types. *Agricultural and Forest Meteorology*, *249*, 275–285. https://doi.org/10.1016/j.agrformet.2017.11.003

Fischer, A. (1994). A model for the seasonal variations of vegetation indices in coarse resolution data and its inversion to extract crop parameters. *Remote Sensing of Environment*, *48*(2), 220–230. https://doi.org/10.1016/0034-4257(94)90143-0

Fisher, J. I., & Mustard, J. F. (2007). Cross-scalar satellite phenology from ground, Landsat, and MODIS data. *Remote Sensing of Environment*, *109*(3), 261–273. https://doi.org/10.1016/j.rse.2007.01.004

Flynn, D. F. B., & Wolkovich, E. M. (2018). Temperature and photoperiod drive spring phenology across all species in a temperate forest community. *The New Phytologist*, *219*(4), 1353–1362. https://doi.org/10.1111/nph.15232

Friedl, M., Gray, J., & Sulla-Menashe, D. (2019). *MCD12Q2 MODIS/Terra+Aqua Land Cover Dynamics Yearly L3 Global 500m SIN Grid V006.* https://doi.org/10.5067/MODIS/MCD12Q2.006

Friedl, M., & Sulla-Menashe, D. (2019). *MCD12Q1 MODIS/Terra+Aqua Land Cover Type Yearly L3 Global 500m SIN Grid V006.* https://doi.org/10.5067/MODIS/MCD12Q1.006

Friedlingstein, P., O'Sullivan, M., Jones, M. W., Andrew, R. M., Bakker, D. C. E., Hauck, J., Landschützer, P., Le Quéré, C., Luijkx, I. T., Peters, G. P., Peters, W., Pongratz, J., Schwingshackl, C., Sitch, S., Canadell, J. G., Ciais, P., Jackson, R. B., Alin, S. R., Anthoni, P., … Zheng, B. (2023). Global Carbon Budget 2023. *Earth System Science Data*, *15*(12), 5301–5369. https://doi.org/10.5194/essd-15-5301-2023

Fu, Y. H., Piao, S., Delpierre, N., Hao, F., Hänninen, H., Geng, X., Peñuelas, J., Zhang, X., Janssens, I. A., & Campioli, M. (2019). Nutrient availability alters the correlation between spring leaf-out and autumn leaf senescence dates. *Tree Physiology*, *39*(8), 1277–1284. https://doi.org/10.1093/treephys/tpz041

Gaertner, B. A., Zegre, N., Warner, T., Fernandez, R., He, Y., & Merriam, E. R. (2019). Climate, forest growing season, and evapotranspiration changes in the central Appalachian Mountains, USA. *The Science of the Total Environment*, *650*(Pt 1), 1371–1381. https://doi.org/10.1016/j.scitotenv.2018.09.129

Gallinat, A. S., Primack, R. B., & Wagner, D. L. (2015). Autumn, the neglected season in climate change research. *Trends in Ecology & Evolution*, *30*(3), 169–176. https://doi.org/10.1016/j.tree.2015.01.004

Ganeva, D., Roumenina, E., Dimitrov, P., Gikov, A., Jelev, G., Dragov, R., Bozhanova, V., & Taneva, K. (2022). Phenotypic Traits Estimation and Preliminary Yield Assessment in Different Phenophases of Wheat Breeding Experiment Based on UAV Multispectral Images. *Remote Sensing*, *14*(4), 1019. https://doi.org/10.3390/rs14041019

Gao, B. (1996). NDWI—A normalized difference water index for remote sensing of vegetation liquid water from space. *Remote Sensing of Environment*, *58*(3), 257–266. https://doi.org/10.1016/S0034-4257(96)00067-3

García-León, D., Contreras, S., & Hunink, J. (2019). Comparison of meteorological and satellite-based drought indices as yield predictors of Spanish cereals. *Agricultural Water Management*, *213*, 388–396. https://doi.org/10.1016/j.agwat.2018.10.030

Garonna, I., Jong, R. de, Wit, A. J. W. de, Mücher, C. A., Schmid, B., & Schaepman, M. E. (2014). Strong contribution of autumn phenology to changes in satellite-derived growing season length estimates across Europe (1982-2011). *Global Change Biology*, *20*(11), 3457–3470. https://doi.org/10.1111/gcb.12625

Gazol, A., & Camarero, J. J. (2022). Compound climate events increase tree drought mortality across European forests. *The Science of the Total Environment*, *816*, 151604. https://doi.org/10.1016/j.scitotenv.2021.151604

GBIF. (2021). *Free and open access to biodiversity data*. https://www.gbif.org/ (accessed 08 November 2023)

GeoBasis-DE / BKG. (2024). *NUTS-Gebiete 1:5 000 000, Stand 31.12. (NUTS5000 31.12.)*. https://gdz.bkg.bund.de/index.php/default/digitale-geodaten/verwaltungsgebiete/nuts-gebiete-1-5-000-000-stand-31-12-nuts5000-31-12.html (accessed 14 March 2024)

Ghassemian, H. (2016). A review of remote sensing image fusion methods. *Information Fusion*, *32*, 75–89. https://doi.org/10.1016/j.inffus.2016.03.003

Gill, A. L., Gallinat, A. S., Sanders-DeMott, R., Rigden, A. J., Short Gianotti, D. J., Mantooth, J. A., & Templer, P. H. (2015). Changes in autumn senescence in northern hemisphere deciduous trees: A meta-analysis of autumn phenology studies. *Annals of Botany*, *116*(6), 875–888. https://doi.org/10.1093/aob/mcv055

Gitelson, A. A., Viña, A., Ciganda, V., Rundquist, D. C., & Arkebauer, T. J. (2005). Remote estimation of canopy chlorophyll content in crops. *Geophysical Research Letters*, *32*(8), Article 2005GL022688. https://doi.org/10.1029/2005GL022688

Glaser, R., Hauter, C., Faust, D., Glawion, R., Saurer, H., Schulte, A., & Sudhaus, D. (2010). Vegetation – Lebensgrundlage für Mensch und Tier. In R. Glaser, C. Hauter, D. Faust, R. Glawion, H. Saurer, A. Schulte, & D. Sudhaus (Eds.), *Physische Geographie kompakt* (pp. 99–116). Springer Berlin Heidelberg. https://doi.org/10.1007/978-3-662-50461-1_6

Goldewijk, K. K. (2001). Estimating global land use change over the past 300 years: The HYDE Database. *Global Biogeochemical Cycles*, *15*(2), 417–433. https://doi.org/10.1029/1999GB001232

Gonzalez-Meler, M. A., Taneva, L., & Trueman, R. J. (2004). Plant respiration and elevated atmospheric CO2 concentration: Cellular responses and global significance. *Annals of Botany*, *94*(5), 647–656. https://doi.org/10.1093/aob/mch189

Grace, J. (1988). 3. Plant response to wind. *Agriculture, Ecosystems & Environment*, *22-23*, 71–88. https://doi.org/10.1016/0167-8809(88)90008-4

Grillakis, M. G. (2019). Increase in severe and extreme soil moisture droughts for Europe under climate change. *The Science of the Total Environment*, *660*, 1245–1255. https://doi.org/10.1016/j.scitotenv.2019.01.001

Grossiord, C., Bachofen, C., Gisler, J., Mas, E., Vitasse, Y., & Didion-Gency, M. (2022). Warming may extend tree growing seasons and compensate for reduced carbon uptake during dry periods. *Journal of Ecology*, *110*(7), 1575–1589. https://doi.org/10.1111/1365-2745.13892

Guenther, A. B., Jiang, X., Heald, C. L., Sakulyanontvittaya, T., Duhl, T., Emmons, L. K., & Wang, X. (2012). The Model of Emissions of Gases and Aerosols from Nature version 2.1 (MEGAN2.1): an extended and updated framework for modeling biogenic emissions. *Geoscientific Model Development*, *5*(6), 1471–1492. https://doi.org/10.5194/gmd-5-1471-2012

Gupta, A., Rico-Medina, A., & Caño-Delgado, A. I. (2020). The physiology of plant responses to drought. *Science (New York, N.Y.)*, *368*(6488), 266–269. https://doi.org/10.1126/science.aaz7614

Gutman, G. G. (1990). Towards Monitoring Droughts from Space. *Journal of Climate*, *3*(2), 282–295. https://doi.org/10.1175/1520-0442(1990)003<0282:TMDFS>2.0.CO;2

Häckel, H. (2016). *Meteorologie* (8., vollständig überarbeitete und erweiterte Auflage). *UTB Geowissenschaften, Ökologie, Agrar- und Forstwissenschaften: Vol. 1338*. Verlag Eugen Ulmer.

Han, Q. (2013). Remote sensing-based quantification of spatial variation in canopy phenology of four dominant tree species in Europe. *Journal of Applied Remote Sensing*, *7*(1), 73485. https://doi.org/10.1117/1.JRS.7.073485

Hänsel, S., Ustrnul, Z., Łupikasza, E., & Skalak, P. (2019). Assessing seasonal drought variations and trends over Central Europe. *Advances in Water Resources*, *127*, 53–75. https://doi.org/10.1016/j.advwatres.2019.03.005

Hari, V., Rakovec, O., Markonis, Y., Hanel, M., & Kumar, R. (2020). Increased future occurrences of the exceptional 2018-2019 Central European drought under global warming. *Scientific Reports*, *10*(1), 12207. https://doi.org/10.1038/s41598-020-68872-9

Harris, I., Osborn, T. J., Jones, P., & Lister, D. (2020). Version 4 of the CRU TS monthly high-resolution gridded multivariate climate dataset. *Scientific Data*, *7*(1), 109. https://doi.org/10.1038/s41597-020-0453-3

Hazaymeh, K., & K. Hassan, Q. (2016). Remote sensing of agricultural drought monitoring: A state of art review. *AIMS Environmental Science*, *3*(4), 604–630. https://doi.org/10.3934/environsci.2016.4.604

Heim, R. R. (2002). A Review of Twentieth-Century Drought Indices Used in the United States. *Bulletin of the American Meteorological Society*, *83*(8), 1149–1166. https://doi.org/10.1175/1520-0477-83.8.1149

Hijmans, R. J., Bivand, R., Pebesma, E., & Sumner, M. D. (2024). *terra: Spatial Data Analysis*. https://cran.r-project.org/web/packages/terra/ (accessed 25 March 2024)

Hijmans, R. J., Phillips, S., Leathwick, J., & Elith, J. (2023a). *dismo: Species Distribution Modeling*. https://cran.r-project.org/web/packages/dismo/index.html (accessed 25 March 2024)

Hijmans, R. J., van Etten, J., Sumner, M., Cheng, J., Baston, D., Bevan, A., Bivand, R., Busetto, L., Canty, M., Fasoli, B., Forrest, D., Ghosh, A., Golicher, D., Gray, J., Greenberg, J. A., Hiemstra, P., Hingee, K., Ilich, A., Institute for Mathematics Applied Geosciences, . . . Wueest, R. (2023b). *raster: Geographic Data Analysis and Modeling*. https://cran.r-project.org/web/packages/raster/index.html (accessed 25 March 2024)

Hoffmann, H., Jensen, R., Thomsen, A., Nieto, H., Rasmussen, J., & Friborg, T. (2016). Crop water stress maps for an entire growing season from visible and thermal UAV imagery. *Biogeosciences*, *13*(24), 6545–6563. https://doi.org/10.5194/bg-13-6545-2016

Houston, W. A. (1999). Severe hail damage to mangroves at Port Curtis, Australia. *Mangroves and Salt Marshes*, *3*(1), 29–40. https://doi.org/10.1023/A:1009946809787

Hu, T., & Smith, R. (2018). The Impact of Hurricane Maria on the Vegetation of Dominica and Puerto Rico Using Multispectral Remote Sensing. *Remote Sensing*, *10*(6), 827. https://doi.org/10.3390/rs10060827

Huang, M., Piao, S., Ciais, P., Peñuelas, J., Wang, X., Keenan, T. F., Peng, S., Berry, J. A., Wang, K., Mao, J., Alkama, R., Cescatti, A., Cuntz, M., Deurwaerder, H. de, Gao, M., He, Y., Liu, Y., Luo, Y., Myneni, R. B., . . . Janssens, I. A. (2019). Air temperature optima of vegetation productivity

across global biomes. *Nature Ecology & Evolution*, *3*(5), 772–779. https://doi.org/10.1038/s41559-019-0838-x

Hübl, E., Burga, C. A., & Klötzli, F. (2007). Landschaft, Flora und Vegetation der Nordostalpen (Bayern–Wiener Becken). *Vierteljahrsschrift Der Naturforschenden Gesellschaft in Zürich*, *152*, 17–26.

Huete, A. R. (2012). Vegetation Indices, Remote Sensing and Forest Monitoring. *Geography Compass*, *6*(9), 513–532. https://doi.org/10.1111/j.1749-8198.2012.00507.x

Huete, A. R., Didan, K., Miura, T., Rodriguez, E., Gao, X., & Ferreira, L. (2002). Overview of the radiometric and biophysical performance of the MODIS vegetation indices. *Remote Sensing of Environment*, *83*(1-2), 195–213. https://doi.org/10.1016/s0034-4257(02)00096-2

Hurtt, G. C., Chini, L., Sahajpal, R., Frolking, S., Bodirsky, B. L., Calvin, K., Doelman, J. C., Fisk, J., Fujimori, S., Klein Goldewijk, K., Hasegawa, T., Havlik, P., Heinimann, A., Humpenöder, F., Jungclaus, J., Kaplan, J. O., Kennedy, J., Krisztin, T., Lawrence, D., … Zhang, X. (2020). Harmonization of global land use change and management for the period 850–2100 (LUH2) for CMIP6. *Geoscientific Model Development*, *13*(11), 5425–5464. https://doi.org/10.5194/gmd-13-5425-2020

Ionita, M., Tallaksen, L. M., Kingston, D. G., Stagge, J. H., Laaha, G., van Lanen, H. A. J., Scholz, P., Chelcea, S. M., & Haslinger, K. (2017). The European 2015 drought from a climatological perspective. *Hydrology and Earth System Sciences*, *21*(3), 1397–1419. https://doi.org/10.5194/hess-21-1397-2017

IPCC. (2023). *Climate Change 2023: Synthesis Report.: Contribution of Working Groups I, II and III to the Sixth Assessment Report of the Intergovernmental Panel on Climate Change*. IPCC. https://doi.org/10.59327/IPCC/AR6-9789291691647

Jia, G., Shevliakova, E., Artaxo, P., Noblet-Ducoudré, N. de, Houghton, R., House, J., Kitajima, K., Lennard, C., Popp, A., Sirin, A., Sukumar, R., & Verchot, L. (2019). Land–climate interactions. In P. R. Shukla, J. Skea, E. Calvo Buendia, V. Masson-Delmotte, H.-O. Pörtner, D. C. Roberts, P. Zhai, R. Slade, S. Connors, R. van Diemen, M. Ferrat, E. Haughey, S. Luz, S. Neogi, M. Pathak, J. Petzold, J. Portugal Pereira, P. Vyas, E. Huntley, … J. Malley (Eds.), *Climate Change and Land: an IPCC special report on climate change, desertification, land degradation, sustainable land management, food security, and greenhouse gas fluxes in terrestrial ecosystems.* https://doi.org/10.1017/9781009157988.004

Jin, H., Jönsson, A. M., Olsson, C., Lindström, J., Jönsson, P., & Eklundh, L. (2019). New satellite-based estimates show significant trends in spring phenology and complex sensitivities to temperature and precipitation at northern European latitudes. *International Journal of Biometeorology*, *63*(6), 763–775. https://doi.org/10.1007/s00484-019-01690-5

Kadereit, J. W., Körner, C., Nick, P., & Sonnewald, U. (2021). *Strasburger - Lehrbuch der Pflanzenwissenschaften* (38. Auflage). Springer Spektrum. https://doi.org/10.1007/978-3-662-61943-8

Kaiser, E., Morales, A., Harbinson, J., Kromdijk, J., Heuvelink, E., & Marcelis, L. F. M. (2015). Dynamic photosynthesis in different environmental conditions. *Journal of Experimental Botany*, *66*(9), 2415–2426. https://doi.org/10.1093/jxb/eru406

Karnieli, A., Agam, N., Pinker, R. T., Anderson, M., Imhoff, M. L., Gutman, G. G., Panov, N., & Goldberg, A. (2010). Use of NDVI and Land Surface Temperature for Drought Assessment: Merits and Limitations. *Journal of Climate*, *23*(3), 618–633. https://doi.org/10.1175/2009JCLI2900.1

Karnieli, A., Bayasgalan, M., Bayarjargal, Y., Agam, N., Khudulmur, S., & Tucker, C. J. (2006). Comments on the use of the Vegetation Health Index over Mongolia. *International Journal of Remote Sensing*, *27*(10), 2017–2024. https://doi.org/10.1080/01431160500121727

Karnieli, A., Ohana-Levi, N., Silver, M., Paz-Kagan, T., Panov, N., Varghese, D., Chrysoulakis, N., & Provenzale, A. (2019). Spatial and Seasonal Patterns in Vegetation Growth-Limiting Factors over Europe. *Remote Sensing*, *11*(20), 2406. https://doi.org/10.3390/rs11202406

Kattge, J., Bönisch, G., Díaz, S., Lavorel, S., Prentice, I. C., Leadley, P., Tautenhahn, S., Werner, G. D. A., Aakala, T., Abedi, M., Acosta, A. T. R., Adamidis, G. C., Adamson, K., Aiba, M., Albert, C. H., Alcántara, J. M., Alcázar C, C., Aleixo, I., Ali, H., . . . Wirth, C. (2020). Try plant trait database - enhanced coverage and open access. *Global Change Biology*, *26*(1), 119–188. https://doi.org/10.1111/gcb.14904

Kazakou, E., Violle, C., Roumet, C., Navas, M.-L., Vile, D., Kattge, J., & Garnier, E. (2014). Are trait-based species rankings consistent across data sets and spatial scales? *Journal of Vegetation Science*, *25*(1), 235–247. https://doi.org/10.1111/jvs.12066

Keenan, T. F., Gray, J., Friedl, M. A., Toomey, M., Bohrer, G., Hollinger, D. Y., Munger, J. W., O'Keefe, J., Schmid, H. P., Wing, I. S., Yang, B., & Richardson, A. D. (2014). Net carbon uptake has increased through warming-induced changes in temperate forest phenology. *Nature Climate Change*, *4*(7), 598–604. https://doi.org/10.1038/nclimate2253

Keenan, T. F., & Richardson, A. D. (2015). The timing of autumn senescence is affected by the timing of spring phenology: Implications for predictive models. *Global Change Biology*, *21*(7), 2634–2641. https://doi.org/10.1111/gcb.12890

Kleinsmann, J., Verbesselt, J., & Kooistra, L. (2023). Monitoring Individual Tree Phenology in a Multi-Species Forest Using High Resolution UAV Images. *Remote Sensing*, *15*(14), 3599. https://doi.org/10.3390/rs15143599

Kloos, S., Klosterhalfen, A., Knohl, A., & Menzel, A. (2024). Decoding autumn phenology: Unraveling the link between observation methods and detected environmental cues. *Global Change Biology*, *30*(3), e17231. https://doi.org/10.1111/gcb.17231

Kloos, S., Yuan, Y., Castelli, M., & Menzel, A. (2021). Agricultural Drought Detection with MODIS Based Vegetation Health Indices in Southeast Germany. *Remote Sensing*, *13*(19), 3907. https://doi.org/10.3390/rs13193907

Knohl, A., Schulze, E.-D., Kolle, O., & Buchmann, N. (2003). Large carbon uptake by an unmanaged 250-year-old deciduous forest in Central Germany. *Agricultural and Forest Meteorology*, *118*(3-4), 151–167. https://doi.org/10.1016/S0168-1923(03)00115-1

Knohl, A., Siebicke, L., Tiedemann, F., Kolle, O., & ICOS Ecosystem Thematic Centre. (2022). *Warm winter 2020 ecosystem eddy covariance flux product from Hainich.* https://doi.org/10.18160/CR66-PJ24

Kogan, F. N. (1995). Application of vegetation index and brightness temperature for drought detection. *Advances in Space Research*, *15*(11), 91–100. https://doi.org/10.1016/0273-1177(95)00079-t

Kogan, F., Guo, W., Strashnaia, A., Kleshenko, A., Chub, O., & Virchenko, O. (2016). Modelling and prediction of crop losses from NOAA polar-orbiting operational satellites. *Geomatics, Natural Hazards and Risk*, *7*(3), 886–900. https://doi.org/10.1080/19475705.2015.1009178

Kogan, F. N. (1997). Global Drought Watch from Space. *Bulletin of the American Meteorological Society*, *78*(4), 621–636. https://doi.org/10.1175/1520-0477(1997)078<0621:GDWFS>2.0.CO;2

Kooistra, L., Berger, K., Brede, B., Graf, L. V., Aasen, H., Roujean, J.-L., Machwitz, M., Schlerf, M., Atzberger, C., Prikaziuk, E., Ganeva, D., Tomelleri, E., Croft, H., Reyes Muñoz, P., Garcia Millan, V., Darvishzadeh, R., Koren, G., Herrmann, I., Rozenstein, O., . . . Verrelst, J. (2024). Reviews and syntheses: Remotely sensed optical time series for monitoring vegetation productivity. *Biogeosciences*, *21*(2), 473–511. https://doi.org/10.5194/bg-21-473-2024

Kowalski, K., Senf, C., Hostert, P., & Pflugmacher, D. (2020). Characterizing spring phenology of temperate broadleaf forests using Landsat and Sentinel-2 time series. *International Journal of Applied Earth Observation and Geoinformation*, *92*, 102172. https://doi.org/10.1016/j.jag.2020.102172

Kowalski, T., & Holdenrieder, O. (2009). Pathogenicity of Chalara fraxinea. *Forest Pathology*, *39*(1), 1–7. https://doi.org/10.1111/j.1439-0329.2008.00565.x

Lamichhane, J. R. (2021). Rising risks of late-spring frosts in a changing climate. *Nature Climate Change*, *11*(7), 554–555. https://doi.org/10.1038/s41558-021-01090-x

Lamigueiro, O. P., Hijmans, R., & Courtiol, A. (2023). *rasterVis: Visualization Methods for Raster Data*. https://cran.r-project.org/web/packages/rasterVis/index.html (accessed 25 March 2024)

Lang, W., Chen, X., Qian, S., Liu, G., & Piao, S. (2019). A new process-based model for predicting autumn phenology: How is leaf senescence controlled by photoperiod and temperature coupling? *Agricultural and Forest Meteorology*, *268*, 124–135. https://doi.org/10.1016/j.agrformet.2019.01.006

Lange, M., & Doktor, D. (2017). *phenex: Auxiliary Functions for Phenological Data Analysis*. https://cran.r-project.org/web/packages/phenex/index.html (accessed 25 March 2024)

Lasslop, G., Reichstein, M., Papale, D., Richardson, A. D., Arneth, A., Barr, A., Stoy, P., & Wohlfahrt, G. (2010). Separation of net ecosystem exchange into assimilation and respiration using a light response curve approach: critical issues and global evaluation. *Global Change Biology*, *16*(1), 187–208. https://doi.org/10.1111/j.1365-2486.2009.02041.x

Lausch, A., Erasmi, S., King, D., Magdon, P., & Heurich, M. (2016). Understanding Forest Health with Remote Sensing -Part I—A Review of Spectral Traits, Processes and Remote-Sensing Characteristics. *Remote Sensing*, *8*(12), 1029. https://doi.org/10.3390/rs8121029

LDBF. (2023). *BayernAtlas*. https://geoportal.bayern.de/bayernatlas/?lang=de&topic=ba&bgLayer=atkis&catalogNode&catalogNodes=11 (accessed 02 November 2023)

Le Du, T. T., Du Bui, D., Nguyen, M. D., & Lee, H. (2018). Satellite-Based, Multi-Indices for Evaluation of Agricultural Droughts in a Highly Dynamic Tropical Catchment, Central Vietnam. *Water*, *10*(5), 659. https://doi.org/10.3390/w10050659

Lechowicz, M. J. (1984). Why Do Temperate Deciduous Trees Leaf Out at Different Times? Adaptation and Ecology of Forest Communities. *The American Naturalist*, *124*(6), 821–842. https://doi.org/10.1086/284319

Lee, B. R., & Ibáñez, I. (2021). Spring phenological escape is critical for the survival of temperate tree seedlings. *Functional Ecology*, *35*(8), 1848–1861. https://doi.org/10.1111/1365-2435.13821

LfStat. (2018). *Bodennutzung der landwirtschaftlichen Betriebe in Bayern 2016: Totalerhebung*. https://www.statistik.bayern.de/mam/produkte/veroffentlichungen/statistische_berichte/c1101c_201651_25313.pdf (accessed 13 April 2021)

Li, Y., Zhao, M., Motesharrei, S., Mu, Q., Kalnay, E., & Li, S. (2015). Local cooling and warming effects of forests based on satellite observations. *Nature Communications*, *6*, 6603. https://doi.org/10.1038/ncomms7603

Lieth, H. (1974). *Phenology and seasonality modeling*. *Ecological studies: Volume 8*. Springer Seience+Business Media LLC.

Lindner, M., Fitzgerald, J. B., Zimmermann, N. E., Reyer, C., Delzon, S., van der Maaten, E., Schelhaas, M.-J., Lasch, P., Eggers, J., van der Maaten-Theunissen, M., Suckow, F., Psomas, A., Poulter, B., & Hanewinkel, M. (2014). Climate change and European forests: What do we know, what are the uncertainties, and what are the implications for forest management? *Journal of Environmental Management*, *146*, 69–83. https://doi.org/10.1016/j.jenvman.2014.07.030

Liu, Q., Fu, Y. H., Zeng, Z., Huang, M., Li, X., & Piao, S. (2016a). Temperature, precipitation, and insolation effects on autumn vegetation phenology in temperate China. *Global Change Biology*, *22*(2), 644–655. https://doi.org/10.1111/gcb.13081

Liu, Q., Fu, Y. H., Zhu, Z., Liu, Y., Liu, Z., Huang, M., Janssens, I. A., & Piao, S. (2016b). Delayed autumn phenology in the Northern Hemisphere is related to change in both climate and spring phenology. *Global Change Biology*, *22*(11), 3702–3711. https://doi.org/10.1111/gcb.13311

Liu, Q., Piao, S., Janssens, I. A., Fu, Y. H., Peng, S., Lian, X., Ciais, P., Myneni, R. B., Peñuelas, J., & Wang, T. (2018). Extension of the growing season increases vegetation exposure to frost. *Nature Communications*, *9*(1), 426. https://doi.org/10.1038/s41467-017-02690-y

Liu, X., Zhu, X., Pan, Y., Li, S., Liu, Y., & Ma, Y. (2016c). Agricultural drought monitoring: Progress, challenges, and prospects. *Journal of Geographical Sciences*, *26*(6), 750–767. https://doi.org/10.1007/s11442-016-1297-9

Liu, Y., & Wu, C. (2020). Understanding the role of phenology and summer physiology in controlling net ecosystem production: a multiscale comparison of satellite, PhenoCam and eddy covariance data. *Environmental Research Letters*, *15*(10), 104086. https://doi.org/10.1088/1748-9326/abb32f

Lovett, G. M., Burns, D. A., Driscoll, C. T., Jenkins, J. C., Mitchell, M. J., Rustad, L., Shanley, J. B., Likens, G. E., & Haeuber, R. (2007). Who needs environmental monitoring? *Frontiers in Ecology and the Environment*, *5*(5), 253–260. https://doi.org/10.1890/1540-9295(2007)5[253:WNEM]2.0.CO;2

Lu, X., & Keenan, T. F. (2022). No evidence for a negative effect of growing season photosynthesis on leaf senescence timing. *Global Change Biology*, *28*(9), 3083–3093. https://doi.org/10.1111/gcb.16104

Marchand, L. J., Dox, I., Gričar, J., Prislan, P., Leys, S., van den Bulcke, J., Fonti, P., Lange, H., Matthysen, E., Peñuelas, J., Zuccarini, P., & Campioli, M. (2020). Inter-individual variability in spring phenology of temperate deciduous trees depends on species, tree size and previous year autumn phenology. *Agricultural and Forest Meteorology*, *290*, 108031. https://doi.org/10.1016/j.agrformet.2020.108031

McKinney, L. V., Nielsen, L. R., Hansen, J. K., & Kjær, E. D. (2011). Presence of natural genetic resistance in Fraxinus excelsior (Oleraceae) to Chalara fraxinea (Ascomycota): An emerging infectious disease. *Heredity*, *106*(5), 788–797. https://doi.org/10.1038/hdy.2010.119

Meier, U. (2018). *Growth stages of mono- and dicotyledonous plants: Bbch Monograph.* https://doi.org/10.5073/20180906-074619

Menzel, A., Sparks, T. H., Estrella, N., Koch, E., Aasa, A., Ahas, R., Alm-Kübler, K., Bissolli, P., Braslavská, O., Briede, A., Chmielewski, F. M., Crepinsek, Z., Curnel, Y., Dahl, Å., Defila, C., Donnelly, A., Filella, Y., Jatczak, K., Måge, F., . . . Zust, A. N. (2006). European phenological response to climate change matches the warming pattern. *Global Change Biology*, *12*(10), 1969–1976. https://doi.org/10.1111/j.1365-2486.2006.01193.x

Menzel, A., Yuan, Y., Matiu, M., Sparks, T. H., Scheifinger, H., Gehrig, R., & Estrella, N. (2020). Climate change fingerprints in recent European plant phenology. *Global Change Biology*, *26*(4), 2599–2612. https://doi.org/10.1111/gcb.15000

Möllmann, J., Buchholz, M., & Musshoff, O. (2019). Comparing the Hedging Effectiveness of Weather Derivatives Based on Remotely Sensed Vegetation Health Indices and Meteorological Indices. *Weather, Climate, and Society*, *11*(1), 33–48. https://doi.org/10.1175/WCAS-D-17-0127.1

Muffler, L., Beierkuhnlein, C., Aas, G., Jentsch, A., Schweiger, A. H., Zohner, C. M., & Kreyling, J. (2016). Distribution ranges and spring phenology explain late frost sensitivity in 170 woody plants from the Northern Hemisphere. *Global Ecology and Biogeography*, *25*(9), 1061–1071. https://doi.org/10.1111/geb.12466

NDMC. (2024). *Types of Drought*. https://www.drought.unl.edu/Education/DroughtIn-depth/TypesofDrought.aspx (accessed 08 February 2024)

Neumann, C., Behling, R., Schindhelm, A., Itzerott, S., Weiss, G., Wichmann, M., & Müller, J. (2020). The colors of heath flowering – quantifying spatial patterns of phenology in Calluna life-cycle phases using high-resolution drone imagery. *Remote Sensing in Ecology and Conservation*, *6*(1), 35–51. https://doi.org/10.1002/rse2.121

Norman, S. P., Koch, F. H., & Hargrove, W. W. (2016). Review of broad-scale drought monitoring of forests: Toward an integrated data mining approach. *Forest Ecology and Management*, *380*, 346–358. https://doi.org/10.1016/j.foreco.2016.06.027

Osada, N., & Hiura, T. (2019). Intraspecific differences in spring leaf phenology in relation to tree size in temperate deciduous trees. *Tree Physiology*, *39*(5), 782–791. https://doi.org/10.1093/treephys/tpz011

Panchen, Z. A., Primack, R. B., Nordt, B., Ellwood, E. R., Stevens, A.-D., Renner, S. S., Willis, C. G., Fahey, R., Whittemore, A., Du, Y., & Davis, C. C. (2014). Leaf out times of temperate woody plants are related to phylogeny, deciduousness, growth habit and wood anatomy. *The New Phytologist*, *203*(4), 1208–1219. https://doi.org/10.1111/nph.12892

Peled, E., Dutra, E., Viterbo, P., & Angert, A. (2010). Technical Note: Comparing and ranking soil drought indices performance over Europe, through remote-sensing of vegetation. *Hydrology and Earth System Sciences*, *14*(2), 271–277. https://doi.org/10.5194/hess-14-271-2010

Peñuelas, J., & Filella, I. (1998). Visible and near-infrared reflectance techniques for diagnosing plant physiological status. *Trends in Plant Science*, *3*(4), 151–156. https://doi.org/10.1016/S1360-1385(98)01213-8

Peñuelas, J., Rutishauser, T., & Filella, I. (2009). Ecology. Phenology feedbacks on climate change. *Science (New York, N.Y.)*, *324*(5929), 887–888. https://doi.org/10.1126/science.1173004

Peterson, C. J. (2000). Catastrophic wind damage to North American forests and the potential impact of climate change. *The Science of the Total Environment*, *262*(3), 287–311. https://doi.org/10.1016/s0048-9697(00)00529-5

Piao, S., Liu, Q., Chen, A., Janssens, I. A., Fu, Y. H., Dai, J., Liu, L., Lian, X., Shen, M., & Zhu, X. (2019). Plant phenology and global climate change: Current progresses and challenges. *Global Change Biology*, *25*(6), 1922–1940. https://doi.org/10.1111/gcb.14619

Plowright, A., & Roussel, J.-R. (2023). *ForestTools: Tools for Analyzing Remote Sensing Forest Data*. https://cran.r-project.org/web/packages/ForestTools/ (accessed 25 March 2024)

Popescu, S. C., & Wynne, R. H. (2004). Seeing the Trees in the Forest. *Photogrammetric Engineering & Remote Sensing*, *70*(5), 589–604. https://doi.org/10.14358/PERS.70.5.589

Prey, L., Hanemann, A., Ramgraber, L., Seidl-Schulz, J., & Noack, P. O. (2022). UAV-Based Estimation of Grain Yield for Plant Breeding: Applied Strategies for Optimizing the Use of Sensors, Vegetation Indices, Growth Stages, and Machine Learning Algorithms. *Remote Sensing*, *14*(24), 6345. https://doi.org/10.3390/rs14246345

Qin, Q., Wu, Z., Zhang, T., Sagan, V., Zhang, Z., Zhang, Y., Zhang, C., Ren, H., Sun, Y., Xu, W., & Zhao, C. (2021). Optical and Thermal Remote Sensing for Monitoring Agricultural Drought. *Remote Sensing*, *13*(24), 5092. https://doi.org/10.3390/rs13245092

Queloz, V., Grünig, C. R., Berndt, R., Kowalski, T., Sieber, T. N., & Holdenrieder, O. (2011). Cryptic speciation in Hymenoscyphus albidus. *Forest Pathology*, *41*(2), 133–142. https://doi.org/10.1111/j.1439-0329.2010.00645.x

R Core Team. (2024). *R: A language and environment for statistical computing*. https://www.r-project.org/ (accessed 25 March 2024)

Rakovec, O., Samaniego, L., Hari, V., Markonis, Y., Moravec, V., Thober, S., Hanel, M., & Kumar, R. (2022). The 2018–2020 Multi-Year Drought Sets a New Benchmark in Europe. *Earth's Future*, *10*(3), Article e2021EF002394. https://doi.org/10.1029/2021EF002394

Ramanathan, V., & Carmichael, G. (2008). Global and regional climate changes due to black carbon. *Nature Geoscience*, *1*(4), 221–227. https://doi.org/10.1038/ngeo156

Reddy, A. R., Rasineni, G. K., & Raghavendra, A. S. (2010). The impact of global elevated CO2 concentration on photosynthesis and plant productivity. *Current Science*, *99*(99), 46–57.

Reichstein, M., Falge, E., Baldocchi, D., Papale, D., Aubinet, M., Berbigier, P., Bernhofer, C., Buchmann, N., Gilmanov, T., Granier, A., Grünwald, T., Havránková, K., Ilvesniemi, H., Janous, D., Knohl, A., Laurila, T., Lohila, A., Loustau, D., Matteucci, G., . . . Valentini, R.

(2005). On the separation of net ecosystem exchange into assimilation and ecosystem respiration: review and improved algorithm. *Global Change Biology*, *11*(9), 1424–1439. https://doi.org/10.1111/j.1365-2486.2005.001002.x

Rice, A., Glick, L., Abadi, S., Einhorn, M., Kopelman, N.M., Salman-Minkov, A. et al., 2015. The Chromosome Counts Database (CCDB) - a community resource of plant chromosome numbers. *The New phytologist 206*(1), 19–26. https://doi.org/10.1111/nph.13191.

Richardson, A. D. (2023). PhenoCam: An evolving, open-source tool to study the temporal and spatial variability of ecosystem-scale phenology. *Agricultural and Forest Meteorology*, *342*, 109751. https://doi.org/10.1016/j.agrformet.2023.109751

Richardson, A. D., Jenkins, J. P., Braswell, B. H., Hollinger, D. Y., Ollinger, S. V., & Smith, M.-L. (2007). Use of digital webcam images to track spring green-up in a deciduous broadleaf forest. *Oecologia*, *152*(2), 323–334. https://doi.org/10.1007/s00442-006-0657-z

Richardson, A. D., Keenan, T. F., Migliavacca, M., Ryu, Y., Sonnentag, O., & Toomey, M. (2013). Climate change, phenology, and phenological control of vegetation feedbacks to the climate system. *Agricultural and Forest Meteorology*, *169*, 156–173. https://doi.org/10.1016/j.agrformet.2012.09.012

Richardson, A. D., & O'Keefe, J. (2009). Phenological Differences Between Understory and Overstory. In A. Noormets (Ed.), *Phenology of ecosystem processes: Applications in global change research* (pp. 87–117). Springer. https://doi.org/10.1007/978-1-4419-0026-5_4

Riedel, T., & Weber, T. K. D. (2020). Review: The influence of global change on Europe's water cycle and groundwater recharge. *Hydrogeology Journal*, *28*(6), 1939–1959. https://doi.org/10.1007/s10040-020-02165-3

Rigo, D. de, Caudullo, G., Houston Durrant, T., & San-Miguel-Ayanz, J. (2016). The European Atlas of Forest Tree Species: modelling, data and information on forest tree species. In J. San-Miguel-Ayanz, D. de Rigo, G. Caudullo, T. Houston Durrant, & A. Mauri (Eds.), *European Atlas of Forest Tree Species* (pp. e01aa69+). Publications Office of the European Union.

Rodriguez-Galiano, V., Dash, J., & Atkinson, P. (2015a). Characterising the Land Surface Phenology of Europe Using Decadal MERIS Data. *Remote Sensing*, *7*(7), 9390–9409. https://doi.org/10.3390/rs70709390

Rodriguez-Galiano, V., Dash, J., & Atkinson, P. (2015b). Intercomparison of satellite sensor land surface phenology and ground phenology in Europe. *Geophysical Research Letters*, *42*(7), 2253–2260. https://doi.org/10.1002/2015GL063586

Rouse, J. W., Haas, R. H., Schell, J. A., & Deering, D. W. (1974). Monitoring vegetation systems in the Great Plains with ERTS. *NASA Spec. Publ.*, *351*(309).

Roussel, J.-R., Auty, D., Boissieu, F. de, Meador, A. S., Jean-François, B., Demetrios, G., Steinmeier, L., Adaszewski, S., & St-Onge, B. (2024). *lidR: Airborne LiDAR Data Manipulation and Visualization for Forestry Applications*. https://cran.r-project.org/web/packages/lidR/index.html (accessed 25 March 2024)

RStudio Team. (2024). *RStudio: Integrated Development for R*. http://www.rstudio.com/ (accessed 25 March 2024)

Rudolf, H. (2023). *Weltwald Freising*. https://www.weltwald.de/fileadmin/user_upload/14-weltwald/pdfs/Weltwald_Freising_2023.pdf (accessed 15 March 2024)

Ruosteenoja, K., Markkanen, T., Venäläinen, A., Räisänen, P., & Peltola, H. (2018). Seasonal soil moisture and drought occurrence in Europe in CMIP5 projections for the 21st century. *Climate Dynamics*, *50*(3-4), 1177–1192. https://doi.org/10.1007/s00382-017-3671-4

Ryu, Y., Lee, G., Jeon, S., Song, Y., & Kimm, H. (2014). Monitoring multi-layer canopy spring phenology of temperate deciduous and evergreen forests using low-cost spectral sensors. *Remote Sensing of Environment*, *149*, 227–238. https://doi.org/10.1016/j.rse.2014.04.015

Schär, C., Vidale, P. L., Lüthi, D., Frei, C., Häberli, C., Liniger, M. A., & Appenzeller, C. (2004). The role of increasing temperature variability in European summer heatwaves. *Nature*, *427*(6972), 332–336. https://doi.org/10.1038/nature02300

Schneider, U., Becker, A., Finger, P., Meyer-Christoffer, A., Rudolf, B., & Ziese, M. (2011). *GPCC Full Data Reanalysis Version 6.0 at 0.5°: Monthly Land-Surface Precipitation from Rain-Gauges built on GTS-based and Historic Data.* https://doi.org/10.5676/DWD_GPCC/FD_M_V6_050

Schönwiese, C.-D. (2020). *Klimatologie* (5. überarb. u. aktual. Aufl.). utb GmbH. https://doi.org/10.36198/9783838553870

Schrodt, F., Kattge, J., Shan, H., Fazayeli, F., Joswig, J., Banerjee, A., Reichstein, M., Bönisch, G., Díaz, S., Dickie, J., Gillison, A., Karpatne, A., Lavorel, S., Leadley, P., Wirth, C. B., Wright, I. J., Wright, S. J., & Reich, P. B. (2015). BHPMF – a hierarchical B ayesian approach to gap-filling and trait prediction for macroecology and functional biogeography. *Global Ecology and Biogeography*, *24*(12), 1510–1521. https://doi.org/10.1111/geb.12335

Schuldt, B., Buras, A., Arend, M., Vitasse, Y., Beierkuhnlein, C., Damm, A., Gharun, M., Grams, T. E., Hauck, M., Hajek, P., Hartmann, H., Hiltbrunner, E., Hoch, G., Holloway-Phillips, M., Körner, C., Larysch, E., Lübbe, T., Nelson, D. B., Rammig, A., . . . Kahmen, A. (2020). A first assessment of the impact of the extreme 2018 summer drought on Central European forests. *Basic and Applied Ecology*, *45*, 86–103. https://doi.org/10.1016/j.baae.2020.04.003

Schultz, J. (2016). *Die Ökozonen der Erde* (5., vollständig überarbeitete Auflage, Online-Ausgabe). *utb-studi-e-book: Vol. 1514*. utb GmbH; Verlag Eugen Ulmer. https://doi.org/10.36198/9783838546285

Sepulcre-Canto, G., Horion, S., Singleton, A., Carrao, H., & Vogt, J. (2012). Development of a Combined Drought Indicator to detect agricultural drought in Europe. *Natural Hazards and Earth System Sciences*, *12*(11), 3519–3531. https://doi.org/10.5194/nhess-12-3519-2012

Shen, M., Piao, S., Jeong, S.-J., Zhou, L., Zeng, Z., Ciais, P., Chen, D., Huang, M., Jin, C.-S., Li, L. Z. X., Li, Y., Myneni, R. B., Yang, K., Zhang, G., Zhang, Y., & Yao, T. (2015). Evaporative cooling over the Tibetan Plateau induced by vegetation growth. *Proceedings of the National Academy of Sciences of the United States of America*, *112*(30), 9299–9304. https://doi.org/10.1073/pnas.1504418112

Sishodia, R. P., Ray, R. L., & Singh, S. K. (2020). Applications of Remote Sensing in Precision Agriculture: A Review. *Remote Sensing*, *12*(19), 3136. https://doi.org/10.3390/rs12193136

Soudani, K., Delpierre, N., Berveiller, D., Hmimina, G., Pontailler, J.-Y., Seureau, L., Vincent, G., & Dufrêne, É. (2021). A survey of proximal methods for monitoring leaf phenology in temperate deciduous forests. *Biogeosciences*, *18*(11), 3391–3408. https://doi.org/10.5194/bg-18-3391-2021

Spinoni, J., Naumann, G., & Vogt, J. V. (2017). Pan-European seasonal trends and recent changes of drought frequency and severity. *Global and Planetary Change*, *148*, 113–130. https://doi.org/10.1016/j.gloplacha.2016.11.013

Spinoni, J., Vogt, J. V., Naumann, G., Barbosa, P., & Dosio, A. (2018). Will drought events become more frequent and severe in Europe? *International Journal of Climatology*, *38*(4), 1718–1736. https://doi.org/10.1002/joc.5291

Sporbert, M., Jakubka, D., Bucher, S. F., Hensen, I., Freiberg, M., Heubach, K., König, A., Nordt, B., Plos, C., Blinova, I., Bonn, A., Knickmann, B., Koubek, T., Linstädter, A., Mašková, T., Primack, R. B., Rosche, C., Shah, M. A., Stevens, A.-D., . . . Römermann, C. (2022). Functional traits influence patterns in vegetative and reproductive plant phenology - a multi-botanical garden study. *The New Phytologist*, *235*(6), 2199–2210. https://doi.org/10.1111/nph.18345

Stagge, J. H., Kingston, D. G., Tallaksen, L. M., & Hannah, D. M. (2017). Observed drought indices show increasing divergence across Europe. *Scientific Reports*, *7*(1), 14045. https://doi.org/10.1038/s41598-017-14283-2

Statistical Offices of the Federation and the States. (2021). *Erträge ausgewählter landwirtschaftlicher Feldfrüchte - Jahressumme - regionale Tiefe: Kreise und krfr. Städte*.

https://www.regionalstatistik.de/genesis/online?operation=previous&levelindex=2&levelid=1618314159666&levelid=1618314123639&step=1#abreadcrumb (accessed 13 April 2021)

Stener, L.-G. (2013). Clonal differences in susceptibility to the dieback of Fraxinus excelsior in southern Sweden. *Scandinavian Journal of Forest Research*, *28*(3), 205–216. https://doi.org/10.1080/02827581.2012.735699

Strengers, B. J., Müller, C., Schaeffer, M., Haarsma, R. J., Severijns, C., Gerten, D., Schaphoff, S., van den Houdt, R., & Oostenrijk, R. (2010). Assessing 20th century climate–vegetation feedbacks of land-use change and natural vegetation dynamics in a fully coupled vegetation–climate model. *International Journal of Climatology*, *30*(13), 2055–2065. https://doi.org/10.1002/joc.2132

Sun, D., & Kafatos, M. (2007). Note on the NDVI-LST relationship and the use of temperature-related drought indices over North America. *Geophysical Research Letters*, *34*(24), Article 2007GL031485. https://doi.org/10.1029/2007GL031485

Tamrakar, R., Rayment, M. B., Moyano, F., Mund, M., & Knohl, A. (2018). Implications of structural diversity for seasonal and annual carbon dioxide fluxes in two temperate deciduous forests. *Agricultural and Forest Meteorology*, *263*, 465–476. https://doi.org/10.1016/j.agrformet.2018.08.027

Tang, J., Körner, C., Muraoka, H., Piao, S., Shen, M., Thackeray, S. J., & Yang, X. (2016). Emerging opportunities and challenges in phenology: a review. *Ecosphere*, *7*(8), Article e01436. https://doi.org/10.1002/ecs2.1436

Thiel, C., Mueller, M. M., Epple, L., Thau, C., Hese, S., Voltersen, M., & Henkel, A. (2020). UAS Imagery-Based Mapping of Coarse Wood Debris in a Natural Deciduous Forest in Central Germany (Hainich National Park). *Remote Sensing*, *12*(20), 3293. https://doi.org/10.3390/rs12203293

Thomas, J. R., Namken, L. N., Oerther, G. F., & Brown, R. G. (1971). Estimating Leaf Water Content by Reflectance Measurements 1. *Agronomy Journal*, *63*(6), 845–847. https://doi.org/10.2134/agronj1971.00021962006300060007x

Tian, F., Cai, Z., Jin, H., Hufkens, K., Scheifinger, H., Tagesson, T., Smets, B., van Hoolst, R., Bonte, K., Ivits, E., Tong, X., Ardö, J., & Eklundh, L. (2021). Calibrating vegetation phenology from Sentinel-2 using eddy covariance, PhenoCam, and PEP725 networks across Europe. *Remote Sensing of Environment*, *260*, 112456. https://doi.org/10.1016/j.rse.2021.112456

TLUBN. (2024). *Kartendienst des TLUBN*. https://antares.thueringen.de/cadenza/pages/map/default/index.xhtml;jsessionid=6877477FE8727D4B77C4B854389311DF?mapId=429f7ba3-9277-40dd-ad05-1a281631215c&repositoryItemGlobalId=Anwendungen.Naturschutz.Schutzgebiete.sgb%2Fschutzgebietskarte.mml&mapSrs=EPSG%3A25832&mapExtent=549081.5077862333%2C5630475.820260193%2C651493.365013037%2C5679121.452442925 (accessed 14 March 2024)

Trnka, M., Hlavinka, P., Možný, M., Semerádová, D., Štěpánek, P., Balek, J., Bartošová, L., Zahradníček, P., Bláhová, M., Skalák, P., Farda, A., Hayes, M., Svoboda, M., Wagner, W., Eitzinger, J., Fischer, M., & Žalud, Z. (2020). Czech Drought Monitor System for monitoring and forecasting agricultural drought and drought impacts. *International Journal of Climatology*, *40*(14), 5941–5958. https://doi.org/10.1002/joc.6557

Tucker, C. J. (1979). Red and photographic infrared linear combinations for monitoring vegetation. *Remote Sensing of Environment*, *8*(2), 127–150. https://doi.org/10.1016/0034-4257(79)90013-0

UFZ. (2021). *Dürremonitor Deutschland*. https://www.ufz.de/index.php?de=37937 (accessed 13 April 2021)

Uphus, L., Lüpke, M., Yuan, Y., Benjamin, C., Englmeier, J., Fricke, U., Ganuza, C., Schwindl, M., Uhler, J., & Menzel, A. (2021). Climate Effects on Vertical Forest Phenology of Fagus

sylvatica L., Sensed by Sentinel-2, Time Lapse Camera, and Visual Ground Observations. *Remote Sensing*, *13*(19), 3982. https://doi.org/10.3390/rs13193982

van Hateren, T. C., Chini, M., Matgen, P., & Teuling, A. J. (2021). Ambiguous Agricultural Drought: Characterising Soil Moisture and Vegetation Droughts in Europe from Earth Observation. *Remote Sensing*, *13*(10), 1990. https://doi.org/10.3390/rs13101990

Verger, A., Filella, I., Baret, F., & Peñuelas, J. (2016). Vegetation baseline phenology from kilometric global LAI satellite products. *Remote Sensing of Environment*, *178*, 1–14. https://doi.org/10.1016/j.rse.2016.02.057

Violle, C., Choler, P., Borgy, B., Garnier, E., Amiaud, B., Debarros, G., Diquelou, S., Gachet, S., Jolivet, C., Kattge, J., Lavorel, S., Lemauviel-Lavenant, S., Loranger, J., Mikolajczak, A., Munoz, F., Olivier, J., & Viovy, N. (2015). Vegetation ecology meets ecosystem science: Permanent grasslands as a functional biogeography case study. *The Science of the Total Environment*, *534*, 43–51. https://doi.org/10.1016/j.scitotenv.2015.03.141

Viovy, N., Arino, O., & Belward, A. S. (1992). The Best Index Slope Extraction (BISE): A method for reducing noise in NDVI time-series. *International Journal of Remote Sensing*, *13*(8), 1585–1590. https://doi.org/10.1080/01431169208904212

Vitasse, Y. (2013). Ontogenic changes rather than difference in temperature cause understory trees to leaf out earlier. *The New Phytologist*, *198*(1), 149–155. https://doi.org/10.1111/nph.12130

Vitasse, Y., Baumgarten, F., Zohner, C. M., Rutishauser, T., Pietragalla, B., Gehrig, R., Dai, J., Wang, H., Aono, Y., & Sparks, T. H. (2022). The great acceleration of plant phenological shifts. *Nature Climate Change*, *12*(4), 300–302. https://doi.org/10.1038/s41558-022-01283-y

Vitasse, Y., Delzon, S., Dufrêne, E., Pontailler, J.-Y., Louvet, J.-M., Kremer, A., & Michalet, R. (2009). Leaf phenology sensitivity to temperature in European trees: Do within-species populations exhibit similar responses? *Agricultural and Forest Meteorology*, *149*(5), 735–744. https://doi.org/10.1016/j.agrformet.2008.10.019

Vitasse, Y., Hoch, G., Randin, C. F., Lenz, A., Kollas, C., Scheepens, J. F., & Körner, C. (2013). Elevational adaptation and plasticity in seedling phenology of temperate deciduous tree species. *Oecologia*, *171*(3), 663–678. https://doi.org/10.1007/s00442-012-2580-9

Vitasse, Y., Lenz, A., & Körner, C. (2014). The interaction between freezing tolerance and phenology in temperate deciduous trees. *Frontiers in Plant Science*, *5*, 541. https://doi.org/10.3389/fpls.2014.00541

Vitasse, Y., Ursenbacher, S., Klein, G., Bohnenstengel, T., Chittaro, Y., Delestrade, A., Monnerat, C., Rebetez, M., Rixen, C., Strebel, N., Schmidt, B. R., Wipf, S., Wohlgemuth, T., Yoccoz, N. G., & Lenoir, J. (2021). Phenological and elevational shifts of plants, animals and fungi under climate change in the European Alps. *Biological Reviews of the Cambridge Philosophical Society*, *96*(5), 1816–1835. https://doi.org/10.1111/brv.12727

Vitra, A., Lenz, A., & Vitasse, Y. (2017). Frost hardening and dehardening potential in temperate trees from winter to budburst. *The New Phytologist*, *216*(1), 113–123. https://doi.org/10.1111/nph.14698

Walentowski, H., Gulder, H.-J., Kölling, C., Ewald, J., & Türk, W. (2001). *Die regionale natürliche Waldzusammensetzung Bayerns.* LWF. https://www.lwf.bayern.de/service/publikationen/lwf_wissen/063195/index.php (accessed 21 March 2024)

Walentowski, H., & Kopp, D. (2006). Leitlinien für eine gesamtdeutsche ökologische Klassifikation der Wald-Naturräume. *Archiv Für Naturschutz Und Landschaftsforschung*, *45*, 135–149.

Wan, Z., Hook, S., & Hulley, G. (2015). *MOD11A2 MODIS/Terra Land Surface Temperature/Emissivity 8-Day L3 Global 1km SIN Grid V006.* https://doi.org/10.5067/MODIS/MOD11A2.006

Wang, R., & Gamon, J. A. (2019). Remote sensing of terrestrial plant biodiversity. *Remote Sensing of Environment*, *231*, 111218. https://doi.org/10.1016/j.rse.2019.111218

Wang, W., Peng, C., Kneeshaw, D. D., Larocque, G. R., & Luo, Z. (2012). Drought-induced tree mortality: ecological consequences, causes, and modeling. *Environmental Reviews*, *20*(2), 109–121. https://doi.org/10.1139/a2012-004

Wei, T., Simko, V., Levy, M., Xie, Y., Jin, Y., Zemla, J., Freidank, M., Cai, J., & Protivinsky, T. (2021). *corrplot: Visualization of a Correlation Matrix*. https://cran.r-project.org/web//packages/corrplot/ (accessed 25 March 2024)

Weiss, M., Jacob, F., & Duveiller, G. (2020). Remote sensing for agricultural applications: A meta-review. *Remote Sensing of Environment*, *236*, 111402. https://doi.org/10.1016/j.rse.2019.111402

West, H., Quinn, N., & Horswell, M. (2019). Remote sensing for drought monitoring & impact assessment: Progress, past challenges and future opportunities. *Remote Sensing of Environment*, *232*, 111291. https://doi.org/10.1016/j.rse.2019.111291

White, M. A., Beurs, K. M. de, Didan, K., Inouye, D. W., Richardson, A. D., Jensen, O. P., O'Keefe, J., Zhang, G., Nemani, R. R., van Leeuwen, W. J. D., Brown, J. F., Wit, A. de, Schaepman, M., Lin, X., Dettinger, M., Bailey, A. S., Kimball, J., Schwartz, M. D., Baldocchi, D., … Lauenroth, W. K. (2009). Intercomparison, interpretation, and assessment of spring phenology in North America estimated from remote sensing for 1982–2006. *Global Change Biology*, *15*(10), 2335–2359. https://doi.org/10.1111/j.1365-2486.2009.01910.x

Wickham, H. (2016). *ggplot2: Elegant Graphics for Data Analysis*. Springer-Verlag New York.

Wickham, H. (2020). *reshape2: Flexibly Reshape Data: A Reboot of the Reshape Package*. https://cran.r-project.org/web/packages/reshape2/index.html (accessed 25 March 2024)

Wickham, H. (2023). *plyr: Tools for Splitting, Applying and Combining Data*. (accessed 25 March 2024)

Wickham, H., Averick, M., Bryan, J., Chang, W., McGowan, L., François, R., Grolemund, G., Hayes, A., Henry, L., Hester, J., Kuhn, M., Pedersen, T., Miller, E., Bache, S., Müller, K., Ooms, J., Robinson, D., Seidel, D., Spinu, V., … Yutani, H. (2019). Welcome to the Tidyverse. *Journal of Open Source Software*, *4*(43), 1686. https://doi.org/10.21105/joss.01686

Wickham, H., François, R., Henry, L., Müller, K., & Vaughan, D. (2023). *dplyr: A Grammar of Data Manipulation: R package version 1.1.4*. https://dplyr.tidyverse.org/ (accessed 25 March 2024)

Wickham, H., Vaughan, D., & Girlich, M. (2024). *tidyr: Tidy Messy Data: R package version 1.3.1*. https://tidyr.tidyverse.org/ (accessed 25 March 2024)

Wilhite, D. A., & Glantz, M. H. (1985). Understanding: the Drought Phenomenon: The Role of Definitions. *Water International*, *10*(3), 111–120. https://doi.org/10.1080/02508068508686328

Woebbecke, D. M., Meyer, G. E., Bargen, K. V., & Mortensen, D. A. (1995). Color Indices for Weed Identification Under Various Soil, Residue, and Lighting Conditions. *Transactions of the ASAE*, *38*(1), 259–269. https://doi.org/10.13031/2013.27838

Xie, J., Hüsler, F., Jong, R. de, Chimani, B., Asam, S., Sun, Y., Schaepman, M. E., & Kneubühler, M. (2021). Spring Temperature and Snow Cover Climatology Drive the Advanced Springtime Phenology (1991–2014) in the European Alps. *Journal of Geophysical Research: Biogeosciences*, *126*(3), Article e2020JG006150. https://doi.org/10.1029/2020JG006150

Xie, Y., Wang, X., Wilson, A. M., & Silander, J. A. (2018). Predicting autumn phenology: How deciduous tree species respond to weather stressors. *Agricultural and Forest Meteorology*, *250-251*, 127–137. https://doi.org/10.1016/j.agrformet.2017.12.259

Yuan, W., Cai, W., Chen, Y., Liu, S., Dong, W., Zhang, H., Yu, G., Chen, Z., He, H., Guo, W., Liu, D., Liu, S., Xiang, W., Xie, Z., Zhao, Z., & Zhou, G. (2016). Severe summer heatwave and drought strongly reduced carbon uptake in Southern China. *Scientific Reports*, *6*, 18813. https://doi.org/10.1038/srep18813

Yuan, Y., Härer, S., Ottenheym, T., Misra, G., Lüpke, A., Estrella, N., & Menzel, A. (2021). Maps, trends, and temperature sensitivities-phenological information from and for decreasing numbers of volunteer observers. *International Journal of Biometeorology*, *65*(8), 1377–1390. https://doi.org/10.1007/s00484-021-02110-3

Zani, D., Crowther, T. W., Mo, L., Renner, S. S., & Zohner, C. M. (2020). Increased growing-season productivity drives earlier autumn leaf senescence in temperate trees. *Science (New York, N.Y.)*, *370*(6520), 1066–1071. https://doi.org/10.1126/science.abd8911

Zargar, A., Sadiq, R., Naser, B., & Khan, F. I. (2011). A review of drought indices. *Environmental Reviews*, *19*(NA), 333–349. https://doi.org/10.1139/a11-013

Zeileis, A., Grothendieck, G., Ryan, J. A., Ulrich, J. M., & Andrews, F. (2023). *zoo: S3 Infrastructure for Regular and Irregular Time Series (Z's Ordered Observations)*. https://cran.r-project.org/web/packages/zoo/index.html (accessed 25 March 2024)

Zeng, L., Wardlow, B. D., Xiang, D., Hu, S., & Li, D. (2020). A review of vegetation phenological metrics extraction using time-series, multispectral satellite data. *Remote Sensing of Environment*, *237*, 111511. https://doi.org/10.1016/j.rse.2019.111511

Zeng, Y., Hao, D., Huete, A. R., Dechant, B., Berry, J., Chen, J. M., Joiner, J., Frankenberg, C., Bond-Lamberty, B., Ryu, Y., Xiao, J., Asrar, G. R., & Chen, M. (2022). Optical vegetation indices for monitoring terrestrial ecosystems globally. *Nature Reviews Earth & Environment*, *3*(7), 477–493. https://doi.org/10.1038/s43017-022-00298-5

Zhang, Y., Peng, C., Li, W., Fang, X., Zhang, T., Zhu, Q., Chen, H., & Zhao, P. (2013). Monitoring and estimating drought-induced impacts on forest structure, growth, function, and ecosystem services using remote-sensing data: recent progress and future challenges. *Environmental Reviews*, *21*(2), 103–115. https://doi.org/10.1139/er-2013-0006

Zhao, J., Zhang, H., Zhang, Z., Guo, X., Li, X., & Chen, C. (2015). Spatial and Temporal Changes in Vegetation Phenology at Middle and High Latitudes of the Northern Hemisphere over the Past Three Decades. *Remote Sensing*, *7*(8), 10973–10995. https://doi.org/10.3390/rs70810973

Zhao, S., Cong, D., He, K., Yang, H., & Qin, Z. (2017). Spatial-Temporal Variation of Drought in China from 1982 to 2010 Based on a modified Temperature Vegetation Drought Index (mTVDI). *Scientific Reports*, *7*(1), 17473. https://doi.org/10.1038/s41598-017-17810-3

Zhou, S., Zhang, Y., Caylor, K. K., Luo, Y., Xiao, X., Ciais, P., Huang, Y., & Wang, G. (2016). Explaining inter-annual variability of gross primary productivity from plant phenology and physiology. *Agricultural and Forest Meteorology*, *226-227*, 246–256. https://doi.org/10.1016/j.agrformet.2016.06.010

Zhou, S., Zhang, Y., Ciais, P., Xiao, X., Luo, Y., Caylor, K. K., Huang, Y., & Wang, G. (2017). Dominant role of plant physiology in trend and variability of gross primary productivity in North America. *Scientific Reports*, *7*, 41366. https://doi.org/10.1038/srep41366

Zink, M., Samaniego, L., Kumar, R., Thober, S., Mai, J., Schäfer, D., & Marx, A. (2016). The German drought monitor. *Environmental Research Letters*, *11*(7), 74002. https://doi.org/10.1088/1748-9326/11/7/074002

Zohner, C. M., Mirzagholi, L., Renner, S. S., Mo, L., Rebindaine, D., Bucher, R., Palouš, D., Vitasse, Y., Fu, Y. H., Stocker, B. D., & Crowther, T. W. (2023). Effect of climate warming on the timing of autumn leaf senescence reverses after the summer solstice. *Science (New York, N.Y.)*, *381*(6653), eadf5098. https://doi.org/10.1126/science.adf5098

Zohner, C. M., Mo, L., Renner, S. S., Svenning, J.-C., Vitasse, Y., Benito, B. M., Ordonez, A., Baumgarten, F., Bastin, J.-F., Sebald, V., Reich, P. B., Liang, J., Nabuurs, G.-J., de-Miguel, S., Alberti, G., Antón-Fernández, C., Balazy, R., Brändli, U.-B., Chen, H. Y. H., . . . Crowther, T. W. (2020). Late-spring frost risk between 1959 and 2017 decreased in North America but increased in Europe and Asia. *Proceedings of the National Academy of Sciences of the United States of America*, *117*(22), 12192–12200. https://doi.org/10.1073/pnas.1920816117

Zohner, C. M., & Renner, S. S. (2017). Innately shorter vegetation periods in North American species explain native-non-native phenological asymmetries. *Nature Ecology & Evolution*, *1*(11), 1655–1660. https://doi.org/10.1038/s41559-017-0307-3

Publication reprints

The following pages show the publications (see section 3) on which this doctoral thesis is based:

1. Simon Kloos, Ye Yuan, Mariapina Castelli & Annette Menzel; Agricultural Drought Detection with MODIS Based Vegetation Health Indices in Southeast Germany (open-access; https://www.mdpi.com/2072-4292/13/19/3907)

2. Simon Kloos, Anne Klosterhalfen, Alexander Knohl & Annette Menzel; Decoding autumn phenology: Unraveling the link between observation methods and detected environmental cues (open-access; https://onlinelibrary.wiley.com/doi/full/10.1111/gcb.17231)

3. Simon Kloos, Marvin Lüpke, Nicole Estrella, Wael Ghada, Jens Kattge, Solveig Franziska Bucher, Allan Buras, & Annette Menzel; The linkage between functional traits and drone-derived phenology of 74 Northern Hemisphere tree species (manuscript and supplementary is still in review and might change due to the review process)

remote sensing

MDPI

Article

Agricultural Drought Detection with MODIS Based Vegetation Health Indices in Southeast Germany

Simon Kloos [1,*], Ye Yuan [1], Mariapina Castelli [2] and Annette Menzel [1,3]

[1] TUM School of Life Sciences, Ecoclimatology, Technical University of Munich, 85354 Freising, Germany; yuan@wzw.tum.de (Y.Y.); annette.menzel@tum.de (A.M.)
[2] Institute for Earth Observation, Eurac Research, 39100 Bolzano-Bozen, Italy; mariapina.castelli@eurac.edu
[3] Institute for Advanced Study, Technical University of Munich, 85748 Garching, Germany
* Correspondence: simon.kloos@tum.de

Abstract: Droughts during the growing season are projected to increase in frequency and severity in Central Europe in the future. Thus, area-wide monitoring of agricultural drought in this region is becoming more and more important. In this context, it is essential to know where and when vegetation growth is primarily water-limited and whether remote sensing-based drought indices can detect agricultural drought in these areas. To answer these questions, we conducted a correlation analysis between the Normalized Difference Vegetation Index (NDVI) and Land Surface Temperature (LST) within the growing season from 2001 to 2020 in Bavaria (Germany) and investigated the relationship with land cover and altitude. In the second step, we applied the drought indices Temperature Condition Index (TCI), Vegetation Condition Index (VCI), and Vegetation Health Index (VHI) to primarily water-limited areas and evaluated them with soil moisture and agricultural yield anomalies. We found that, especially in the summer months (July and August), on agricultural land and grassland and below 800 m, NDVI and LST are negatively correlated and thus, water is the primary limiting factor for vegetation growth here. Within these areas and periods, the TCI and VHI correlate strongly with soil moisture and agricultural yield anomalies, suggesting that both indices have the potential to detect agricultural drought in Bavaria.

Keywords: NDVI; LST; TCI; VCI; VHI; soil moisture; crop yield; remote sensing; drought monitoring; corn

Citation: Kloos, S.; Yuan, Y.; Castelli, M.; Menzel, A. Agricultural Drought Detection with MODIS Based Vegetation Health Indices in Southeast Germany. *Remote Sens.* **2021**, *13*, 3907. https://doi.org/10.3390/rs13193907

Academic Editor: Won-Ho Nam

Received: 15 September 2021
Accepted: 25 September 2021
Published: 30 September 2021

1. Introduction

Drought is a complex, globally occurring phenomenon that affects humans and nature alike [1]. It can be examined from different perspectives: meteorological (precipitation deficit), agricultural (soil moisture deficit), hydrological (runoff and water storage deficit), and socio-economic drought (consideration of water supply and demand) [2–4]. Drought events in Europe have far-reaching impacts and economic costs within different sectors of society [5,6]. Within the European Union and United Kingdom, the annual economic losses (1981–2010) from drought are estimated at EUR 9 billion year^{-1} [7]. In Central Europe, and thus also in Bavaria, extreme drought events in recent years have repeatedly resulted in massive damage and losses in agriculture and forestry [8–11].

Since the beginning of the 21st century, Central Europe has experienced recurrent periods of exceptional drought, with the years 2003, 2015, and 2018, in particular, being extremely hot and/or dry [12–15]. While climate data from the past do not yet allow a consistent statement on drought trends in Central Europe [16–19], future projections mainly assume an increase in drought frequency and severity during the growing season [20–23]. In addition, there could be a significant increase in the risk of consecutive droughts and their affected areas in the future [15].

In this context, the detection and forecast of drought are becoming more and more important, a major challenge being the monitoring of the impacts of agricultural drought

on vegetation. In addition to in-situ measurements, remote sensing based observations allow a broad scale detection and can identify and fill relevant knowledge gaps within this thematic area. A variety of approaches based on remote sensing exist to detect drought impacts on vegetation [24–26], some of which have already been applied in Central Europe, with different methodologies. The majority of existing studies made use of remotely sensed vegetation indices (VIs).

One possibility is the comparison of VIs with meteorological drought indices. It has been shown that the Normalized Difference Vegetation Index (NDVI) and Vegetation Optical Depth (VOD) could capture agricultural drought events in response to meteorological droughts within Europe [27]. In addition, it has been found that meteorological drought indices for shorter periods were associated with crop stress (defined via the Vegetation Condition Index (VCI) and Vegetation Health Index (VHI)), while longer accumulation periods correlated better with the vegetation status of forest areas. At the same time, the magnitude of regional differences in drought impacts within Europe was pointed out [28]. Equally, when the NDVI and Standardized Precipitation Index (SPI) data in spring and summer were compared to each other, high positive correlations were detected, especially in Eastern Europe and on the Iberian Peninsula [29].

Another approach within VI use is the analysis and comparison with soil moisture data. Comparing the NDVI with soil moisture indices such as the Palmer Drought Severity Index, the Self-Calibrating Palmer Drought Severity Index and the Normalized total depth Soil Moisture (NSM), clear differences in correlations have been observed across Europe [29]. Here, the NSM achieved the highest correlations (also in Eastern Europe and on the Iberian Peninsula), whereby this was explained primarily with the additional information included in NSM compared to the other indices about soil moisture in deeper soil layers. Using the NSM as a soil moisture variable, it was also found that in European areas with a warmer summer climate, the NDVI only responded to fluctuations in soil moisture, but not in temperature. In spring, this dependency was reversed. In colder regions, the NDVI was only dependent on temperature in both seasons. Furthermore, during the 2018 agricultural drought in the Netherlands, negative soil moisture anomalies occurred 2–3 weeks before the first VI reduction, using near-infrared reflectance of terrestrial vegetation and VOD as VI [30]. When comparing NDVI and Climate Change Initiative soil moisture data, an offset between soil moisture drought and vegetation drought in Europe was also found [31].

In Central Europe, analyses of VIs have been used to assess the impact of agricultural droughts on corn and winter wheat yields. Corn yields at the NUTS3 level in Germany correlated well with VCI and VHI in August, although clear spatial correlation differences could also be seen [28]. On the other hand, comparing Temperature Condition Index (TCI), VCI and VHI with winter wheat yields in northern and eastern Germany, VHI, in particular, was able to achieve higher correlations than meteorological indices [32]. Comparing the VIs NDVI and Enhanced Vegetation Index (EVI) with climatic datasets, it was shown that during the extreme drought in July 2018, 1.5 times more area within Europe was negatively impacted than during the extreme drought in August 2003. Differences within land-use types were also found [33].

Within remote sensing of agricultural drought, there are also studies which developed combined drought monitoring in Central Europe. Sepulcre-Canto et al. [34], for example, applied a combination of SPI, soil moisture anomaly, and the fraction of Absorbed Photosynthetically Active Radiation (fAPAR), while Trnka et al. [35] used a combination of soil moisture data (remotely sensed, modelled, and reported) and EVI in the Czech Republic and Slovakia. Both approaches were shown to be promising. Finally, approaches also exist within this topic to determine areas and time periods where water is the primary limiting factor for plant growth. In Europe, a correlation analysis between LST and NDVI has revealed that energy was a limiting factor mainly in northern Europe, at high altitudes, and in spring, while water limited plant growth mainly in southern Europe and in summer [36].

Despite the large numbers of existing studies on agricultural and vegetation-based drought in Central Europe using remote sensing, uncertainties and larger knowledge gaps

still exist. For example, the spatial as well as temporal resolution of results indicating where and when water is the limiting factor for vegetation growth is still rather limited. There are also hardly any evaluations that deal with other explanatory environmental variables for vegetation stress caused by drought. In Bavaria in particular, there are still hardly any approaches for continuous drought monitoring via remote sensing-based VIs that can demonstrate an appropriate spatial and temporal resolution. Therefore, our study aims, for the first time, to provide results with a much better spatial and temporal resolution than currently exists as to where and when in Central Europe water is the limiting factor for vegetation growth. Second, the analysis of this limitation incorporates other environmental conditions to explain it, which has rarely been done before. Finally, an approach not yet practiced in Bavaria is presented to perform continuous drought monitoring via remote sensing-based VIs at an appropriate spatial and temporal resolution.

Addressing the aforementioned gaps in knowledge, the general objective of this study is to detect agricultural drought using remote sensing in Central Europe on water-limited areas for vegetation growth. Specifically, this means, with a spatial resolution of up to 250 m and a temporal resolution of up to 8 days:

1. To determine, by means of a correlation analysis between Moderate Resolution Imaging Spectroradiometer (MODIS) NDVI and LST, areas and time periods in which water is the limiting factor for vegetation growth. In addition, it will be examined whether and to what extent the factors of land cover and altitude influence these conditions;
2. To carry out drought monitoring using the TCI, VCI, and VHI, as well as to evaluate their results by soil moisture and agricultural yields. The question to be addressed here is whether and to what extent these indices can be used to detect agricultural drought.

2. Materials and Methods

The general work-flow of this study is shown in Figure 1, including preprocessing of data, the classified correlation analysis between NDVI and LST, and the calculation and evaluation of the drought indices. All relevant analyses were carried out in R (version 4.0.3). More details on the following steps are provided in the respective subsections.

2.1. Study Area

The study area of Bavaria is located between 47°N and 50.5°N, and between 9°E and 14°E, in the southeastern part of Germany, Central Europe (Figure 2). The climate of the region is mainly influenced by strong relief, with higher elevations in the south (northern edge of the Alps) and east (Bavarian Forest and Fichtel Mountains; Figure S1 in Supplementary Materials). The mean annual temperature ranges from −3.3 to 11 °C, but in the majority of the territory, it is between 8 and 10 °C (Figure S2, based on data from the German Meteorological Service, 1991–2020). The mean annual precipitation sums range from 515 to 3184 mm, with wetter conditions in the southern part of Bavaria (Figure S3). The land cover in Bavaria is largely dominated by agriculture (54.58%) and forest (35.38%). The agricultural areas are mainly found in the northwest and southeast of Bavaria, while forest cover dominates towards the Alps and in the east of Bavaria. Open grasslands and larger water areas are mostly localized in the Alpine region and Alpine foothills. Munich and Nuremberg constitute the largest urbanized areas (Figure 2, based on Corine Land Cover (CLC) 2018 data). Bavaria is divided into 96 counties (based on the yield data for agricultural crops/Statistical Offices of the Federation and the states).

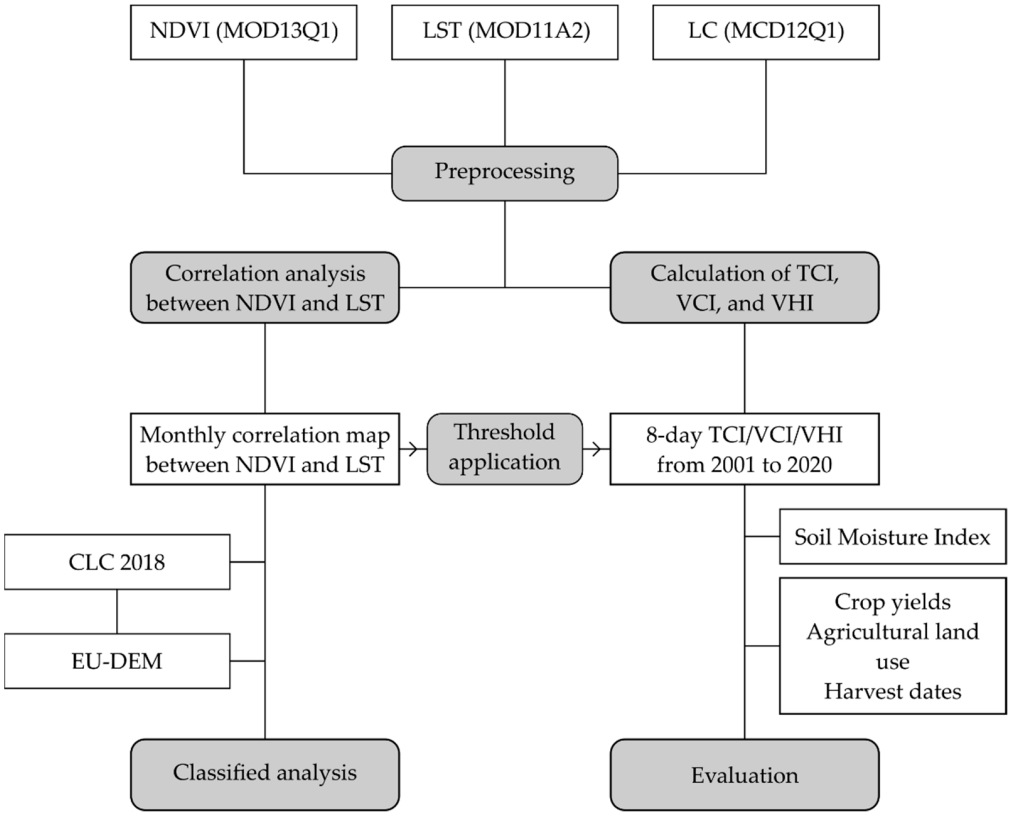

Figure 1. Flowchart of data used and processed (white boxes) and methodology applied (gray boxes; NDVI = Normalized Difference Vegetation Index; LST = Land Surface Temperature; LC = Land Cover; TCI = Temperature Condition Index; VCI = Vegetation Condition Index; VHI = Vegetation Health Index; CLC = Corine Land Cover; EU-DEM = European Digital Elevation Model).

2.2. Data

MODIS NDVI, LST, and Land Cover (LC) products were used for both the correlation analysis between NDVI and LST and the calculation of drought indices. The chosen period for all MODIS products was from 2001 to 2020. The NDVI raster data (MOD13Q1) have a spatial resolution of 250 m and a temporal resolution of 16 days [37]. The LST raster data (MOD11A2) provide Daytime Land Surface Temperature [K] with a spatial resolution of 1 km and a temporal resolution of 8 days [38]. The LC product from MODIS (MCD12Q1) is issued annually with a spatial resolution of 500 m. We used the International Geosphere-Biosphere Programme (IGBP) classification (LC Type 1) [39].

Both the LST and LC data were resampled first to a spatial resolution of 250 m in order to be compatible with the NDVI data. In addition, an annual vegetation mask (Table S2) was created using the MODIS LC data and applied to the NDVI and LST data to preemptively avoid misinterpretation, especially with respect to NDVI. Finally, the 16-day NDVI grid data were linearly interpolated to an 8-day temporal resolution in order to perform both the correlation analysis between NDVI and LST and the calculation of drought indices in 8-day time steps.

In addition, we used the land cover product CLC 2018 and the European Digital Elevation Model (EU-DEM) v1.1 for a better and more differentiated evaluation of the correlation analysis between NDVI and LST. The CLC and EU-DEM datasets are produced within the framework of the EU Copernicus Service coordinated by the European Environment Agency (EEA) and have a spatial resolution of 100 [40] and 25 m [41], respectively. To combine the two datasets, the elevation model was aggregated to a spatial resolution of 100 m using the arithmetic mean.

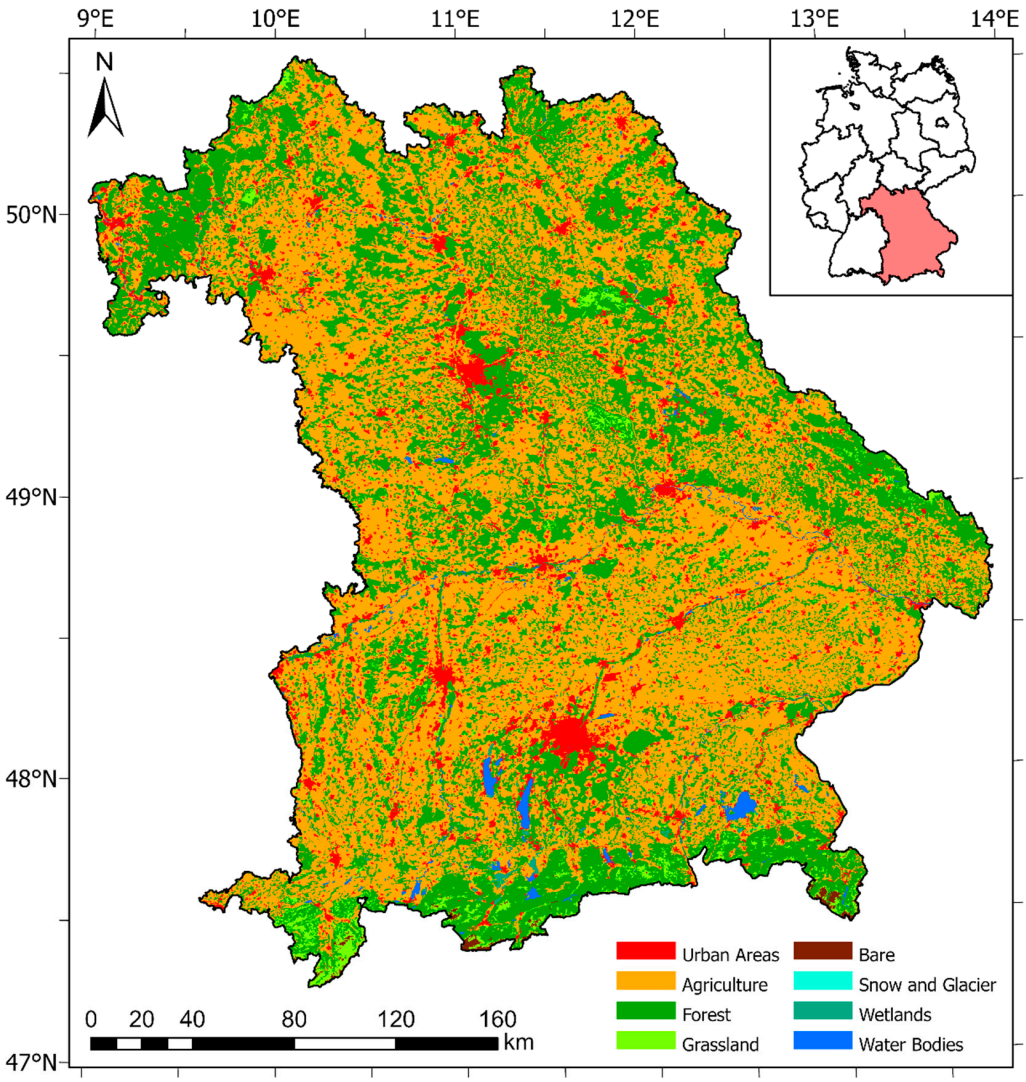

Figure 2. Land cover in Bavaria based on CLC 2018 (simplified according to Table S1). Agricultural land (orange) dominates mainly in the northwest and southeast of Bavaria, while forested land (dark green) mainly dominates in the northeast and south. All further results and representations refer to this area, whereby a further longitude and latitude indication was omitted.

To evaluate the calculated drought indices VCI, TCI, and VHI (see Section 2.4), soil moisture index data from 2001 to 2020, as well as yield data for agricultural crops in combination with land use data were used. The present work exploits the Soil Moisture Index (SMI) published by the Helmholtz Centre for Environmental Research (UFZ). SMI represents the percentile of soil moisture content in the topsoil up to a depth of 25 cm, relative to its frequency distribution in the period 1951–2019. The data have a monthly temporal resolution and a spatial resolution of 4 km [42,43]. In order to compare the data with the calculated raster data of the drought indices, the soil moisture index data were bilinearly resampled to a spatial resolution of 250 m.

The yield data for agricultural crops from 2001 to 2019 are published in the Regional Database Germany, which is operated by the Statistical Offices of the Federation and the states. The data are given as the annual mean yield per hectare in dt ha^{-1} and are provided at county level [44]. The land use data for the agricultural holdings in Bavaria originate from the Bavarian State Office for Statistics and refer to the reference year 2016. The cultivated area of the respective field crop is also given for each county [45]. In the present paper, the area ratios of the individual cultivated crops within the counties are assumed to be relatively stable and thus refer to the observation period of the yield statistics (2001 to

2019). For the selection of yield data to be included in the analysis, data on annual harvest dates in Bavaria from 2001 to 2019 were used based on selected phenological observations of the respective crops (Phase ID 24—"Ernte") from the German Meteorological Service (DWD) [46].

2.3. Correlation Analysis between NDVI and LST

The first step of the present study is a correlation analysis between NDVI and LST to determine when and where water is the limiting factor for vegetation growth. NDVI is one of the most widely used vegetation indices in remote sensing and is defined as follows [47,48]:

$$NDVI = \frac{\rho_{NIR} - \rho_R}{\rho_{NIR} + \rho_R}, \quad (1)$$

where ρ_{NIR} is the reflectance in the near-infrared band and ρ_R is the reflectance in the red band. NDVI allows one to distinguish between healthy and stressed vegetation and to determine the growth status of vegetation, and thus a measure of general vegetation health [26,49,50]. In addition, NDVI can also be an effective indicator of the vegetation-moisture condition [51]. LST, in turn, mirrors soil moisture conditions, evapotranspiration, and vegetation water stress. Because evapotranspiration cools the earth's surface, rising surface temperatures may be linked to decreasing water content or a soil moisture deficit and thus water stress in the vegetation canopy [52,53]. If both variables are well correlated, the limiting factor for vegetation growth can be determined depending on the season and location: The NDVI-LST correlation is negative if water is the limiting factor, but it is positive if energy is the limiting factor [36,54,55].

Here the correlation analysis between NDVI and LST was performed at pixel level, at a monthly time scale, following the method of Abdi et al. [56]. The Bravais-Pearson correlation coefficient was calculated for each pixel and month in the vegetation period from March to October using all available MODIS data from 2001 to 2020 (Table 1).

Table 1. Monthly subdivision of Moderate Resolution Imaging Spectroradiometer (MODIS) day numbers for pixel-based monthly correlation analysis between NDVI and LST.

Month	MODIS Day Numbers
March	065–089
April	097–113
May	121–145
June	153–177
July	185–209
August	217–241
September	249–273
October	281–297

The calculated correlation coefficients were additionally analyzed by land cover, altitude, and their combination. For this, the monthly NDVI-LST correlation maps were resampled to 100 m spatial resolution. Subsequently, both the land cover data (CLC 2018) and the digital elevation model data (EU-DEM v1.1) were classified into different classes (Table 2). The selected land cover classes had to meet two criteria: (1) contain vegetation; and (2) cover at least 1% of the Bavarian land area. The altitude classification followed relevant papers with a reasonable number of classes [57–60]. The respective independent masks were then intersected with the monthly NDVI-LST correlation maps and finally characterized using boxplots.

Table 2. Land cover (CLC 2018) and elevation (EU-DEM v1.1) classes and their IDs applied to the monthly NDVI-LST correlation maps.

ID	Land Cover Classes (CLC 2018)	ID	Altitude Classes (EU-DEM v1.1)
NAL	Non-irrigated arable land	AL1	<300 m
PAS	Pastures	AL2	300–500 m
BLF	Broad-leaved forest	AL3	500–800 m
CFF	Coniferous forest	AL4	800–1200 m
MXF	Mixed forest	AL5	>1200 m
NGL	Natural grasslands		

When combining both classifications, the land cover masks were intersected with the altitude masks. All 30 (6 land cover classes × 5 altitude classes) combined masks were then intersected with the monthly NDVI-LST correlation maps, for which the median was determined for each class.

2.4. Calculation and Evaluation of the Drought Indices VCI, TCI, and VHI

The VHI consists of two components, i.e., VCI and TCI. The VCI is defined as follows [61–63]:

$$VCI = 100 * \frac{(NDVI - NDVI_{min})}{(NDVI_{max} - NDVI_{min})}. \quad (2)$$

The NDVI is the smoothed 8-day NDVI, the $NDVI_{min,}$ and the $NDVI_{max}$ the corresponding multiyear absolute maximum and minimum. The VCI is accordingly scaled from 0 to 100 and takes on larger values the higher the NDVI is. The TCI is defined as follows [61–63]:

$$TCI = 100 * \frac{(T_{max} - T)}{(T_{max} - T_{min})}, \quad (3)$$

where T is the smoothed 8-day temperature, T_{min} and the T_{max} are the corresponding multiyear absolute maximum and minimum. The TCI is also scaled accordingly from 0 to 100 but takes on higher values the lower T is. In this work, T is defined via the LST. The combination of both described indices results in the VHI [61,62,64]:

$$VHI = \alpha * VCI + (1 - \alpha) * TCI, \quad (4)$$

where α determines the share of VCI and TCI in the VHI. Since this share depending on location and time is unknown, the weight of both indices was assumed to be equal ($\alpha = 0.5$) [64–66]. The value range of the VHI is also from 0 (severe vegetation stress) to 100 (very favorable conditions). The VHI is based on the assumption that there is a negative correlation between NDVI and LST: During a drought period, the NDVI tends to be low, while the LST tends to be high [54].

In this work, all three drought indices were calculated pixel-based for Bavaria in 8-day resolution within the growing season (March–October) from 2001 to 2020. Due to the VHI assumption of a negative correlation between NDVI and LST, it is important to exclude all areas with a non-negative NDVI-LST correlation in order to avoid misinterpretations. For this purpose, a threshold value of -0.1 was applied to all monthly NDVI-LST correlation maps, and all areas with a correlation coefficient >-0.1 were then removed from the respective drought index time series on a monthly basis.

For the evaluation of the drought indices time series, TCI, VCI, and VHI were compared with the SMI and the yield data. For the comparison with the monthly SMI, we calculated the monthly arithmetic means of the 8-days drought indices, based on Table 1. Subsequently, the Bravais-Pearson correlation coefficients were determined between the SMI and the drought index data-sets for the complete time series (monthly and total vegetation period). Agricultural yield data comprised winter wheat, winter rye, summer barley, oat, sugar beet, winter rapeseed, and silage corn, i.e., major crops for which harvest dates in Bavaria were available and which were on average harvested at the end of July at the

earliest (Day of year > 200; Table 3). The reason for this threshold value was the inclusion of at least one month (July) in the evaluation, in which water can be assumed as the limiting factor for vegetation growth over large areas in Bavaria.

Table 3. List of selected crop yield data from the Regional Database Germany and the corresponding mean harvest dates (as the day of the year) from 2001 to 2019 in Bavaria in the evaluation study.

Selected Crops in The Yield Statistics (Regional Database Germany)	Mean Harvest Date (Day of The Year) in Bavaria from 2001 to 2019
Winter wheat	215
Winter rye	212
Summer barley	211
Oat	221
Sugar beet	283
Winter rapeseed	205
Silage corn	266

To be compared with crop yield data, drought indices were averaged pixel-wise and annually for a crop-specific period of influence, i.e., all months from May to July for winter wheat, winter rye, summer barley, oat, and winter rapeseed or May to September for sugar beet and silage corn. Then, mean drought indices were determined for each county. A correlation analysis was then performed between the mean annual drought indices and the respective relative annual yield anomaly at county level in Bavaria. These correlations were accordingly also determined within the counties. In order to avoid misinterpretations, counties, where, for a specific cultivated crop, the area share of the total area of the seven selected crops was less than 3%, were excluded from the spatial correlation analysis.

In order to summarize the results across the individual crops, an additional analysis was carried out based on weighted relative crop yield anomalies. For this purpose, the share of the total area of the seven selected crops was determined for each county and each crop. Subsequently, the respective annual crop yield anomalies were weighted with the area shares for each county and each year and summed up. In any case, years in which data were not available for all crops grown in that county were removed to ensure comparability. Mean annual drought indices (May to July or May to September) were also weighted at the county level according to the corresponding area shares of the crop and added up to obtain a weighted drought index. Finally, an overall correlation analysis, as well as a spatial correlation analysis differentiated by county between the relatively weighted crop yield anomalies and the weighted drought indices, were carried out.

3. Results

3.1. Correlations between NDVI and LST

As evidenced by the monthly correlation analysis between NDVI and LST for the period 2001 to 2020, NDVI-LST relationships clearly depend on several factors. The first factor is the time of the year. Across Bavaria (Figure 3 and Table S3), positive NDVI-LST correlations occurred above all both at the beginning (March to May) and at the end (September and October) of the vegetation period. In contrast, in the middle of the vegetation period or summer season (June to August), negative correlations prevailed. Regardless of the season, areas in the Alps, the Bavarian Forest, and the Spessart region showed consistently positive correlations, while negative correlations prevailed for the main part of the vegetation period within the Main-Franconian Plates or the Isar-Inn Hills.

This seasonal influence on the sign of the correlation between NDVI and LST was also confirmed when being classified by land cover, altitude, and their combination. Similarly, the correlation coefficients were higher at the beginning and end of the growing season than in the summer months of June, July, and August. Negative NDVI-LST correlations occurred especially in these summer months, while in the marginal months of March, April,

and October only positive correlations were observed in almost all classes (Figures 4 and 5; Table 4).

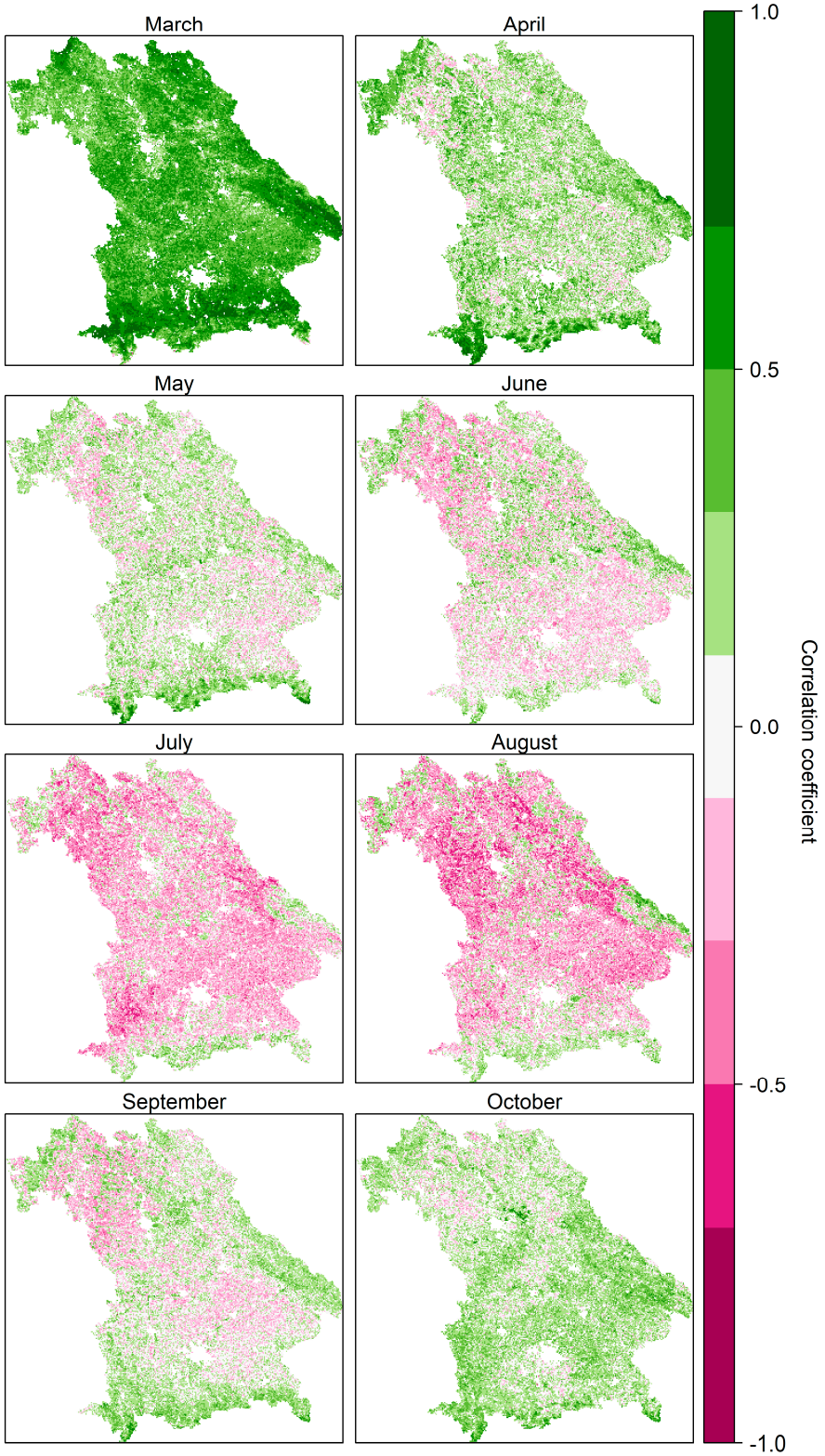

Figure 3. Pixel-based monthly correlation coefficients (Bravais-Pearson) between 8-day NDVI and LST in Bavaria from 2001 to 2020 during the vegetation period (March to October; corresponding *p*-values: Figure S4; corresponding scatterplots: Figure S5).

The second factor that significantly influences the NDVI-LST relationship is land cover (Figure 4) with a clear dichotomy of the results. Except for the marginal months of March and October, the medians of the correlation coefficients of the agricultural classes (non-irrigated arable land (NAL) and pastures (PAS)) were always significantly lower than those of the forest and grassland areas. While the agricultural areas showed predominantly negative correlation values, especially in summer (June, July, and August), none or only positive correlations occurred in the other classes.

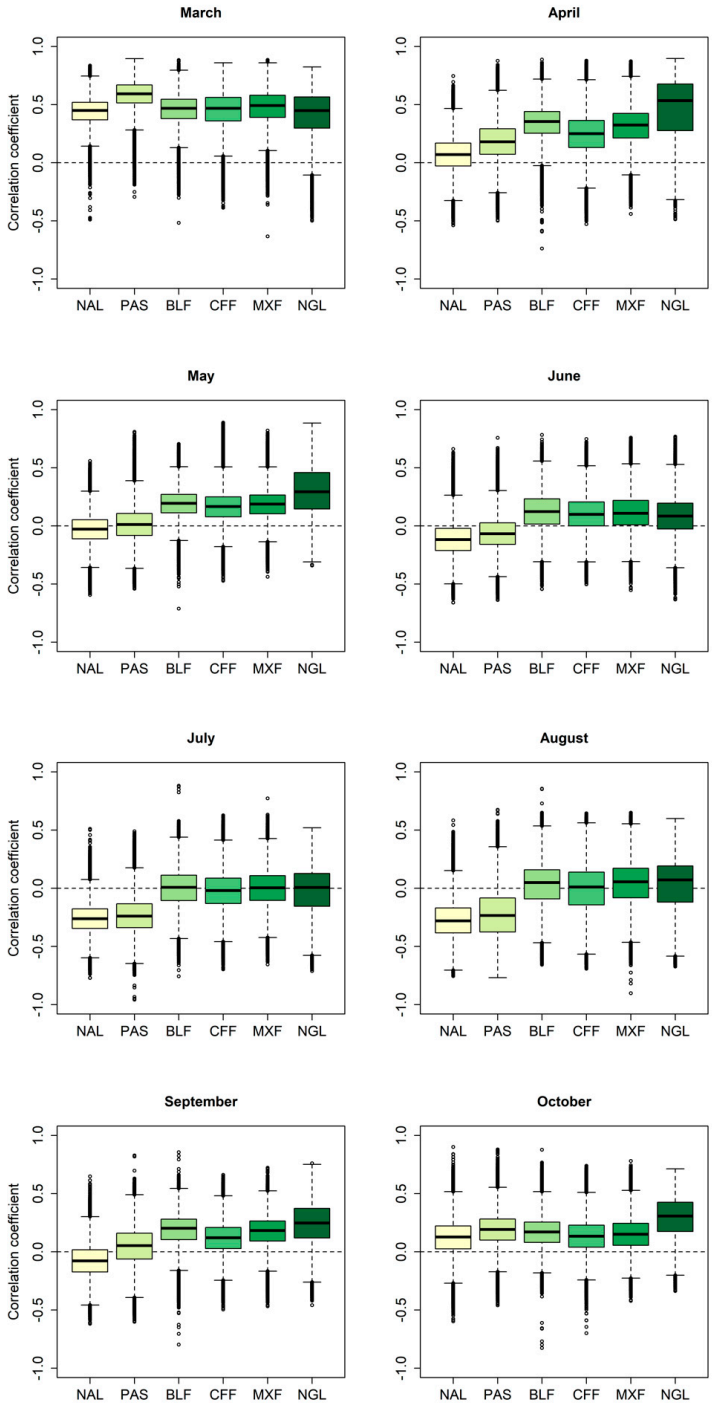

Figure 4. Pixel-based monthly correlation coefficients (Bravais-Pearson) between 8-day NDVI and LST by land cover in Bavaria from 2001 to 2020. Land cover classes according to CLC 2018 (Table 2) are non-irrigated arable land (NAL), pastures (PAS), broad-leaved forest (BLF), coniferous forest (CFF), mixed forest (MXF), and natural grasslands (NGL).

When combining the factors land cover and altitude (Table 4), natural grasslands (NGL) at lower altitudes, in addition to the agricultural classes NAL and PAS, also showed significantly lower correlation coefficients than the forest areas except for March and October. Altitudes below 800 m which constitute more than 90% of the total area were characterized by this negative NDVI-LST correlation in the summer months, while forest areas showed no or a slightly positive correlation in summer. Above 800 m the effect of the dichotomy decreased significantly since forests predominated.

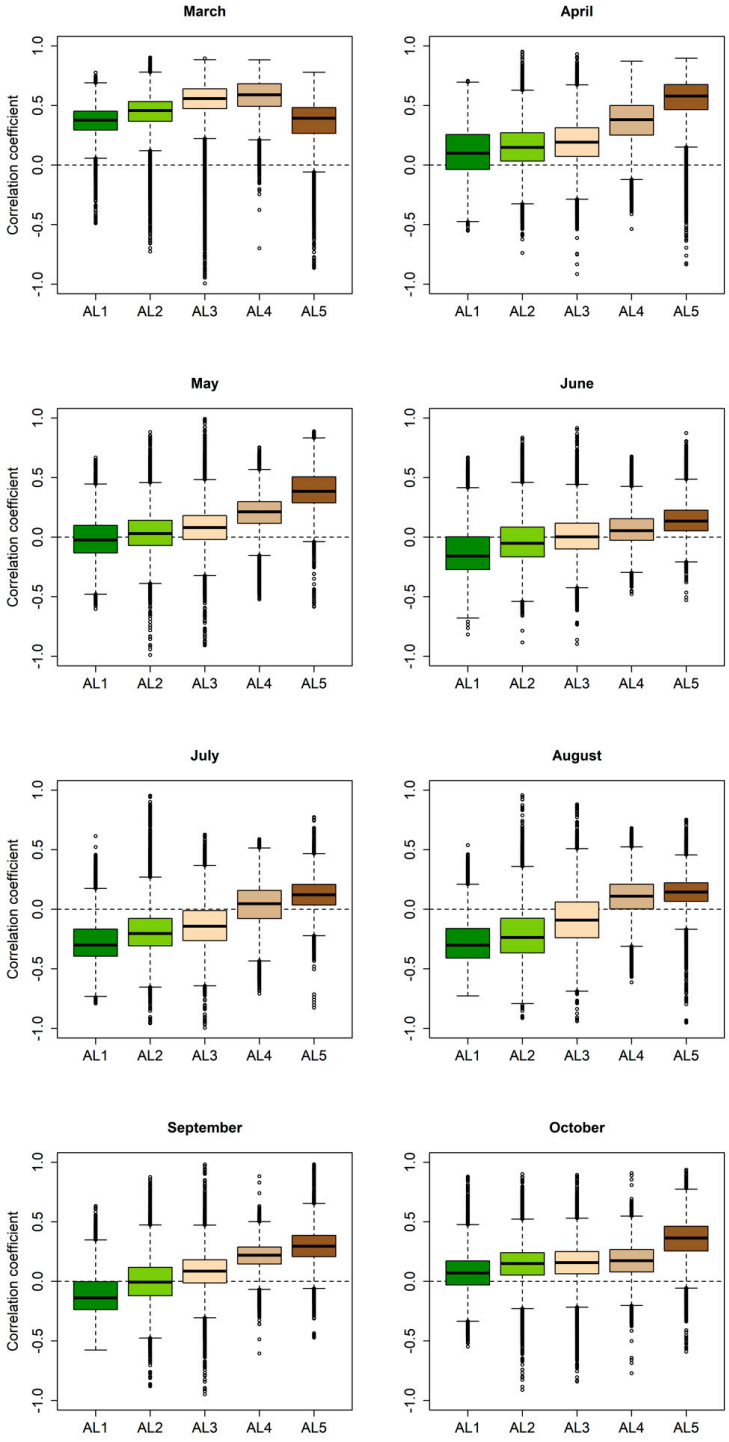

Figure 5. Pixel-based monthly correlation coefficients (Bravais-Pearson) between 8-day NDVI and LST by altitude levels in Bavaria from 2001 to 2020. Altitude levels (Table 2) are <300 m (AL1), 300–500 m (AL2), 500–800 m (AL3), 800–1200 m (AL4), and >1200 m (AL5).

Table 4. Median pixel-based monthly correlation coefficients (Bravais-Pearson) between NDVI and LST in Bavaria from 2001 to 2020, by altitude and land cover classes. The percentage (in parentheses) of the respective altitude class indicates the area share of this class in the total area of Bavaria. The percentage of the respective land cover class indicates the area share of this land cover in the total area of the respective altitude class. The color-coding of the individual median values is based on Figure 3. Land cover classes according to CLC 2018 are non-irrigated arable land (NAL), pastures (PAS), broad-leaved forest (BLF), coniferous forest (CFF), mixed forest (MXF), and natural grasslands (NGL). Altitude levels are <300 m (AL1), 300–500 m (AL2), 500–800 m (AL3), 800–1200 m (AL4), and >1200 m (AL5; Table 2).

Altitude	CLC 2018	Number of Pixels	March	April	May	June	July	August	September	October
AL1	**NAL**	240,901 (48.69%)	0.35	0.00	−0.09	−0.23	−0.35	−0.33	−0.19	0.01
(7.01%)	**PAS**	77,745 (15.71%)	0.46	0.19	0.01	−0.12	−0.29	−0.36	−0.14	0.12
	NGL	1650 (0.33%)	0.46	0.09	−0.01	−0.08	−0.43	−0.41	−0.19	0.15
	BLF	38,559 (7.79%)	0.42	0.32	0.16	0.08	−0.06	−0.06	0.12	0.18
	CFF	24,399 (4.93%)	0.31	0.31	0.16	0.14	−0.03	−0.05	0.13	0.12
	MXF	22,339 (4.51%)	0.36	0.38	0.17	0.14	−0.03	−0.02	0.14	0.18
AL2	**NAL**	1,603,322 (43.47%)	0.44	0.07	−0.03	−0.12	−0.26	−0.29	−0.08	0.14
(52.28%)	**PAS**	609,244 (16.52%)	0.55	0.16	−0.01	−0.09	−0.26	−0.33	−0.01	0.18
	NGL	13,274 (0.36%)	0.44	0.19	0.09	−0.03	−0.23	−0.29	0.08	0.16
	BLF	253,590 (6.88%)	0.45	0.35	0.19	0.14	−0.01	0.04	0.20	0.18
	CFF	627,277 (17.01%)	0.40	0.22	0.15	0.10	−0.05	−0.07	0.10	0.12
	MXF	239,313 (6.49%)	0.44	0.31	0.17	0.13	−0.02	−0.01	0.16	0.17
AL3	**NAL**	511,891 (22.01%)	0.51	0.09	0.00	−0.07	−0.24	−0.21	−0.02	0.14
(32.96%)	**PAS**	646,484 (27.80%)	0.64	0.18	0.02	−0.06	−0.22	−0.16	0.10	0.20
	NGL	8681 (0.37%)	0.61	0.24	0.11	0.00	−0.18	−0.15	0.10	0.17
	BLF	92,655 (3.98%)	0.53	0.34	0.19	0.12	0.00	0.05	0.20	0.15
	CFF	595,578 (25.61%)	0.53	0.24	0.16	0.10	−0.02	0.03	0.11	0.13
	MXF	254,112 (10.93%)	0.53	0.30	0.18	0.09	−0.01	0.06	0.17	0.13
AL4	**NAL**	0 (0.00%)	n.a.	n.a.	n.a.	n.a.	n.a.	n.a.	n.a.	n.a.
(5.51%)	**PAS**	95,015 (24.43%)	0.71	0.35	0.09	−0.02	−0.13	−0.02	0.21	0.23
	NGL	15,785 (4.06%)	0.60	0.54	0.27	0.03	−0.01	0.08	0.25	0.27
	BLF	37,420 (9.62%)	0.52	0.40	0.27	0.10	0.15	0.14	0.25	0.11
	CFF	129,960 (33.42%)	0.55	0.37	0.24	0.08	0.08	0.14	0.20	0.16
	MXF	94,833 (24.38%)	0.54	0.39	0.27	0.11	0.10	0.16	0.25	0.13
AL5	**NAL**	0 (0.00%)	n.a.	n.a.	n.a.	n.a.	n.a.	n.a.	n.a.	n.a.
(2.23%)	**PAS**	747 (0.47%)	0.34	0.69	0.43	0.13	0.13	0.16	0.29	0.40
	NGL	35,529 (22.58%)	0.34	0.66	0.46	0.17	0.10	0.16	0.36	0.42
	BLF	8214 (5.22%)	0.47	0.51	0.32	0.08	0.16	0.14	0.25	0.24
	CFF	58,431 (37.14%)	0.42	0.53	0.34	0.11	0.14	0.14	0.27	0.31
	MXF	14,883 (9.46%)	0.47	0.53	0.34	0.10	0.16	0.13	0.28	0.27

Thirdly, monthly NDVI-LST correlations vary with altitude in Bavaria (Figure 5). Except for the altitude level above 1200 m in March, the correlation coefficients increased continuously with altitude in all months. Negative correlations were on average only achieved at altitudes up to 800 m, and at altitudes below 300 m, the median of the correlation coefficients was clearly negative (from June to September). When combining altitude and land cover classes (Table 4), the results of the simple altitude classification were confirmed, whereby here even negative correlations could occur up to 1200 m in the median (July). Finally, it is important to note that hardly any strong relationships are observed within the NDVI-LST correlation analysis with respect to all described perspectives.

3.2. Drought Indices VCI, TCI, and VHI and Their Evaluation Results

Figure 6 is showing the prominent drought year 2003 as an example: The VHI is a clear combination of both indices, with weeks of low drought stress taking higher values (e.g., day 129) and weeks of high drought stress taking lower values (e.g., day 193–233). The TCI basically changes more dynamically than the VCI, both spatially and temporally. From the 20-year time series of the VCI, TCI, and VHI, all areas with a monthly mean NDVI-LST correlation coefficient >-0.1 had to be removed. While in the summer months of July and August a large part of the area was still retained (62.25 and 58.83%, respectively), in the marginal months of March (0.15%), April (8.00%), and October (5.95%) hardly any area was included in the analysis. The months of May (18.15%), June (34.31%), and September (24.04%) represented intermediate stages, in which mainly focal areas in the south-east and north-west of Bavaria were included in the analysis (Figure S6 and Table S3).

When evaluating for the above described sensitive areas the drought indices TCI, VCI, and VHI with the SMI (Table 5), several observations could be made. Over the entire growing season, similar ranges of values were found for the correlation coefficients of SMI with TCI (0.54) or VHI (0.48), while the one between VCI and SMI was considerably lower (0.27). This tendency of lower VCI than TCI/VHI correspondence to SMI could be observed across all months, especially in the summer months of July and August. Generally, the MODIS-based drought indices corresponded much better to the SMI in summer than at the beginning and end of the growing season.

Table 5. Bravais-Pearson correlation coefficients between Soil Moisture Index (SMI) and the MODIS-based drought index data sets for the complete time series from 2001 to 2020 (monthly and total). All correlation coefficients are statistically significant (p-value < 0.05). The corresponding scatterplots for the complete time series (March to October) are included in Figure S7.

SMI vs.	TCI	VCI	VHI
March	0.26	0.09	0.25
April	0.52	0.11	0.37
May	0.38	0.16	0.32
June	0.34	0.15	0.30
July	0.63	0.26	0.52
August	0.69	0.37	0.61
September	0.47	0.38	0.51
October	0.07	0.05	0.08
Total	**0.54**	**0.27**	**0.48**

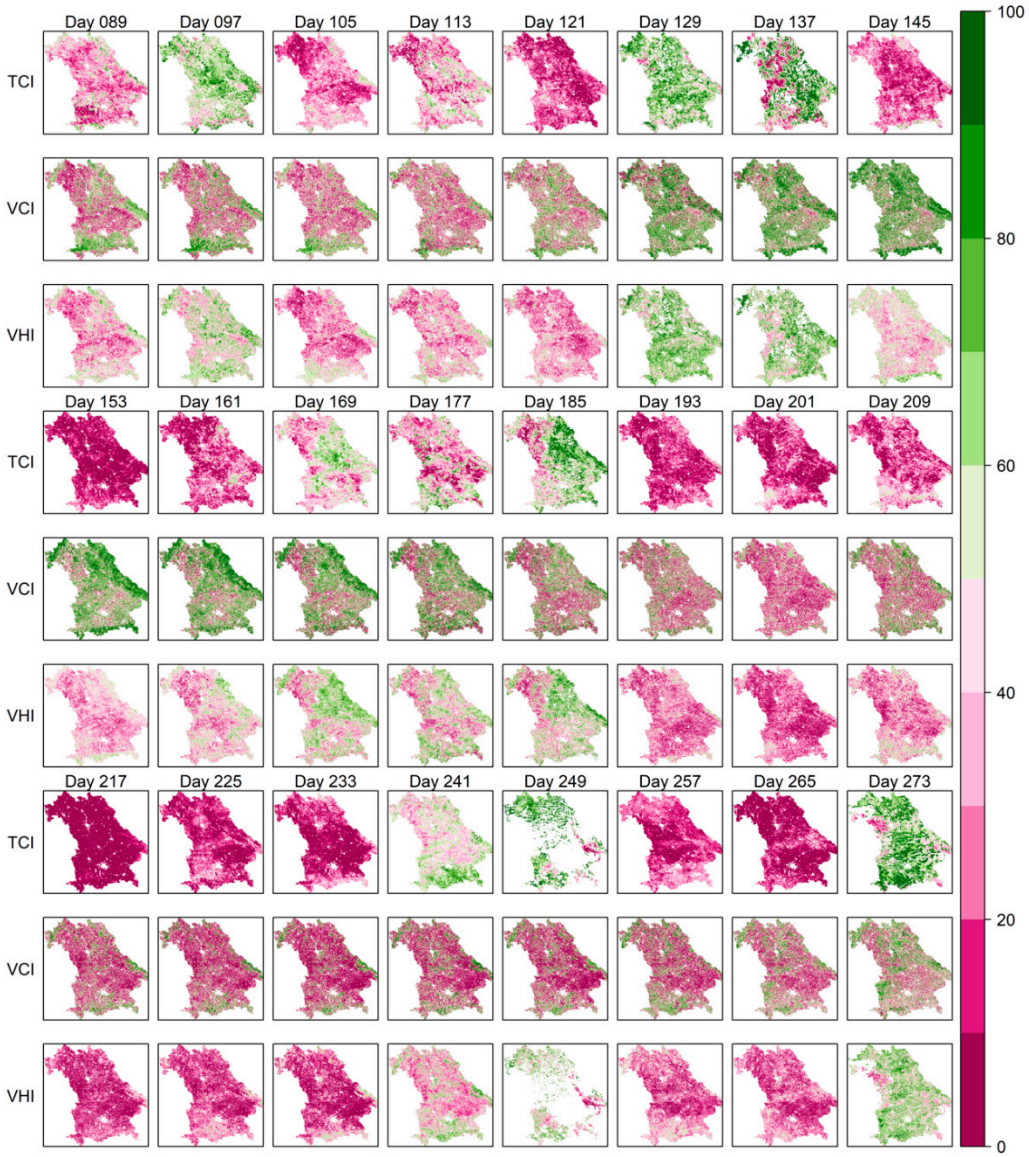

Figure 6. TCI, VCI, and VHI in Bavaria in the drought year 2003 from day 089 (30 March) to day 273 (30 September).

When comparing the MODIS-based drought indices with annual yield data for different crops, positive correlations of varying strength were found (Table 6). In contrast to SMI, the correlations of all the three drought indices with the yield anomalies were in a similar value range, e.g., across all field crops as indicated by the weighted yield; they ranged between 0.45 (VCI) and 0.49 (VHI). Additionally for the individual crops, no obvious differences were apparent among TCI, VCI, and VHI correspondence to yield anomalies. However, the correlation varied considerably for individual crops. While especially winter wheat, summer barley, and winter rapeseed showed low positive correlations, the correlations of sugar beet and silage corn were high.

The correlations between weighted crop yield anomalies and the corresponding TCI, VCI, and VHI at county level highlighted spatial patterns across Bavaria (Figures 7c and S9e,f). Similar to Table 6, for each of the drought indices, almost all correlations were positive, with significant variations across counties. There were hardly any differences between the maps of the individual drought indices. However, all counties in the north of Bavaria tended to have higher correlation values than southern areas. Another focus area with positive correlations was the northwest of Bavaria, with statistically significant correlations

>0.8. One county in the south, was also striking, showing a slight to medium negative linear correlation for all the three drought indices.

Table 6. Bravais-Pearson correlation coefficients (r) between crop-specific mean drought index values and the respective annual field crop or weighted yield anomalies (county level). All correlation coefficients are statistically significant (p-value < 0.05). The corresponding scatterplots between weighted yield anomaly and weighted annual mean drought index are included in Figure S8.

r	Winter Wheat	Winter Rye	Summer Barley	Oat	Sugar Beet	Winter Rapeseed	Silage Corn	Weighted Yield
TCI	0.12	0.34	0.10	0.28	0.38	0.10	0.62	**0.47**
VCI	0.21	0.25	0.19	0.25	0.50	0.09	0.51	**0.45**
VHI	0.16	0.33	0.14	0.28	0.46	0.10	0.61	**0.49**

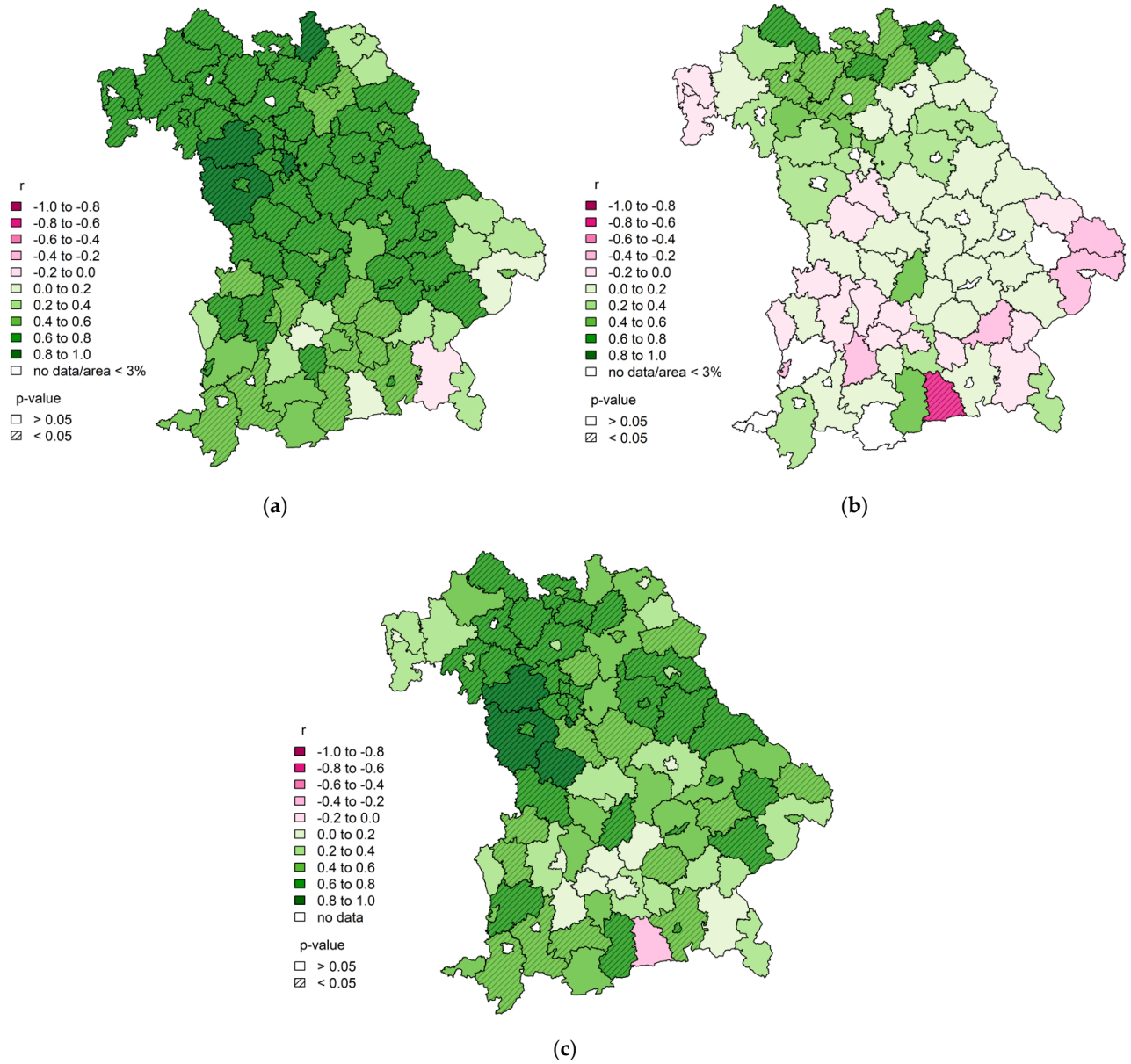

Figure 7. Bravais-Pearson correlation coefficients between (**a**) the relative annual silage corn yield anomalies and the annual mean VHI, (**b**) the relative annual winter wheat yield anomalies and the annual mean VHI, and (**c**) the annual relatively weighted crop yield anomalies and the annual weighted VHI differentiated by county. The corresponding maps with TCI and VCI are provided in Figure S9.

Within the correlation maps between the individual field crop yield anomalies and the drought indices TCI, VCI, and VHI, clear differences could be recognized depending on the crop type (Figures 7a,b and S9–S12). While silage corn, oats, winter rye, and sugar beet showed a homogeneous picture of positive correlations, winter wheat, winter rapeseed, and summer barley showed a predominantly heterogeneous picture of positive and negative correlations. In addition, it became clear that the correlations in northern Bavaria generally had higher values than in the south. The strongly negative outlier in the southern county was also confirmed in the maps of individual crops. In contrast, there were hardly any notable differences between the individual drought indices. In conclusion, it must also be noted within this subsection that, as with the NDVI-LST correlation analysis, few strong relationships emerged in the evaluation of the drought indices.

4. Discussion

This study addresses three research questions that are not satisfactorily answered in the current literature. First, it provides results with much better spatial and temporal resolution than the current one to determine where and when water is the limiting factor for vegetation growth in Central Europe. Second, the analysis of this constraint incorporates other environmental conditions to explain it, which has rarely been the case before. Finally, an approach not yet practiced in Bavaria is presented to perform continuous drought monitoring using remote sensing-based VIs at appropriate spatial and temporal resolution.

Our study showed that the correlation between NDVI and LST depends on the season, land cover, and altitude, and that the TCI and VHI correlate well with both soil moisture and yield data in Bavaria. Considering that the NDVI-LST correlation is negative when water is the limiting factor for vegetation growth and positive when energy is the limiting factor, several conclusions can be drawn from the results presented. In Bavaria, this relationship is, firstly, dependent on the season: At the beginning and end of the vegetation period the correlation between NDVI and LST is predominantly positive, whereas in the summer months it is predominantly negative. Accordingly, the primary growth-limiting factor of energy is replaced by the factor of water, especially in July and August. This seasonal dependence of the NDVI-LST relationship has already been demonstrated globally, for example in China [67] and North America [54,55] and even both from temporal and spatial perspectives in Europe [36], although not in such a detailed spatial and temporal resolution.

Classifying the correlations according to land cover, it is noticeable that only agricultural land and grassland show negative NDVI-LST correlations in the summer months, while forest shows none or only positive correlations throughout the year. This indicates that forests have a greater water storage capacity and/or a higher resilience to drought stress than agricultural plants and grasses. Accordingly, the growth of forests in Bavaria in summer seems in this study primarily energy-limited, while water is the primary limiting factor for arable plants and grasses. However, it is important to emphasize that this is an averaging analysis over 20 years: Extreme drought years also affect forest areas in Central Europe and are associated with tree mortality [9,68].

The fact that the relationship between NDVI and LST varies depending on the land cover or vegetation type has also already been demonstrated in several regions of interest, e.g., on the Iberian Peninsula [69], in the Arctic [70], Mongolia [71], and North America [54]. The differences in forest areas and other vegetation types have only been investigated in Mongolia [71] and North America [54]. Similar correlation differences were found in Mongolia as well, although the analysis does not include seasonal differentiation. In North America, it was also shown that forest areas are less prone to negative NDVI-LST correlations than agricultural areas or grasslands. However, the different data, classification, and geographical conditions must be taken into account when making these comparisons.

The third factor that significantly influences the relationship between NDVI and LST is altitude. An increase in the correlation coefficient between NDVI and LST with altitude has similarly been observed in other parts of the world before, for example in North America [54], Mongolia [71], and Europe [36].

Additionally, in Bavaria the correlation coefficient increases with altitude in all months, with negative correlations only occurring below 800 m a.s.l. on average. Thus, especially in summer at low altitudes in Bavaria (<800 m), water is the primary limiting factor for vegetation growth, while above this altitude energy continues to be the primary factor.

Looking at the calculated drought index maps from TCI, VCI, and VHI (Figure 6), it can be seen that MODIS data can primarily capture the temporal and spatial dynamics of NDVI and LST. Comparing this with drought index calculations from other satellites (e.g., [72,73]), this is an advantage in drought monitoring, especially in the temporal dimension. However, some compromises have to be made within the spatial resolution. In general, it can thus be argued that MODIS data are particularly useful for near-real-time drought monitoring, while general classifications at selected time periods with high spatial resolution are more useful with other platforms.

When evaluating the drought indices TCI, VCI, and VHI, with the soil moisture index, two aspects are particularly relevant. Firstly, TCI and VHI show higher correlations with soil moisture than VCI, with TCI resulting in the highest correlation overall. It can be concluded from this that surface temperature generally reacts faster to changes in soil moisture than vegetation state. Further studies with similar methodology exist mainly for Asia and North America. Positive correlations between soil moisture and VHI have been observed also in [74–76]. In Mongolia, the correlation between TCI and soil moisture is higher than that for VCI, firstly, at different soil depths (but only with lagged measurements) [77] and secondly, in areas with predominant vegetation cover [78]. In China, soil moisture measurements and TCI also correlate higher than VCI in different months [79]. A similar picture emerges for rice fields in Vietnam, and only on forest land do both indices show a similar soil moisture correlation [80]. The results for Bavaria are thus largely supported in other regions of the world.

The second relevant aspect of the correlation analysis between soil moisture and the drought indices is the seasonal course. In summer, all indices correlate more strongly with soil moisture than at the beginning and end of the vegetation period. This suggests that soil moisture in summer has a stronger influence on both the surface temperature and the status of the vegetation. This can be explained by the fact that water is the primary limiting factor for plant growth in the warmer or hot summer months when the biomass to be sustained is high: If soil moisture shows negative or positive anomalies in summer, this has a stronger influence on the water balance of the vegetation and thus also on the temperature [81] than in the other seasons, in which energy is the primary limiting factor.

When comparing the agricultural yield data with the drought indices, three aspects are particularly central. Firstly, all three indices (TCI, VCI, and VHI) show similarly high positive correlations in general, i.e., as indicated in the weighted yields. Also, there is no general tendency for the superiority of any index for the individual crops. All three indices thus reflect the annual anomaly of agricultural yields in Bavaria well. Two aspects are noticeable here: VHI shows only slightly superior correlations here than its two components separately. On the other hand, VCI and TCI correlate with yield at the same level, although VCI is assumed to have a much more direct link to agricultural yield via NDVI than the TCI via LST. This suggests that drought, which is reflected in higher than normal vegetation thermal conditions, was the main cause of yield losses in the study area. Other correlation studies in Europe involving yield data have also shown positive correlations with the three drought indices almost without exception [61,64,82,83]. However, a direct comparison is usually difficult due to the different methodologies, data situations, selected crops, and geographical locations. When comparing with the most methodologically similar study by Bachmair et al. [28], the results are confirmed in terms of both correlation strength and spatial distribution, although in the other study the VCI shows slightly higher correlations than the VHI. The added value in the present paper compared to this study is mainly the analysis of several crops and the inclusion of the TCI.

The second aspect worth mentioning is the difference in correlation strength between the individual crops. Especially sugar beet and silage corn show higher correlations than

the others, which can be explained primarily in the monitoring period: While most crops are harvested at the end of July/beginning of August, sugar beet and silage corn are harvested at the end of September/beginning of October (Table 3). Thus, for these two crops, more growing time and area (especially in August) is included in the correlation analysis, which is obviously reflected in the drought indices. In comparison with other studies, it is noticeable that winter wheat yields in north-eastern Germany [32] show higher correlations with the VIs used than in Bavaria. The decisive difference here, however, is in the methodological choice to include only relevant areas in north-eastern Germany in the monitoring or the correlation analysis, whereas in our study all vegetation areas with negative NDVI-LST correlation were included. Our results of the yields for wheat and barley in connection with the drought indices are also confirmed by a Europe-wide temporal correlation analysis between NDVI and wheat and barley yields [84]. Here, both correlations in Germany decrease significantly from June onwards (Day 153) and reach similar value ranges as in our analysis.

The third and last aspect to be noted is the spatial difference within the correlation analysis. The general impression is that for all indices and crops the correlation between yield and drought index is higher in northern/eastern Bavaria than in southern Bavaria. The reason for this can be traced in the different precipitation conditions (Figure S3): In drier northern Bavaria, the sensitivity of both the drought indices and agricultural yields to a change in the water balance is higher than that in wetter southern Bavaria. The higher sensitivity causes a higher correlation and thus a stronger relationship between the two variables.

Nevertheless, certain limitations of this study should be noted. The spatial resolution of the underlying data should be thoroughly considered. Due to the small-scale features of the landscape in Bavaria, mixed pixels often occur, especially in the remote sensing data, which can lead to inaccuracies both in the correlation analysis between NDVI and LST and in the index calculation. Within the evaluation data, this indication is equally true for both the soil moisture data (4 km) and the agricultural yield data (county level). In addition, it must be noted that the data in this paper show significant differences within temporal and spatial resolution. In order to match the data, they are adjusted on both levels (e.g., via resampling or interpolation). This causes additional inaccuracies and could be an explanation for partially low correlations within the results. In addition, the assumption of a 19-year identical distribution of crop shares within the counties introduces—to some extent—further uncertainties.

Another aspect worth discussing is the general use of VIs for estimating vegetation growth and the application of NDVI in particular. Thus, VIs only ever provide an indirect vegetation proxy, and several limitations must be considered here: On the one hand, detection on heterogeneous surfaces and at different canopy heights is problematic, and on the other hand, factors such as sensor calibration, sensor viewing conditions, solar illumination geometry and soil moisture, also influence the data quality of the indices [85–87]. NDVI in particular is one of the most widely used vegetation indices and thus offers a wide range of comparisons. It allows a large number of estimations of different vegetation properties and, in addition, it has a sensitivity to green vegetation even on areas with low vegetation cover. Nevertheless, the NDVI also brings uncertainties in the detection due to the influence of soil brightness, soil color, clouds and cloud shadows as well as leaf canopy shadows and a saturation problem in the presence of high vegetation diversity [86,88–90].

From a methodological point of view, two aspects, in particular, should always be kept in mind: Firstly, the application of the drought indices is in part severely limited in terms of area due to the threshold value set for the correlation coefficient between NDVI and LST (which refers to the entire period and partially masks individual drier years). The evaluation of the indices is thus only of limited significance, especially in the marginal months of the vegetation period and in counties with little area included. On the other hand, the area included in the analysis is always the same when evaluating the

drought indices with the individual crop yields and no differentiation is made between the individual crops.

5. Conclusions

In this study, we aimed at identifying by means of a correlation analysis between NDVI and LST when and where in Bavaria vegetation growth is primarily water-limited and how this is related to the factors of land cover and altitude. In addition, we investigated whether and to what extent the remote sensing-based drought indices TCI, VCI, and VHI can capture agricultural drought and yield losses within these areas. The indices were calculated from 2001 to 2020 within the growing season and evaluated with both soil moisture and yield anomalies of agricultural crops.

We found that in Bavaria, especially in the summer months of July and August, on agricultural land and grassland and below 800 m, water is the primary limiting factor for plant growth. Within these areas and periods, the remote sensing-based drought indices TCI and VHI correlate strongly with soil moisture and agricultural yield anomalies. From both a soil- and a vegetation-based perspective, both indices have the potential to detect agricultural and vegetation-based drought, respectively.

However, there are also further research potentials within this thematic focus. With regard to the LST-NDVI relationship, it would be particularly interesting to include in the correlation analysis other relevant variables, such as evapotranspiration, precipitation, and global radiation and to specifically analyze individual drought years with regard to this relationship. Within the evaluation of the drought indices, further soil- and vegetation-related variables could be included in the analysis. In addition, a temporally differentiated (e.g., monthly) correlation analysis between the drought indices and the field crop yield anomalies would be desirable to determine possible seasonal focal points in the context.

Supplementary Materials: The following are available online at https://www.mdpi.com/article/10.3390/rs13193907/s1, Figure S1: Map of altitude distribution in Bavaria, Figure S2: Overview map of mean annual air temperature (2 m) for Bavaria from 1991 to 2020, Figure S3: Overview map of mean annual precipitation sum in Bavaria from 1991 to 2020, Table S1: Simplified land cover classification according to CLC 2018 classification applied in Figure 2, Table S2: Classification of the MCD12Q1 International Geosphere-Biosphere Programme (IGBP) classes into the vegetation mask and the non-vegetation mask, Figure S4: P-values of the pixel-based monthly correlation coefficients (Bravais-Pearson) between NDVI and LST in Bavaria from 2001 to 2020 during the vegetation period, Table S3: Pixel-based monthly correlation coefficients (Bravais-Pearson) between NDVI and LST in Bavaria from 2001 to 2020 during the vegetation period, Figure S5: Pixel-based scatterplot between 8-day NDVI and LST in Bavaria from 2001 to 2020 in March, April, May, June, July, August, September, and October, Figure S6: Pixel-based monthly correlation coefficients (Bravais-Pearson) between NDVI and LST in Bavaria from 2001 to 2020 during the vegetation period, Figure S7: Pixel-based scatterplot between SMI and TCI, VCI and VHI in Bavaria from 2001 to 2020, Figure S8: Scatterplot between weighted yield anomaly and weighted annual mean TCI, VCI and VHI in Bavaria from 2001 to 2019, Figure S9: Bravais-Pearson correlation coefficients between the relative annual silage corn yield anomalies and the annual mean TCI or VCI, the relative annual winter wheat yield anomalies and the annual mean TCI or VCI, and the annual relatively weighted crop yield anomalies and the annual weighted TCI or VCI differentiated by county, Figure S10: Bravais-Pearson correlation coefficients between the relative annual oat yield anomalies and the annual mean TCI/VCI/VHI and the relative annual winter rapeseed yield anomalies and the annual mean TCI/VCI/VHI differentiated by county, Figure S11: Bravais-Pearson correlation coefficients between the relative annual summer barley yield anomalies and the annual mean TCI/VCI/VHI and the relative annual winter rye yield anomalies and the annual mean TCI/VCI/VHI differentiated by county, Figure S12: Bravais-Pearson correlation coefficients between the relative annual sugar beet yield anomalies and the annual mean TCI/VCI/VHI differentiated by county.

Author Contributions: Conceptualization, S.K. and A.M.; methodology, S.K., Y.Y., M.C. and A.M.; software, S.K.; validation, S.K., Y.Y. and A.M.; formal analysis, S.K.; investigation, S.K.; data curation, S.K.; writing—original draft preparation, S.K.; writing—review and editing, S.K., Y.Y., M.C. and A.M.;

visualization, S.K.; supervision, A.M.; project administration, A.M.; funding acquisition, A.M. All authors have read and agreed to the published version of the manuscript.

Funding: This study was performed using the framework of the project BAYSICS (Bavarian Citizen Science Portal for Climate Research and Science Communication), which is sponsored by the Bavarian State Ministry of Science and the Arts in the context of the Bavarian Climate Research Network (bayklif). M. Castelli was partially funded by the project ADO, Alpine Drought Observatory, 2019–2022, co-financed by the European Regional Development Fund through the Interreg Alpine Space program.

Institutional Review Board Statement: Not applicable.

Informed Consent Statement: Not applicable.

Data Availability Statement: Publicly available datasets were analyzed in this study. This data can be found here: [MODIS NDVI] LP DAAC. 2021. MCD12Q1 v006; https://lpdaac.usgs.gov/products/mcd12q1v006/ (access on 8 July 2021); [MODIS LST] LP DAAC. 2021. MOD11A2 v006; https://lpdaac.usgs.gov/products/mod11a2v006/ (access on 8 July 2021); [MODIS LC] LP DAAC. 2021. MOD13Q1 v006; https://lpdaac.usgs.gov/products/mod13q1v006/ (access on 8 July 2021); [CLC 2018] Copernicus Land Monitoring Service. 2020. Corine Land Cover (CLC) 2018, Version 2020_20u1; https://land.copernicus.eu/pan-european/corine-land-cover/clc2018?tab=download (access on 8 July 2021); [EU-DEM] Copernicus Land Monitoring Service. 2016. European Digital Elevation Model (EU-DEM), version 1.1; https://land.copernicus.eu/imagery-in-situ/eu-dem/eu-dem-v1.1?tab=download (access on 8 July 2021); [SMI] UFZ-Dürremonitor/Helmholtz-Zentrum für Umweltforschung. 2020. SMI data 1951–2020; https://www.ufz.de/index.php?de=37937 (access on 8 July 2021); [yield data for agricultural crops] Statistische Ämter des Bundes und der Länder. 2021. 41241-Ernte- und Betriebsberichterstattungen (EBE); https://www.regionalstatistik.de/genesis/online?operation=statistic&levelindex=0&levelid=1619013679238&code=41241&option=table&info=on#abreadcrumb (access on 8 July 2021); [land use data for the agricultural holdings] Bayerisches Landesamt für Statistik. 2018. Bodennutzung der landwirtschaftlichen Betriebe in Bayern 2016; https://www.statistik.bayern.de/mam/produkte/veroffentlichungen/statistische_berichte/c1101c_201651_25313.pdf (access on 8 July 2021); [harvest dates] DWD Climate Data Center (CDC). 2021. Phenological observations of crops from sowing to harvest (annualreporters, historical), Version v006; https://opendata.dwd.de/climate_environment/CDC/observations_germany/phenology/annual_reporters/crops/historical/ (access on 8 July 2021).

Acknowledgments: The authors would like to thank the Land Processes Distributed Active Archive Center (LP DAAC), the European Environment Agency (EEA), the UFZ Drought Monitor/Helmholtz Centre for Environmental Research, the Statistical Offices of the Federation and the states, the Bavarian State Office for Statistics, and the DWD Climate Data Center (CDC) for making the data freely available.

Conflicts of Interest: The authors declare no conflict of interest.

References

1. Heim, R.R. A Review of Twentieth-Century Drought Indices Used in the United States. *Bull. Am. Meteor. Soc.* **2002**, *83*, 1149–1166. [CrossRef]
2. Dai, A. Drought under global warming: A review. *WIREs Clim Chang.* **2011**, *2*, 45–65. [CrossRef]
3. Wilhite, D.A. (Ed.) Drought as a Natural Hazard: Concepts and Definitions. In *Drought: A Global Assessment*; Routledge: London, UK, 2000; pp. 3–18.
4. Wilhite, D.A.; Glantz, M.H. Understanding: The Drought Phenomenon: The Role of Definitions. *Water Int.* **1985**, *10*, 111–120. [CrossRef]
5. European Environment Agency. Mapping the Impacts of Natural Hazards and Technological Accidents in Europe: An Overview of the Last Decade. Available online: https://www.eea.europa.eu/publications/mapping-the-impacts-of-natural (accessed on 21 May 2021).
6. DG Environment—European Commission. Water Scarcity and Droughts: Second Interim Report. Available online: https://ec.europa.eu/environment/water/quantity/pdf/comm_droughts/2nd_int_report.pdf (accessed on 21 May 2021).
7. Cammalleri, C.; Naumann, G.; Mentaschi, L.; Formetta, G.; Forzieri, G.; Gosling, S.; Bisselink, B.; de Roo, A.; Feyen, L. *Global Warming and Drought Impacts in the EU*; Publications Office of the European Union: Luxembourg, 2020; ISBN 978-92-76-12947-9.

8. Buras, A.; Schunk, C.; Zeiträg, C.; Herrmann, C.; Kaiser, L.; Lemme, H.; Straub, C.; Taeger, S.; Gößwein, S.; Klemmt, H.-J.; et al. Are Scots pine forest edges particularly prone to drought-induced mortality? *Environ. Res. Lett.* **2018**, *13*, 25001. [CrossRef]
9. Schuldt, B.; Buras, A.; Arend, M.; Vitasse, Y.; Beierkuhnlein, C.; Damm, A.; Gharun, M.; Grams, T.E.; Hauck, M.; Hajek, P.; et al. A first assessment of the impact of the extreme 2018 summer drought on Central European forests. *Basic Appl. Ecol.* **2020**, *45*, 86–103. [CrossRef]
10. de Bono, A.; Peduzzi, P.; Kluser, S.; Giuliani, G. Impacts of Summer 2003 Heat Wave in Europe. Available online: https://archive-ouverte.unige.ch/unige:32255 (accessed on 1 June 2021).
11. Bavarian State Ministry for the Environment and Consumer Protection. Klima-Report Bayern 2021: Klimawandel, Auswirkungen, Anpassungs- und Forschungsaktivitäten. Available online: https://www.bestellen.bayern.de/application/eshop_app000000?SID=961655746&DIR=eshop&ACTIONxSETVAL(artdtl.htm,APGxNODENR:1325,AARTxNR:stmuv_klima_012,AARTxNODENR:358070,USERxBODYURL:artdtl.htm,KATALOG:StMUG,AKATxNAME:StMUG,ALLE:x)=X (accessed on 20 July 2021).
12. Bakke, S.J.; Ionita, M.; Tallaksen, L.M. The 2018 northern European hydrological drought and its drivers in a historical perspective. *Hydrol. Earth Syst. Sci.* **2020**, *24*, 5621–5653. [CrossRef]
13. Ionita, M.; Tallaksen, L.M.; Kingston, D.G.; Stagge, J.H.; Laaha, G.; van Lanen, H.A.J.; Scholz, P.; Chelcea, S.M.; Haslinger, K. The European 2015 drought from a climatological perspective. *Hydrol. Earth Syst. Sci.* **2017**, *21*, 1397–1419. [CrossRef]
14. Schär, C.; Vidale, P.L.; Lüthi, D.; Frei, C.; Häberli, C.; Liniger, M.A.; Appenzeller, C. The role of increasing temperature variability in European summer heatwaves. *Nature* **2004**, *427*, 332–336. [CrossRef] [PubMed]
15. Hari, V.; Rakovec, O.; Markonis, Y.; Hanel, M.; Kumar, R. Increased future occurrences of the exceptional 2018-2019 Central European drought under global warming. *Sci. Rep.* **2020**, *10*, 12207. [CrossRef]
16. Hänsel, S.; Ustrnul, Z.; Łupikasza, E.; Skalak, P. Assessing seasonal drought variations and trends over Central Europe. *Adv. Water Resour.* **2019**, *127*, 53–75. [CrossRef]
17. Spinoni, J.; Naumann, G.; Vogt, J.V. Pan-European seasonal trends and recent changes of drought frequency and severity. *Glob. Planet. Chang.* **2017**, *148*, 113–130. [CrossRef]
18. Stagge, J.H.; Kingston, D.G.; Tallaksen, L.M.; Hannah, D.M. Observed drought indices show increasing divergence across Europe. *Sci. Rep.* **2017**, *7*, 14045. [CrossRef] [PubMed]
19. Vicente-Serrano, S.M.; Domínguez-Castro, F.; Murphy, C.; Hannaford, J.; Reig, F.; Peña-Angulo, D.; Tramblay, Y.; Trigo, R.M.; Mac Donald, N.; Luna, M.Y.; et al. Long-term variability and trends in meteorological droughts in Western Europe (1851–2018). *Int. J. Climatol.* **2021**, *41*, E690–E717. [CrossRef]
20. Spinoni, J.; Barbosa, P.; Bucchignani, E.; Cassano, J.; Cavazos, T.; Christensen, J.H.; Christensen, O.B.; Coppola, E.; Evans, J.; Geyer, B.; et al. Future Global Meteorological Drought Hot Spots: A Study Based on CORDEX Data. *J. Clim.* **2020**, *33*, 3635–3661. [CrossRef]
21. Spinoni, J.; Vogt, J.V.; Naumann, G.; Barbosa, P.; Dosio, A. Will drought events become more frequent and severe in Europe? *Int. J. Climatol.* **2018**, *38*, 1718–1736. [CrossRef]
22. Ruosteenoja, K.; Markkanen, T.; Venäläinen, A.; Räisänen, P.; Peltola, H. Seasonal soil moisture and drought occurrence in Europe in CMIP5 projections for the 21st century. *Clim. Dyn.* **2018**, *50*, 1177–1192. [CrossRef]
23. Grillakis, M.G. Increase in severe and extreme soil moisture droughts for Europe under climate change. *Sci. Total Environ.* **2019**, *660*, 1245–1255. [CrossRef]
24. West, H.; Quinn, N.; Horswell, M. Remote sensing for drought monitoring & impact assessment: Progress, past challenges and future opportunities. *Remote Sens. Environ.* **2019**, *232*, 111291. [CrossRef]
25. Hazaymeh, K.; Hassan, Q.K. Remote sensing of agricultural drought monitoring: A state of art review. *AIMS Environ. Sci.* **2016**, *3*, 604–630. [CrossRef]
26. AghaKouchak, A.; Farahmand, A.; Melton, F.S.; Teixeira, J.; Anderson, M.C.; Wardlow, B.D.; Hain, C.R. Remote sensing of drought: Progress, challenges and opportunities. *Rev. Geophys.* **2015**, *53*, 452–480. [CrossRef]
27. Afshar, M.H.; Al-Yaari, A.; Yilmaz, M.T. Comparative Evaluation of Microwave L-Band VOD and Optical NDVI for Agriculture Drought Detection over Central Europe. *Remote Sens.* **2021**, *13*, 1251. [CrossRef]
28. Bachmair, S.; Tanguy, M.; Hannaford, J.; Stahl, K. How well do meteorological indicators represent agricultural and forest drought across Europe? *Environ. Res. Lett.* **2018**, *13*, 34042. [CrossRef]
29. Peled, E.; Dutra, E.; Viterbo, P.; Angert, A. Technical Note: Comparing and ranking soil drought indices performance over Europe, through remote-sensing of vegetation. *Hydrol. Earth Syst. Sci.* **2010**, *14*, 271–277. [CrossRef]
30. Buitink, J.; Swank, A.M.; van der Ploeg, M.; Smith, N.E.; Benninga, H.-J.F.; van der Bolt, F.; Carranza, C.D.U.; Koren, G.; van der Velde, R.; Teuling, A.J. Anatomy of the 2018 agricultural drought in the Netherlands using in situ soil moisture and satellite vegetation indices. *Hydrol. Earth Syst. Sci.* **2020**, *24*, 6021–6031. [CrossRef]
31. van Hateren, T.C.; Chini, M.; Matgen, P.; Teuling, A.J. Ambiguous Agricultural Drought: Characterising Soil Moisture and Vegetation Droughts in Europe from Earth Observation. *Remote Sens.* **2021**, *13*, 1990. [CrossRef]
32. Möllmann, J.; Buchholz, M.; Musshoff, O. Comparing the Hedging Effectiveness of Weather Derivatives Based on Remotely Sensed Vegetation Health Indices and Meteorological Indices. *Weather Clim. Soc.* **2019**, *11*, 33–48. [CrossRef]
33. Buras, A.; Rammig, A.; Zang, C.S. Quantifying impacts of the 2018 drought on European ecosystems in comparison to 2003. *Biogeosciences* **2020**, *17*, 1655–1672. [CrossRef]

34. Sepulcre-Canto, G.; Horion, S.; Singleton, A.; Carrao, H.; Vogt, J. Development of a Combined Drought Indicator to detect agricultural drought in Europe. *Nat. Hazards Earth Syst. Sci.* **2012**, *12*, 3519–3531. [CrossRef]
35. Trnka, M.; Hlavinka, P.; Možný, M.; Semerádová, D.; Štěpánek, P.; Balek, J.; Bartošová, L.; Zahradníček, P.; Bláhová, M.; Skalák, P.; et al. Czech Drought Monitor System for monitoring and forecasting agricultural drought and drought impacts. *Int. J. Climatol.* **2020**, *40*, 5941–5958. [CrossRef]
36. Karnieli, A.; Ohana-Levi, N.; Silver, M.; Paz-Kagan, T.; Panov, N.; Varghese, D.; Chrysoulakis, N.; Provenzale, A. Spatial and Seasonal Patterns in Vegetation Growth-Limiting Factors over Europe. *Remote Sens.* **2019**, *11*, 2406. [CrossRef]
37. LP DAAC. MOD13Q1 v006: MODIS/Terra Vegetation Indices 16-Day L3 Global 250 m SIN Grid. Available online: https://lpdaac.usgs.gov/products/mod13q1v006/ (accessed on 13 April 2021).
38. LP DAAC. MOD11A2 v006: MODIS/Terra Land Surface Temperature/Emissivity 8-Day L3 Global 1 km SIN Grid. Available online: https://lpdaac.usgs.gov/products/mod11a2v006/ (accessed on 13 April 2021).
39. LP DAAC. MCD12Q1 v006: MODIS/Terra+Aqua Land Cover Type Yearly L3 Global 500 m SIN Grid. Available online: https://lpdaac.usgs.gov/products/mcd12q1v006/ (accessed on 13 April 2021).
40. European Environment Agency. CLC 2018. Available online: https://land.copernicus.eu/pan-european/corine-land-cover/clc2018?tab=metadata (accessed on 13 April 2021).
41. European Environment Agency. EU-DEM v1.1. Available online: https://land.copernicus.eu/imagery-in-situ/eu-dem/eu-dem-v1.1?tab=metadata (accessed on 13 April 2021).
42. UFZ Drought Monitor/Helmholtz Centre for Environmental Research. Dürremonitor Deutschland. Available online: https://www.ufz.de/index.php?de=37937 (accessed on 13 April 2021).
43. Zink, M.; Samaniego, L.; Kumar, R.; Thober, S.; Mai, J.; Schäfer, D.; Marx, A. The German drought monitor. *Environ. Res. Lett.* **2016**, *11*, 74002. [CrossRef]
44. Statistical Offices of the Federation and the States. Erträge ausgewählter landwirtschaftlicher Feldfrüchte—Jahressumme—regionale Tiefe: Kreise und krfr. Städte. Available online: https://www.regionalstatistik.de/genesis/online?operation=previous&levelindex=2&levelid=1618314159666&levelid=1618314123639&step=1#abreadcrumb (accessed on 13 April 2021).
45. Bavarian State Office for Statistics. Bodennutzung der landwirtschaftlichen Betriebe in Bayern 2016: Totalerhebung. Available online: https://www.statistik.bayern.de/mam/produkte/veroffentlichungen/statistische_berichte/c1101c_201651_25313.pdf (accessed on 13 April 2021).
46. DWD Climate Data Center. Phenological Observations of Crops from Sowing to Harvest (Annual Reporters, Historical). Available online: https://opendata.dwd.de/climate_environment/CDC/observations_germany/phenology/annual_reporters/crops/historical/ (accessed on 20 April 2021).
47. Rouse, J.W.; Haas, R.H.; Schell, J.A.; Deering, D.W. *Monitoring the Vernal Advancement and Retrogradation (Green Wave Effect) of Natural Vegetation*; Remote Sensing Centre, TEXAS A&M University: College Station, TX, USA, 1973.
48. Tucker, C.J. Red and photographic infrared linear combinations for monitoring vegetation. *Remote Sens. Environ.* **1979**, *8*, 127–150. [CrossRef]
49. Norman, S.P.; Koch, F.H.; Hargrove, W.W. Review of broad-scale drought monitoring of forests: Toward an integrated data mining approach. *For. Ecol. Manag.* **2016**, *380*, 346–358. [CrossRef]
50. Zhang, Y.; Peng, C.; Li, W.; Fang, X.; Zhang, T.; Zhu, Q.; Chen, H.; Zhao, P. Monitoring and estimating drought-induced impacts on forest structure, growth, function, and ecosystem services using remote-sensing data: Recent progress and future challenges. *Environ. Rev.* **2013**, *21*, 103–115. [CrossRef]
51. Ji, L.; Peters, A.J. Assessing vegetation response to drought in the northern Great Plains using vegetation and drought indices. *Remote Sens. Environ.* **2003**, *87*, 85–98. [CrossRef]
52. Anderson, M.; Kustas, W.P. Thermal Remote Sensing of Drought and Evapotranspiration. *Eos Trans. Am. Geophys. Union* **2008**, *89*, 233–240. [CrossRef]
53. Anderson, M.C.; Norman, J.M.; Mecikalski, J.R.; Otkin, J.A.; Kustas, W.P. A climatological study of evapotranspiration and moisture stress across the continental United States based on thermal remote sensing: 2. Surface moisture climatology. *J. Geophys. Res.* **2007**, *112*. [CrossRef]
54. Karnieli, A.; Agam, N.; Pinker, R.T.; Anderson, M.; Imhoff, M.L.; Gutman, G.G.; Panov, N.; Goldberg, A. Use of NDVI and Land Surface Temperature for Drought Assessment: Merits and Limitations. *J. Clim.* **2010**, *23*, 618–633. [CrossRef]
55. Sun, D.; Kafatos, M. Note on the NDVI-LST relationship and the use of temperature-related drought indices over North America. *Geophys. Res. Lett.* **2007**, *34*. [CrossRef]
56. Abdi, A.M.; Vrieling, A.; Yengoh, G.T.; Anyamba, A.; Seaquist, J.W.; Ummenhofer, C.C.; Ardö, J. The El Niño—La Niña cycle and recent trends in supply and demand of net primary productivity in African drylands. *Clim. Chang.* **2016**, *138*, 111–125. [CrossRef]
57. Walentowski, H.; Kopp, D. Leitlinien für eine gesamtdeutsche ökologische Klassifikation der Wald-Naturräume. *Arch. Für Nat. Und Landsch.* **2006**, *45*, 135–149.
58. Hübl, E.; Burga, C.A.; Klötzli, F. Landschaft, Flora und Vegetation der Nordostalpen (Bayern–Wiener Becken). *Vierteljahrsschr. Der Nat. Ges. Zürich* **2007**, *152*, 17–26.
59. Bayerische Staatsforsten AöR. Waldbauhandbuch Bayerische Staatsforsten: Richtlinie für die Waldbewirtschaftung im Hochgebirge. Available online: https://www.baysf.de/fileadmin/user_upload/04-wald_verstehen/Publikationen/WNJF-RL-006_Bergwaldrichtlinie.pdf (accessed on 15 April 2021).

60. Walentowski, H.; Gulder, H.-J.; Kölling, C.; Ewald, J.; Türk, W. *Die Regionale Natürliche Waldzusammensetzung Bayerns*; Bayerische Landesanstalt für Wald und Forstwirtschaft (LWF): Freising, Germany, 2001.
61. Kogan, F. Global Drought Watch from Space. *Bull. Am. Meteorol. Soc.* **1997**, *78*, 621–636. [CrossRef]
62. Kogan, F. Application of Vegetation Index and Brightness Temperature for Drought Detection. *Adv. Space Res.* **1995**, *15*, 91–100. [CrossRef]
63. Kogan, F. Satellite-Observed Sensitivity of World Land Ecosystems to El Nino/La Nina. *Remote Sens. Environ.* **2000**, *74*, 445–462. [CrossRef]
64. Kogan, F.; Guo, W.; Strashnaia, A.; Kleshenko, A.; Chub, O.; Virchenko, O. Modelling and prediction of crop losses from NOAA polar-orbiting operational satellites. *Geomat. Nat. Hazards Risk* **2016**, *7*, 886–900. [CrossRef]
65. Gidey, E.; Dikinya, O.; Sebego, R.; Segosebe, E.; Zenebe, A. Analysis of the long-term agricultural drought onset, cessation, duration, frequency, severity and spatial extent using Vegetation Health Index (VHI) in Raya and its environs, Northern Ethiopia. *Environ. Syst. Res.* **2018**, *7*. [CrossRef]
66. Pei, F.; Wu, C.; Liu, X.; Li, X.; Yang, K.; Zhou, Y.; Wang, K.; Xu, L.; Xia, G. Monitoring the vegetation activity in China using vegetation health indices. *Agric. For. Meteorol.* **2018**, *248*, 215–227. [CrossRef]
67. Hu, X.; Ren, H.; Tansey, K.; Zheng, Y.; Ghent, D.; Liu, X.; Yan, L. Agricultural drought monitoring using European Space Agency Sentinel 3A land surface temperature and normalized difference vegetation index imageries. *Agric. For. Meteorol.* **2019**, *279*, 107707. [CrossRef]
68. Senf, C.; Buras, A.; Zang, C.S.; Rammig, A.; Seidl, R. Excess forest mortality is consistently linked to drought across Europe. *Nat. Commun.* **2020**, *11*, 6200. [CrossRef]
69. Julien, Y.; Sobrino, J.A.; Mattar, C.; Ruescas, A.B.; Jiménez-Muñoz, J.C.; Sòria, G.; Hidalgo, V.; Atitar, M.; Franch, B.; Cuenca, J. Temporal analysis of normalized difference vegetation index (NDVI) and land surface temperature (LST) parameters to detect changes in the Iberian land cover between 1981 and 2001. *Int. J. Remote Sens.* **2011**, *32*, 2057–2068. [CrossRef]
70. Raynolds, M.; Comiso, J.; Walker, D.; Verbyla, D. Relationship between satellite-derived land surface temperatures, arctic vegetation types, and NDVI. *Remote Sens. Environ.* **2008**, *112*, 1884–1894. [CrossRef]
71. Karnieli, A.; Bayasgalan, M.; Bayarjargal, Y.; Agam, N.; Khudulmur, S.; Tucker, C.J. Comments on the use of the Vegetation Health Index over Mongolia. *Int. J. Remote Sens.* **2006**, *27*, 2017–2024. [CrossRef]
72. Ghaleb, F.; Mario, M.; Sandra, A. Regional Landsat-Based Drought Monitoring from 1982 to 2014. *Climate* **2015**, *3*, 563–577. [CrossRef]
73. Zuhro, A.; Tambunan, M.P.; Marko, K. Application of vegetation health index (VHI) to identify distribution of agricultural drought in Indramayu Regency, West Java Province. *IOP Conf. Ser. Earth Environ. Sci.* **2020**, *500*, 12047. [CrossRef]
74. Choi, M.; Jacobs, J.M.; Anderson, M.C.; Bosch, D.D. Evaluation of drought indices via remotely sensed data with hydrological variables. *J. Hydrol.* **2013**, *476*, 265–273. [CrossRef]
75. Cong, D.; Zhao, S.; Chen, C.; Duan, Z. Characterization of droughts during 2001–2014 based on remote sensing: A case study of Northeast China. *Ecol. Inform.* **2017**, *39*, 56–67. [CrossRef]
76. Li, Y.; Dong, Y.; Yin, D.; Liu, D.; Wang, P.; Huang, J.; Liu, Z.; Wang, H. Evaluation of Drought Monitoring Effect of Winter Wheat in Henan Province of China Based on Multi-Source Data. *Sustainability* **2020**, *12*, 2801. [CrossRef]
77. Chang, S.; Chen, H.; Wu, B.; Nasanbat, E.; Yan, N.; Davdai, B. A Practical Satellite-Derived Vegetation Drought Index for Arid and Semi-Arid Grassland Drought Monitoring. *Remote Sens.* **2021**, *13*, 414. [CrossRef]
78. Chang, S.; Wu, B.; Yan, N.; Davdai, B.; Nasanbat, E. Suitability Assessment of Satellite-Derived Drought Indices for Mongolian Grassland. *Remote Sens.* **2017**, *9*, 650. [CrossRef]
79. Zhao, S.; Cong, D.; He, K.; Yang, H.; Qin, Z. Spatial-Temporal Variation of Drought in China from 1982 to 2010 Based on a modified Temperature Vegetation Drought Index (mTVDI). *Sci. Rep.* **2017**, *7*, 17473. [CrossRef]
80. Le Du, T.T.; Du Bui, D.; Nguyen, M.D.; Lee, H. Satellite-Based, Multi-Indices for Evaluation of Agricultural Droughts in a Highly Dynamic Tropical Catchment, Central Vietnam. *Water* **2018**, *10*, 659. [CrossRef]
81. Miralles, D.G.; Gentine, P.; Seneviratne, S.I.; Teuling, A.J. Land-atmospheric feedbacks during droughts and heatwaves: State of the science and current challenges. *Ann. N. Y. Acad. Sci.* **2019**, *1436*, 19–35. [CrossRef] [PubMed]
82. Dabrowska-Zielinska, K.; Kogan, F.; Ciolkosz, A.; Gruszczynska, M.; Kowalik, W. Modelling of crop growth conditions and crop yield in Poland using AVHRR-based indices. *Int. J. Remote Sens.* **2002**, *23*, 1109–1123. [CrossRef]
83. García-León, D.; Contreras, S.; Hunink, J. Comparison of meteorological and satellite-based drought indices as yield predictors of Spanish cereals. *Agric. Water Manag.* **2019**, *213*, 388–396. [CrossRef]
84. Panek, E.; Gozdowski, D. Relationship between MODIS Derived NDVI and Yield of Cereals for Selected European Countries. *Agronomy* **2021**, *11*, 340. [CrossRef]
85. Bannari, A.; Morin, D.; Bonn, F.; Huete, A.R. A review of vegetation indices. *Remote Sens. Rev.* **1995**, *13*, 95–120. [CrossRef]
86. Xue, J.; Su, B. Significant Remote Sensing Vegetation Indices: A Review of Developments and Applications. *J. Sens.* **2017**, *2017*, 1353691. [CrossRef]

87. Glenn, E.P.; Huete, A.R.; Nagler, P.L.; Nelson, S.G. Relationship Between Remotely-sensed Vegetation Indices, Canopy Attributes and Plant Physiological Processes: What Vegetation Indices Can and Cannot Tell Us About the Landscape. *Sensors* **2008**, *8*, 2136–2160. [CrossRef]
88. Huang, S.; Tang, L.; Hupy, J.P.; Wang, Y.; Shao, G. A commentary review on the use of normalized difference vegetation index (NDVI) in the era of popular remote sensing. *J. For. Res.* **2021**, *32*, 1–6. [CrossRef]
89. Kumari, N.; Srivastava, A.; Dumka, U.C. A Long-Term Spatiotemporal Analysis of Vegetation Greenness over the Himalayan Region Using Google Earth Engine. *Climate* **2021**, *9*, 109. [CrossRef]
90. Shahzaman, M.; Zhu, W.; Bilal, M.; Habtemicheal, B.A.; Mustafa, F.; Arshad, M.; Ullah, I.; Ishfaq, S.; Iqbal, R. Remote Sensing Indices for Spatial Monitoring of Agricultural Drought in South Asian Countries. *Remote Sens.* **2021**, *13*, 2059. [CrossRef]

Received: 13 October 2023 | Revised: 2 February 2024 | Accepted: 9 February 2024

DOI: 10.1111/gcb.17231

Global Change Biology WILEY

RESEARCH ARTICLE

Decoding autumn phenology: Unraveling the link between observation methods and detected environmental cues

Simon Kloos[1] | Anne Klosterhalfen[2] | Alexander Knohl[2,3] | Annette Menzel[1,4]

[1]TUM School of Life Sciences, Ecoclimatology, Technical University of Munich, Freising, Germany

[2]Bioclimatology, University of Göttingen, Göttingen, Germany

[3]Centre of Biodiversity and Sustainable Land Use (CBL), University of Göttingen, Göttingen, Germany

[4]Institute for Advanced Study, Technical University of Munich, Garching, Germany

Correspondence
Simon Kloos, TUM School of Life Sciences, Ecoclimatology, Technical University of Munich, Freising 85354, Germany.
Email: simon.kloos@tum.de

Funding information
Bavarian State Ministry of Science and the Arts; German Federal Ministry of Education and Research; Deutsche Forschungsgemeinschaft, Grant/Award Number: INST 186/1118-1 FUGG; Ministry of Lower-Saxony for Science and Culture, Grant/Award Number: ZN 3679

Abstract

Leaf coloring and fall mark the end of the growing season (EOS), playing essential roles in nutrient cycling, resource allocation, ecological interactions, and as climate change indicators. However, understanding future changes in autumn phenology is challenging due to the multitude of likely environmental cues and substantial variations in timing caused by different derivation methods. Yet, it remains unclear whether these two factors are independent or if methodological uncertainties influence the environmental cues determined. We derived start of growing season (SOS) and EOS at a mixed beech forest in Central Germany for the period 2000–2020 based on four different derivation methods using a unique long-term data set of in-situ data, canopy imagery, eddy covariance measurements, and satellite remote sensing data and determined their influence on a predictor analysis of leaf senescence. Both SOS and EOS exhibited substantial ranges in mean onset dates (39.5 and 28.6 days, respectively) across the different methods, although inter-annual variations and advancing SOS trends were similar across methods. Depending on the data, EOS trends were advanced or delayed, but inter-annual patterns correlated well (mean $r = .46$). Overall, warm, dry, and less photosynthetically productive growing seasons were more likely to be associated with a delayed EOS, while colder, wetter, and more photosynthetically productive vegetation periods resulted in an earlier EOS. In addition, contrary to recent results, no clear influence of pre-solstice vegetation activity on the timing of senescence was detected. However, most notable were the large differences in sign and strength of potential drivers both in the univariate and multivariate analyses when comparing derivation methodologies. The results suggest that an ensemble analysis of all available phenological data sources and derivation methods is needed for general statements on autumn phenology and its influencing variables and correct implementation of the senescence process in ecosystem models.

KEYWORDS
eddy covariance, end of season, Hainich, ICOS, leaf coloring, phenocam, photosynthesis, remote sensing, temperature, water availability

1 | INTRODUCTION

Autumn phenology significantly determines biogeochemical cycles in terrestrial ecosystems, such as the carbon cycle (Keenan et al., 2014; Piao et al., 2007; Richardson et al., 2010; Wu, Chen, et al., 2013; Wu, Gough, et al., 2013) or the water cycle (Gaertner et al., 2019; Kim et al., 2018), by directly ending carbon uptake or evapotranspiration. These changes in the growing season also exert biophysical feedback on the climate system (Peñuelas et al., 2009; Richardson et al., 2013; Stéfanon et al., 2012). In the past, a general trend towards a delay in autumn senescence has been observed in the northern hemisphere, whereby the magnitude, direction, and significance of the autumn phenological trends differ significantly depending on the species, the observation period, and the study region (Garonna et al., 2016; Gill et al., 2015; Liu, Fu, Zhu, et al., 2016; Menzel & Fabian, 1999; Menzel et al., 2020; Piao et al., 2019). To explain these observed features as well as to model and forecast future autumn phenology, it is of tremendous importance to fully understand all (environmental) drivers of leaf senescence; however, recent studies found varying and contradicting results.

The temperature is a main driver for leaf discoloration and leaf fall of deciduous trees in autumn (Gallinat et al., 2015; Gill et al., 2015), however with varying seasonal and daily patterns. Numerous current studies have shown that higher temperatures before senescence or all-year warming result in a delay in the phenological autumn (Fu et al., 2018; Lang et al., 2019; Liu, Fu, Zeng, et al., 2016; Liu, Fu, Zhu, et al., 2016; Menzel et al., 2020; Zohner & Renner, 2019). However, mostly likely due to different temporal resolutions and influencing periods, several studies have shown a differentiated picture in this temperature-senescence relationship: Chen et al. (2020) noted a delay in leaf coloration only with warming night-time temperatures—while warmer daytime temperatures cause it to start earlier. Estrella and Menzel (2006), Liu et al. (2018), and Lu and Keenan (2022) detected a delay in autumn phenology only with warmer autumn temperatures but not with higher temperatures in summer or in the growing season. This could be because heat stress was shown to lead to earlier rather than later autumn phenology (Xie et al., 2015, 2018). Furthermore, Zohner et al. (2023) recently noted a solstice effect in temperature, with increased temperatures before solstice leading to earlier senescence and after solstice leading to a lengthening of the autumn growing season. Finally, temperature-related effects on senescence seem to be also species-dependent (Grossiord et al., 2022).

Besides air temperature, other factors have also been studied to trigger leaf coloring and leaf fall in autumn. Water availability, characterized by precipitation amounts, soil moisture or vapor pressure deficit, has been frequently tested, but the results are also contradictory. While drier conditions are generally associated with earlier senescence (Gill et al., 2015), there are also study results that ascribe no or even opposite effects of water availability on autumn phenology (Estrella & Menzel, 2006; Liu et al., 2018; Xie et al., 2015, 2018; Zani et al., 2020). The study region, the biome, the type of phenology recorded, and the tree species also represent differentiating factors in this relationship (Bigler & Vitasse, 2021; Grossiord et al., 2022; Liu, Fu, Zeng, et al., 2016; Liu, Fu, Zhu, et al., 2016; Lu & Keenan, 2022). Other less considered and discussed factors for autumn senescence are photoperiod (Gill et al., 2015; Lang et al., 2019), nutrient availability (Fu et al., 2019), insolation (Liu, Fu, Zeng, et al., 2016; Liu, Fu, Zhu, et al., 2016; Lu & Keenan, 2022), and legacy or carryover effects, such as the timing of preceding leaf unfolding (Fu et al., 2019; Keenan & Richardson, 2015; Liu, Fu, Zhu, et al., 2016; Zani et al., 2020), and—more recently—growing season photosynthesis (Lu & Keenan, 2022; Norby, 2021; Zani et al., 2020; Zohner et al., 2023).

In addition to the multiple potential factors influencing autumn phenology, there is also a second source of uncertainty for future predictions: the used datasets and methods to derive phenological events. While many studies have compared remote sensing and ground-observed phenology (e.g., Berra & Gaulton, 2021; Mariën et al., 2019), only a few studies—mostly based in the US—have compared multiple data sources in autumn phenology. For mixed forests, Garrity et al. (2011) observed little agreement, while Zhao et al. (2020) found just minor differences between remote sensing derived and ground-observed autumn phenology. In contrast, Melaas et al. (2016) found varying correlations between autumn phenology from satellite remote sensing, eddy covariance measurements, canopy images and in-situ observations in North America, depending on the study area and data source. The spatial resolution of the data and the tree species composition may play a major role in this context (Klosterman et al., 2018). Accordingly, for deciduous forests in Europe, significant differences in the autumn phenology from remote sensing indices, eddy covariance measurements, and ground-based observations, such as in-situ or camera data, have been reported (Jin et al., 2017; Soudani et al., 2021). In contrast, comparatively good agreement was obtained by Liu et al. (2019) for leaf fall in a Chinese deciduous forest, using radiometer as well as satellite remote sensing data and leaf-litterfall measurements. Thus, D'Odorico et al. (2015) concluded on the phenological data mismatch for the entire northern hemisphere, that depending on the data source, derivation methodology, period and study site, the autumn phenology of deciduous forests is only partially (if at all) consistent with other data sources.

Based on the research findings regarding autumn phenology in deciduous forests, two imminent research gaps merge: First, there are hardly any detailed and long-term evaluations in Central Europe comparing different data sources for deriving autumn phenology. Second, most studies investigating the tricky influential factors of autumn phenology of deciduous forests rely on a single data source for phenology derivation, despite the potentially significant differences in derived phenology among datasets. To our knowledge, no study has explored the combined impact of these two sources of uncertainty. Consequently, there is a knowledge gap on how divergent phenological metrics further complicate the identification of drivers of autumn phenology. This study addresses these gaps through a detailed analysis of long-term data from Hainich National Park, Germany, which has one of the longest time series of canopy camera (CC) datasets in combination with continuous eddy covariance

measurements worldwide. Our research aims to answer the following key research questions:

1. What are the differences in spring and autumn phenology of a European deciduous forest when derived indirectly from satellite remote sensing data and eddy covariance measurements or directly from canopy imagery and in-situ phenological observations?
2. How do uncertainties and variations in derived phenology impact the univariate and multivariate analysis of potential factors influencing early, mid, and late autumn phenology in deciduous forests?

2 | MATERIALS AND METHODS

2.1 | Study site

The study site with its associated flux tower is located in Central Europe in the Hainich National Park (51.079407°N, 10.452089°E; 440 m a.s.l.; Germany; Figure 1). The National Park with an area of approximately 7600 ha was established for beech forest protection in 1997. Due to relatively undisturbed development, some trees are up to 270 years old. It has also been a UNESCO World Heritage Site since 2011 (Thiel et al., 2020). The forest of the National Park consists mainly of European beech (*Fagus sylvatica* L., 64%) and European ash (*Fraxinus excelsior* L., 28%; Tamrakar et al., 2018). During the study period from 2000 to 2020, the mean annual temperature at the flux tower site was 8.6°C, and the mean annual precipitation sum was 716 mm. The flux tower is located on a slightly inclined north slope (2°–3°; Knohl et al., 2003). Further information on the study area and location can be found in Knohl et al. (2003) or Tamrakar et al. (2018).

2.2 | In-situ phenology

Phenological observations are available from the network of the German Meteorological Service (DWD). The data set contains annual point measurements of 50 different phenological phases, which are then interpolated for a grid with a spatial resolution of 1 × 1 km over Germany: For this interpolation, Germany is

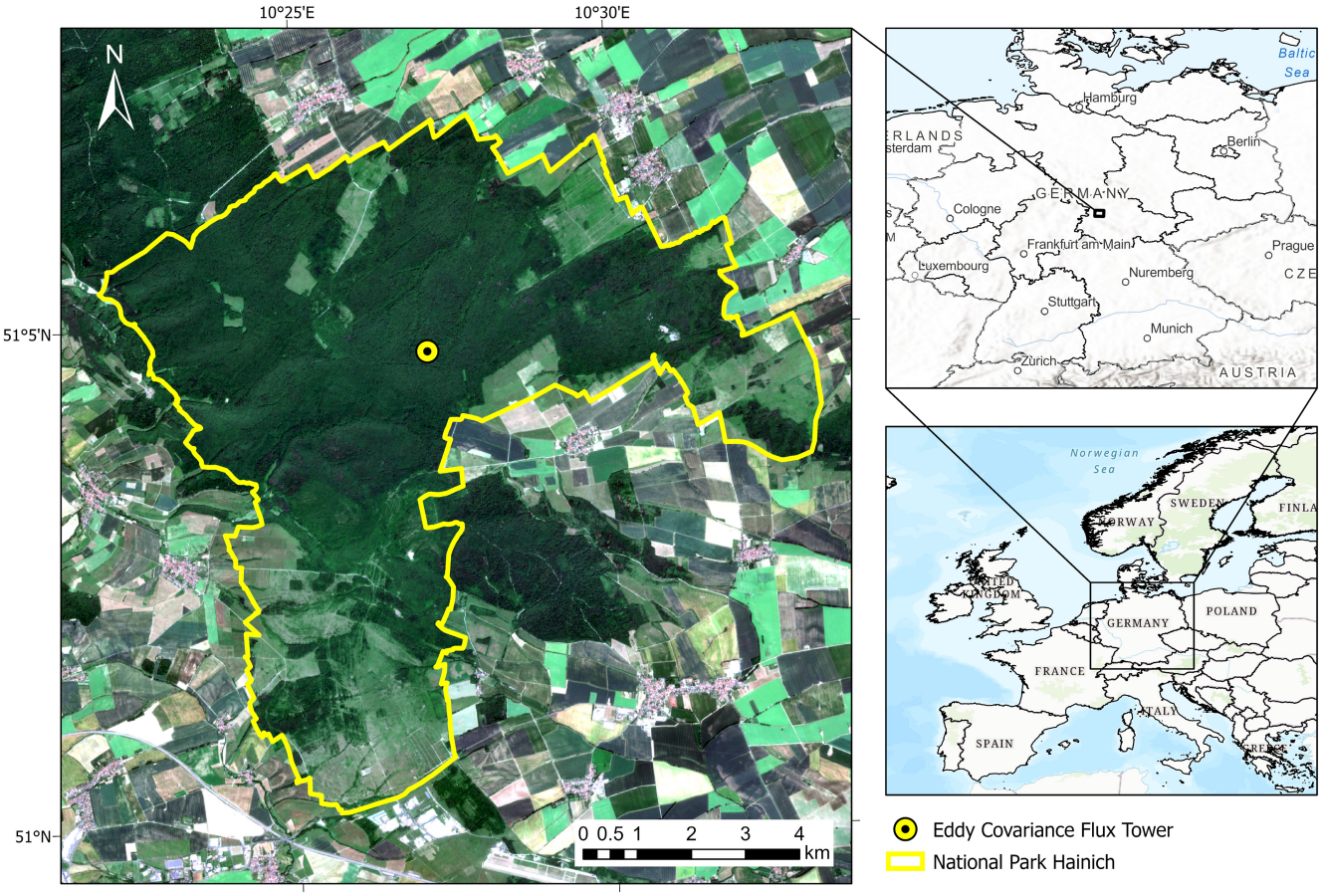

FIGURE 1 General map of Hainich National Park (left) and its location in Germany and Europe (right). The boundaries of the National Park are marked in yellow; the site of the eddy covariance flux tower is marked with a black and yellow dot (Source: Sentinel-2 [Copernicus SciHub], Esri, FAO, NOAA, USGS; GDI-Th, Earthstar Geographics; HERE, Garmin). Map lines delineate study areas and do not necessarily depict accepted national boundaries.

segmented into 20 regions, each comprising overlapping circles of uniform size. Within each region, all observations undergo multiple linear regression analysis, considering altitude, longitude, and latitude as regression coefficients. The regression coefficients for the four neighboring circles at a specific location are then weighted based on the distances to the circle centers. Finally, for each 1 × 1 km grid cell, annual onset dates are then interpolated based on these local regression coefficients (DWD Climate Data Center, 2022; Yuan et al., 2021).

The grid was used for the complete study period from 2000 to 2020. As the Hainich National Park mainly consists of beech forest, the dataset RBUBO (European beech—beginning of unfolding of leaves: the first leaves have entirely pushed out of the bud and unfolded up to the stalk; DWD:LU) was used for spring phenology, and the datasets RBUBV (European beech—autumn leaf coloring: about half of the leaves on the observation tree have turned autumnal; DWD:LC) and RBUBF (European beech—autumn leaf fall: about half the leaves of the observation tree have fallen off; DWD:LF) for autumn phenology. Unfortunately, leaf unfolding, coloring and fall of European ash are not part of the DWD phenological program, thus this phase could not be included in the in-situ data. Further information regarding the data can be found at DWD Climate Data Center (2022). The respective onset dates (DOY, day of year) were extracted bilinearly from all raster files for the coordinates of the flux tower.

2.3 | Satellite phenology

The remote sensing based phenology was extracted from the MODIS Land Cover Dynamics Product MCD12Q2 (Gray et al., 2019), which has been used in many studies dealing with remote sensing of phenology (e.g., Lu & Keenan, 2022; Zohner et al., 2023). Plant phenology is derived globally from 2-band Enhanced Vegetation Index (EVI) data with a resolution of 500 m. For spring phenology, the phases Greenup (date when EVI2 first crossed 15% of the segment EVI2 amplitude; MODIS:GU) and MidGreenup (date when EVI2 first crossed 50% of the segment EVI2 amplitude; MODIS:MGU) were used. For autumn phenology, the phases senescence (date when EVI2 last crossed 90% of the segment EVI2 amplitude; MODIS:SE) and dormancy (date when EVI2 last crossed 15% of the segment EVI2 amplitude; MODIS:DO) were used. Data were available from 2001 to 2019. To improve the quality of the data set, the quality assurance layer was applied to the existing raster files. The layer consists of scores (0 = "best"; 1 = "good"; 2 = "fair"; 3 = "poor"), which are composed of various criteria for calculating the phenology (fraction of missing or filled EVI data in the cycle, spline goodness-of-fit) for each pixel. In our study, we only used the highest quality class (=0) in the data set. Subsequently, the corresponding DOY for the respective phenological phase was extracted bilinearly from all raster files using the flux tower coordinates.

2.4 | CC phenology

The CC is placed on top of the flux tower above the tree canopy and provided recordings from 2001 to 2020. From 2001 to 2019, the pictures were always taken at 12:00 noon, since August 2020, every 30 min throughout the day. As the camera position changed a few times, and in some cases, there were longer data gaps in the dataset, the annual phenology could only be estimated visually from the pictures.

As far as the data availability for a year allowed, both start of season (SOS; BBCH 11 = first leaves unfold) and end of season (EOS; BBCH 95 = 50% of the leaves have fallen/discolored) were determined (for the BBCH (Biologische Bundesanstalt für Land- und Forstwirtschaft, Bundessortenamt und CHemische Industrie) coding see Meier, 2018). Due to the different camera positions, an individual region of interest (ROI) was created for each year and phase (SOS/EOS). The ROI was always set for the two main tree species of the Hainich National Park: *F. sylvatica* (CC:Fagus) and *F. excelsior* (CC:Fraxinus). The process of manually estimating the spring and autumn phenology via the CC images was carried out independently by three experienced and trained bioclimatologists. The mean of the three SOS/EOS estimates represented the respective CC phenology (CC:Fraxinus and CC:Fagus).

2.5 | Flux tower data

The data from the flux tower in the Hainich National Park are part of the Integrated Carbon Observation System (ICOS) network (DE-Hai; https://www.icos-cp.eu/) and cover the period 2000–2020 on a half-hourly or daily basis (Knohl et al., 2022). A variety of both meteorological and ecosystem CO_2 exchange-related variables are measured, but only the following variables were used in this study:

- Air temperature (°C)
- Precipitation (mm).
- Vapor pressure deficit (VPD) (hPa)
- Soil water content (16 cm depth) (%)
- Net ecosystem exchange (NEE) (g C m^{-2} day^{-1})
- Gross primary production, from daytime partitioning method (GPP:DT) (g C m^{-2} day^{-1})
- Gross primary production, from nighttime partitioning method (GPP:NT) (g C m^{-2} day^{-1})

Here, we included GPP derived from nighttime and from daytime flux-based partitioning methods, respectively, because they slightly differ in their approaches and assumptions (Wutzler et al., 2018). The nighttime source partitioning method (after Reichstein et al., 2005) first derives a relationship between (air or soil) temperature and the measured NEE during nighttime, which then only consists of respiratory fluxes. By extrapolating this temperature-respiration response function, ecosystem respiration (Reco) can also be estimated for daytime hours and with

calculating the balance between measured NEE and estimated Reco also GPP can be obtained. The daytime source partitioning method (after Lasslop et al., 2010) derives GPP and Reco during daytime based on a rectangular hyperbolic light-response curve, fitting this function to measured NEE data during daytime. Thus, this daytime source partitioning approach also considers the impact of varying meteorological conditions, such as incoming radiation and VPD, on GPP. Finally, Reco during nighttime is again derived based on a temperature-respiration response function.

2.5.1 | Flux tower phenology

To derive the phenology of Hainich National Park from the flux tower data, NEE, as well as GPP:DT and GPP:NT, were analyzed. Daily resolved data from 2000 to 2020 was used for all three variables. As a first step, all NEE values were converted to net ecosystem production (NEP) values (NEP = −NEE) to create a consistent positive sign for CO_2 uptake with NEP and GPP. To derive SOS and EOS from the NEP data, the smoothed-threshold approach was chosen (Barnard et al., 2018). A moving-window mean was calculated (central, 5 days) and a threshold of 0 g C m^{-2} day^{-1} was set. SOS was defined as the day this threshold value was overshot for the first time (CO_2 uptake) and remained overshot for 20 consecutive days. Inversely, EOS was defined as the day on which the NEP undershot the threshold value again for the first time and was no longer above it for 20 days in a row. The phenology of GPP:DT and GPP:NT was determined in a comparable method, but here the threshold was defined as a 10% value of the mean annual GPP maximum from 2000 to 2020 (Zhou et al., 2016, 2017). Thus, SOS was defined as the day this threshold value was exceeded for the first time in a year and EOS as the day this threshold was not met for the first time. In addition, SOS < 30 and EOS > 330 were discarded as extreme outliers.

2.5.2 | EOS predictor variables

To detect potential influencing factors on autumn phenology in Hainich National Park, 20 predictor variables from phenology, meteorology and ecosystem CO_2 exchange were selected and derived (Table 1) from literature including Zani et al. (2020). We additionally calculated a Dryness-Wetness Index (DWI) to incorporate the aspect of drought as a potential driver of autumn phenology. Since dryness/drought can be defined from different perspectives (Wilhite & Glantz, 1985), an index calculation combining different drought-related variables was chosen. For the annual DWI used in this study, six different variables were included in the index calculation:

- Growing season precipitation: Precipitation sum from March to October (mm)
- Summer precipitation: Precipitation sum in June, July, and August (mm)
- Growing season VPD: VPD sum from March to October (hPa)
- Summer VPD: VPD sum in June, July, and August (hPa)
- Growing season soil water content: Mean soil water content (16 cm depth) from March to October (%)
- Summer soil water content: Mean soil water content (16 cm depth) in June, July, and August (%)

For precipitation and for soil water content both in the growing season and in summer, the following index was calculated annually for the study period 2000–2020 on the basis of daily data:

$$\text{Index} = \frac{x_i - x_{\min}}{x_{\max} - x_{\min}}. \quad (1)$$

x_i represents the respective value of the year, $x_{\max}$ and $x_{\min}$, the respective maxima and minima in the period from 2000 to 2020. The value range of the index is accordingly between 0 and 1. The closer the index is to 0, the drier the conditions in the respective year. An index was also calculated for the VPD both in the growing season and in summer:

$$\text{Index} = \frac{x_{\max} - x_i}{x_{\max} - x_{\min}}. \quad (2)$$

The variables are congruent with Equation (1); here, values range from 0 to 1. The closer the index is to 0, the drier the VPD conditions. Finally, all six calculated indices were added up annually and defined as DWI. The range of values here extends from 0 (*very dry*) to 6 (*very wet*).

2.6 | Statistical analyses

Phenological data were analyzed using descriptive statistics, including trend analysis via linear regression with the year as predictor over the observation period, as well as a Pearson-correlation analysis for the spring and autumn datasets. We identified the factors that influence autumn phenology using univariate and multivariate analyses. In the univariate analysis, we calculated Spearman-rank correlation coefficients between all EOS data and the predictor variables (see Section 2.5.2). For the multivariate analysis, a common predictor dataset from the three main predictor groups temperature, water availability and photosynthetic activity was selected from the 20 predictor variables. To achieve this, the previously calculated SOS variables from different data sources were averaged for each year. Subsequently, to prevent multicollinearity within the dataset, variables with a strong ($r > .7$) and statistically significant ($p < .05$) Spearman correlation coefficient (Table S1) were not included in the analysis. Finally, for all EOS data sets, multiple linear regressions with two and three predictor variable combinations were calculated and the individual models were compared with each other. For reasons of clarity, we have decided to show only the 3- and 2-predictor combinations of the most common temperature (T_{AU} and T_{SU}) and water availability (P_{HY}) variables as well as the only directly measured photosynthesis variable (NEP). Combinations with other variables from

TABLE 1 Predictor variables for autumn phenology used including abbreviation, description, and unit. The hydrological year runs from 01.11. of the previous year to 31.10. of the current year.

Variable	Abbreviation	Description	Unit
Start of season	SOS	Respective SOS of the data source, for MODIS: Greenup	Day of year
Summer temperature	T_{SU}	Mean daily temperature in June, July, and August	°C
Autumn temperature	T_{AU}	Mean daily minimum temperature in September and October	°C
Extreme heat events	T_{EX}	Number of days with maximum temperature >30°C in the hydrological year	Days
Frost days	F_{HY}	Number of days with minimum temperature <0°C in the hydrological year	Days
Frost days in spring	F_{SP}	Number of days with minimum temperature <0°C from SOS until 60 days later	Days
Annual precipitation	P_{HY}	Number of days with >2 mm precipitation in the hydrological year	Days
Summer precipitation	P_{SU}	Number of days with >2 mm precipitation in June, July, and August	Days
Heavy rain days	P_{EX}	Number of days with >20 mm precipitation in the hydrological year	Days
Growing season vapor pressure deficit	VPD	Sum of daily VPD between SOS and September (30 September/DOY: 274)	hPa
Dryness-Wetness-Index	DWI	Combined drought index ranging between 0 (*very dry*) and 6 (*very wet*)	—
Growing season net ecosystem production	N_T	Sum of daily NEP between SOS and September (30 September/DOY: 274)	g C m^{-2}
Growing season gross primary production, daytime method	GD_T	Sum of daily GPP:DT between SOS and September (30 September/DOY: 274)	g C m^{-2}
Growing season gross primary production, nighttime method	GN_T	Sum of daily GPP:NT between SOS and September (30 September/DOY: 274)	g C m^{-2}
Growing season first half net ecosystem production	N_1	Sum of daily NEP in April, May, and June	g C m^{-2}
Growing season second half net ecosystem production	N_2	Sum of daily NEP in July, August, and September	g C m^{-2}
Growing season first half gross primary production, daytime method	GD_1	Sum of daily GPP:DT in April, May and June	g C m^{-2}
Growing season second half gross primary production, daytime method	GD_2	Sum of daily GPP:DT in July, August, and September	g C m^{-2}
Growing season first half gross primary production, nighttime method	GN_1	Sum of daily GPP:NT in April, May and June	g C m^{-2}
Growing season second half gross primary production, nighttime method	GN_2	Sum of daily GPP:NT in July, August, and September	g C m^{-2}

the same predictor groups led to similar results, which is why they are not shown here.

Following Zohner et al. (2023), who identify pre-solstice vegetation activity/temperature and autumn temperature as the main drivers of autumn phenology, two additional analyses were performed. First, for each derivation methodology, a multiple linear regression was calculated with the respective EOS as the dependent variable and growing season first half-NEP (N_1) and autumn temperature (T_{AU}) as predictors. Using the median of one predictor variable and the dynamic variable of the other predictor, regression lines were then calculated for the respective methodology.

To gain a better understanding of the interaction of autumn temperature and NEP, particularly in extreme years, we dissected the observed period (2000–2020; 21 years) into all possible combinations of these two variables: years with low T_{AU} and N_1 (scenario 1), high T_{AU} and N_1 (scenario 2), low T_{AU} and high N_1 (scenario 3), and high T_{AU} and low N_1 (scenario 4). To ensure comparability, 5 years were allocated to each scenario as follows: The 10 years with the lowest or highest photosynthetic activity in the first half of the growing season (according to N_1) were determined, excluding the median N_1 year. Within these 10-year subgroups, the 5 years with the coldest or warmest autumn temperatures (by T_{AU})

were then selected. Remarkably, the reverse classification order (first by T_{AU} then by N_1) yielded almost identical results. Finally, for each of the four 5-year subgroups, the mean EOS for each derivation methodology was determined and compared to each other. The general workflow of this study is shown in Figure 2. All relevant work steps were carried out in R (version 4.2.1; R Core Team, 2022).

3 | RESULTS

3.1 | Spring and autumn phenology

Mean SOS in the Hainich National Park started between the beginning of April (94.6; MODIS:GU) and mid-May (134.1; CC:Fraxinus), depending on the source of data (see Figure 3 and Table S2). The single SOS metrics exhibited strong year-to-year fluctuations (SDs) between 5.75 (DWD:LU) and 11.48 (GPP:NT) days. The earliest SOS in the observation period was recorded in mid-March 2019 (DOY 69; GPP:NT), the latest in late May 2017 (DOY 145; CC:Fraxinus; Figure 4). The linear SOS trends from 2000 to 2020 mostly indicated advancing onset dates (−0.23 to −0.78 days per year), and even a statistically significant trend for MODIS:GU. A clear exception is the SOS for ash observed via CC (CC:Fraxinus), which showed a significant positive, that is delayed, trend of 0.82 days per year. It is also worth noting that metrices from indirect derivation methods (MODIS/GPP) are more likely to indicate spring phenology earlier than those from direct methods (DWD/CC).

Comparing the SOS of different data sources, the large range of values was striking (Figure 4): In some extreme years, the difference between individual data sources was more than 70 days, and in general, the SOS values diverged by almost 40 days. The earliest values were detected on average by MODIS (Greenup data, MODIS:GU), usually followed by GPP data. The mean onset dates of DWD, NEP, and MODIS:MGU data, as well as the CC data of the beech (CC:Fagus) were similar and highly correlated (Figure S1). The latest SOS was usually observed for the ash tree via CC (CC:Fraxinus), which was less well correlated with the other SOS variables, such as GPP:DT and GPP:NT.

The mean start of autumn phenology (2000–2020) in the Hainich National Park ranged from the beginning of October (DWD:LC, MODIS:SE) to the beginning of November (MODIS:DO) for the period from 2000 to 2020 (Figure 3 and Table S3). Unlike spring phenology, the variation between individual years was smaller and ranged from 3.09 to 11.09 days SD. The earliest recorded autumn phenology was in late September 2004 (DOY 268; CC:Fagus) and the latest in mid-November 2009 (DOY 320; MODIS:DO; Figure 5). The linear trends from 2000 to 2020 were by far not as clear for autumn as for spring phenology: Six of nine data sources indicated a weak delay (0.06–0.94 days per year), and three data sources indicated a weak trend towards earliness (−0.10 to −0.26 days per year). None of the autumn trends was statistically significant.

A comparison between the individual data sources of autumn phenology also showed extreme differences in the annual range of values, mostly between 30 and 40 days (Figure 5). The senescence detected by MODIS and DWD data usually was at the start of autumn, followed by CC and flux tower data. Autumn ended with DWD leaf fall (DWD:LF) and the subsequent dormancy by MODIS (MODIS:DO). Thus, a clear temporal separation of the two main phases of autumn phenology, leaf discoloration and leaf fall, could be observed with derivation methods that measure these specifically (DWD/MODIS). Derivation methods that did not imply this differentiation (GPP/NEP/CC) are settled in between. Compared to spring phenology, there was even a larger agreement in EOS variables, as indicated by correlation coefficients (Figure S2).

3.2 | Drivers of autumn phenology

Spring phenology correlated only weakly with EOS (r_s = −.28–.19, not significant), depending on the data source (Figure 6). Temperature-related explanatory variables, such as summer (r_s = −.06–.62, not

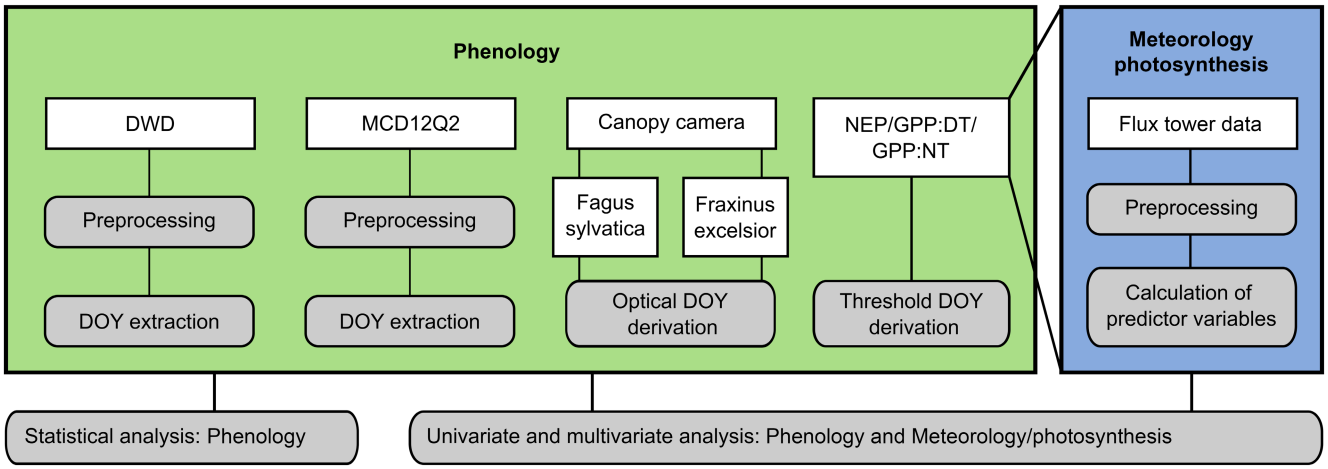

FIGURE 2 Flowchart of used data sources (white boxes) and applied methodology (grey boxes). The main aim is to relate plant phenology data (green box) and meteorological or ecosystem CO_2 exchange-related data (blue box).

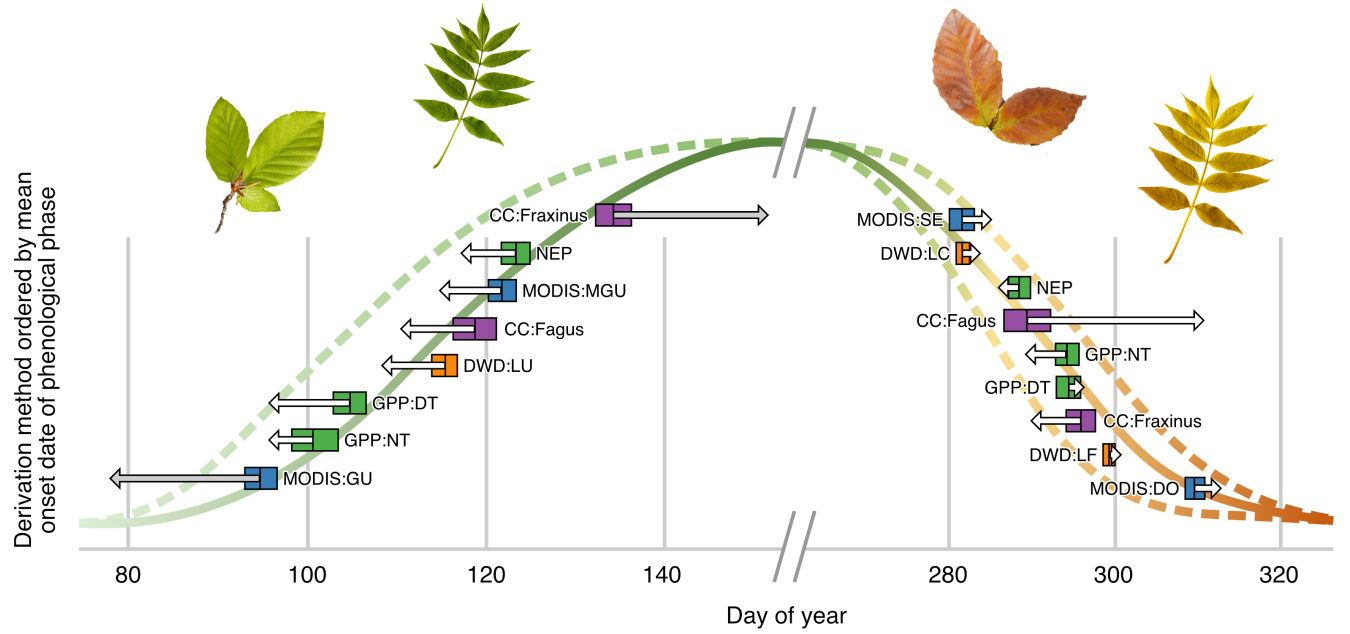

FIGURE 3 Schematic representation of the descriptive statistics of spring and autumn phenology from 2000 to 2020 for the respective data sources (orange: in-situ observation; blue: satellite remote sensing; green: flux tower; purple: canopy camera), ordered by mean DOY. The middle line within each box indicates the mean, the outer boundaries ±one SD. The arrows represent the trends over the observation period of 21 years, with gray coloring indicating statistical significance ($p < .05$). The dashed lines correspond to possible (extrapolated) future trends based on the arrows. The exact values of means, SD and trends are summarized in Tables S2 and S3.

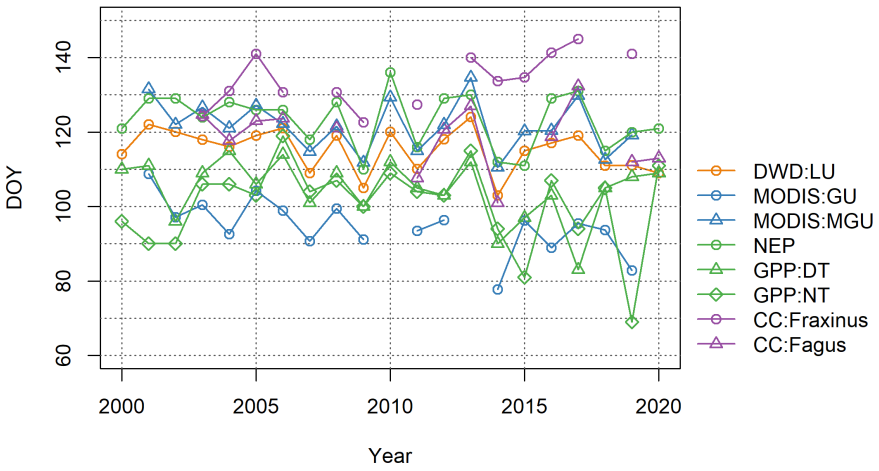

FIGURE 4 Time series of the derived spring phenology from the different data sources (orange: in-situ observation; blue: satellite remote sensing; green: flux tower; purple: canopy camera) in the Hainich National Park from 2000 to 2020.

significant) or autumn temperature ($r_s = .09–.33$, not significant), as well as extreme heat days ($r_s = .04–.64$, not significant), correlated mostly positively for the EOS, indicating that under warm/hot conditions in summer or assessed by extreme heat days, EOS should be observed later. Throughout positive correlations could also be seen for annual frost days ($r_s = .02–.55$, not significant; i.e., frosty winters should be linked to later EOS in autumn). In contrast, spring frost gave ambiguous results depending on the data source ($r_s = -.16–.32$, not significant).

The different variables of water availability had an evident (and sometimes significant) influence on autumn phenology: The less water—be it defined by precipitation in the hydrological year ($r_s = -.76–.08$) or during summer ($r_s = -.69–.05$), by VPD ($r_s = -.52$ to $-.02$, not significant) or DWI ($r_s = -.58$ to $-.18$, not significant)—was available, the later EOS took place (significant: $r_s = -.76$ and p-value $= .0007$ for P_{HY} and CC:Fagus; $r_s = -.67$ and p-value $= .0046$ for P_{SU} and CC:Fagus).

The variables of ecosystem CO_2 exchange provided a differentiated picture: The lower the NEP or GPP (and correspondingly less CO_2 uptake), the later EOS usually was. These effects were especially pronounced for the entire and the second half of the growing season and the NEP/GPP:NT explanatory variables ($r_s = -.60–.31$, not significant). In contrast, regarding the variables concerning the first half of the annual growth period (N_1, GD_1, GN_1), the correlations with the EOS were more spread, including positive and negative associations depending on the data source ($r_s = -.39–.51$, not significant).

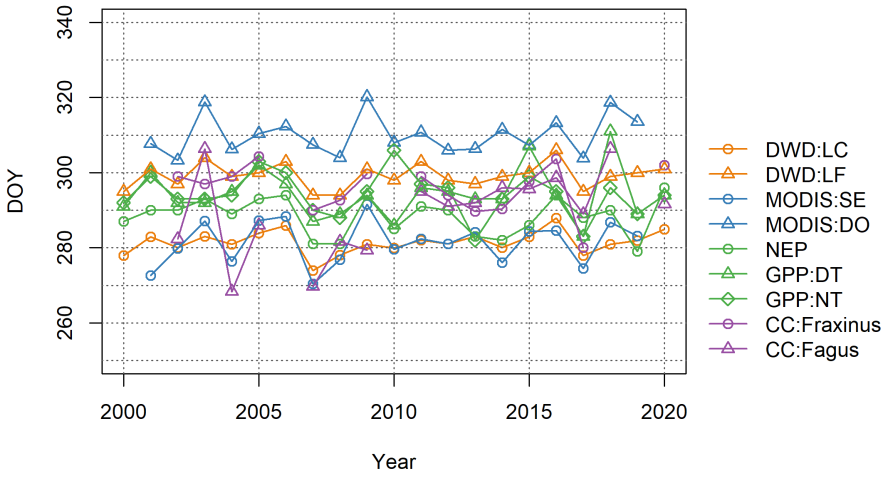

FIGURE 5 Time series of the derived autumn phenology from the different data sources (orange: in-situ observation; blue: satellite remote sensing; green: flux tower; purple: canopy camera) in the Hainich National Park from 2000 to 2020.

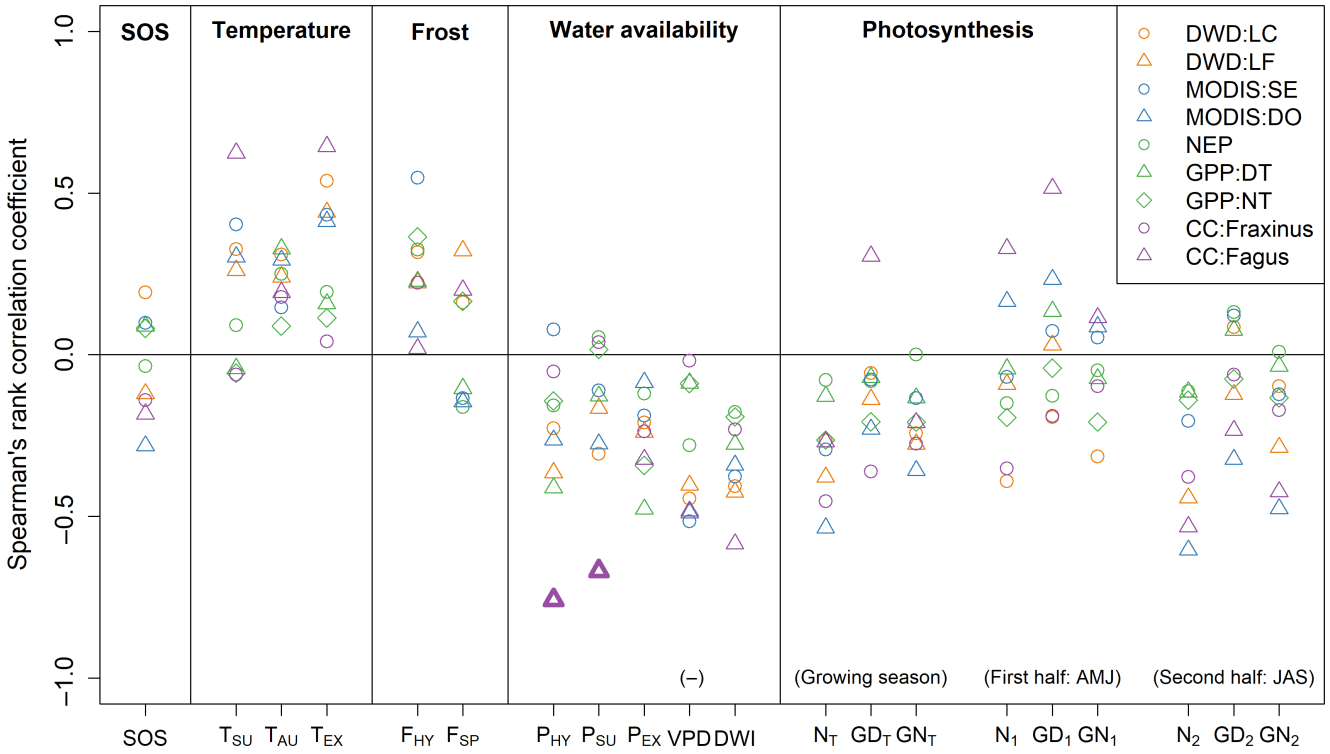

FIGURE 6 Spearman's rank correlation coefficient between the derived EOS and the respective predictor (variables see Table 1). Positive correlations indicate a delay in the EOS, while negative correlations mean an advance in EOS if the amount of the respective variable increases. To simplify the interpretation of the graph, the sign of VPD (−) has been changed (high VPD therefore means humid conditions). Symbols marked in bold represent a statistically significant correlation ($p < .05$, Bonferroni corrected).

If only the direct methods (DWD and CC) are considered in this respect, a similar picture emerges: While spring phenology and photosynthetic activity in April, May, and June indicate an ambiguous influence, higher temperatures in summer and autumn, more frost days, drier conditions, and lower photosynthetic activity in the growing season and in July, August, and September are associated with a later EOS.

This general variance in the sign and/or strength of correlation coefficients depending on the data source and variable was striking (Figure 6; e.g., summer temperature or precipitation). Among the phenological metrics, in-situ, CC, and remote sensing approaches tended to display stronger correlation coefficients (except T_{AU} and P_{EX}) than flux-related ones (NEP, GPP:DT, GPP:NT). Differences between direct (DWD/CC) and indirect (MODIS/GPP/NEP) derivation methodologies and between early (DWD:LC/MODIS:SE) and late autumn phenological (DWD:LF/MODIS:DO) metrics could not be detected in the univariate analysis.

In the multivariate analysis, the results of the univariate analyses were mostly confirmed (Figure 7 and Figures S3–S5). In the combination of the predictors from the groups of temperature, precipitation and photosynthesis, an increased autumn temperature and, in some cases, an increased summer temperature had an EOS-delaying

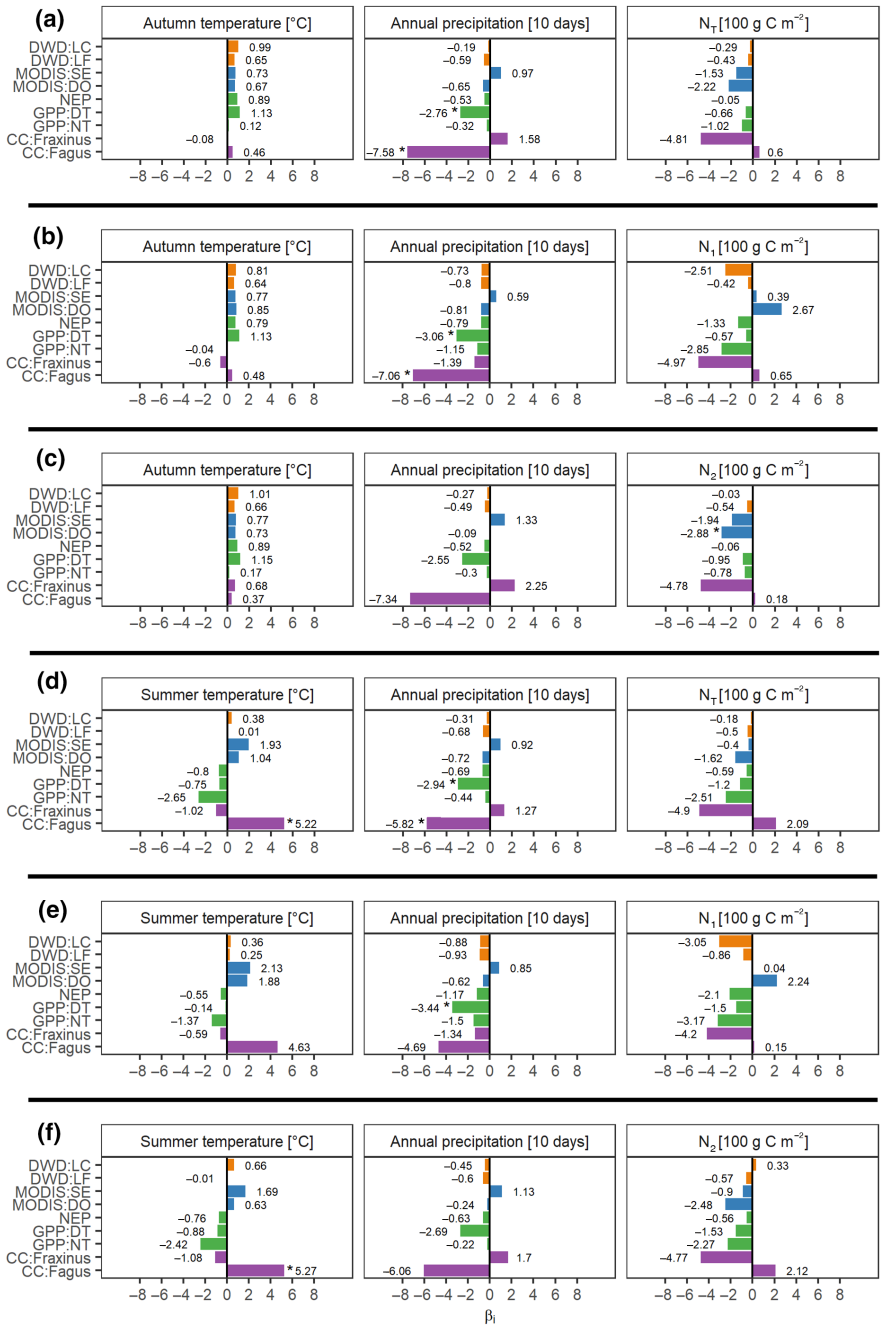

FIGURE 7 Regression coefficients of the respective predictor variable within the linear multiple regression models between EOS metrics and (a) T_{AU}, P_{HY}, and N_T; (b) T_{AU}, P_{HY}, and N_1; (c) T_{AU}, P_{HY}, and N_2; (d) T_{SU}, P_{HY}, and N_T; (e) T_{SU}, P_{HY}, and N_1; (f) T_{SU}, P_{HY}, and N_2. Statistically significant ($p < .05$) regression coefficients are marked with an asterisk.

effect. In contrast, wetter conditions and increased photosynthetic activity over the entire vegetation period and in the second half (July/August/September) had an advancing effect on the EOS, while photosynthetic activity in the first half of the vegetation period (April/May/June) showed diverging results depending on the data source. This also applies if only the direct methods (CC and DWD) are considered, except for photosynthetic activity in the first half of the growing season (the higher, the earlier EOS).

In general, the data source significantly influenced the sign, magnitude, and significance of the regression coefficient of the multiple linear regression models. This also became clear in the key statistics of the individual models (Table 2): With the identical predictor data set and only changing EOS data source, R^2 (.03–.62), adjusted R^2 (–.17–.52) and p-value (.01–.91) varied considerably. As in the univariate analysis, differences between direct (DWD/CC) and indirect (MODIS/GPP/NEP) derivation methodologies and between early (DWD:LC/MODIS:SE) and late autumn phenological (DWD:LF/MODIS:DO) metrics could not be detected.

The data source played a crucial role in investigating the interplay between EOS, N_1, and T_{AU}, as proposed by Zohner et al. (2023). When keeping autumn temperature constant, the various EOS responses showed a nuanced pattern relative to N_1 (Figure 8a): While higher photosynthetic activity in the first half of the growing season lead to a delay in the autumn phenology of GPP:DT, MODIS:DO, and especially CC:Fagus, some of the EOS variables were hardly affected, or even occurred earlier (CC:Fraxinus, GPP:NT, and DWD:LC). Conversely, under stable N_1 conditions, a rise in autumn temperature predominantly resulted in delayed EOS (except CC:Fraxinus and GPP:NT).

TABLE 2 Statistical ratios (coefficient of determination, adjusted coefficient of determination and *p*-value) of the multiple linear models between the respective EOS and the three predictor variable variants (see Figure 7).

	Variable combination	Statistical ratio	DWD: LC	DWD: LF	MODIS: SE	MODIS: DO	NEP	GPP: DT	GPP: NT	CC: Fraxinus	CC: Fagus
(a)	T_{AU}	R^2	.21	.18	.10	.30	.07	.34	.05	.29	.46
	P_{HY}	R^2 (adj.)	.06	.03	−.08	.16	−.10	.22	−.13	.10	.32
	N_T	*p*-value	.27	.34	.67	.14	.74	.07	.84	.26	.05
(b)	T_{AU}	R^2	.30	.17	.03	.16	.08	.34	.05	.08	.46
	P_{HY}	R^2 (adj.)	.17	.01	−.16	.00	−.09	.21	−.13	−.17	.32
	N_1	*p*-value	.11	.39	.91	.43	.69	.08	.83	.80	.05
(c)	T_{AU}	R^2	.20	.19	.13	.40	.07	.35	.03	.23	.46
	P_{HY}	R^2 (adj.)	.05	.04	−.04	.28	−.10	.23	−.15	.02	.32
	N_2	*p*-value	.29	.33	.54	.04	.74	.07	.91	.39	.05
(d)	T_{SU}	R^2	.06	.12	.15	.30	.04	.31	.19	.31	.62
	P_{HY}	R^2 (adj.)	−.12	−.05	−.02	.16	−.14	.18	.04	.12	.52
	N_T	*p*-value	.81	.56	.46	.14	.87	.11	.32	.23	.01
(e)	T_{SU}	R^2	.21	.11	.15	.26	.06	.29	.11	.08	.59
	P_{HY}	R^2 (adj.)	.07	−.06	−.02	.12	−.12	.16	−.06	−.17	.49
	N_1	*p*-value	.27	.58	.47	.19	.79	.13	.60	.81	.01
(f)	T_{SU}	R^2	.06	.12	.17	.38	.04	.32	.15	.24	.61
	P_{HY}	R^2 (adj.)	−.11	−.05	.00	.25	−.14	.19	−.01	.03	.52
	N_2	*p*-value	.79	.53	.42	.06	.88	.10	.44	.38	.01

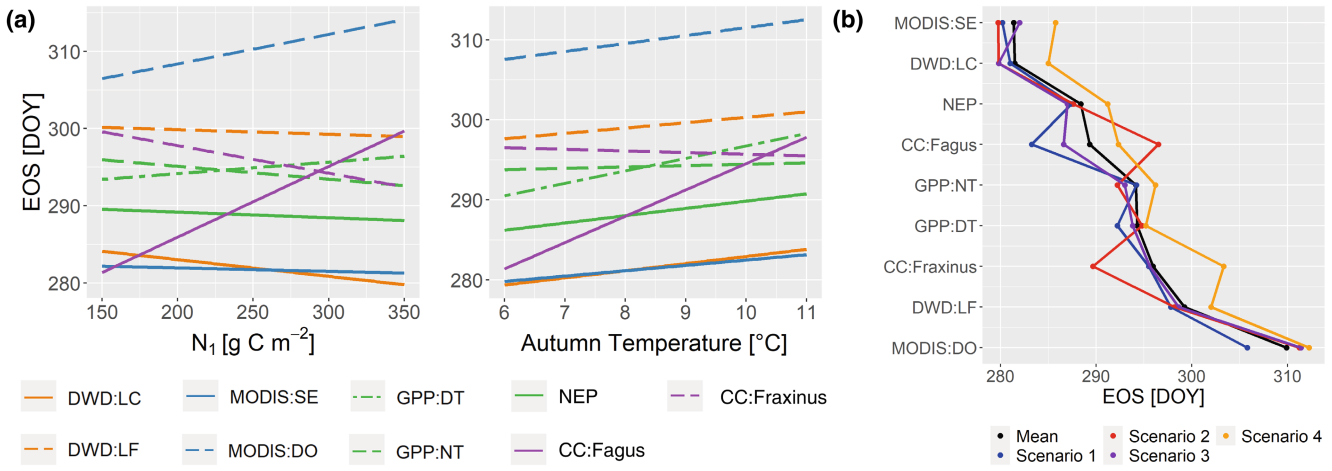

FIGURE 8 Analysis of EOS metrics in combination with the predictor variables autumn temperature (T_{AU}) and growing season first half net ecosystem production (N_1): (a) Multiple linear regressions with the other variable kept constant (median); (b) mean EOS (metrics ordered by mean date of onset), for 5 years each with low T_{AU} and N_1 (scenario 1), with high T_{AU} and N_1 (scenario 2), with low T_{AU} and high N_1 (scenario 3), with high T_{AU} and low N_1 (scenario 4), and for the total period (mean).

When comparing four 5-year scenarios across the EOS metrics (Figure 8b), it is most noticeable that in years with low photosynthetic activity in the first half of the growing season and high autumn temperature at the same time, a delayed EOS is observed in most of the methodologies. All other scenarios behave differently depending on the methodology, but the EOS values are always close to each other. In both analyses, no differences were observed between direct/indirect and early and late autumn phenological metrics.

4 | DISCUSSION

Both spring and autumn phenology in the Hainich National Park over the last 20 years differed widely by up to 1.5 months when different sources of derivation, such as remote sensing, carbon fluxes, CC images, or in-situ observations, are considered. However, the resulting time series still had remarkable similarities in their temporal courses. Whereas there is largely consensus that spring phenology in temperate deciduous forests is mainly driven by spring temperatures (besides winter chilling and photoperiod), the drivers of autumn phenology are less clear and heavily debated (e.g., Lu & Keenan, 2022). Consequently, our main intention was to analyze whether EOS data sources influence analyses' outcome on autumn phenology drivers, such as temperature, water availability, and/or photosynthetic activity. In the following sections, we will discuss the considerable differences found between the data sources and their implications for predicting changes in the growing season length of deciduous forests under climate change.

4.1 | Spring and autumn phenology

Spring phenology metrics from different data sources, such as satellite remote sensing, carbon flux data, CC, and in-situ observations, are well-known to differ (Berra & Gaulton, 2021). However, their seasonal order seems not random but well justified by inherent properties of the different indices. The MODIS Greenup, with its low threshold of 15% of EVI2 amplitude, mainly focuses on the greening of understory vegetation such as *Allium ursinum* L., *Mercurialis perennis* L., *Anemone nemorosa* L., usually occurring earlier in the year than the greening of the overstory (Filippa et al., 2018; Ryu et al., 2014; Uphus et al., 2021). Equally, the flux tower phenology also partially records the photosynthetic activity of the understory, leading to earlier GPP-based SOS dates (D'Odorico et al., 2015), albeit slightly later than MODIS:GU. This difference can be interpreted to signify as meaning that the greening of understory vegetation occurs before any relevant carbon uptake processes are initiated. The observation that indirect derivation methods are the first to indicate the start of spring phenology, compared to direct methods observing the trees themselves can therefore be primarily explained by the recording of the understory, which shows a clear drawback of the recording method. Unsurprisingly, the CC and the interpolated DWD phenology of *F. sylvatica* largely match. Corresponding to literature findings (Ahrends et al., 2009; Smith & Ramsay, 2020) *F. excelsior* leaves out later than *F. sylvatica*.

Advancing trends of SOS in the Hainich National Park from 2000 to 2020 are predominantly in line with the current literature (Caparros-Santiago et al., 2021; Menzel et al., 2020; Piao et al., 2019) and are mainly caused by rising spring temperatures (Hamunyela et al., 2013; Jin et al., 2019). On the contrary, the statistically significant delay of *F. excelsior* SOS might be a consequence of the pathogenic fungus *Hymenoscyphus pseudoalbidus*, which is currently damaging ash trees across Europe (Kowalski & Holdenrieder, 2009; but then Queloz et al., 2011). This phenomenon is also increasingly observed in the Hainich National Park. More severely damaged trees tend to leave out later than healthy ones (McKinney et al., 2011; Stener, 2013). These results highlight that "ecosystem-scale" indirect approaches are not very reliable in addressing species-specific phenology trends and could lead to large errors for species experiencing a phenological shift that is

inverse to the other plants in the community. Furthermore, since SOS dates are often used as predictors for EOS onset dates (assuming a constant length of the growing season; for example, Keenan & Richardson, 2015; Liu, Fu, Zhu, et al., 2016), it is essential to note that all SOS data sources, except for the ash CC, show similarly inter-annually varying time series and have a similar range (e.g., MODIS:MGU, DWD:LU, NEP, CC:Fagus). This indicates that for this specific assumed driver of EOS, differences in SOS metrics should not play a major role.

In autumn, as in spring, the order of the determined phenology was in line with the current process understanding. The data sources that explicitly detect the beginning of autumn phenology—namely leaf discoloration—(DWD:LC and MODIS:SE) estimated the earliest onset dates on average. The data sources indicating a later EOS were related to leaf fall (DWD:LF and MODIS:DO), with the MODIS data occurring significantly later (over 10 days on average).

The other autumn phenology metrics had a similar range of values in between, whereby two points are particularly noteworthy: Firstly, the DWD:LC data (which are based on 50% leaf discoloration of *F. sylvatica*) were more than 1 week earlier than CC:Fagus, although by definition the same is measured—in the top canopy (CC) and from the ground (DWD). This lag of 1 week could be because the phenological variability of individual trees is quite large and differences within certain phenological phases of more than 7 days are not uncommon (Capdevielle-Vargas et al., 2015; Marchand et al., 2020). Moreover, the DWD data are interpolated data, which per se represents an uncertainty factor, and thus can explain these differences. The Hainich site is slightly elevated to the Thuringen Becken, so it could be that the interpolation does not capture properly the elevational effect at this site. Secondly, ash leaf discoloration or leaf fall was later than the corresponding autumn phenology of beech, as also reported by Ahrends et al. (2009) for the Hainich National Park. The CC analysis clearly showed the dissimilarity: While *F. sylvatica* has intensive leaf discoloration and both leaf discoloration and leaf fall are longer lasting processes, the leaves of *F. excelsior* hardly change color and then fall to the ground relatively abruptly.

The autumn phenological trends across different data sources were rather delayed than advanced (but no single significant trend in either direction). This aligns well with existing research (Gill et al., 2015; Piao et al., 2019), although no directly comparable study with a similar observation period and area is available. Another striking difference is the sign of the two species observed via the CC. While the ash tends to enter dormancy earlier, the phenological autumn of the beech is clearly delayed. Contrasting the results of McKinney et al. (2011) and Stener (2013), we assume an influence of ash dieback also on the autumn phenology, which can be seen due to an advance in leaf senescence. The observed differences can be justified here based on a different research area, method, and period. In summary, there were thus two opposing trends in the length of the growing season for the Hainich National Park: a lengthening for *F. sylvatica* and a shortening for *F. excelsior*. Despite the high variance of the individual data sources in the value range of EOS, there is a high degree of temporal agreement. Above all, DWD:LC, DWD:LF, MODIS:SE, NEP and CC:Fraxinus show similar temporal courses and thus form a solid EOS construct for the Hainich National Park.

4.2 | Predictor analysis of autumn phenology

The predictor analysis of autumn phenology revealed that spring phenology, spring frost, and (partly) summer temperatures exhibit minor or contradicting effects—depending on the data source for autumn phenology. However, years with higher autumn (and partly summer) temperatures and more heat and frost days tend to be associated with a later EOS. These outcomes hold a dual nature, aligning with some and diverging from other research findings. While many studies support the idea that higher autumn temperatures cause leaves to change color and fall later (e.g., Gallinat et al., 2015; Gill et al., 2015; Zohner et al., 2023), there are some studies that do not offer evidence for a later EOS with higher summer temperatures (Liu et al., 2018; Lu & Keenan, 2022). However, a noteworthy discrepancy arises concerning our consistently positive link between the number of extreme hot days and the EOS, that is more hot days are associated with later autumn senescence contrasting with results of Xie et al. (2015, 2018) who associate extreme heat stress with an earlier autumn phenology. This discrepancy could be due to the methodology: Xie et al. (2015) analyzed remote sensing data in the US from 2001 to 2012, defining heat stress in July and August as temperatures exceeding 32 or 35°C, whereas Xie et al. (2018) also considered ground observations with a threshold of 35°C. Their findings on the relationship between heat stress and EOS changed depending on the threshold (Xie et al., 2015) and tree species (Xie et al., 2018), which is in agreement with our results. Consequently, there is a need to further investigate in detail whether higher temperature thresholds than applied in our study lead to the detection of possible drought effects associated with heat waves in remote sensing products, resulting in this reverse relationship with EOS.

A clear influence was seen for water availability: the less precipitation falls in the previous hydrological year, in summer, and as extremes, the later the autumn phenology. This finding was also confirmed for VPD and DWI influences in our study. When considering the impact of water availability, some studies observe a later EOS in drier conditions (Xie et al., 2015, 2018), although other studies cannot confirm this finding (Bigler & Vitasse, 2021; Liu et al., 2018; Zani et al., 2020). In general, the understanding of this topic is still unclear, since there are many different variables (e.g., precipitation, soil moisture, VPD) and methods (mean values or extremes) involved.

The impact of photosynthetic activity on EOS requires a more differentiated assessment, particularly given the conflicting statements in current literature. While some studies support the idea that photosynthetic activity regulates autumn phenology (Zani et al., 2020; Zohner et al., 2023), others oppose this hypothesis (Lu & Keenan, 2022; Norby, 2021). We found that the effect for the first part of the growing season varied based on how EOS is determined, and the analysis method used (univariate/multivariate). This was equally the case, when only photosynthetic activity in the first half

of the growing season and autumn temperature were considered as predictor variables. On the other hand, reduced photosynthetic activity over the entire growing season and in the second half of the season (July, August, September) was more likely to delay EOS. Nevertheless, the dominating effect was autumn temperature, with a high temperature being associated with a later EOS in most cases. Consequently, years with low photosynthesis in April, May, and June and high autumn temperature were particularly associated with delayed EOS, indicating the autumn temperature effect. However, in detail this was again true not for all EOS data sources and the photosynthesis definition (NEP, GPP) influenced the results significantly.

Recent results by Zohner et al. (2023), according to which increased pre-solstice vegetation activity advances senescence in Northern Hemisphere forests, cannot be confirmed by our study. EOS metrics determined the overall picture and the phases specifically related to the beginning of senescence (e.g., MODIS:SE and DWD:LC) provided different results, which makes this hypothesis questionable, at least in a temperate mid-latitude deciduous forest.

One finding is valid for all influencing factors: the different data sources for phenology matter. Although some studies already link derived autumn phenology with potential predictors using different data sources and methodologies (e.g., Keenan & Richardson, 2015; Lu & Keenan, 2022), to our knowledge, there is no systematic evaluation of how different derivation approaches of EOS affect a predictor analysis in a given study area. We found large differences in the magnitude, sign, and significance of effects on autumn phenology depending on the data source and derivation methodology. For example, beech CC EOS dates were highly correlated with temperature and water variables, suggesting a strong relationship, whereas correlations for the same variables were much weaker or even opposite for flux tower phenology. Similar observations can be made at the multivariate level, where, for example, the NEP, GPP, and ash CC autumn phenology were negatively related to summer temperature. In contrast, the DWD and MODIS phenology showed (mostly) a positive correlation. Both examples illustrate that conclusions about drivers of autumn phenology can diverge considerably depending on the data source. This finding is noteworthy, as many studies within this field of research base statements about relationships between phenology and possible influencing factors on only one data source and derivation methodology. On the other hand, however, it must also be noted that despite the large number of different data sources and derivation methods, the correlations in the more general variable groups (temperature, water availability, photosynthesis) with the EOS variables provide a largely uniform picture. There were no discernible structural differences in the relationships with the individual predictor variables found either in the differentiation between direct and indirect recording methods or in early, mid-, and late autumn phenological metrics.

However, the choice of methods can lead to substantial variations in EOS-related findings (especially just looking at one predictor variable), whereby for general statements on potential predictors of autumn phenology, an ensemble evaluation of all available data sources of a study area is recommendable but requires considerably larger data sets. In the context of machine learning ensemble analysis, the fundamental premise is that inherent inaccuracies of individual models can be mitigated through the combination of multiple models. This approach is expected to enhance predictive accuracy compared to relying on single models (Sagi & Rokach, 2018). In our specific context, where various phenological data sources or derivation methods were employed for a given location and observation period to analyze phenological trends and their drivers, we constructed several regression models using a singular model type. Thus, this above-mentioned methodology would open up new avenues, particularly for extensive phenological data sets which amalgamate diverse data sources. However, ensemble methods from the field of machine learning, such as boosting (Elith et al., 2008) and bagging (Breiman, 1996), have not yet received much attention in plant phenology but hold potential for refining models for various research questions. Nevertheless, for differentiated views, especially concerning spatial resolution (ecosystem, species, individual tree, etc.), individual data sources still have importance for specific applications.

In light of our study findings, it is evident across all EOS metrics that warmer and drier growing seasons lead to a later EOS. At the same time, cooler and wetter conditions tend to prompt an earlier EOS in the Hainich National Park, with the role of photosynthetic activity remaining unclear, contingent on the definition, observation period, and EOS methodology.

4.3 | Limitations of the data sources

However, there are also specific limitations related to the data and methods. Only individual trees of the respective species were observed by DWD and CC data. As previously mentioned, there can be substantial variability within a phenological phase among trees (Capdevielle-Vargas et al., 2015; Marchand et al., 2020), and thus, in the worst case, the determined phenological phase might not accurately represent the species studied. The interpolation of DWD data adds another layer of uncertainty. Particularly worth noting is the manual and, thus semi-objective nature of evaluating phenology in the case of the CC data. Also, since the camera position changed several times over the time series, the same tree was not always observed consistently. In the case of the remote sensing and flux tower data, the homogeneous and spatially undifferentiated observation must be pointed out, which can lead to distorted results, especially in respect to the understory. Across all data sources and phenology studies (Berra & Gaulton, 2021; Templ et al., 2018; Zeng et al., 2020), there is also concern about consistent definitions of the phenological phases. Especially in autumn, due to the more complex process of leaf discoloration and fall, phenology can be measured differently. Additionally, indirect measurement methods such as remote sensing or derivation via ecosystem CO_2 exchange, can sometimes lack clarity in terms of what exactly is being measured, making comparisons challenging. For eddy covariance data, uncertainties arise from quality checks, gap-filling, and the source partitioning approach. Finally, GPP:DT and GPP:NT are just modelled values; only NEP is directly measured. Uncertainties also extend to the predictor variables. The

defined threshold values and the periods can be designed differently, influencing evaluations. However, careful selection of robust variables was prioritized when avoiding collinearity within the multiple linear regression models. Lastly, the limitations of the statistical analyses conducted here should be acknowledged. The dataset size (maximum 21 years) upon which the statistical metrics are based was relatively small, making it sensitive to outliers.

5 | CONCLUSION

The analysis of spring and autumn phenology in the Hainich National Park from different data sources revealed significant variability in the determined onset dates and corresponding trends, dependent on the specific data source employed. While spring phenology generally exhibited advancement over the observed period (except for European ash), autumn trends were less distinct, aside from the delayed leaf coloring in European beech. The factors possibly influencing autumn phenology include temperature, water availability, and/or photosynthetic activity. Warmer and drier years tend to be linked to a delayed end of season, although the exact role of photosynthesis remains unclear. Notably, the predictors derived for autumn phenology exhibit substantial disparities across the EOS data sources, whereby no structural differences are found between direct and indirect data sources or between early and late autumn phenological metrics. Considering these findings, it appears prudent to adopt an ensemble approach by using multiple phenological data sources in future research, particularly when addressing broader questions concerning plant phenology.

AUTHOR CONTRIBUTIONS

Simon Kloos: Conceptualization; data curation; formal analysis; investigation; methodology; software; validation; visualization; writing – original draft; writing – review and editing. **Anne Klosterhalfen:** Data curation; investigation; resources; writing – review and editing. **Alexander Knohl:** Data curation; funding acquisition; project administration; resources; writing – review and editing. **Annette Menzel:** Conceptualization; funding acquisition; methodology; project administration; supervision; writing – review and editing.

ACKNOWLEDGMENTS

The authors thank the Land Processes Distributed Active Archive Center (LP DAAC), the DWD Climate Data Center (CDC), and the Integrated Carbon Observation System (ICOS) data portal for providing the data free of charge. We thank the technical staff from the Bioclimatology Group of the University of Göttingen for their continuous support in data acquisition and instrument maintenance and Matthias Neumair and Donna P. Ankerst for statistical advice. Thanks also go to Johanna Kauffert and Lars Uphus for manually determining the CC phenology. Finally, we thank the administration of the Hainich National Park for the opportunity for research within the National Park. Open Access funding enabled and organized by Projekt DEAL.

FUNDING INFORMATION

This study was performed within the project BAYSICS (Bavarian Citizen Science Portal for Climate Research and Science Communication), funded by the Bavarian State Ministry of Science and the Arts in the context of the Bavarian Climate Research Network (bayklif). We acknowledge support by the German Federal Ministry of Education and Research (BMBF) as part of the European Integrated Carbon Observation System (ICOS), by the Deutsche Forschungsgemeinschaft (INST 186/1118-1 FUGG), and the Digital Forest project funded by Niedersächsisches Vorab (ZN 3679), Ministry of Lower-Saxony for Science and Culture (MWK).

CONFLICT OF INTEREST STATEMENT

The authors declare no conflicts of interest.

DATA AVAILABILITY STATEMENT

The phenological data that support the findings of this study are openly available in figshare at https://doi.org/10.6084/m9.figshare.22040828, the DWD data are publicly available at https://opendata.dwd.de/climate_environment/CDC/grids_germany/annual/phenology/ (RBUBO, RBUBV, and RBUBF), the flux tower data are openly available in the ICOS data portal at https://doi.org/10.18160/cr66-pj24, and the MODIS data were downloaded with the R package MODIStsp (Busetto & Ranghetti, 2016). The canopy camera images are publicly available at https://doi.org/10.25625/6IWFIY.

ORCID

Simon Kloos https://orcid.org/0000-0002-9242-1456
Anne Klosterhalfen https://orcid.org/0000-0001-7999-8966
Alexander Knohl https://orcid.org/0000-0002-7615-8870
Annette Menzel https://orcid.org/0000-0002-7175-2512

REFERENCES

Ahrends, H. E., Etzold, S., Kutsch, W. L., Stoeckli, R., Bruegger, R., Jeanneret, F., Wanner, H., Buchmann, N., & Eugster, W. (2009). Tree phenology and carbon dioxide fluxes: Use of digital photography for process-based interpretation at the ecosystem scale. *Climate Research*, *39*, 261–274. https://doi.org/10.3354/cr00811

Barnard, D. M., Knowles, J. F., Barnard, H. R., Goulden, M. L., Hu, J., Litvak, M. E., & Molotch, N. P. (2018). Reevaluating growing season length controls on net ecosystem production in evergreen conifer forests. *Scientific Reports*, *8*(1), 17973. https://doi.org/10.1038/s41598-018-36065-0

Berra, E. F., & Gaulton, R. (2021). Remote sensing of temperate and boreal forest phenology: A review of progress, challenges and opportunities in the intercomparison of in-situ and satellite phenological metrics. *Forest Ecology and Management*, *480*, 118663. https://doi.org/10.1016/j.foreco.2020.118663

Bigler, C., & Vitasse, Y. (2021). Premature leaf discoloration of European deciduous trees is caused by drought and heat in late spring and cold spells in early fall. *Agricultural and Forest Meteorology*, *307*, 108492. https://doi.org/10.1016/j.agrformet.2021.108492

Breiman, L. (1996). Bagging predictors. *Machine Learning*, *24*(2), 123–140. https://doi.org/10.1007/BF00058655

Busetto, L., & Ranghetti, L. (2016). MODIStsp: An R package for automatic preprocessing of MODIS land products time series.

Computers & Geosciences, *97*, 40–48. https://doi.org/10.1016/j.cageo.2016.08.020

Caparros-Santiago, J. A., Rodriguez-Galiano, V., & Dash, J. (2021). Land surface phenology as indicator of global terrestrial ecosystem dynamics: A systematic review. *ISPRS Journal of Photogrammetry and Remote Sensing*, *171*, 330–347. https://doi.org/10.1016/j.isprsjprs.2020.11.019

Capdevielle-Vargas, R., Estrella, N., & Menzel, A. (2015). Multiple-year assessment of phenological plasticity within a beech (*Fagus sylvatica* L.) stand in southern Germany. *Agricultural and Forest Meteorology*, *211-212*, 13–22. https://doi.org/10.1016/j.agrformet.2015.03.019

Chen, L., Hänninen, H., Rossi, S., Smith, N. G., Pau, S., Liu, Z., Feng, G., Gao, J., & Liu, J. (2020). Leaf senescence exhibits stronger climatic responses during warm than during cold autumns. *Nature Climate Change*, *10*(8), 777–780. https://doi.org/10.1038/s41558-020-0820-2

D'Odorico, P., Gonsamo, A., Gough, C. M., Bohrer, G., Morison, J., Wilkinson, M., Hanson, P. J., Gianelle, D., Fuentes, J. D., & Buchmann, N. (2015). The match and mismatch between photosynthesis and land surface phenology of deciduous forests. *Agricultural and Forest Meteorology*, *214-215*, 25–38. https://doi.org/10.1016/j.agrformet.2015.07.005

DWD Climate Data Center. (2022). Annual grids of several phenological plant stages in Germany, version 0.x. https://opendata.dwd.de/climate_environment/CDC/grids_germany/annual/phenology/

Elith, J., Leathwick, J. R., & Hastie, T. (2008). A working guide to boosted regression trees. *The Journal of Animal Ecology*, *77*(4), 802–813. https://doi.org/10.1111/j.1365-2656.2008.01390.x

Estrella, N., & Menzel, A. (2006). Responses of leaf colouring in four deciduous tree species to climate and weather in Germany. *Climate Research*, *32*, 253–267. https://doi.org/10.3354/cr032253

Filippa, G., Cremonese, E., Migliavacca, M., Galvagno, M., Sonnentag, O., Humphreys, E., Hufkens, K., Ryu, Y., Verfaillie, J., Di Morra Cella, U., & Richardson, A. D. (2018). NDVI derived from near-infrared-enabled digital cameras: Applicability across different plant functional types. *Agricultural and Forest Meteorology*, *249*, 275–285. https://doi.org/10.1016/j.agrformet.2017.11.003

Fu, Y. H., Piao, S., Delpierre, N., Hao, F., Hänninen, H., Geng, X., Peñuelas, J., Zhang, X., Janssens, I. A., & Campioli, M. (2019). Nutrient availability alters the correlation between spring leaf-out and autumn leaf senescence dates. *Tree Physiology*, *39*(8), 1277–1284. https://doi.org/10.1093/treephys/tpz041

Fu, Y. H., Piao, S., Delpierre, N., Hao, F., Hänninen, H., Liu, Y., Sun, W., Janssens, I. A., & Campioli, M. (2018). Larger temperature response of autumn leaf senescence than spring leaf-out phenology. *Global Change Biology*, *24*(5), 2159–2168. https://doi.org/10.1111/gcb.14021

Gaertner, B. A., Zegre, N., Warner, T., Fernandez, R., He, Y., & Merriam, E. R. (2019). Climate, forest growing season, and evapotranspiration changes in the central Appalachian Mountains, USA. *The Science of the Total Environment*, *650*(Pt 1), 1371–1381. https://doi.org/10.1016/j.scitotenv.2018.09.129

Gallinat, A. S., Primack, R. B., & Wagner, D. L. (2015). Autumn, the neglected season in climate change research. *Trends in Ecology & Evolution*, *30*(3), 169–176. https://doi.org/10.1016/j.tree.2015.01.004

Garonna, I., de Jong, R., & Schaepman, M. E. (2016). Variability and evolution of global land surface phenology over the past three decades (1982-2012). *Global Change Biology*, *22*(4), 1456–1468. https://doi.org/10.1111/gcb.13168

Garrity, S. R., Bohrer, G., Maurer, K. D., Mueller, K. L., Vogel, C. S., & Curtis, P. S. (2011). A comparison of multiple phenology data sources for estimating seasonal transitions in deciduous forest carbon exchange. *Agricultural and Forest Meteorology*, *151*(12), 1741–1752. https://doi.org/10.1016/j.agrformet.2011.07.008

Gill, A. L., Gallinat, A. S., Sanders-DeMott, R., Rigden, A. J., Short Gianotti, D. J., Mantooth, J. A., & Templer, P. H. (2015). Changes in autumn senescence in northern hemisphere deciduous trees: A meta-analysis of autumn phenology studies. *Annals of Botany*, *116*(6), 875–888. https://doi.org/10.1093/aob/mcv055

Gray, J., Sulla-Menashe, D., & Friedl, M. A. (2019). *User guide to collection 6 MODIS land cover dynamics (MCD12Q2) product*. https://lpdaac.usgs.gov/products/mcd12q2v006/

Grossiord, C., Bachofen, C., Gisler, J., Mas, E., Vitasse, Y., & Didion-Gency, M. (2022). Warming may extend tree growing seasons and compensate for reduced carbon uptake during dry periods. *Journal of Ecology*, *110*(7), 1575–1589. https://doi.org/10.1111/1365-2745.13892

Hamunyela, E., Verbesselt, J., Roerink, G., & Herold, M. (2013). Trends in spring phenology of Western European deciduous forests. *Remote Sensing*, *5*(12), 6159–6179. https://doi.org/10.3390/rs5126159

Jin, H., Jönsson, A. M., Bolmgren, K., Langvall, O., & Eklundh, L. (2017). Disentangling remotely-sensed plant phenology and snow seasonality at northern Europe using MODIS and the plant phenology index. *Remote Sensing of Environment*, *198*, 203–212. https://doi.org/10.1016/j.rse.2017.06.015

Jin, H., Jönsson, A. M., Olsson, C., Lindström, J., Jönsson, P., & Eklundh, L. (2019). New satellite-based estimates show significant trends in spring phenology and complex sensitivities to temperature and precipitation at northern European latitudes. *International Journal of Biometeorology*, *63*(6), 763–775. https://doi.org/10.1007/s00484-019-01690-5

Keenan, T. F., Gray, J., Friedl, M. A., Toomey, M., Bohrer, G., Hollinger, D. Y., Munger, J. W., O'Keefe, J., Schmid, H. P., Wing, I. S., Yang, B., & Richardson, A. D. (2014). Net carbon uptake has increased through warming-induced changes in temperate forest phenology. *Nature Climate Change*, *4*(7), 598–604. https://doi.org/10.1038/nclimate2253

Keenan, T. F., & Richardson, A. D. (2015). The timing of autumn senescence is affected by the timing of spring phenology: Implications for predictive models. *Global Change Biology*, *21*(7), 2634–2641. https://doi.org/10.1111/gcb.12890

Kim, J. H., Hwang, T., Yang, Y., Schaaf, C. L., Boose, E., & Munger, J. W. (2018). Warming-induced earlier greenup leads to reduced stream discharge in a temperate mixed forest catchment. *Journal of Geophysical Research: Biogeosciences*, *123*(6), 1960–1975. https://doi.org/10.1029/2018JG004438

Klosterman, S., Melaas, E., Wang, J. A., Martinez, A., Frederick, S., O'Keefe, J., Orwig, D. A., Wang, Z., Sun, Q., Schaaf, C., Friedl, M., & Richardson, A. D. (2018). Fine-scale perspectives on landscape phenology from unmanned aerial vehicle (UAV) photography. *Agricultural and Forest Meteorology*, *248*, 397–407. https://doi.org/10.1016/j.agrformet.2017.10.015

Knohl, A., Schulze, E.-D., Kolle, O., & Buchmann, N. (2003). Large carbon uptake by an unmanaged 250-year-old deciduous forest in Central Germany. *Agricultural and Forest Meteorology*, *118*(3–4), 151–167. https://doi.org/10.1016/S0168-1923(03)00115-1

Knohl, A., Siebicke, L., Tiedemann, F., Kolle, O., & ICOS Ecosystem Thematic Centre. (2022). *Warm winter 2020 ecosystem eddy covariance flux product from Hainich*. https://doi.org/10.18160/CR66-PJ24

Kowalski, T., & Holdenrieder, O. (2009). Pathogenicity of *Chalara fraxinea*. *Forest Pathology*, *39*(1), 1–7. https://doi.org/10.1111/j.1439-0329.2008.00565.x

Lang, W., Chen, X., Qian, S., Liu, G., & Piao, S. (2019). A new process-based model for predicting autumn phenology: How is leaf senescence controlled by photoperiod and temperature coupling? *Agricultural and Forest Meteorology*, *268*, 124–135. https://doi.org/10.1016/j.agrformet.2019.01.006

Lasslop, G., Reichstein, M., Papale, D., Richardson, A. D., Arneth, A., Barr, A., Stoy, P., & Wohlfahrt, G. (2010). Separation of net ecosystem exchange into assimilation and respiration using a light response

curve approach: Critical issues and global evaluation. *Global Change Biology*, *16*(1), 187–208. https://doi.org/10.1111/j.1365-2486.2009.02041.x

Liu, F., Wang, X., & Wang, C. (2019). Autumn phenology of a temperate deciduous forest: Validation of remote sensing approach with decadal leaf-litterfall measurements. *Agricultural and Forest Meteorology*, *279*, 107758. https://doi.org/10.1016/j.agrformet.2019.107758

Liu, G., Chen, X., Zhang, Q., Lang, W., & Delpierre, N. (2018). Antagonistic effects of growing season and autumn temperatures on the timing of leaf coloration in winter deciduous trees. *Global Change Biology*, *24*(8), 3537–3545. https://doi.org/10.1111/gcb.14095

Liu, Q., Fu, Y. H., Zeng, Z., Huang, M., Li, X., & Piao, S. (2016). Temperature, precipitation, and insolation effects on autumn vegetation phenology in temperate China. *Global Change Biology*, *22*(2), 644–655. https://doi.org/10.1111/gcb.13081

Liu, Q., Fu, Y. H., Zhu, Z., Liu, Y., Liu, Z., Huang, M., Janssens, I. A., & Piao, S. (2016). Delayed autumn phenology in the Northern Hemisphere is related to change in both climate and spring phenology. *Global Change Biology*, *22*(11), 3702–3711. https://doi.org/10.1111/gcb.13311

Lu, X., & Keenan, T. F. (2022). No evidence for a negative effect of growing season photosynthesis on leaf senescence timing. *Global Change Biology*, *28*(9), 3083–3093. https://doi.org/10.1111/gcb.16104

Marchand, L. J., Dox, I., Gričar, J., Prislan, P., Leys, S., van den Bulcke, J., Fonti, P., Lange, H., Matthysen, E., Peñuelas, J., Zuccarini, P., & Campioli, M. (2020). Inter-individual variability in spring phenology of temperate deciduous trees depends on species, tree size and previous year autumn phenology. *Agricultural and Forest Meteorology*, *290*, 108031. https://doi.org/10.1016/j.agrformet.2020.108031

Mariën, B., Balzarolo, M., Dox, I., Leys, S., Lorène, M. J., Geron, C., Portillo-Estrada, M., AbdElgawad, H., Asard, H., & Campioli, M. (2019). Detecting the onset of autumn leaf senescence in deciduous forest trees of the temperate zone. *The New Phytologist*, *224*(1), 166–176. https://doi.org/10.1111/nph.15991

McKinney, L. V., Nielsen, L. R., Hansen, J. K., & Kjær, E. D. (2011). Presence of natural genetic resistance in *Fraxinus excelsior* (Oleraceae) to *Chalara fraxinea* (Ascomycota): An emerging infectious disease. *Heredity*, *106*(5), 788–797. https://doi.org/10.1038/hdy.2010.119

Meier, U. (2018). Growth stages of mono- and dicotyledonous plants: BBCH monograph. Open Agrar Repositorium https://www.openagrar.de/receive/openagrar_mods_00042351, https://doi.org/10.5073/20180906-074619

Melaas, E. K., Sulla-Menashe, D., Gray, J. M., Black, T. A., Morin, T. H., Richardson, A. D., & Friedl, M. A. (2016). Multisite analysis of land surface phenology in North American temperate and boreal deciduous forests from Landsat. *Remote Sensing of Environment*, *186*, 452–464. https://doi.org/10.1016/j.rse.2016.09.014

Menzel, A., & Fabian, P. (1999). Growing season extended in Europe. *Nature*, *397*(6721), 659. https://doi.org/10.1038/17709

Menzel, A., Yuan, Y., Matiu, M., Sparks, T., Scheifinger, H., Gehrig, R., & Estrella, N. (2020). Climate change fingerprints in recent European plant phenology. *Global Change Biology*, *26*, 2599–2612. https://doi.org/10.1111/gcb.15000

Norby, R. J. (2021). Comment on "Increased growing-season productivity drives earlier autumn leaf senescence in temperate trees". *Science*, *371*(6533), eabg1438. https://doi.org/10.1126/science.abg1438

Peñuelas, J., Rutishauser, T., & Filella, I. (2009). Phenology feedbacks on climate change. *Science*, *324*(5929), 887–888. https://doi.org/10.1126/science.1173004

Piao, S., Friedlingstein, P., Ciais, P., Viovy, N., & Demarty, J. (2007). Growing season extension and its impact on terrestrial carbon cycle in the Northern Hemisphere over the past 2 decades. *Global Biogeochemical Cycles*, *21*(3), GB3018. https://doi.org/10.1029/2006GB002888

Piao, S., Liu, Q., Chen, A., Janssens, I. A., Fu, Y., Dai, J., Liu, L., Lian, X., Shen, M., & Zhu, X. (2019). Plant phenology and global climate change: Current progresses and challenges. *Global Change Biology*, *25*(6), 1922–1940. https://doi.org/10.1111/gcb.14619

Queloz, V., Grünig, C. R., Berndt, R., Kowalski, T., Sieber, T. N., & Holdenrieder, O. (2011). Cryptic speciation in *Hymenoscyphus albidus*. *Forest Pathology*, *41*(2), 133–142. https://doi.org/10.1111/j.1439-0329.2010.00645.x

R Core Team. (2022). *R: A language and environment for statistical computing*. https://www.R-project.org/

Reichstein, M., Falge, E., Baldocchi, D., Papale, D., Aubinet, M., Berbigier, P., Bernhofer, C., Buchmann, N., Gilmanov, T., Granier, A., Grünwald, T., Havránková, K., Ilvesniemi, H., Janous, D., Knohl, A., Laurila, T., Lohila, A., Loustau, D., Matteucci, G., … Valentini, R. (2005). On the separation of net ecosystem exchange into assimilation and ecosystem respiration: Review and improved algorithm. *Global Change Biology*, *11*(9), 1424–1439. https://doi.org/10.1111/j.1365-2486.2005.001002.x

Richardson, A. D., Black, T. A., Ciais, P., Delbart, N., Friedl, M. A., Gobron, N., Hollinger, D. Y., Kutsch, W. L., Longdoz, B., Luyssaert, S., Migliavacca, M., Montagnani, L., Munger, J. W., Moors, E., Piao, S., Rebmann, C., Reichstein, M., Saigusa, N., Tomelleri, E., … Varlagin, A. (2010). Influence of spring and autumn phenological transitions on forest ecosystem productivity. *Philosophical Transactions of the Royal Society of London. Series B, Biological Sciences*, *365*(1555), 3227–3246. https://doi.org/10.1098/rstb.2010.0102

Richardson, A. D., Keenan, T. F., Migliavacca, M., Ryu, Y., Sonnentag, O., & Toomey, M. (2013). Climate change, phenology, and phenological control of vegetation feedbacks to the climate system. *Agricultural and Forest Meteorology*, *169*, 156–173. https://doi.org/10.1016/j.agrformet.2012.09.012

Ryu, Y., Lee, G., Jeon, S., Song, Y., & Kimm, H. (2014). Monitoring multilayer canopy spring phenology of temperate deciduous and evergreen forests using low-cost spectral sensors. *Remote Sensing of Environment*, *149*, 227–238. https://doi.org/10.1016/j.rse.2014.04.015

Sagi, O., & Rokach, L. (2018). Ensemble learning: A survey. *WIREs Data Mining and Knowledge Discovery*, *8*(4), e1249. https://doi.org/10.1002/widm.1249

Smith, A. M., & Ramsay, P. M. (2020). A comparison of ground-based methods for obtaining large-scale, high-resolution data on the spring leaf phenology of temperate tree species. *International Journal of Biometeorology*, *64*(3), 521–531. https://doi.org/10.1007/s00484-019-01839-2

Soudani, K., Delpierre, N., Berveiller, D., Hmimina, G., Pontailler, J.-Y., Seureau, L., Vincent, G., & Dufrêne, É. (2021). A survey of proximal methods for monitoring leaf phenology in temperate deciduous forests. *Biogeosciences*, *18*(11), 3391–3408. https://doi.org/10.5194/bg-18-3391-2021

Stéfanon, M., Drobinski, P., D'Andrea, F., & Noblet-Ducoudré, N. d. (2012). Effects of interactive vegetation phenology on the 2003 summer heat waves. *Journal of Geophysical Research Biogeosciences*, *117*(D24). https://doi.org/10.1029/2012JD018187

Stener, L.-G. (2013). Clonal differences in susceptibility to the dieback of *Fraxinus excelsior* in southern Sweden. *Scandinavian Journal of Forest Research*, *28*(3), 205–216. https://doi.org/10.1080/02827581.2012.735699

Tamrakar, R., Rayment, M. B., Moyano, F., Mund, M., & Knohl, A. (2018). Implications of structural diversity for seasonal and annual carbon dioxide fluxes in two temperate deciduous forests. *Agricultural and Forest Meteorology*, *263*, 465–476. https://doi.org/10.1016/j.agrformet.2018.08.027

Templ, B., Koch, E., Bolmgren, K., Ungersböck, M., Paul, A., Scheifinger, H., Rutishauser, T., Busto, M., Chmielewski, F.-M., Hájková, L., Hodzić, S., Kaspar, F., Pietragalla, B., Romero-Fresneda, R., Tolvanen, A., Vučetič, V., Zimmermann, K., & Zust, A. (2018). Pan

European phenological database (PEP725): A single point of access for European data. *International Journal of Biometeorology*, *62*(6), 1109–1113. https://doi.org/10.1007/s00484-018-1512-8

Thiel, C., Mueller, M. M., Epple, L., Thau, C., Hese, S., Voltersen, M., & Henkel, A. (2020). UAS imagery-based mapping of coarse wood debris in a natural deciduous forest in Central Germany (Hainich National Park). *Remote Sensing*, *12*(20), 3293. https://doi.org/10.3390/rs12203293

Uphus, L., Lüpke, M., Yuan, Y., Benjamin, C., Englmeier, J., Fricke, U., Ganuza, C., Schwindl, M., Uhler, J., & Menzel, A. (2021). Climate effects on vertical Forest phenology of *Fagus sylvatica* L., sensed by Sentinel-2, time lapse camera, and visual ground observations. *Remote Sensing*, *13*(19), 3982. https://doi.org/10.3390/rs13193982

Wilhite, D. A., & Glantz, M. H. (1985). Understanding: The drought phenomenon: The role of definitions. *Water International*, *10*(3), 111–120. https://doi.org/10.1080/02508068508686328

Wu, C., Chen, J. M., Black, T. A., Price, D. T., Kurz, W. A., Desai, A. R., Gonsamo, A., Jassal, R. S., Gough, C. M., Bohrer, G., Dragoni, D., Herbst, M., Gielen, B., Berninger, F., Vesala, T., Mammarella, I., Pilegaard, K., & Blanken, P. D. (2013). Interannual variability of net ecosystem productivity in forests is explained by carbon flux phenology in autumn. *Global Ecology and Biogeography*, *22*(8), 994–1006. https://doi.org/10.1111/geb.12044

Wu, C., Gough, C. M., Chen, J. M., & Gonsamo, A. (2013). Evidence of autumn phenology control on annual net ecosystem productivity in two temperate deciduous forests. *Ecological Engineering*, *60*, 88–95. https://doi.org/10.1016/j.ecoleng.2013.07.019

Wutzler, T., Lucas-Moffat, A., Migliavacca, M., Knauer, J., Sickel, K., Šigut, L., Menzer, O., & Reichstein, M. (2018). Basic and extensible post-processing of eddy covariance flux data with REddyProc. *Biogeosciences*, *15*(16), 5015–5030. https://doi.org/10.5194/bg-15-5015-2018

Xie, Y., Wang, X., & Silander, J. A. (2015). Deciduous forest responses to temperature, precipitation, and drought imply complex climate change impacts. *Proceedings of the National Academy of Sciences of the United States of America*, *112*(44), 13585–13590. https://doi.org/10.1073/pnas.1509991112

Xie, Y., Wang, X., Wilson, A. M., & Silander, J. A. (2018). Predicting autumn phenology: How deciduous tree species respond to weather stressors. *Agricultural and Forest Meteorology*, *250-251*, 127–137. https://doi.org/10.1016/j.agrformet.2017.12.259

Yuan, Y., Härer, S., Ottenheym, T., Misra, G., Lüpke, A., Estrella, N., & Menzel, A. (2021). Maps, trends, and temperature sensitivities-phenological information from and for decreasing numbers of volunteer observers. *International Journal of Biometeorology*, *65*(8), 1377–1390. https://doi.org/10.1007/s00484-021-02110-3

Zani, D., Crowther, T. W., Mo, L., Renner, S. S., & Zohner, C. M. (2020). Increased growing-season productivity drives earlier autumn leaf senescence in temperate trees. *Science*, *370*(6520), 1066–1071. https://doi.org/10.1126/science.abd8911

Zeng, L., Wardlow, B. D., Xiang, D., Hu, S., & Li, D. (2020). A review of vegetation phenological metrics extraction using time-series, multispectral satellite data. *Remote Sensing of Environment*, *237*, 111511. https://doi.org/10.1016/j.rse.2019.111511

Zhao, B., Donnelly, A., & Schwartz, M. D. (2020). Evaluating autumn phenology derived from field observations, satellite data, and carbon flux measurements in a northern mixed forest, USA. *International Journal of Biometeorology*, *64*(5), 713–727. https://doi.org/10.1007/s00484-020-01861-9

Zhou, S., Zhang, Y., Caylor, K. K., Luo, Y., Xiao, X., Ciais, P., Huang, Y., & Wang, G. (2016). Explaining inter-annual variability of gross primary productivity from plant phenology and physiology. *Agricultural and Forest Meteorology*, *226-227*, 246–256. https://doi.org/10.1016/j.agrformet.2016.06.010

Zhou, S., Zhang, Y., Ciais, P., Xiao, X., Luo, Y., Caylor, K. K., Huang, Y., & Wang, G. (2017). Dominant role of plant physiology in trend and variability of gross primary productivity in North America. *Scientific Reports*, *7*, 41366. https://doi.org/10.1038/srep41366

Zohner, C. M., Mirzagholi, L., Renner, S. S., Mo, L., Rebindaine, D., Bucher, R., Palouš, D., Vitasse, Y., Fu, Y. H., Stocker, B. D., & Crowther, T. W. (2023). Effect of climate warming on the timing of autumn leaf senescence reverses after the summer solstice. *Science*, *381*(6653), eadf5098. https://doi.org/10.1126/science.adf5098

Zohner, C. M., & Renner, S. S. (2019). Ongoing seasonally uneven climate warming leads to earlier autumn growth cessation in deciduous trees. *Oecologia*, *189*(2), 549–561. https://doi.org/10.1007/s00442-019-04339-7

SUPPORTING INFORMATION

Additional supporting information can be found online in the Supporting Information section at the end of this article.

How to cite this article: Kloos, S., Klosterhalfen, A., Knohl, A., & Menzel, A. (2024). Decoding autumn phenology: Unraveling the link between observation methods and detected environmental cues. *Global Change Biology*, *30*, e17231. https://doi.org/10.1111/gcb.17231

The linkage between functional traits and drone-derived phenology of 74 Northern Hemisphere tree species

Simon Kloos[1], Marvin Lüpke[1], Nicole Estrella[1], Wael Ghada[1], Jens Kattge[2,3], Solveig Franziska Bucher[3,4], Allan Buras[5], Annette Menzel[1,6,*]

[1]TUM School of Life Sciences, Ecoclimatology, Technical University of Munich; Hans-Carl-von-Carlowitz-Platz 2, 85354 Freising, Germany; simon.kloos@tum.de, marvin.luepke@tum.de, estrella@tum.de, annette.menzel@tum.de

[2]Max Planck Institute for Biogeochemistry; Hans-Knöll-Straße 10, 07745 Jena, Germany; jkattge@bgc-jena.mpg.de

[3]German Centre for Integrative Biodiversity Research (iDiv) Halle-Jena-Leipzig; Puschstraße 4, 04103 Leipzig, Germany

[4]Institute of Ecology and Evolution, Plant Biodiversity Group, Friedrich Schiller University Jena; Philosophenweg 16, 07743 Jena, Germany; solveig.franziska.bucher@uni-jena.de

[5]TUM School of Life Sciences, Land Surface-Atmosphere Interactions, Technical University of Munich; Hans-Carl-von-Carlowitz-Platz 2, 85354 Freising, Germany; allan.buras@tum.de

[6]Institute for Advanced Study, Technical University of Munich; Lichtenbergstraße 2a, 85748 Garching, Germany

[*]Correspondence: annette.menzel@tum.de; ORCID iD: 0000-0002-7175-2512

Abstract: Tree phenology is a major component of the global carbon and water cycle, serving as a fingerprint of climate change, and exhibiting significant variability both within and between species. In the emerging field of drone monitoring, it remains unclear whether this phenological variability can be effectively captured across numerous tree species. Additionally, the drivers behind interspecific variations in the phenology of deciduous trees are poorly understood, although they may be linked to plant functional traits. In this study, we derived the start of season (SOS), end of season (EOS), and length of season (LOS) for 3,099 individuals from 74 deciduous tree species of the Northern Hemisphere at a unique study site in southeast Germany using drone imagery. We validated these phenological metrics with in-situ data and analyzed the interspecific variability in terms of plant functional traits. The drone-derived SOS and EOS showed high agreement with ground observations of leaf unfolding (R^2 = 0.49) and leaf discoloration (R^2 = 0.79), indicating that this methodology robustly captures phenology at the individual level with low temporal and human effort. Both intra- and interspecific phenological variability were high in spring and autumn, leading to differences in the LOS of up to two months under almost identical environmental conditions. Functional traits such as seed dry mass, chromosome number, and continent of origin played significant roles in explaining interspecific phenological differences in SOS, EOS, and LOS, respectively. In total, 55 %, 39%, and 45 % of interspecific variation in SOS, EOS, and LOS could be explained by the Boosted Regression Tree (BRT) models based on functional traits. Our findings encourage new research avenues in tree phenology and advance our understanding of the growth strategies of key tree species in the Northern Hemisphere.

Keywords: UAV, leaf unfolding, senescence, growing season, phenological variability, plant traits

1. Introduction

Plant phenology is an important indicator of the ecological impacts of climate change (Cleland et al., 2007; Menzel et al., 2020; Piao et al., 2019) and influences essential functions of terrestrial ecosystems such as photosynthetic activity (Keenan et al., 2014; Piao et al., 2007; Tang et al., 2016) or evapotranspiration (Gaertner et al., 2019; Kim et al., 2018). Spring phenology is primarily controlled by temperature (Ettinger et al., 2020; Flynn and Wolkovich, 2018; Menzel et al., 2006) and shows mostly advancing trends in the northern hemisphere due to global warming in recent decades (Melaas et al., 2018; Menzel et al., 2020; Vitasse et al., 2022). In contrast, autumn phenology is slightly delayed with global warming, but the responses are much more heterogeneous (Garonna et al., 2016; Piao et al., 2019) and the drivers are still not fully understood (Gill et al., 2015; Kloos et al., 2024; Lu and Keenan, 2022; Zohner et al., 2023). Offsetting the onset dates of spring and autumn phenology against each other, the growing season length (phenological season; Körner et al., 2023) can be obtained.

In analyses of both trends and drivers for spring and autumn phenology, as well as the resulting growing season length, phenological variability is a frequently underestimated factor. For example, in twelve years of phenological observations in a North American forest (16 canopy species), roughly six weeks of interspecific difference in budburst and almost three weeks of difference in leaf coloration were observed (Richardson and O'Keefe, 2009). Two years of in-situ budburst observations in six deciduous tree species and a total of 825 individuals in a European woodland showed species-specific differences of up to 42 days (Cole and Sheldon, 2017). On the other hand, phenological variability can also be observed within tree species: Budburst, for example, has been observed to vary between individuals of *Quercus petraea* by up to 26 days and the onset of senescence by up to 51 days between individuals of *Betula pendula* at the same location. In general the autumn phenology seems to exhibit a higher intraspecific variability (Capdevielle-Vargas et al., 2015; Delpierre et al., 2017; Marchand et al., 2020). The age and height of the trees play an important role in observing spring and autumn phenology for smaller and subcanopy individuals in a stand (Augspurger and Bartlett, 2003; Gressler et al., 2015; Osada and Hiura, 2019; Uphus et al., 2021).

For trend- and driver-analyses in plant phenology, these forms of variability primarily translate into unexplained variance. From an ecological perspective, phenological variability may also constitute a major factor for resilience against extremes, e.g., late spring frost damage (Diez et al., 2012). Consequently, this inter-and intraspecific variability is of great interest. The correlation of interspecific variation of phenology to biotic factors (and especially plant functional traits) could be used to get a better understanding of climate-resilient forest species and to open avenues to extrapolation of single species results. In the last decades, many studies have demonstrated the significance of functional traits for the onset dates of certain phenological phases of different, however mostly herbaceous species: In previous studies, for example, plant height (e.g., Horbach et al., 2023; Sporbert et al., 2022; Sun and Frelich, 2011), seed dry mass (e.g., Bolmgren and Cowan, 2008; Du and Qi, 2010; Segrestin et al., 2020), leaf area (Liu ZhiGuo et al., 2011; Sun et al., 2006) and thickness (Craine et al., 2012; Horbach et al., 2023), leaf area per leaf dry mass (specific leaf area, SLA; Bucher et al., 2018; Bucher and Römermann, 2021; Horbach et al., 2023; Sporbert et al., 2022), leaf dry mass per leaf fresh mass (leaf dry matter content, LDMC; Horbach et al., 2023; Sporbert et al., 2022) and chemical properties of the leaf such as phosphorus (P; Bucher et al.,

2018), carbon (C; Bucher and Römermann, 2021; Sporbert et al., 2022) or nitrogen (N; Bucher et al., 2018; Craine et al., 2012; Sporbert et al., 2022) content were associated with different phenological phases. Less recognized traits in connection with plant phenology are the rooting depth (Dorji et al., 2013) and the diameter of the spring/xylem vessels (Lechowicz, 1984; Panchen et al., 2014). Finally, Zohner and Renner (2017) revealed that the region of origin of a plant also has an influence on spring and autumn phenology and can therefore determine the length of the growing season.

However, up to date, the link between onset dates of phenological phases, especially the beginning and end of the growing season, and functional traits has hardly been studied for deciduous tree species. On the one hand, this is because there are barely any sites with an adequate number of different tree species with mature individuals. On the other hand, the in-situ observation of different phenological phases and functional traits on the individual level is extremely time-consuming and resource-intensive. A relatively new approach for solving the phenological monitoring problem is the derivation of plant phenology via unmanned aerial vehicles (UAV): Various phenological metrics (especially SOS and EOS) can be monitored via drone images and the resulting spectral indices (e.g., Dandois and Ellis, 2013; Klosterman and Richardson, 2017; Kleinsmann et al., 2023). The main advantage of this method is that, compared to satellite remote sensing, the spatial resolution is much higher, and thus analyses at the individual level are possible. At the same time, a larger area and more individuals can be covered than with in-situ observations. Studies specifically analyzing deciduous tree phenology have received ambiguous but acceptable results when comparing drone-derived phenology and the phenology deduced from other data sources such as in-situ observations or satellite remote sensing (Berra et al., 2019; Berra and Gaulton, 2021). Only a few studies exist which evaluate the phenology of several deciduous tree species via drone: Wu et al. (2021) combined PlanetScope and drone data for the autumn phenology of eleven canopy tree species in northeast China and found high agreement with phenocams, while Fawcett et al. (2021) showed understory effects in the drone-derived spring phenology of a heterogeneous ecosystem in the UK. These understory effects might also explain poor drone coverage of inter- and intraspecific spring phenological variability in a Japanese study (19 deciduous broad-leaved species; Budianti et al., 2021), whereas a follow-up study with 17 species showed partly significant correlation between drone and ground-observed phenometrics (Budianti et al., 2022).

However, several research gaps appear: First, there are (to our knowledge) no analyses in the still young research field of drone monitoring that have tested whether realistic phenological data sets can be generated for a large number (> 20) of deciduous tree species using a drone flight series. Second, there are hardly any studies available that systematically analyze the inter- and intraspecific variability of spring and autumn phenology and the length of the growing season for a large number of deciduous tree species at one site. As a result, there is little knowledge about the relationship or influence of functional traits on different phenological phases and metrics, such as SOS, EOS, or LOS, especially for deciduous tree species. Applying a year-round drone monitoring of 74 deciduous tree species from the Northern Hemisphere with a total of 3099 individuals at a unique study site in southeast Germany, our study asks the following research questions:

1. Can the spring and autumn phenology, along with the resulting length of the growing season, of a diverse array of deciduous tree species at a single site be accurately determined using drone data and a universal method applicable to all species?

2. To what extent do the determined phenological metrics (SOS, EOS, LOS) vary between and within the individual tree species under almost identical environmental conditions?
3. Can the observed interspecific phenological variability be explained by functional traits of the respective tree species, and if so, which traits play a dominant role?

2. Materials and Methods

2.1. Study site

The study was conducted in the "Weltwald Freising" (World Forest), which is located in southeastern Germany (48°24'50''N, 11°40'00''E; 462 to 508 m a.s.l.; State Office for Digitization, Broadband and Surveying, 2023; Figure 1). The area of the forest is about 100 ha and more than 400 tree and shrub species of the Northern Hemisphere have been planted there since 1987 (Rudolf, 2023). The arboretum is divided according to the continental origin of the tree and shrub species. Species are planted in plots, each containing from a few single individuals to nearly 200 specimens of the respective species. Only deciduous tree species were selected for the analysis since their phenological phases are easier and more robust to detect using drone data than for evergreen species.

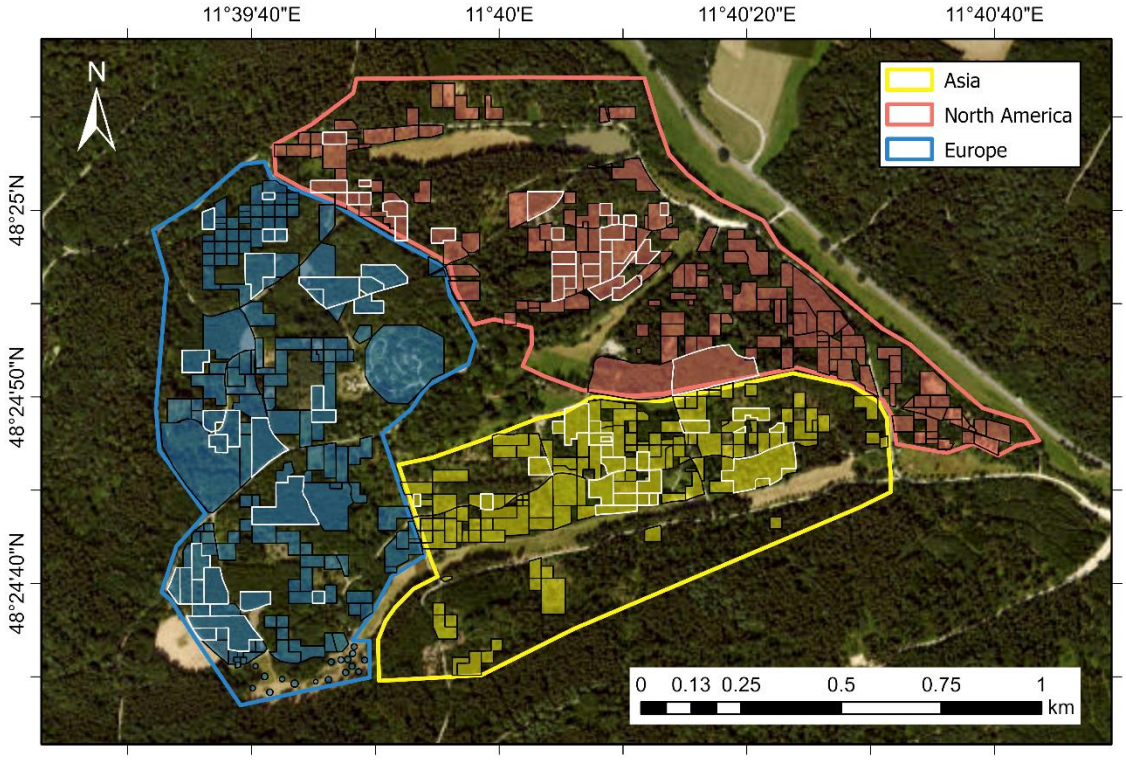

Figure 1: Map of Weltwald Freising. The areas marked in color represent the individual tree species plots, whereby the plots framed in white are the analyzed tree species plots within this study (for the selection criteria see section 2.3.1; yellow: Asia; blue: Europe; red: North America; background map: Maxar, Microsoft; polygon data: Bavarian State Forestry, 2022).

Most of the soils in the study area are deep, mixed substrates of Tertiary (gravels, sands) and Quaternary (loess loam) sediments, which have a high nutrient availability and water retention capacity. The regional climate is subatlantic to subcontinental, the mean annual temperature is

9.4 °C and the mean annual precipitation is 736 mm (2001-2020; DWD, 2024; Rudolf, 2023). In the observation year 2022, the mean temperature in the study area was 9.6 °C, and the annual precipitation total was 829 mm (for further details see Figure S1; data provided by the Bavarian State Institute of Forestry). The microclimate should be homogeneous within the study area and between the individual continental areas due to the small differences in altitude (see Figure S2).

2.2. Data

2.2.1. Drone imagery

To observe the phenological development at the study site, in total 27 flights with a Phantom 4 multispectral UAV (DJI, Nanshan, Shenzhen, China) at 100 m a.g.l. flight height with a ground sampling distance of 5-8 cm were performed in 2022. Images were taken once per second at the red (650 nm ± 16 nm), near-infrared (NIR; 840 nm ± 26 nm), and RGB cameras at a 2 MP resolution in NADIR position. The drone used an integrated dual-band high precision Real Time Kinematic (RTK) GPS with Networked Transport of RTCM via Internet Protocol (NTRIP) network service to get a repeatable position accuracy (up to 0.1 m vertical and horizontal precision according to the manufacturer manual). To enhance accuracy further, at least five measured ground control points were placed in each flight area. The flight grid was set up with a frontal and lateral overlap of 85%. The orientation of the grid was set by the flight software automatically according to sun direction, sun angle, and date to avoid disturbance from sunlight on the camera sensor. This was important since flights were also conducted in early spring and late autumn with typically lower sun angles compared to summer months.

All settings were optimized for the highest flight speed and therefore to achieve largest coverage and avoid strong shadow movement. Optimal drone orthomosaics are usually generated under overcast and calm (no wind) conditions, as images with even illumination do not have any shadows and canopies are not blurred due to movement. Since such conditions are rare, flight days with uniform clear skies or overcast conditions and low wind speeds were targeted. The flight time was typically set around noon with highest sun angle, in order to avoid long shadows. The exact flight dates are listed in Table S1.

Before each flight, a picture of a calibration reflectance panel (AgEagle Aerial Systems Inc., Wichita, Kansas, USA) was taken since this was a requirement for the processing software PIX4d to calculate reflectance values for both spectral channels. The drone images were processed in PIX4d mapper Version 4.75 (Pix4D, Prilly, Switzerland) to generate RGB orthomosaics, Normalized Difference Vegetation Index (NDVI) maps, a digital terrain model (DTM), a digital surface model (DSM), and 3D point clouds. A custom configuration was used to process the images (Table S2) since the standard setting worked insufficiently with the drone cameras. The output resolution for all images was set to 10 cm, except the DTM with 1 m resolution.

2.2.2. In-situ observations

For validation purposes, the phenology of selected tree species was observed from the ground in spring and autumn 2022. In spring, 45 of the 74 tree species observed with the drone were monitored from in-situ (Table S3). From the end of March to the end of May, the phenological phase of each tree species was recorded plot-wise twice a week based on a categorical scale (Vitasse et al., 2013):

- 0: buds closed (no bud activity)
- 1: budburst (buds are open and leaves are partially visible)
- 2: leaf emergence (leaves fully emerged from the buds but are still folded, crinkled or pendant)
- 3: leaf unfolding (for each tree at least one leaf is fully unfolded)

For the validation of the drone-derived SOS, the date on which phase 3 was observed for the first time from the ground was selected for each tree species.

In autumn, 27 of the 74 species monitored with the drone were additionally observed from the ground (Table S3). Between mid-September and early December, the degree of leaf discoloration and leaf fall of the respective tree species was estimated plot-wise twice a week in 10% steps. For leaf discoloration, this included fallen leaves on the ground in the estimates. For validation with the drone-based EOS, the degree of leaf discoloration was finally interpolated at a daily time resolution and the date on which the proportion of discolored leaves for the first time reached at least 50% was determined as ground-truth EOS. To validate the drone-derived phenology with the in-situ data, a simple linear regression was calculated between the two data sets, and the associated coefficient of determination and p-value were defined. The mean difference between the two onset dates and the percentage of species exhibiting at maximum five days of deviation was used as a further evaluation measure for spring and autumn. Not all drone-monitored species were validated on the ground due to the extensive study area, which demanded significant time and personnel resources for on-site observations.

2.2.3. Functional traits

To explain differences in the interspecific variability of phenology in the study area as derived from drone flights, 13 functional traits of the tree species (Table 1) were included in the analysis, selected from an initial set of 23 numerical traits (Table S4). The age of the tree species was determined from planting dates provided by the Bavarian State Forestry (2022), whereas the mean tree height and crown area of each tree species were derived from the drone data (via crown extraction and selection, see 2.3.1.). The number of chromosomes was determined for the individual tree species using the CCBD (Chromosome Counts Database; Rice et al., 2015) whereby the respective median was assigned to each species. In addition to the numerical traits, the continent of origin was included as a categorical trait variable for each tree species.

The other numerical traits were extracted from the TRY plant trait database (Kattge et al., 2020): Originally, a trait matrix with the trait measurements for all available species from the TRY database was created. The data were transformed into a normal distribution and then z-transformed. The gaps in the matrix were then filled using the Bayesian hierarchical probabilistic matrix factorization (BHPMF) gap-filling algorithm (Schrodt et al., 2015), which is based on probabilistic matrix factorization (PMF) and the taxonomic hierarchy of the plant kingdom. Subsequently, the matrix values were transformed back, and finally outliers were removed based on the z-transformation.

For 70 study species (*Alnus rugosa*, *Carya tomentosa*, *Populus trichocarpa*, and *Pterocarya fraxinifolia* are not included in TRY), a mean value was then calculated for each trait and species from the individual values in the TRY data set. Based on the "stable species hierarchy" hypothesis, it can be assumed that although these mean values do not necessarily correspond to the values for the study area in absolute terms, the hierarchical arrangement of values between

species should remain approximately the same (e.g., Kazakou et al., 2014; Cordlandwehr et al., 2013; Violle et al., 2015).

The final selection of numerical traits (Table 1) for the Boosted Regression Trees (BRT) analysis (section 2.3.3.) was based on two criteria: In the first step, all traits were selected for which a connection to plant phenology had already been established in the existing literature (see Table 1). In the second step, additional traits were included which showed a statistically significant correlation with the phenological metrics determined from the drone data (Table S4; section 2.3.2.).

Table 1: Functional traits used for analysis of interspecific variability in phenology. The table indicates their units, lists studies that have linked the relationship of the respective trait to a plant phenological phase, and summarizes the respective type of correlation. The table distinguishes between tree species (black) and non-tree species (gray) studies.

Plant trait	Unit	Link to plant phenology	Correlation between trait and phenological onset date
Tree (plant) height	m	Horbach et al., 2023; Sporbert et al., 2022; Liu et al., 2021; Segrestin et al., 2020; König et al., 2018; Lauterbach et al., 2013; Sun and Frelich, 2011; Du and Qi, 2010; Bolmgren and Cowan, 2008; Vile et al., 2006; Louault et al., 2005	Positive (all phenophases, especially flowering)
Leaf area	mm^2	Sporbert et al., 2022; Segrestin et al., 2020; Craine et al., 2012; Liu ZhiGuo et al., 2011; Sun et al., 2006	Positive (leaf unfolding) and negative (flowering, fruiting, senescence)
Leaf thickness	mm	Horbach et al., 2023; Craine et al., 2012	Negative (leaf unfolding and flowering)
Leaf area per leaf dry mass (SLA)	mm^2 mg^{-1}	Horbach et al., 2023; Sporbert et al., 2022; Bucher and Römermann, 2021; Bucher et al., 2018; König et al., 2018; Lauterbach et al., 2013; Sun and Frelich, 2011; Vile et al., 2006	Positive (fruiting) and negative (leaf unfolding)
Leaf dry mass per leaf fresh mass (LDMC)	$g\ g^{-1}$	Horbach et al., 2023; Sporbert et al., 2022; Bucher and Römermann, 2021; König et al., 2018	Positive (leaf unfolding) and negative (flowering)
Seed dry mass	mg	Sporbert et al., 2022; Liu et al., 2021; Segrestin et al., 2020; Craine et al., 2012; Du and Qi, 2010; Bolmgren and	Negative (flowering)

		Cowan, 2008; Vile et al., 2006; Louault et al., 2005	
Leaf N content per leaf dry mass	mg g^{-1}	Sporbert et al., 2022; Bucher and Römermann, 2021; Segrestin et al., 2020; Bucher et al., 2018; Craine et al., 2012	Negative (leaf unfolding, flowering, fruiting)
Leaf C content per leaf dry mass	mg g^{-1}	Sporbert et al., 2022; Bucher and Römermann, 2021; Craine et al., 2012	Positive (leaf unfolding, fruiting, senescence)
Leaf P content per leaf dry mass	mg g^{-1}	Segrestin et al., 2020; Bucher et al., 2018	Negative (flowering)
Root rooting depth	m	Dorji et al., 2013	Positive (flowering)
Stem conduit diameter	micro m	Lechowicz, 1984; Panchen et al., 2014	Positive (leaf unfolding)
Chromosome number	n	Included due to high correlation values with extracted phenological metrics (2.3.2; Table S4)	Negative (senescence)
Fine root length per fine root dry mass (specific root length, SRL)	cm g^{-1}	Included due to high correlation values with extracted phenological metrics (2.3.2; Table S4)	Positive (leaf unfolding)

2.2.4. Climate distances

To represent the climatic origin of each tree species, we combined species-specific distribution maps with so-called climate distances (Buras and Menzel, 2019). These climate distances represent conflated Manhattan distances of the 30-year climatology of 11 climate variables (e.g. growing season length, climatic water balance of the driest month, for details see supplementary Table S2 in Buras and Menzel, 2019) representing the period 1961-1990. Climate distances were based on CRU TS (v 4.01; Harris et al., 2020) temperature data and GPCC precipitation data (Schneider et al., 2011) which are available at monthly temporal and 0.5° spatial resolution. To represent the climatic distance of each species under investigation, we extracted the climate distances to the grid-cell representative of our study site (48.25°N, 11.25°E) for all terrestrial grid cells on Earth. Thus, the extracted values represent a measure of the dissimilarity of each grid cells' climate to the climate in our study site. Further details on the derivation of climate distances are specified in Buras and Menzel (2019).

To assign a climate distance for each tree species, the distribution area of the respective species was determined. For European species, the distribution in terms of chorological maps (Caudullo et al., 2017) and relative probability of presence (RPP; de Rigo et al., 2016) were obtained from the website of the Joint Research Centre of the European Commission. Synanthropic occurrences were excluded to keep the focus on the natural distribution of the species. Equally, we excluded fragmented isolated occurrences to avoid including entire grid cells for the sake of only a few observations. For all other species, the GBIF (Global Biodiversity Information Facility, 2021) occurrence data were used. We limited our research to tree-species observations after 1900 and

excluded species that did not occur in at least 100 grid cells considering a global resolution of 0.5° x 0.5°. For the resulting 60 (of 74) individual species distributions, we extracted all climate distances for further processing. To avoid the effect of a large distribution area, we identified for each tree species the regions in the chorological map where the climate distance to the study area was within the lower 20% quantile. Within these regions, we calculated the median of climate distances to the study area.

2.3. Methods

2.3.1. Extraction and selection of tree crowns

To extract phenology on an individual tree level, single tree canopies needed to be identified from the drone images. As input for the tree detection algorithms a canopy height model (CHM) was calculated from the difference between the DSM and the DTM. DTMs were constructed from the end of March (22nd and 28th) drone images, when all deciduous trees had no leaves, and the ground was clearly visible. DSM was obtained from drone images at the end of July (27th) when all canopies were fully developed.

Treetops were detected by a variable window filter (Popescu and Wynne, 2004) using the *vwf* function in the R (R Core Team, 2022) package *ForestTools* (v.1.0.1; Plowright and Roussel, 2023). The algorithm detects local maxima, which correspond to a treetop, via a specific window filter size in the CHM. The window size was set by a height-dependent function, starting from 3 m to 8 m CHM height with a constant value of 1, growing windows with a linear function (height * 0.06 + 0.52) from 8-35 m CHM height and a final constant of 2.62 above a CHM height of 35 m. The function was derived by comparing different functions against a manually derived treetop map. All treetops below 5 m were ignored since these mostly included shrubs and/or saplings. In a further step, unrealistic and falsely detected treetops were removed, and missing treetops were added by comparing the tops with multiple orthomosaics from spring, summer, and autumn.

Crowns were segmented from the filtered treetops with the algorithm by Dalponte and Coomes (2016) using the R (R Core Team, 2022) package *lidR* (v3.1.0; Roussel et al., 2023; Roussel et al., 2020). The algorithm used a height threshold of 5 m, a growing threshold 1 of 0.35, a growing threshold 2 of 0.55, and a maximum amount of 90 pixels for the crown diameter of a detected tree.

After the extraction of the tree crowns for the study area, the canopy area (in m^2) was calculated for all crowns. All individuals with a canopy area < 3 m^2 were removed from the analysis to avoid tree crowns with a low pixel count. Within each plot, tree crowns were manually filtered, removing "non-circular" crowns (incorrectly determined by the algorithm, significantly longer than wide) from the final dataset. In addition, only crowns that were located within the planted plots and species (derived from Bavarian State Forestry, 2022) with a minimum number of five individuals within the plot were included in the analyses to ensure a higher representativeness of the results. In the last step, 10 cm (one pixel) reverse buffers were calculated around each tree crown to avoid overlaps and mixed pixels from two crowns. After the selection process, 74 tree species (Table S3) and 3099 individuals were included in the final analysis.

2.3.2. Extraction of phenological metrics

The extraction of the phenological metrics for the single trees was done in R (R Core Team, 2022) with the *phenex* package (v.1.4-5; Lange and Doktor, 2022). In the first step, a raster stack of all

27 NDVI images of the year was created. Subsequently, we computed the median of the NDVI pixels within each of the respective tree crowns for each of the 27 scenes. A double logistic function was then fitted (Fischer, 1994) for each tree crown using the non-corrected 27 median NDVI values. To determine individual SOS and EOS dates from these fitted NDVI curves, percentage thresholds were set between the lowest, early-season (i.e., before peak-season NDVI) and highest NDVI value (SOS) and the highest and lowest, late-season NDVI (EOS) in the time series ("local" threshold). The SOS/EOS dates were then defined on the day when NDVI first exceeded or fell below these thresholds. Each threshold was tested in 10 percent increments and the SOS/EOS results were compared to the observed in-situ data. The best validation results were obtained with a threshold of 0.5 for SOS and 0.7 for EOS. These phenological metrics were then used for all further analyses (for illustration, see Figure S3). Finally, the length of the growing season (LOS) was calculated by subtracting SOS from EOS for each tree crown. To analyze differences in tree species phenology with respect to the continent of origin, a two-sided Wilcoxon test was calculated between the respective continent groups.

2.3.3. Boosted Regression Trees (BRT)

To explain the interspecific variability of SOS, EOS, and LOS in the study area by traits (2.2.3.), a BRT analysis was conducted. BRTs are a combination of regression trees and boosting, a machine-learning algorithm. They have the advantage that predictor variables of any type (numeric, binary, categorical) can be used and that they are relatively insensitive to outliers and collinearity, which means that no variance inflation has to be calculated in advance (Elith et al., 2008; Sporbert et al., 2022). We altogether computed three BRTs, i.e. each one to model the variance of the tree species median SOS/EOS/LOS. As predictor variables we used 1) the 13 selected numerical traits (Table 1), 2) the continent of origin of the tree species as a categorical variable, and 3) the climatic distance calculated in each case (section 2.2.4.). The models were set up in R (R Core Team, 2022) using the package *dismo* (v1.3-14; Hijmans et al., 2023). We used a Gaussian error distribution, a tree complexity of 1, a learning rate of 0.003, and a bag fraction of 0.5 for all models. Finally, partial dependency plots and the relative importance (%) of all predictor variables in the models were calculated. To evaluate the model performance, we used cross-validation (cv) correlation and predicted (BRT) vs. observed (drone-derived) SOS, EOS, and LOS plots (see Figure S4-6).

3. Results

3.1. Validation of drone phenology

When comparing the ground observations (first leaf unfolding) and the drone-derived spring phenology (SOS, local threshold: 0.5) for the individual tree species, a good agreement of the dates was found ($R^2 = 0.49$; $p < 0.001$; Figure 2). 53 % of the observed tree species had an in-situ/drone SOS difference of at most five days and the mean difference between drone-derived and in-situ SOS was 5.6 days. For early leaf-unfolding species, the drone-derived SOS tended to be recorded later than the observed leaf emergence, while later sprouting species had the tendency to be assigned with earlier SOS values in comparison to the in-situ data. Validation differences between the individual continents of origin could not be determined, although North American species tended to leaf out later compared to the other continents.

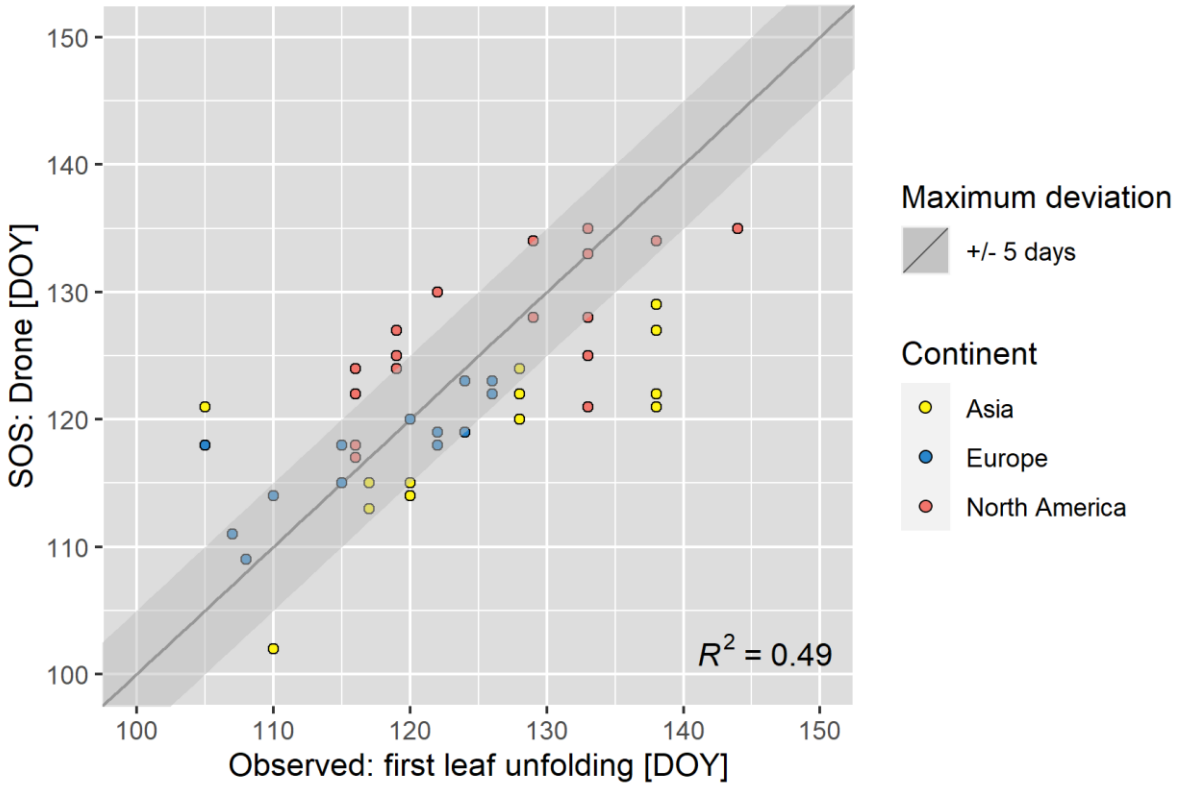

Figure 2: Scatterplot of the observed first leaf unfolding, and the calibrated SOS determined by the drone images for the respective tree species. The observed tree species are color-coded according to the continent of origin (yellow: Asia; blue: Europe; red: North America). The dark gray line in the plot represents the area where the in-situ data and the drone data for spring phenology match perfectly. The dark gray area marks a maximum deviation of five days between in-situ and drone phenology (inside: 53 % of the observed tree species). The coefficient of determination is shown at the bottom right of the plot.

When comparing the autumn phenology data, even higher agreement between the drone EOS (local threshold: 0.7) and the ground observations (50 % leaf discoloration) was observed than in spring (R^2 = 0.79; $p < 0.001$; Figure 3). 93 % of the data points were within the 5-day deviation between drone-derived and observed autumn phenology and the mean difference between drone and in-situ EOS was 2.8 days. No differences were found within the validation in the distinction between early and late senescent species or in the continent of origin, whereas North American species were more likely to be early senescing species.

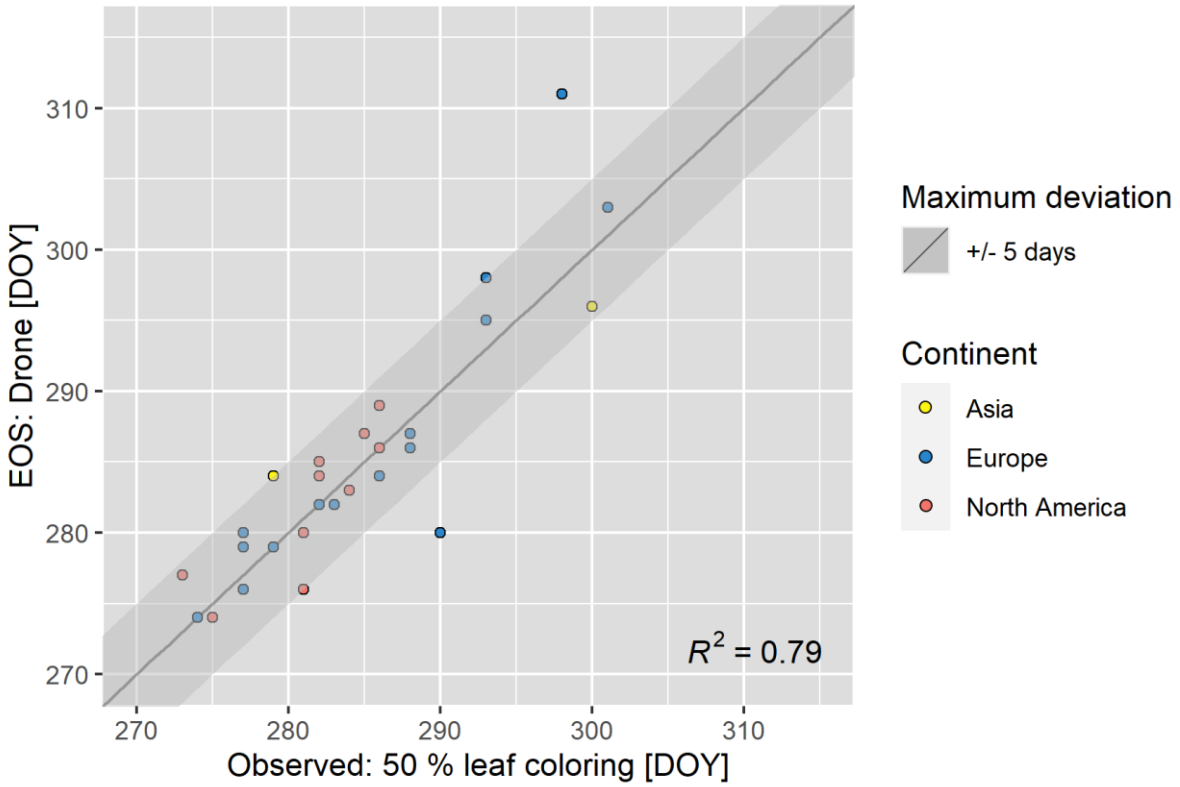

Figure 3: Scatterplot between the observed 50 % leaf coloring, and the calibrated EOS determined by the drone images for the respective tree species. The observed tree species are color-coded according to the continent of origin (yellow: Asia; blue: Europe; red: North America). The dark gray line in the plot represents the area where the in-situ data and the drone data for autumn phenology match perfectly. The dark gray area marks a maximum deviation of five days between in-situ and drone phenology (inside: 93 % of the observed tree species). The coefficient of determination is shown at the bottom right of the plot.

3.2. Tree phenology

The spring phenology (SOS) of the 74 tree species observed in the study area in 2022 ranged from the end of March to the end of May, with a difference of 41 days between the median of the first (*Prunus padus*; 4th of April) and the last leaf-unfolding species (*Carya tomentosa*; 15th of May; Figure 4). In addition, it should be noted that there were a few species (*Prunus padus*, *Larix gemlinii var. principis-rupprechtii*, *Larix decidua var. polonica*) that unfolded their leaves/needles much earlier (6-14 days median difference) than the vast majority. Remarkable differences in SOS were also observed within species (*Fraxinus pennsylvanica* with an interquartile range (IQR) of 11 days as well as *Betula costata* and *Quercus alba* with an IQR of 9 days each as the three most variable species). Notably the North American species leaved out significantly later compared to species of the other two continents (10-day difference to Europe in the median and 8 days to Asia; Asia/North America: $W = 82.5$, $p < 0.001$; Europe/North America: $W = 112$, $p < 0.001$).

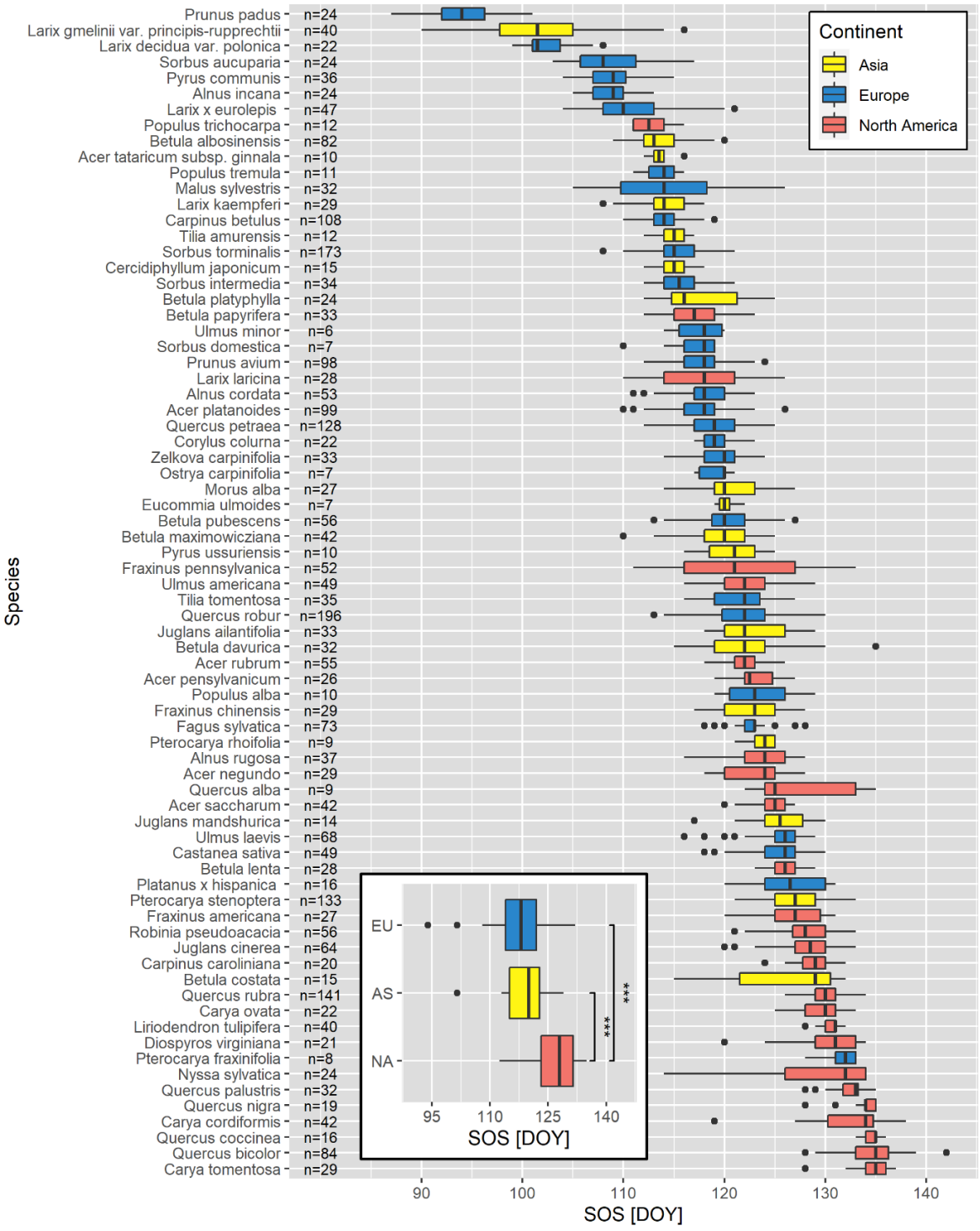

Figure 4: Drone-derived SOS for the 74 tree species observed in the study area, ordered by median. The respective boxplots are composed of the SOS of the individuals and the tree species are colored according to the continent of origin (yellow: Asia; blue: Europe; red: North America). The number (n) of observed individuals of the respective tree species is indicated on the left-hand side. Small figure: SOS of the tree species of the respective continent of origin, which is composed of the medians of the large figure. The asterisks mark the significance of a two-sided Wilcoxon test between the respective continents (* = p-value < 0.05; ** = p-value < 0.01; *** = p-value < 0.001, Bonferroni corrected).

Autumn phenology (EOS) for the observed species extended from late August to mid-November. The median of the first (*Fraxinus pennsylvanica*, 18th of September) and the last senescing species

(*Ostrya carpinifolia*, 7th of November) had a difference of 50 days (Figure 5). As in spring, there were also considerable differences within the species (IQR of 19 days for *Larix kaempferi* and 18.5 and 16.5 days for *Populus alba* and *Larix x eurolepis*, respectively, as the three most variable species). When comparing the continental areas of origin, no significant phenological differences were found between the different continents.

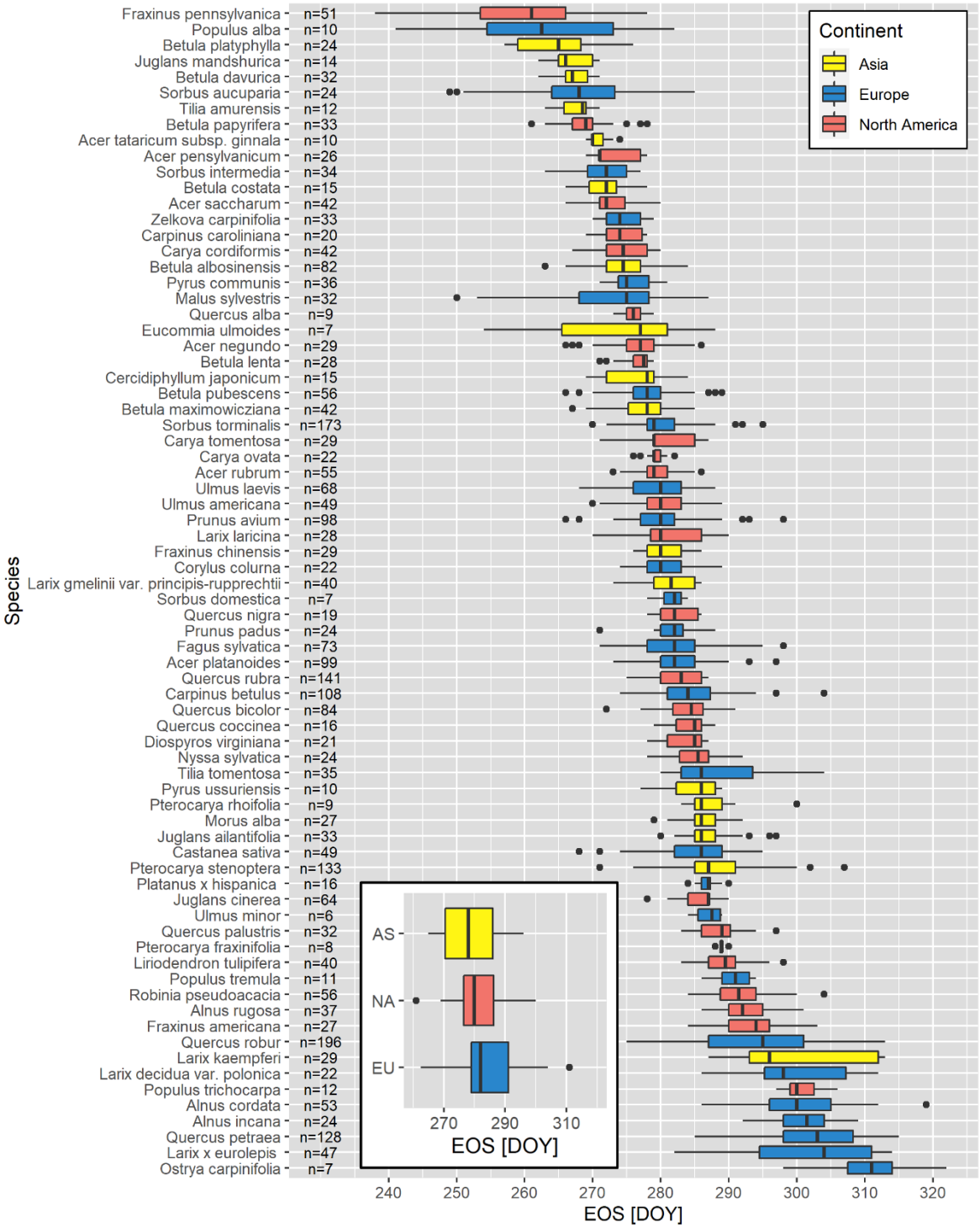

Figure 5: Drone-derived EOS for the 74 tree species observed in the study area, ordered by median. The respective boxplots are composed of the EOS of the individuals and the tree species are colored according to the continent of origin (yellow: Asia; blue: Europe; red: North America). The number (n) of observed individuals of the respective tree species

is indicated on the left-hand side. Small figure: EOS of the tree species of the respective continent of origin, which is composed of the medians of the large figure. The asterisks mark the significance of a two-sided Wilcoxon test between the respective continents (* = p-value < 0.05; ** = p-value < 0.01; *** = p-value < 0.001, Bonferroni corrected).

The length of the growing season (LOS) calculated from SOS and EOS ranged from 108 to 213 days (Figure 6). The difference between the median of the species with the shortest (*Fraxinus pennsylvanica*, 137 days) and the longest vegetation period (*Larix decidua var. polonica*, 196 days) was 59 days. As in spring, it should also be noted that a small proportion (approx. 14 %) of the species observed had a remarkably longer vegetation period than most of the other species (~ >180 days LOS in Figure 6). Here, too, there was considerable intraspecific variability (IQR of 20 days for *Larix kaempferi* and 19.5 and 17.75 for *Fraxinus pennsylvanica* and *Malus sylvestris*, respectively, as the three most variable species). From a continental origin perspective, European species had a significantly longer vegetation period than North American species (11-day difference in the median; $W = 653.5$, $p < 0.001$).

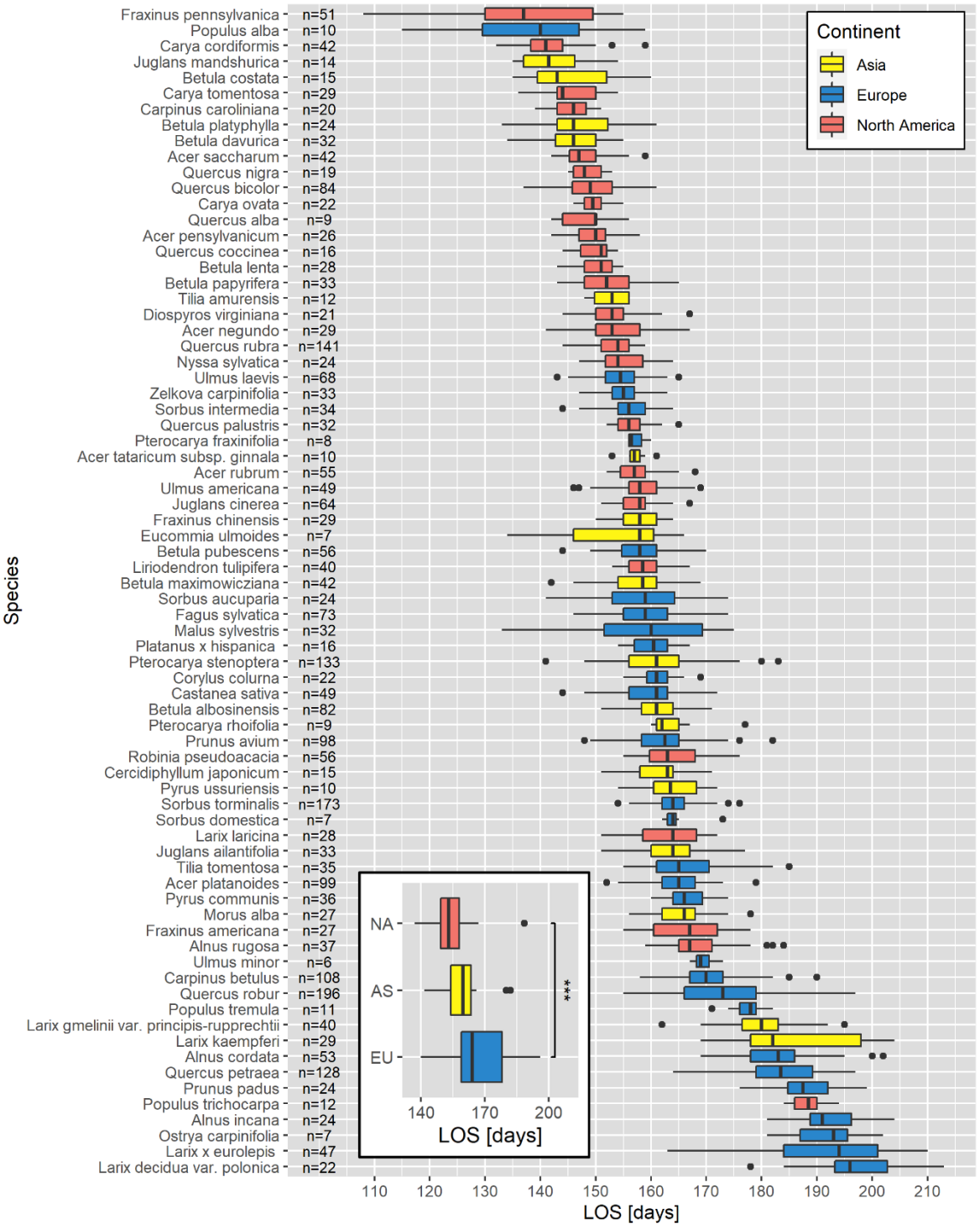

Figure 6: Drone-derived LOS for the 74 tree species observed in the study area. Large figure: LOS of the respective tree species, ordered by median. The respective boxplots are composed of the LOS of the individuals and the tree species are colored according to the continent of origin (yellow: Asia; blue: Europe; red: North America). The number (n) of observed individuals of the respective tree species is indicated on the left-hand side. Small figure: LOS of the tree species of the respective continent of origin, which is composed of the medians of the large figure. The asterisks mark the significance of a two-sided Wilcoxon test between the respective continents (* = p-value < 0.05; ** = p-value < 0.01; *** = p-value < 0.001, Bonferroni corrected).

3.3. Relationship between phenology, functional traits, and climate distances

In the BRT analysis of the SOS and the functional traits as well as climate distance (cv correlation = 0.63), the three most important explanatory variables were the seed dry mass (relative influence: 20.2 %), the continent of origin (20.1 %) and the leaf thickness (12.8 %; Figure 7a). If the tree species came from North America, a significant delay in SOS was observed, while the continents of Europe and Asia showed only minor differences (Figure S7). A positive relationship between SOS and the traits mentioned was found for seed dry mass, with tree species with lighter seeds (< 500 mg) leafing out earlier. In contrast, there was a negative relationship for leaf thickness, where later SOS was associated with tree species with a lower leaf thickness (< 0.2 mm).

In the BRTs for EOS (cv correlation = 0.20), the number of chromosomes (15.7 %), the stem conduit diameter (15.7 %), and the SRL (12.6 %; Figure 7b) were the three most important explanatory variables. A positive relationship between EOS and traits was found for stem conduit diameter, whereby an earlier EOS was more likely for tree species that had a smaller stem conduit diameter (< 100 µm; Figure S8). In contrast, the number of chromosomes and SRL had a negative relationship with EOS: tree species with fewer chromosomes (< 20) and a lower SRL (< 2000 cm g^{-1}) were more likely to be associated with a later EOS.

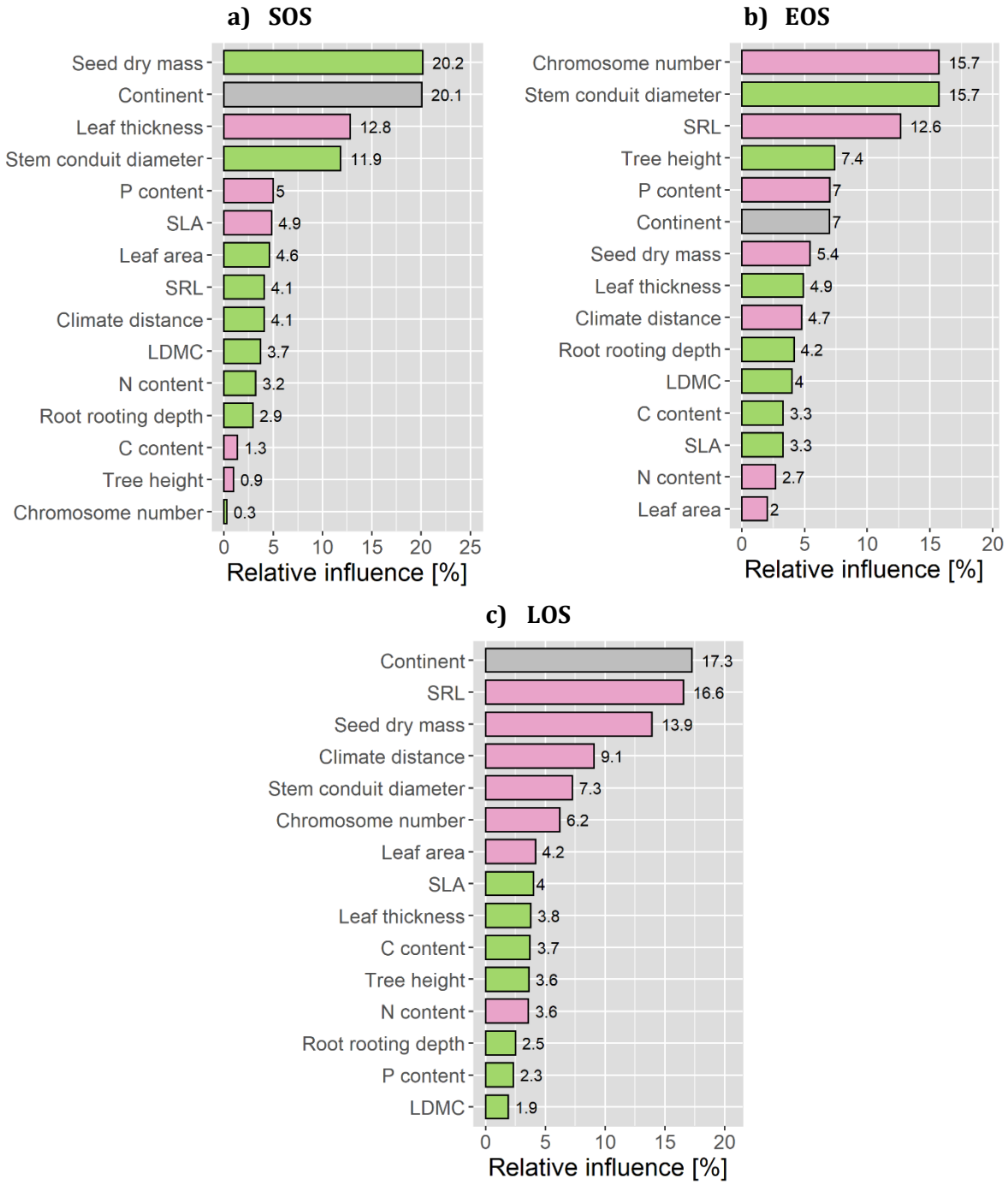

Figure 7: Relative importance (%) of the functional traits and the climate distance for the individual phenological metrics (a: SOS; b: EOS; c: LOS) from the BRT analysis. Positive correlations between the respective traits and the phenological metrics are marked in green and negative correlations in red; the continent is marked in gray due to its three categorical characteristics. The corresponding partial dependency plots can be found in Figure S7-9. The respective cv correlation was 0.63 (SOS), 0.20 (EOS) and 0.37 (LOS).

457

458 Finally, the BRT analysis for the LOS (cv correlation = 0.37) showed a combination of the results
459 of SOS and EOS (Figure 7c). The most important explanatory variables were the continent of origin
460 (17.3 %), SRL (16.6 %) and seed dry mass (13.9 %). If the tree species came from Europe, a
461 significant longer LOS was observed, while the continents of Asia and North America showed only
462 minor differences (Figure S9). The other variables were negatively related to EOS, with tree

463 species with lighter seeds (< 50 mg) and a lower SRL (< 2500 cm g^{-1}) being associated with a
464 longer LOS.

465

466 4. Discussion

467 When assessing multiple phenological metrics using drone images across 74 deciduous tree
468 species, both the drone-derived spring and, notably autumn phenology demonstrated a high
469 degree of agreement with in-situ observations. A high inter- and intraspecific variability was
470 found in the SOS, EOS, and LOS and a considerable part of the interspecific variability of up to 55
471 % can be related to functional traits, with the continent of origin, seed dry mass and number of
472 chromosomes being among the most important ones.

473

474 4.1. Measuring deciduous tree phenology with a drone at a multi-species site: 475 possibilities and limitations

476 The drone spring and autumn crown phenology for a variety of deciduous tree species derived
477 from a single uniform method (non-corrected NDVI values, double logistic function, "local"
478 threshold) matched in-situ observations mostly well. This confirms previous studies (e.g.,
479 Klosterman and Richardson, 2017; Berra et al., 2019) reporting that reliable and robust recording
480 of plant phenology at the individual level is possible by drone monitoring. Compared to similar
481 study approaches (Budianti et al., 2021; Budianti et al., 2022; Fawcett et al., 2021; Wu et al., 2021),
482 equal or even better agreements between drone- and in-situ-based phenology could be shown
483 here, especially as these former studies even used different species, derivation methodologies and
484 measurement devices.

485 The fact that the drone-based spring phenology shows less agreement with in-situ observations
486 than the autumn phenology can be explained by the understory-overstory interaction: In spring,
487 the understory vegetation shows an earlier greening compared to the adult tree crowns (e.g.,
488 Richardson and O'Keefe, 2009; Vitasse, 2013) and is therefore included in the (mixed-pixel) NDVI
489 images of early spring. This temporal mismatch in spring is a general problem in remote sensing
490 at different scales (e.g., Filippa et al., 2018; Ryu et al., 2014; Budianti et al., 2021), primarily
491 explaining that NDVI data inconsistently predict an earlier SOS date than the observed onset of
492 leaf unfolding. In autumn, however, the understory vegetation only influences the images after the
493 leaves of the trees have fallen and therefore does not distort the drone-derived onset of leaf
494 discoloration.

495 Tree species exhibiting a later SOS according to drone data compared to in-situ observations also
496 underscore the methodological uncertainty inherent in phenological assessments. While drone-
497 derived phenology addresses each individual tree, field observations rely on assumptions of
498 representativeness for the plot, given that the entire area cannot be observed from the ground. In
499 addition, ground truth data encompass specific phenological stages (such as budburst, leaf-out,
500 and first leaf unfolded), whereas drone data only assesses a calculated index based on the
501 greenness of the vegetation. This obviously leads to a larger discrepancy in spring compared to
502 autumn phenology, as leaf discoloration is much easier monitored visually and on a larger scale.
503 To increase the quality of drone-based phenological onset dates, a comparison with canopy or
504 hemispherical camera images (as applied by Fawcett et al. (2021) or Klosterman et al. (2018)) can
505 add more precision. Nevertheless, the evaluation results obtained in this study promise robust

statements about key phases in the phenology of different tree species and their inter- and intraspecific variability.

4.2. Explaining intra- and interspecific variability of deciduous tree phenology

The trees exhibited high interspecific (up to 50-day difference in medians) and intraspecific (up to a 19-day interquartile range) phenological variability under nearly identical environmental conditions in both spring and autumn. This resulted in differences in the length of the growing season of up to almost two months between individual trees.

A large phenological variability of individuals within a tree species was also observed in previous analyses (e.g., Marchand et al., 2020; Delpierre et al., 2017; Prislan et al., 2013). The reasons for this intraspecific variability are often the age and height of the trees observed (Augspurger and Bartlett, 2003; Marchand et al., 2020; Osada and Hiura, 2019), but also the microclimate (Delpierre et al., 2017; Osada and Hiura, 2019) and genetic diversity (Capdevielle-Vargas et al., 2015; Delpierre et al., 2017; Schmeddes et al., 2023). In our study area, all individuals of a tree species are planted in the same year and therefore differ only slightly in height, which is why the variability cannot be explained by the previous factors. Temporal patterns (as later leaf-out and earlier senescence mean less variability; Denéchère et al., 2021) are also not observable in both spring and autumn. In contrast, the large intraspecific variability is striking. In addition, as in comparable studies (e.g., Denéchère et al., 2021; Marchand et al., 2020; Capdevielle-Vargas et al., 2015), the intraspecific variability is lower in spring than in autumn events. This can be explained by the fact that the onset of senescence is more complex and therefore dependent on more factors than spring phenology (Gill et al., 2015; Lu and Keenan, 2022). Accordingly, the sensitivity to individual drivers can have accumulated effects on different individuals and thus result in greater autumnal phenological plasticity.

Comparing the phenological onset dates between the species, the interspecific phenological variability in spring was in line with previous studies (e.g., Cole and Sheldon, 2017; Panchen et al., 2014; Richardson and O'Keefe, 2009; Wesołowski and Rowiński, 2006). In contrast, the variability of autumn phenology was comparatively high (e.g., compared to Budianti et al., 2022; Budianti et al., 2021; Wu et al., 2021; Archetti et al., 2013; Richardson and O'Keefe, 2009), which can be explained by the high number and diversity of the species considered. Even though a comparison with other studies is only possible to a limited extent due to different meteorological and environmental conditions, parallels can be recognized in the chronological order of the phenological onset dates of the tree species: While species such as *Alnus incana* (Donnelly et al., 2017) or the genera *Prunus*, *Populus* (Richardson and O'Keefe, 2009) or *Corylus* (Wesołowski and Rowiński, 2006) tend to leaf out early, greening of *Nyssa sylvatica* or the genera *Quercus* (Richardson and O'Keefe, 2009) and *Fraxinus* (Cole and Sheldon, 2017) are more likely to be observed later in the spring. In autumn, on the other hand, early leaf discoloration seems to be common, especially in *Acer rubrum* (Archetti et al., 2013; Richardson and O'Keefe, 2009), while the genera *Populus* and *Quercus* mainly senesce later in the year (Archetti et al., 2013; Richardson and O'Keefe, 2009; Wu et al., 2021).

Both in spring and in autumn, the variation in phenological timing between the tree species can be interpreted as different growth strategies: While early leafing-out plant genera such as *Larix* or various species of the Rosaceae family (*Prunus padus*, *Pyrus communis*, *Sorbus aucuparia, Malus sylvestris*) or late senescing genera such as *Larix* or *Quercus* pursue maximization of carbon sequestration and use of seasonally limited resources (i.e., light) over a prolonged growth period

("phenological escape"; e.g., Lee and Ibáñez, 2021; Richardson and O'Keefe, 2009), genera such as *Quercus* or *Carya* presumably try to minimize the risk of late frost by late leaf emergence in spring (Bennie et al., 2010; Vitasse et al., 2014).

These strategies seem to have some inherent logic, but the phenological behavior of a specific single species is difficult to derive from these general statements. One possibility is to link the growth strategies to continents of origin and to respective functional traits of the tree species. Our study shows that North American tree species and species with higher seed dry mass and lower leaf thickness are associated with later leaf-out. Interestingly, other studies have also linked the time of leaf emergence or phenological sensitivity to continental differences (Lee et al., 2022; Zohner and Renner, 2017), whereby a later leaf-out in North American species is primarily explained by higher variability of North American spring temperatures and the associated risk avoidance strategy with regard to late frost events (Zohner et al., 2017). In contrast to Zohner and Renner (2017) earlier leaf discoloration of North American species is hardly observed in our study. Frost avoidance could also be the driver for other traits: tree species with heavier seeds may invest a lot of energy in reproduction and are therefore more likely to lower risks associated with energy loss due to late frost. Furthermore, tree species with thinner leaves are more susceptible to low temperatures and the resulting frost damage (Bucher et al., 2019; Bucher and Rosbakh, 2021) and therefore may exhibit a later leaf-out date, similar to Horbach et al. (2023).

A significantly distinct picture emerges when considering traits related to autumn phenology: tree species with a lower chromosome number and SRL as well as a larger stem conduit diameter tend to enter senescence later. A potential influence of chromosome numbers represents a totally novel aspect in plant phenology, with only a few papers offering insights into potential explanatory connections. For example, it is known that species with monoploid large genomes are more likely to invest in inflorescence preformation and thus flower and senesce earlier (Schnablová et al., 2021). In principle, different chromosome numbers in angiosperm tree genera hint at phylogenetic differences (Carta et al., 2018). Interestingly, for Italian vascular plant species, chromosome numbers were poorly related to climatic conditions, but to environmental categorical variables suggesting an evolutionary role. Carta et al. (2018) reported that lower chromosome numbers were associated with open, disturbed, drought-prone, i.e. instable habitats, while species in stable environments (favoring higher recombination rates) and with longer life cycles had generally higher chromosome numbers. Translating our findings into Carta's scheme would indicate that species from stable environments should have EOS earlier, whereas pioneers or species from disturbed habitats may profit from later EOS. With regard to the stem conduit diameter, due to the positive correlation with both spring and autumn phenology, it can be assumed that the species that unfolded their leaves later due to the strategy of frost avoidance with a larger conduit diameter (Lechowicz, 1984; Panchen et al., 2014) now make up for the initially lower carbon sequestration compared to other species through later senescence. Regarding SRL, our findings might be linked to nutrient and water acquisition as good water-use efficiency was linked to later dates of senescence (Bucher and Römermann, 2021).

Another aspect that should also be mentioned in this context is the drought summer of 2022 (Toreti et al., 2022). Regarding the general influence of drought on autumn phenology, the current study situation is contradictory (Gill et al., 2015; Lu and Keenan, 2022; Zani et al., 2020), with tree species' phenology reacting individually to drought stress (Bigler and Vitasse, 2021; Grossiord et al., 2022). Both visually in the field and in the NDVI data, no drought stress could be detected within the plots of the study area in the summer of 2022, most likely due to optimal soils with high water storage capacities, which meant that no analyses could be carried out in this context.

Nevertheless, this circumstance should be included in the final assessment when considering autumn phenological variability.

The length of the growing season, which results from SOS and EOS, is a clear combination of the SOS/EOS-trait relationships. European species start leaf emergence earliest and change color later than North American and Asian species, resulting in a significantly longer growing season. Furthermore, a higher SRL is associated with earlier leaf discoloration and thus a shorter LOS. Finally, a high seed dry mass tends to result in later leaf emergence, which also results in a shorter LOS.

4.3. Limitations and uncertainties

Due to the large number of trait data sets and the complex methodology to derive single tree crown phenological onset dates, there are also several uncertainties and limitations in our study. Regarding the drone data it should be noted that there are different illumination conditions depending on the season and weather, which can influence the calculation of the NDVI values (Fawcett et al., 2021). In addition, the orthorectification also induces inaccuracies of up to 30 centimeters, which can primarily distort the edge pixels of the respective crowns. The in-situ observations were only observed plot-wise. As shown in the study though, there are clear intraspecific phenological differences, which cannot be described in a plot-by-plot summary. Not all individuals were clearly visible, especially in larger plots, which made the assessment even more difficult. In addition, only a subset of the species analyzed with the drone could be observed on the ground and the temporal frequency of the drone and in-situ data do not match. Regarding the functional traits used in the study, most of the traits were not measured on-site, but were only retrieved from database values, of which some were based on a gap-filling algorithm. Different values would certainly be measured on site, although the magnitude of the values should be realistic depending on the species (e.g., Kazakou et al., 2014; Cordlandwehr et al., 2013; Violle et al., 2015).

Regarding the methodology, it is particularly noteworthy that the polygons of the respective tree crowns are created automatically and therefore only represent the real crown shape to a limited extent, even if unrealistic crowns were removed in the selection process. With more than 3000 individuals, we cannot rule out with 100% certainty that another species has spread naturally somewhere in the plots and - due to very similar phenology - this individual has not been noticed. When extracting the phenology from the drone images, curve fitting represents a simplification of the phenological curve, but is also a well-accepted (Zeng et al., 2020) method to reduce the influence of false outliers (snow cover, drought influence). In addition, setting a general NDVI threshold for over 3000 individuals and 74 species is a clear simplification of the phenological conditions. Regarding the BRT, it should be noted that models based on 74 data points (species) do not promise the highest robustness but are appropriate in this context.

5. Conclusion

Analyzing the phenology of 74 deciduous tree species and 3099 individuals using drone images, our study generates important new insights from both technical and ecophysiological perspectives. We showed that the derivation of SOS, EOS, and LOS via drone images for a large number of tree species using just one methodology achieves robust results and is a promising approach for monitoring phenology on the tree-individual level. Significant phenological

differences were found both within and between tree species, which led to differences in the length of the growing season of up to two months under nearly identical environmental conditions. The interspecific phenological variation could be explained by functional traits, with the continent of origin, seed dry mass and leaf thickness in spring explaining the variability with the strategy of frost avoidance. In autumn, the number of chromosomes, the SRL and the stem conduit diameter played a dominant role. The results encourage new research approaches in the field of plant phenology and form an important basis for understanding different growth strategies of dominant deciduous tree species in the Northern Hemisphere. Finally, the methodological support with camera data and traits measured on-site offer further potential to generate in-depth phenological insights within this research field in the future.

Acknowledgments: The authors would like to thank the Bavarian State Forests (BaySF) and the Bavarian State Institute of Forestry for the permission to conduct research in Weltwald Freising and for the provision and use of study area data. Furthermore, we would like to thank all supporters of the drone monitoring, here notably Niklas Kessel for operating many drone flights during spring and testing different tree detection and canopy delineation algorithms. For the phenological ground observations, we especially thank Yahya Ghalayini, Teresa Mühlbauer, Katharina Brückl, and Louise Harms.

Funding Information: This work was supported by the Bavarian State Ministry of Science and the Arts (F.7-F5121.14.2.3/14/6) in the context of the Bavarian Climate Research Network (bayklif) within the project BAYSICS (Bavarian Citizen Science Portal for Climate Research and Science Communication). Additionally, funding from the Bavarian State Ministry of Food, Agriculture and Forestry (StMELF) (klifW013: 7831-1/1014, klifW012: 7831-1/1078, and project M029) was received.

Data Availability Statement: The phenological and trait-related data that support the findings of this study are openly available in *figshare* (DOI: *10.6084/m9.figshare.24926256*). Further data sets from this study are available on request.

References

Archetti, M., Richardson, A.D., O'Keefe, J., Delpierre, N., 2013. Predicting climate change impacts on the amount and duration of autumn colors in a New England forest. PloS one 8(3), e57373. https://doi.org/10.1371/journal.pone.0057373.

Augspurger, C.K., Bartlett, E.A., 2003. Differences in leaf phenology between juvenile and adult trees in a temperate deciduous forest. Tree physiology 23(8), 517–525. https://doi.org/10.1093/treephys/23.8.517.

Bavarian State Forestry, 2022. (C) Geodata. https://services1.arcgis.com/dzpA3ZtAF0zx03DV/arcgis/rest/services/Weltwald_Update_05_2022/FeatureServer (accessed 10 January 2024).

Bennie, J., Kubin, E., Wiltshire, A., Huntley, B., Baxter, R., 2010. Predicting spatial and temporal patterns of bud-burst and spring frost risk in north-west Europe: the implications of local adaptation to climate. Global change biology 16(5), 1503–1514. https://doi.org/10.1111/j.1365-2486.2009.02095.x.

Berra, E.F., Gaulton, R., 2021. Remote sensing of temperate and boreal forest phenology: A review of progress, challenges and opportunities in the intercomparison of in-situ and satellite

phenological metrics. Forest Ecology and Management 480, 118663. https://www.sciencedirect.com/science/article/pii/S0378112720314328.
Berra, E.F., Gaulton, R., Barr, S., 2019. Assessing spring phenology of a temperate woodland: A multiscale comparison of ground, unmanned aerial vehicle and Landsat satellite observations. Remote Sensing of Environment 223, 229–242. https://doi.org/10.1016/j.rse.2019.01.010.
Bigler, C., Vitasse, Y., 2021. Premature leaf discoloration of European deciduous trees is caused by drought and heat in late spring and cold spells in early fall. Agricultural and Forest Meteorology 307, 108492. https://doi.org/10.1016/j.agrformet.2021.108492.
Bolmgren, K., Cowan, P.D., 2008. Time – size tradeoffs: a phylogenetic comparative study of flowering time, plant height and seed mass in a north-temperate flora. Oikos 117(3), 424–429. https://doi.org/10.1111/j.2007.0030-1299.16142.x.
Bucher, S.F., Feiler, R., Buchner, O., Neuner, G., Rosbakh, S., Leiterer, M. et al., 2019. Temporal and spatial trade-offs between resistance and performance traits in herbaceous plant species. Environmental and Experimental Botany 157, 187–196. https://doi.org/10.1016/j.envexpbot.2018.10.015.
Bucher, S.F., König, P., Menzel, A., Migliavacca, M., Ewald, J., Römermann, C., 2018. Traits and climate are associated with first flowering day in herbaceous species along elevational gradients. Ecology and evolution 8(2), 1147–1158. https://doi.org/10.1002/ece3.3720.
Bucher, S.F., Römermann, C., 2021. The timing of leaf senescence relates to flowering phenology and functional traits in 17 herbaceous species along elevational gradients. Journal of Ecology 109(3), 1537–1548. https://doi.org/10.1111/1365-2745.13577.
Bucher, S.F., Rosbakh, S., 2021. Foliar summer frost resistance measured via electrolyte leakage approach as related to plant distribution, community composition and plant traits. Functional Ecology 35(3), 590–600. https://doi.org/10.1111/1365-2435.13740.
Budianti, N., Mizunaga, H., Iio, A., 2021. Crown Structure Explains the Discrepancy in Leaf Phenology Metrics Derived from Ground- and UAV-Based Observations in a Japanese Cool Temperate Deciduous Forest. Forests 12(4), 425. https://doi.org/10.3390/f12040425.
Budianti, N., Naramoto, M., Iio, A., 2022. Drone-Sensed and Sap Flux-Derived Leaf Phenology in a Cool Temperate Deciduous Forest: A Tree-Level Comparison of 17 Species. Remote Sensing 14(10), 2505. https://doi.org/10.3390/rs14102505.
Buras, A., Menzel, A., 2019. Projecting Tree Species Composition Changes of European Forests for 2061-2090 Under RCP 4.5 and RCP 8.5 Scenarios. Frontiers in plant science 9, 1986. https://doi.org/10.3389/fpls.2018.01986.
Capdevielle-Vargas, R., Estrella, N., Menzel, A., 2015. Multiple-year assessment of phenological plasticity within a beech (Fagus sylvatica L.) stand in southern Germany. Agricultural and Forest Meteorology 211-212, 13–22. https://doi.org/10.1016/j.agrformet.2015.03.019.
Carta, A., Bedini, G., Peruzzi, L., 2018. Unscrambling phylogenetic effects and ecological determinants of chromosome number in major angiosperm clades. Scientific reports 8(1), 14258. https://doi.org/10.1038/s41598-018-32515-x.
Caudullo, G., Welk, E., San-Miguel-Ayanz, J., 2017. Chorological maps for the main European woody species. Data in brief 12, 662–666. https://doi.org/10.1016/j.dib.2017.05.007.
Cleland, E.E., Chuine, I., Menzel, A., Mooney, H.A., Schwartz, M.D., 2007. Shifting plant phenology in response to global change. Trends in Ecology & Evolution 22(7), 357–365. https://www.cell.com/trends/ecology-evolution/fulltext/s0169-5347(07)00130-9.
Cole, E.F., Sheldon, B.C., 2017. The shifting phenological landscape: Within- and between-species variation in leaf emergence in a mixed-deciduous woodland. Ecology and evolution 7(4), 1135–1147. https://doi.org/10.1002/ece3.2718.

Cordlandwehr, V., Meredith, R.L., Ozinga, W.A., Bekker, R.M., van Groenendael, J.M., Bakker, J.P., 2013. Do plant traits retrieved from a database accurately predict on-site measurements? Journal of Ecology 101(3), 662–670. https://doi.org/10.1111/1365-2745.12091.

Craine, J.M., Wolkovich, E.M., Gene Towne, E., Kembel, S.W., 2012. Flowering phenology as a functional trait in a tallgrass prairie. The New phytologist 193(3), 673–682. https://doi.org/10.1111/j.1469-8137.2011.03953.x.

Dalponte, M., Coomes, D.A., 2016. Tree-centric mapping of forest carbon density from airborne laser scanning and hyperspectral data. Methods in ecology and evolution 7(10), 1236–1245. https://doi.org/10.1111/2041-210X.12575.

Dandois, J.P., Ellis, E.C., 2013. High spatial resolution three-dimensional mapping of vegetation spectral dynamics using computer vision. Remote Sensing of Environment 136, 259–276. https://doi.org/10.1016/j.rse.2013.04.005.

Delpierre, N., Guillemot, J., Dufrêne, E., Cecchini, S., Nicolas, M., 2017. Tree phenological ranks repeat from year to year and correlate with growth in temperate deciduous forests. Agricultural and Forest Meteorology 234-235, 1–10. https://doi.org/10.1016/j.agrformet.2016.12.008.

Denéchère, R., Delpierre, N., Apostol, E.N., Berveiller, D., Bonne, F., Cole, E. et al., 2021. The within-population variability of leaf spring and autumn phenology is influenced by temperature in temperate deciduous trees. International journal of biometeorology 65(3), 369–379. https://doi.org/10.1007/s00484-019-01762-6.

Diez, J.M., Ibáñez, I., Miller-Rushing, A.J., Mazer, S.J., Crimmins, T.M., Crimmins, M.A. et al., 2012. Forecasting phenology: from species variability to community patterns. Ecology letters 15(6), 545–553. https://doi.org/10.1111/j.1461-0248.2012.01765.x.

Donnelly, A., Yu, R., Caffarra, A., Hanes, J., Liang, L., Desai, A.R. et al., 2017. Interspecific and interannual variation in the duration of spring phenophases in a northern mixed forest. Agricultural and Forest Meteorology 243, 55–67. https://doi.org/10.1016/j.agrformet.2017.05.007.

Dorji, T., Totland, O., Moe, S.R., Hopping, K.A., Pan, J., Klein, J.A., 2013. Plant functional traits mediate reproductive phenology and success in response to experimental warming and snow addition in Tibet. Global change biology 19(2), 459–472. https://doi.org/10.1111/gcb.12059.

Du, G., Qi, W., 2010. Trade-offs between flowering time, plant height, and seed size within and across 11 communities of a QingHai-Tibetan flora. Plant Ecol 209(2), 321–333. https://doi.org/10.1007/s11258-010-9763-4.

DWD, 2024. Historische tägliche Stationsbeobachtungen (Temperatur, Druck, Niederschlag, Sonnenscheindauer, etc.) für Deutschland, Version v23.3: München-Flughafen. https://opendata.dwd.de/climate_environment/CDC/observations_germany/climate/daily/kl/historical/ (accessed 13 March 2024).

Elith, J., Leathwick, J.R., Hastie, T., 2008. A working guide to boosted regression trees. The Journal of animal ecology 77(4), 802–813. https://doi.org/10.1111/j.1365-2656.2008.01390.x.

Ettinger, A.K., Chamberlain, C.J., Morales-Castilla, I., Buonaiuto, D.M., Flynn, D.F.B., Savas, T. et al., 2020. Winter temperatures predominate in spring phenological responses to warming. Nature Clim Change 10(12), 1137–1142. https://doi.org/10.1038/s41558-020-00917-3.

Fawcett, D., Bennie, J., Anderson, K., 2021. Monitoring spring phenology of individual tree crowns using drone-acquired NDVI data. Remote Sens Ecol Conserv 7(2), 227–244. https://doi.org/10.1002/rse2.184.

Filippa, G., Cremonese, E., Migliavacca, M., Galvagno, M., Sonnentag, O., Humphreys, E. et al., 2018. NDVI derived from near-infrared-enabled digital cameras: Applicability across different plant

functional types. Agricultural and Forest Meteorology 249, 275–285. https://doi.org/10.1016/j.agrformet.2017.11.003.
Fischer, A., 1994. A model for the seasonal variations of vegetation indices in coarse resolution data and its inversion to extract crop parameters. Remote Sensing of Environment 48(2), 220–230. https://www.sciencedirect.com/science/article/pii/0034425794901430.
Flynn, D.F.B., Wolkovich, E.M., 2018. Temperature and photoperiod drive spring phenology across all species in a temperate forest community. The New phytologist 219(4), 1353–1362. https://doi.org/10.1111/nph.15232.
Gaertner, B.A., Zegre, N., Warner, T., Fernandez, R., He, Y., Merriam, E.R., 2019. Climate, forest growing season, and evapotranspiration changes in the central Appalachian Mountains, USA. The Science of the total environment 650(Pt 1), 1371–1381. https://doi.org/10.1016/j.scitotenv.2018.09.129.
Garonna, I., Jong, R. de, Schaepman, M.E., 2016. Variability and evolution of global land surface phenology over the past three decades (1982-2012). Global change biology 22(4), 1456–1468. https://doi.org/10.1111/gcb.13168.
Gill, A.L., Gallinat, A.S., Sanders-DeMott, R., Rigden, A.J., Short Gianotti, D.J., Mantooth, J.A. et al., 2015. Changes in autumn senescence in northern hemisphere deciduous trees: a meta-analysis of autumn phenology studies. Annals of botany 116(6), 875–888. https://doi.org/10.1093/aob/mcv055.
Global Biodiversity Information Facility, 2021. Free and open access to biodiversity data. https://www.gbif.org/ (accessed 08 November 2023).
Gressler, E., Jochner, S., Capdevielle-Vargas, R.M., Morellato, L.P.C., Menzel, A., 2015. Vertical variation in autumn leaf phenology of Fagus sylvatica L. in southern Germany. Agricultural and Forest Meteorology 201, 176–186. https://doi.org/10.1016/j.agrformet.2014.10.013.
Grossiord, C., Bachofen, C., Gisler, J., Mas, E., Vitasse, Y., Didion-Gency, M., 2022. Warming may extend tree growing seasons and compensate for reduced carbon uptake during dry periods. Journal of Ecology 110(7), 1575–1589. https://doi.org/10.1111/1365-2745.13892.
Harris, I., Osborn, T.J., Jones, P., Lister, D., 2020. Version 4 of the CRU TS monthly high-resolution gridded multivariate climate dataset. Scientific data 7(1), 109. https://doi.org/10.1038/s41597-020-0453-3.
Hijmans, R.J., Phillips, S., Leathwick, J., Elith, J., 2023. Package 'dismo'. https://cran.r-project.org/web/packages/dismo/index.html (accessed 02 November 2023).
Horbach, S., Rauschkolb, R., Römermann, C., 2023. Flowering and leaf phenology are more variable and stronger associated to functional traits in herbaceous compared to tree species. Flora 300, 152218. https://doi.org/10.1016/j.flora.2023.152218.
Kattge, J., Bönisch, G., Díaz, S., Lavorel, S., Prentice, I.C., Leadley, P. et al., 2020. TRY plant trait database - enhanced coverage and open access. Global change biology 26(1), 119–188. https://doi.org/10.1111/gcb.14904.
Kazakou, E., Violle, C., Roumet, C., Navas, M.-L., Vile, D., Kattge, J. et al., 2014. Are trait-based species rankings consistent across data sets and spatial scales? J Veg Sci 25(1), 235–247. https://doi.org/10.1111/jvs.12066.
Keenan, T.F., Gray, J., Friedl, M.A., Toomey, M., Bohrer, G., Hollinger, D.Y. et al., 2014. Net carbon uptake has increased through warming-induced changes in temperate forest phenology. Nature Clim Change 4(7), 598–604. https://doi.org/10.1038/nclimate2253.
Kim, J.H., Hwang, T., Yang, Y., Schaaf, C.L., Boose, E., Munger, J.W., 2018. Warming-Induced Earlier Greenup Leads to Reduced Stream Discharge in a Temperate Mixed Forest Catchment. JGR Biogeosciences 123(6), 1960–1975. https://doi.org/10.1029/2018JG004438.

826 Kleinsmann, J., Verbesselt, J., Kooistra, L., 2023. Monitoring Individual Tree Phenology in a Multi-
827 Species Forest Using High Resolution UAV Images. Remote Sensing 15(14), 3599.
828 https://doi.org/10.3390/rs15143599.
829 Kloos, S., Klosterhalfen, A., Knohl, A., Menzel, A., 2024. Decoding autumn phenology: Unraveling
830 the link between observation methods and detected environmental cues. Global change
831 biology 30(3). https://doi.org/10.1111/gcb.17231.
832 Klosterman, S., Melaas, E., Wang, J.A., Martinez, A., Frederick, S., O'Keefe, J. et al., 2018. Fine-scale
833 perspectives on landscape phenology from unmanned aerial vehicle (UAV) photography.
834 Agricultural and Forest Meteorology 248, 397–407.
835 https://doi.org/10.1016/j.agrformet.2017.10.015.
836 Klosterman, S., Richardson, A.D., 2017. Observing Spring and Fall Phenology in a Deciduous Forest
837 with Aerial Drone Imagery. Sensors (Basel, Switzerland) 17(12).
838 https://doi.org/10.3390/s17122852.
839 König, P., Tautenhahn, S., Cornelissen, J.H.C., Kattge, J., Bönisch, G., Römermann, C., 2018. Advances
840 in flowering phenology across the Northern Hemisphere are explained by functional traits.
841 Global Ecology and Biogeography 27(3), 310–321. https://doi.org/10.1111/geb.12696.
842 Körner, C., Möhl, P., Hiltbrunner, E., 2023. Four ways to define the growing season. Ecology letters
843 26(8), 1277–1292. https://doi.org/10.1111/ele.14260.
844 Lange, M., Doktor, D., 2022. Package 'phenex'. https://cran.r-
845 project.org/web/packages/phenex/index.html (accessed 31 October 2023).
846 Lauterbach, D., Römermann, C., Jeltsch, F., Ristow, M., 2013. Factors driving plant rarity in dry
847 grasslands on different spatial scales: a functional trait approach. Biodivers Conserv 22(10),
848 2337–2352. https://doi.org/10.1007/s10531-013-0455-y.
849 Lechowicz, M.J., 1984. Why Do Temperate Deciduous Trees Leaf Out at Different Times?
850 Adaptation and Ecology of Forest Communities. The American Naturalist 124(6), 821–842.
851 https://doi.org/10.1086/284319.
852 Lee, B.R., Ibáñez, I., 2021. Spring phenological escape is critical for the survival of temperate tree
853 seedlings. Functional Ecology 35(8), 1848–1861. https://doi.org/10.1111/1365-2435.13821.
854 Lee, B.R., Miller, T.K., Rosche, C., Yang, Y., Heberling, J.M., Kuebbing, S.E. et al., 2022. Wildflower
855 phenological escape differs by continent and spring temperature. Nature communications
856 13(1), 7157. https://doi.org/10.1038/s41467-022-34936-9.
857 Liu, Y., Li, G., Wu, X., Niklas, K.J., Yang, Z., Sun, S., 2021. Linkage between species traits and plant
858 phenology in an alpine meadow. Oecologia 195(2), 409–419.
859 https://doi.org/10.1007/s00442-020-04846-y.
860 Liu ZhiGuo, Li Kai, Cai YongLi, Fang Yan, 2011. Correlations between leafing phenology and traits:
861 woody species of evergreen broad-leaved forests in subtropical China. Polish Journal of
862 Ecology 59(3), 463–473.
863 Louault, F., v.d. Pillar, Aufrère, J., Garnier, E., Soussana, J.-F., 2005. Plant traits and functional types
864 in response to reduced disturbance in a semi-natural grassland. J Veg Sci 16(2), 151–160.
865 https://doi.org/10.1111/j.1654-1103.2005.tb02350.x.
866 Lu, X., Keenan, T.F., 2022. No evidence for a negative effect of growing season photosynthesis on
867 leaf senescence timing. Global change biology 28(9), 3083–3093.
868 https://doi.org/10.1111/gcb.16104.
869 Marchand, L.J., Dox, I., Gričar, J., Prislan, P., Leys, S., van den Bulcke, J. et al., 2020. Inter-individual
870 variability in spring phenology of temperate deciduous trees depends on species, tree size and
871 previous year autumn phenology. Agricultural and Forest Meteorology 290, 108031.
872 https://doi.org/10.1016/j.agrformet.2020.108031.

Melaas, E.K., Sulla-Menashe, D., Friedl, M.A., 2018. Multidecadal Changes and Interannual Variation in Springtime Phenology of North American Temperate and Boreal Deciduous Forests. Geophysical Research Letters 45(6), 2679–2687. https://doi.org/10.1002/2017GL076933.

Menzel, A., Sparks, T.H., Estrella, N., Koch, E., Aasa, A., Ahas, R. et al., 2006. European phenological response to climate change matches the warming pattern. Global change biology 12(10), 1969–1976. https://doi.org/10.1111/j.1365-2486.2006.01193.x.

Menzel, A., Yuan, Y., Matiu, M., Sparks, T., Scheifinger, H., Gehrig, R. et al., 2020. Climate change fingerprints in recent European plant phenology. Global change biology. https://doi.org/10.1111/gcb.15000.

Osada, N., Hiura, T., 2019. Intraspecific differences in spring leaf phenology in relation to tree size in temperate deciduous trees. Tree physiology 39(5), 782–791. https://doi.org/10.1093/treephys/tpz011.

Panchen, Z.A., Primack, R.B., Nordt, B., Ellwood, E.R., Stevens, A.-D., Renner, S.S. et al., 2014. Leaf out times of temperate woody plants are related to phylogeny, deciduousness, growth habit and wood anatomy. The New phytologist 203(4), 1208–1219. https://doi.org/10.1111/nph.12892.

Piao, S., Friedlingstein, P., Ciais, P., Viovy, N., Demarty, J., 2007. Growing season extension and its impact on terrestrial carbon cycle in the Northern Hemisphere over the past 2 decades. Global Biogeochemical Cycles 21(3). https://doi.org/10.1029/2006GB002888.

Piao, S., Liu, Q., Chen, A., Janssens, I.A., Fu, Y., Dai, J. et al., 2019. Plant phenology and global climate change: Current progresses and challenges. Global change biology 25(6), 1922–1940. https://doi.org/10.1111/gcb.14619.

Plowright, A., Roussel J.-R., 2023. Package 'ForestTools'. https://cran.r-project.org/web/packages/ForestTools/index.html (accessed 07 November 2023).

Popescu, S.C., Wynne, R.H., 2004. Seeing the Trees in the Forest. photogramm eng remote sensing 70(5), 589–604. https://doi.org/10.14358/PERS.70.5.589.

Prislan, P., Gričar, J., Luis, M. de, Smith, K.T., Čufar, K., 2013. Phenological variation in xylem and phloem formation in Fagus sylvatica from two contrasting sites. Agricultural and Forest Meteorology 180, 142–151. https://doi.org/10.1016/j.agrformet.2013.06.001.

R Core Team, 2022. R: A language and environment for statistical computing. R Foundation for Statistical Computing, Vienna, Austria. https://www.R-project.org/.

Rice, A., Glick, L., Abadi, S., Einhorn, M., Kopelman, N.M., Salman-Minkov, A. et al., 2015. The Chromosome Counts Database (CCDB) - a community resource of plant chromosome numbers. The New phytologist 206(1), 19–26. https://doi.org/10.1111/nph.13191.

Richardson, A.D., O'Keefe, J., 2009. Phenological Differences Between Understory and Overstory, in: Noormets, A., (Ed.), Phenology of ecosystem processes: Applications in global change research. Springer, Dordrecht, Heidelberg, pp. 87–117.

Rigo, D. de, Caudullo, G., Houston Durrant, T., San-Miguel-Ayanz, J., 2016. The European Atlas of Forest Tree Species: modelling, data and information on forest tree species, in: San-Miguel-Ayanz, J., Rigo, D. de, Caudullo, G., Houston Durrant, T., Mauri, A., (Eds.), European Atlas of Forest Tree Species. Publications Office of the European Union, Luxembourg, pp. e01aa69+.

Roussel, J.-R., Auty, D., Boissieu, F. de, Meador, A.S., Jean-Francois, B., Demetrios, G. et al., 2023. Package 'lidR'. https://cran.r-project.org/web/packages/lidR/index.html (accessed 07 November 2023).

Roussel, J.-R., Auty, D., Coops, N.C., Tompalski, P., Goodbody, T.R., Meador, A.S. et al., 2020. lidR: An R package for analysis of Airborne Laser Scanning (ALS) data. Remote Sensing of Environment 251, 112061. https://doi.org/10.1016/j.rse.2020.112061.

Rudolf, H., 2023. Weltwald Freising. https://www.weltwald.de/fileadmin/user_upload/14-weltwald/pdfs/Weltwald_Freising_2023.pdf (accessed 27 September 2023).

Ryu, Y., Lee, G., Jeon, S., Song, Y., Kimm, H., 2014. Monitoring multi-layer canopy spring phenology of temperate deciduous and evergreen forests using low-cost spectral sensors. Remote Sensing of Environment 149, 227–238. https://doi.org/10.1016/j.rse.2014.04.015.

Schmeddes, J., Muffler, L., Barbeta, A., Beil, I., Bolte, A., Holm, S. et al., 2023. High phenotypic variation found within the offspring of each mother tree in Fagus sylvatica regardless of the environment or source population. Global Ecology and Biogeography. https://doi.org/10.1111/geb.13794.

Schnablová, R., Huang, L., Klimešová, J., Šmarda, P., Herben, T., 2021. Inflorescence preformation prior to winter: a surprisingly widespread strategy that drives phenology of temperate perennial herbs. The New phytologist 229(1), 620–630. https://doi.org/10.1111/nph.16880.

Schneider, U., Becker, A., Finger, P., Meyer-Christoffer, A., Rudolf, B., Ziese, M. GPCC Full Data Reanalysis Version 6.0 at 0.5°: Monthly Land-Surface Precipitation from Rain-Gauges built on GTS-based and Historic Data; 2011.

Schrodt, F., Kattge, J., Shan, H., Fazayeli, F., Joswig, J., Banerjee, A. et al., 2015. BHPMF - a hierarchical Bayesian approach to gap-filling and trait prediction for macroecology and functional biogeography. Global Ecology and Biogeography 24(12), 1510–1521. https://doi.org/10.1111/geb.12335.

Segrestin, J., Navas, M.-L., Garnier, E., 2020. Reproductive phenology as a dimension of the phenotypic space in 139 plant species from the Mediterranean. The New phytologist 225(2), 740–753. https://doi.org/10.1111/nph.16165.

Sporbert, M., Jakubka, D., Bucher, S.F., Hensen, I., Freiberg, M., Heubach, K. et al., 2022. Functional traits influence patterns in vegetative and reproductive plant phenology - a multi-botanical garden study. The New phytologist 235(6), 2199–2210. https://doi.org/10.1111/nph.18345.

State Office for Digitization, Broadband and Surveying, 2023. BayernAtalas. https://geoportal.bayern.de/bayernatlas/?lang=de&topic=ba&bgLayer=atkis&catalogNodes=11&E=697066.10&N=5365947.32&zoom=11&layers=tk_by (accessed 02 November 2023).

Sun, S., Frelich, L.E., 2011. Flowering phenology and height growth pattern are associated with maximum plant height, relative growth rate and stem tissue mass density in herbaceous grassland species. Journal of Ecology 99(4), 991–1000. https://doi.org/10.1111/j.1365-2745.2011.01830.x.

Sun, S., Jin, D., Li, R., 2006. Leaf emergence in relation to leaf traits in temperate woody species in East-Chinese Quercus fabri forests. Acta Oecologica 30(2), 212–222. https://doi.org/10.1016/j.actao.2006.04.001.

Tang, J., Körner, C., Muraoka, H., Piao, S., Shen, M., Thackeray, S.J. et al., 2016. Emerging opportunities and challenges in phenology: a review. Ecosphere 7(8). https://doi.org/10.1002/ecs2.1436.

Toreti, A., Bavera, D., Acosta Navarro, J., Cammalleri, C., Jager, A. de, Di Ciollo, C. et al., 2022. Drought in Europe August 2022. Publications Office of the European Union, Luxembourg.

Uphus, L., Lüpke, M., Yuan, Y., Benjamin, C., Englmeier, J., Fricke, U. et al., 2021. Climate Effects on Vertical Forest Phenology of Fagus sylvatica L., Sensed by Sentinel-2, Time Lapse Camera, and Visual Ground Observations. Remote Sensing 13(19), 3982. https://doi.org/10.3390/rs13193982.

965 Vile, D., Shipley, B., Garnier, E., 2006. A structural equation model to integrate changes in
966 functional strategies during old-field succession. Ecology 87(2), 504–517.
967 https://doi.org/10.1890/05-0822.
968 Violle, C., Choler, P., Borgy, B., Garnier, E., Amiaud, B., Debarros, G. et al., 2015. Vegetation ecology
969 meets ecosystem science: Permanent grasslands as a functional biogeography case study. The
970 Science of the total environment 534, 43–51.
971 https://doi.org/10.1016/j.scitotenv.2015.03.141.
972 Vitasse, Y., 2013. Ontogenic changes rather than difference in temperature cause understory trees
973 to leaf out earlier. The New phytologist 198(1), 149–155.
974 https://doi.org/10.1111/nph.12130.
975 Vitasse, Y., Baumgarten, F., Zohner, C.M., Rutishauser, T., Pietragalla, B., Gehrig, R. et al., 2022. The
976 great acceleration of plant phenological shifts. Nature Clim Change 12(4), 300–302.
977 https://doi.org/10.1038/s41558-022-01283-y.
978 Vitasse, Y., Hoch, G., Randin, C.F., Lenz, A., Kollas, C., Scheepens, J.F. et al., 2013. Elevational
979 adaptation and plasticity in seedling phenology of temperate deciduous tree species.
980 Oecologia 171(3), 663–678. https://doi.org/10.1007/s00442-012-2580-9.
981 Vitasse, Y., Lenz, A., Körner, C., 2014. The interaction between freezing tolerance and phenology
982 in temperate deciduous trees. Frontiers in plant science 5, 541.
983 https://doi.org/10.3389/fpls.2014.00541.
984 Wesołowski, T., Rowiński, P., 2006. Timing of bud burst and tree-leaf development in a
985 multispecies temperate forest. Forest Ecology and Management 237(1-3), 387–393.
986 https://doi.org/10.1016/j.foreco.2006.09.061.
987 Wu, S., Wang, J., Yan, Z., Song, G., Chen, Y., Ma, Q. et al., 2021. Monitoring tree-crown scale autumn
988 leaf phenology in a temperate forest with an integration of PlanetScope and drone remote
989 sensing observations. ISPRS Journal of Photogrammetry and Remote Sensing 171, 36–48.
990 https://doi.org/10.1016/j.isprsjprs.2020.10.017.
991 Zani, D., Crowther, T.W., Mo, L., Renner, S.S., Zohner, C.M., 2020. Increased growing-season
992 productivity drives earlier autumn leaf senescence in temperate trees. Science (New York,
993 N.Y.) 370(6520), 1066–1071. https://doi.org/10.1126/science.abd8911.
994 Zeng, L., Wardlow, B.D., Xiang, D., Hu, S., Li, D., 2020. A review of vegetation phenological metrics
995 extraction using time-series, multispectral satellite data. Remote Sensing of Environment 237,
996 111511. https://doi.org/10.1016/j.rse.2019.111511.
997 Zohner, C.M., Benito, B.M., Fridley, J.D., Svenning, J.-C., Renner, S.S., 2017. Spring predictability
998 explains different leaf-out strategies in the woody floras of North America, Europe and East
999 Asia. Ecology letters 20(4), 452–460. https://doi.org/10.1111/ele.12746.
1000 Zohner, C.M., Mirzagholi, L., Renner, S.S., Mo, L., Rebindaine, D., Bucher, R. et al., 2023. Effect of
1001 climate warming on the timing of autumn leaf senescence reverses after the summer solstice.
1002 Science (New York, N.Y.) 381(6653), eadf5098. https://doi.org/10.1126/science.adf5098.
1003 Zohner, C.M., Renner, S.S., 2017. Innately shorter vegetation periods in North American species
1004 explain native-non-native phenological asymmetries. Nature ecology & evolution 1(11),
1005 1655–1660. https://doi.org/10.1038/s41559-017-0307-3.

Supplementary Material: The linkage between functional traits and drone-derived phenology of 74 Northern Hemisphere tree species

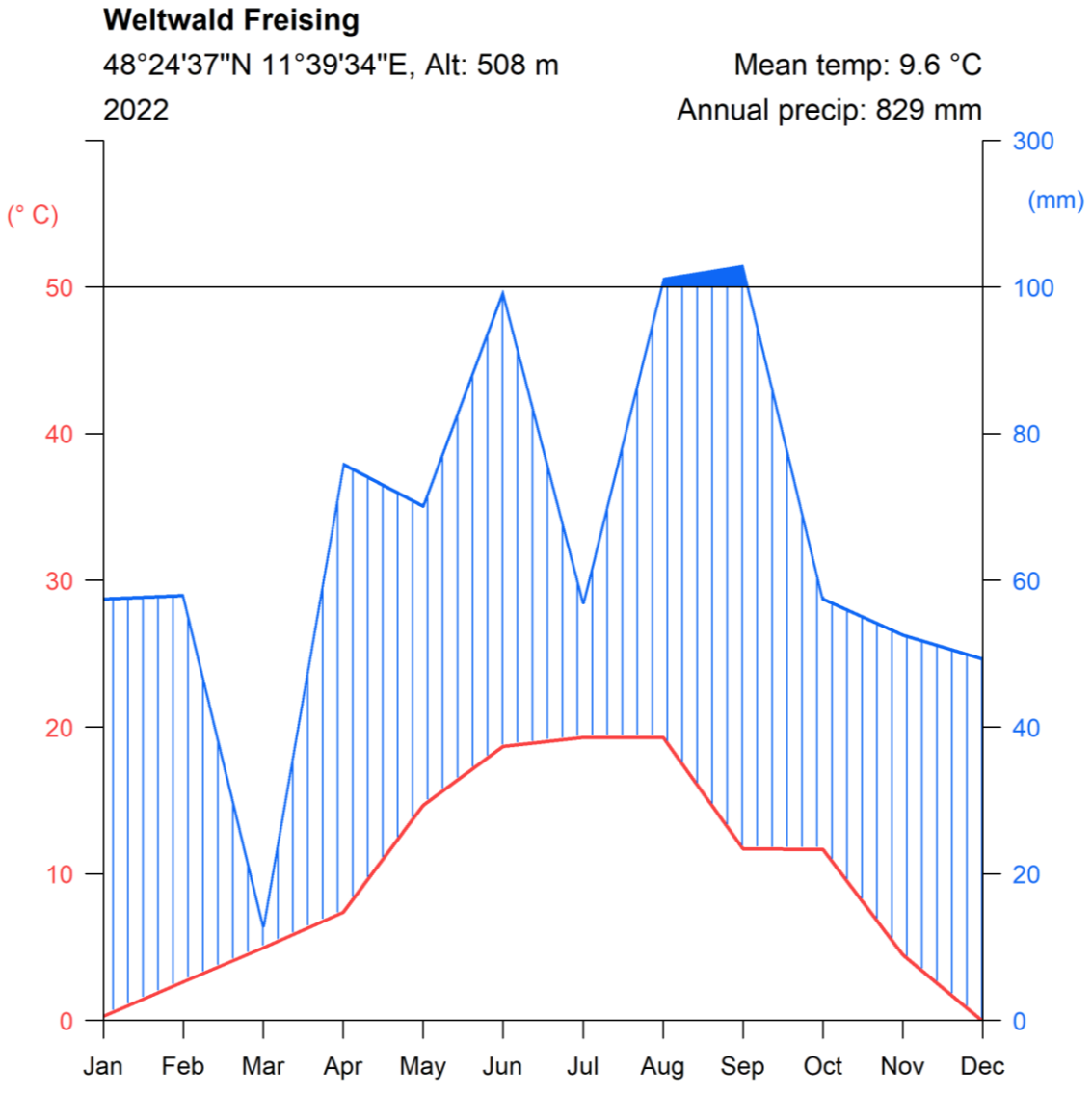

Figure S1: Monthly mean temperature and precipitation sum of the meteorological measuring station in the "Weltwald" Freising for the observation year 2022 in Walther-Lieth format (red: temperature; blue: precipitation; data provided by the Bavarian State Institute of Forestry).

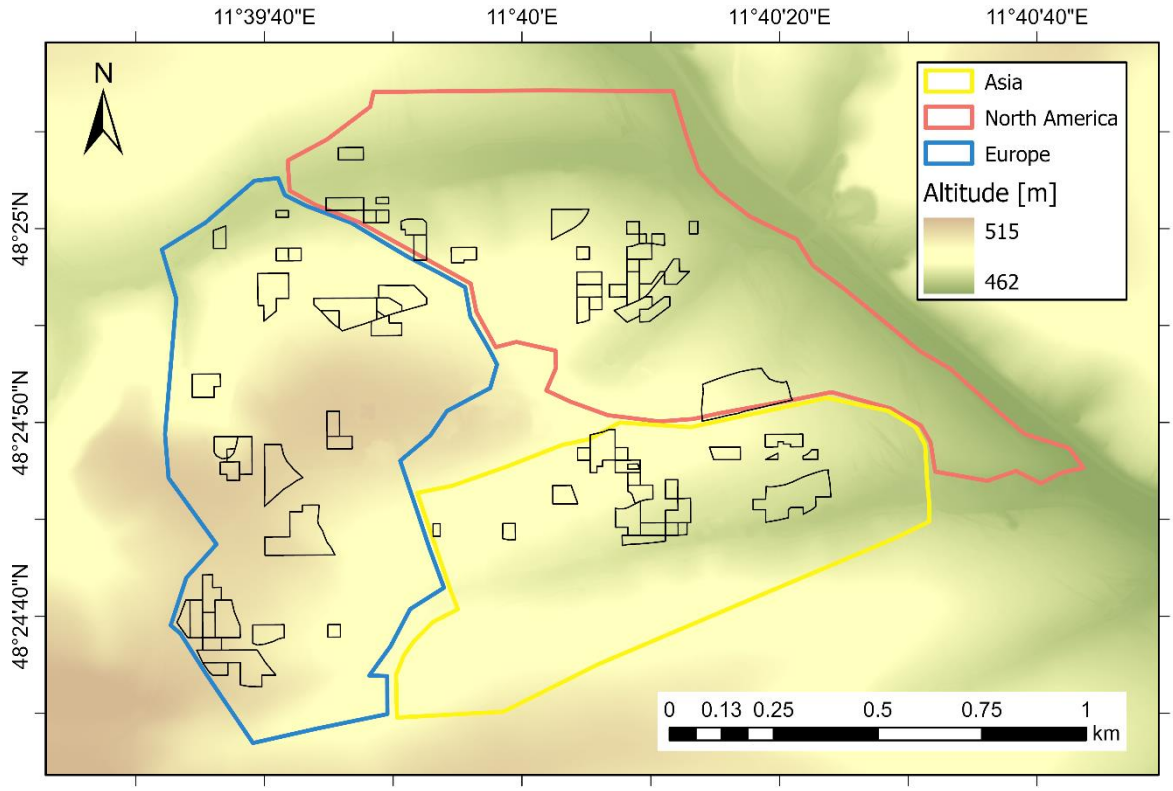

Figure S2: Topographic map of Weltwald Freising. The plots framed in black are the analyzed tree species plots within this study (for the selection criteria see section 2.3.1; yellow: Asia; blue: Europe; red: North America; background map: Bavarian Surveying Administration, 2024; polygon data: Bavarian State Forestry, 2022).

Table S1: Flight dates in the year 2022. Overall, 27 drone flights were performed to derive the phenological metrics for the study site.

Day	Month
03rd, 22nd, 28th	March
06th, 12th, 20th, 28th	April
04th, 10th, 19th, 25th	May
02nd, 14th	June
19th, 27th	July
03rd, 23rd	August
12th, 22nd, 26th	September
05th, 13th, 18th, 26th	October
08th, 21st	November
07th	December

Table S2: Processing options for PIX4D mapper.

Initial Processing Details

Image Coordinate System	WGS 84
Ground Control Point (GCP) Coordinate System	WGS 84
Output Coordinate System	WGS 84 / UTM zone 32N

Processing Options

Detected Template	MS_RGB_COMB_V2*
Keypoints Image Scale Full, Image Scale	1

Advanced: Matching Image Pairs	Aerial Grid or Corridor
Advanced: Matching Strategy	Use Geometrically Verified Matching: no
Advanced: Keypoint Extraction Targeted Number of Keypoints:	Custom, Number of Keypoints: 20000
Advanced: Calibration	Calibration Method: Geolocation Based
	Internal Parameters Optimization: All
	External Parameters Optimization: Rotation
Rematch	Auto, no
Rig «MS_ALL» processing	Ignore rig

Point Cloud Densification details

Image Scale	multiscale, 1 (original image size, slow)
Point Density	Optimal
Minimum Number of Matches	2
3D Textured Mesh Generation	No
LOD Generated	No
Advanced: Image Groups	Group1
Advanced: Use Processing Area	Yes
Advanced: Use Annotations	Yes

DSM, Orthomosaic and Index Details

DSM Filters	Noise Filtering: yes
	Surface Smoothing: yes, Type: sharp
Raster DSM	Generated: yes
	Method: Inverse Distance Weighting
	Merge Tiles: yes
Orthomosaic	Generated: yes
	Merge Tiles: yes
	GeoTIFF Without Transparency: no
	Google Maps Tiles and KML: no
Radiometric calibration with reflectance target	Yes
Index Calculator: Reflectance Map	Generated: yes
	Resolution: 10 [cm/pixel]
	Merge Tiles: yes
Index Calculator:	Indices Red_red, NIR_nir, ndvi_MS

Table S3: Drone-analyzed tree species in the "Weltwald Freising" and their continental area of origin (Rudolf, 2023), the year of planting (Bavarian State Forestry, 2022), the number of individuals in each plot, and whether the phenology was observed from the ground.

Species	Continent	Year of planting	Number of individuals	Ground observations in spring	Ground observations in autumn
Acer negundo	North America	2002	29	X	
Acer pensylvanicum	North America	2002	26		
Acer platanoides	Europe	1991	99	X	X
Acer rubrum	North America	2002	55	X	
Acer saccharum	North America	2002	42	X	X

Acer tataricum subsp. ginnala	Asia	2012	10	X	
Alnus cordata	Europe	2012	53		
Alnus incana	Europe	2014	24		
Alnus rugosa	North America	2002	37	X	
Betula albosinensis	Asia	2010	82	X	
Betula costata	Asia	2004	15	X	
Betula davurica	Asia	2004	32	X	
Betula lenta	North America	2002	28		
Betula maximowicziana	Asia	2015	42	X	X
Betula papyrifera	North America	2014	33	X	
Betula platyphylla	Asia	2004	24		
Betula pubescens	Europe	2014	56		
Carpinus betulus	Europe	1994	108	X	X
Carpinus caroliniana	North America	2002	20		
Carya cordiformis	North America	2001	42	X	X
Carya ovata	North America	2003	22		
Carya tomentosa	North America	2002	29		
Castanea sativa	Europe	2012	49	X	X
Cercidiphyllum japonicum	Asia	1991	15	X	
Corylus colurna	Europe	1995	22		X
Diospyros virginiana	North America	2002	21		X
Eucommia ulmoides	Asia	2011	7		
Fagus sylvatica	Europe	1995	73	X	X
Fraxinus americana	North America	2002	27		
Fraxinus chinensis	Asia	2004	29	X	
Fraxinus pennsylvanica	North America	2002	52		
Juglans ailantifolia	Asia	1991	33	X	
Juglans cinerea	North America	2002	64	X	
Juglans mandshurica	Asia	2011	14		
Larix decidua var. polonica	Europe	2015	22		X
Larix gmelinii var. principis-rupprechtii	Asia	2004	40	X	
Larix kaempferi	Asia	NA	29	X	X
Larix laricina	North America	2001	28	X	X
Larix x eurolepis	Europe	NA	47		
Liriodendron tulipifera	North America	2015	40	X	X
Malus sylvestris	Europe	NA	32		
Morus alba	Asia	2010	27	X	
Nyssa sylvatica	North America	2002	24		
Ostrya carpinifolia	Europe	2017	7		X
Platanus x hispanica	Europe	1994	16		X
Populus alba	Europe	1997	10		
Populus tremula	Europe	1997	11		
Populus trichocarpa	North America	1997	12		

Prunus avium	Europe	1996	98	X	X
Prunus padus	Europe	NA	24		
Pterocarya fraxinifolia	Europe	1994	8		
Pterocarya rhoifolia	Asia	1991	9	X	
Pterocarya stenoptera	Asia	2011	133	X	
Pyrus communis	Europe	NA	36	X	
Pyrus ussuriensis	Asia	2011	10	X	
Quercus alba	North America	2001	9	X	X
Quercus bicolor	North America	2001	84	X	X
Quercus coccinea	North America	1996	16	X	
Quercus nigra	North America	2003	19	X	
Quercus palustris	North America	2001	32	X	X
Quercus petraea	Europe	1996	128	X	X
Quercus robur	Europe	1987	196	X	X
Quercus rubra	North America	1987	141	X	X
Robinia pseudoacacia	North America	2015	56	X	X
Sorbus aucuparia	Europe	1992	24	X	
Sorbus domestica	Europe	1993	7	X	
Sorbus intermedia	Europe	1994	34		
Sorbus torminalis	Europe	1994	173	X	X
Tilia amurensis	Asia	2011	12	X	
Tilia tomentosa	Europe	2013	35		X
Ulmus americana	North America	2016	49	X	
Ulmus laevis	Europe	NA	68	X	X
Ulmus minor	Europe	2015	6		
Zelkova carpinifolia	Europe	1997	33	X	X

Table S4: Correlation values of Spearman's rank correlation analysis between the functional traits and the extracted phenological metrics. Additionally, lines 24 and 25 show the correlation values between the phenological metrics. Statistically significant correlations are marked with an asterisk (p-value < 0.05 = *; p-value < 0.01 = **; p-value < 0.001 = ***). The traits marked in bold were finally used in the BRT analysis.

	Plant trait	SOS	EOS	LOS
1	Age (y)	0.02	-0.03	0.01
2	**Tree height (m)**	0.04	0.22	0.12
3	Crown area (m^2)	0.01	0.21	0.14
4	**Leaf area (mm^2)**	0.44***	-0.01	-0.27*
5	**Leaf thickness (mm)**	-0.49***	0.09	0.35**
6	**Leaf area per leaf dry mass (specific leaf area, SLA; $mm^2\ mg^{-1}$)**	0.15	-0.19	-0.19
7	**Leaf dry mass per leaf fresh mass (leaf dry matter content, LDMC; $g\ g^{-1}$)**	-0.06	0.05	0.08
8	**Seed dry mass (mg)**	0.49***	0.17	-0.16
9	Seed number per reproduction unit (n)	-0.21	0.06	0.13
10	Leaf water content per leaf dry mass (not saturated; $g\ g^{-1)}$	-0.08	-0.09	0.01

11	**Leaf nitrogen (N) content per leaf dry mass (mg g^{-1})**	0.14	0.02	-0.09
12	**Leaf carbon (C) content per leaf dry mass (mg g^{-1})**	-0.18	0.02	0.08
13	**Leaf phosphorus (P) content per leaf dry mass (mg g^{-1})**	-0.24*	-0.20	-0.05
14	Leaf carbon nitrogen ratio (g g^{-1})	0.03	-0.03	-0.02
15	**Stem conduit diameter (micro m)**	0.43***	0.17	-0.15
16	Wood rays per millimeter (wood ray density; mm^{-1})	0.03	-0.11	-0.13
17	Wood vessel element length (micro m)	-0.21	0.01	0.12
18	Wood fiber lengths (micro m)	-0.09	0.11	0.09
19	**Chromosome number (n)**	-0.08	-0.27*	-0.15
20	Chromosome cDNA content (pg)	-0.06	0.12	0.11
21	Root length per root dry mass (specific root length, SRL; cm g^{-1})	0.20	-0.10	-0.23
22	**Fine root length per fine root dry mass (specific root length, SRL; cm g^{-1})**	0.29*	-0.15	-0.33**
23	**Root rooting depth (m)**	0.20	0.14	0.01
Pheno-metrics	SOS (DOY)	-	0.05	-0.60***
	EOS (DOY)	0.05	-	0.72***

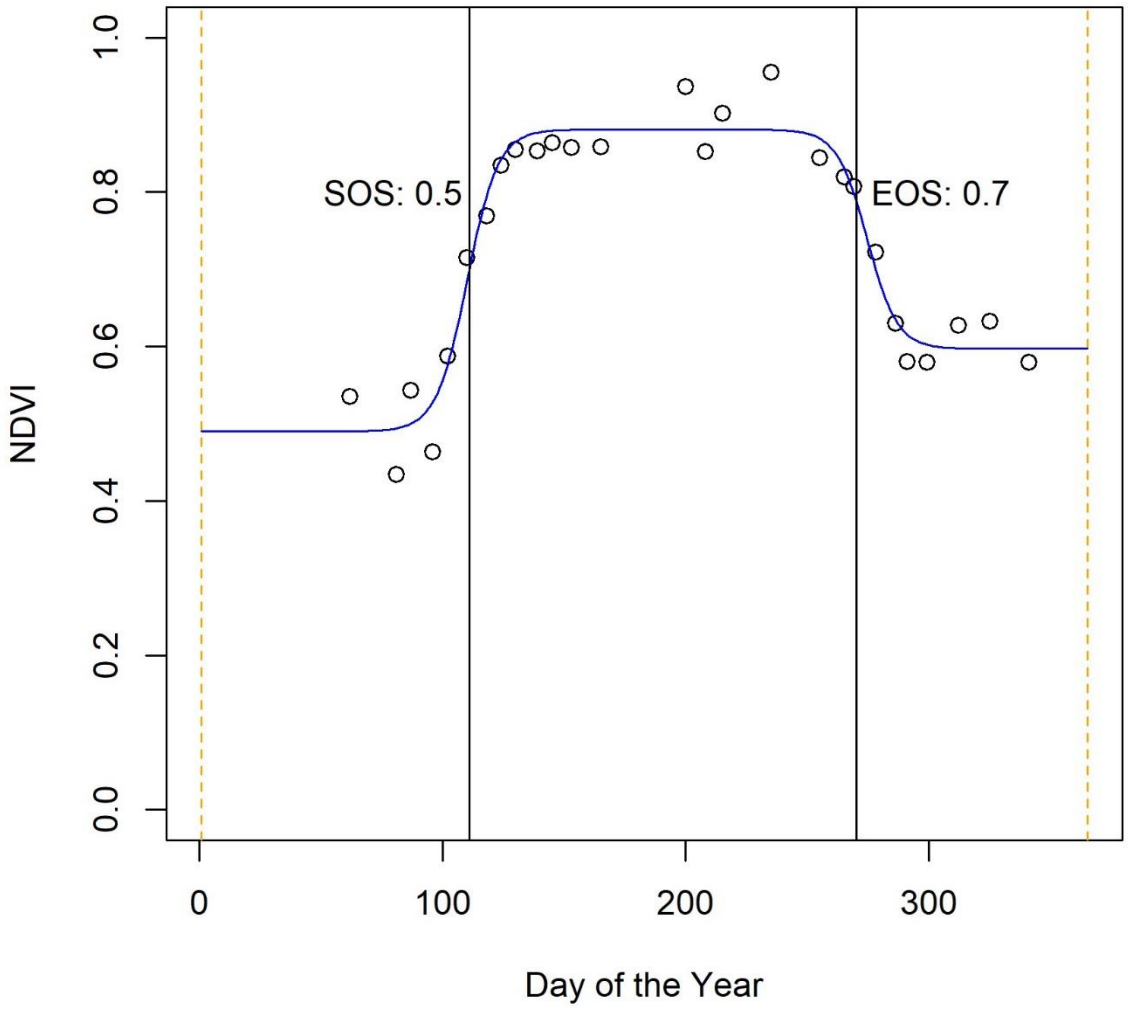

Figure S3: Example plot for extracting the phenological metrics for a tree. The 27 NDVI crown medians (white dots), the blue fitted NDVI curve (double-logistic) and the two threshold lines (SOS: 0.5, EOS: 0.7), which determine the SOS and EOS, are shown.

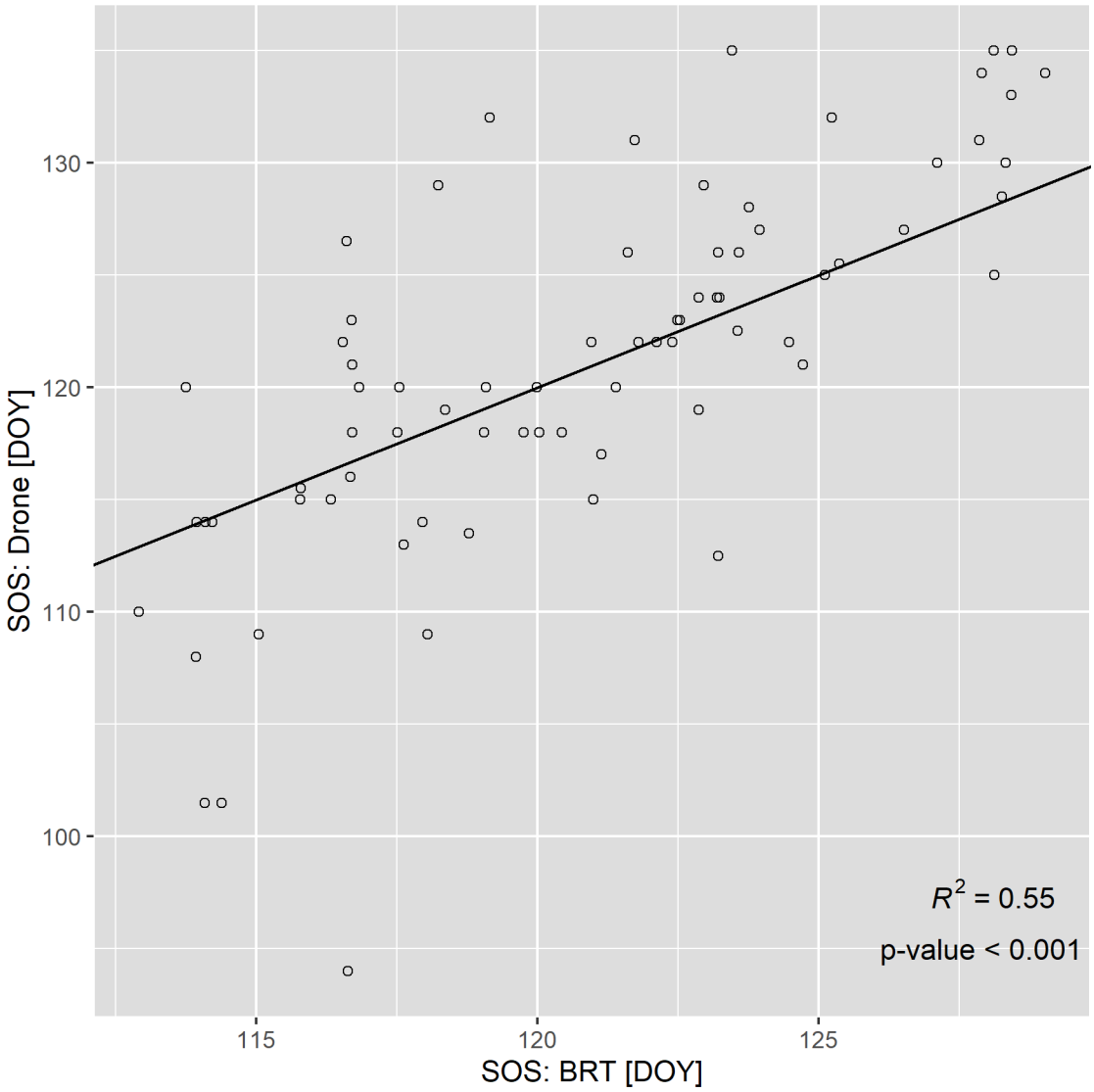

Figure S4: Scatterplot of the predicted (BRT) and observed (drone-derived) SOS values. The coefficient of determination and the p-value of the linear regression model of both data sets are shown at the bottom right. The black line represents the 1:1 line.

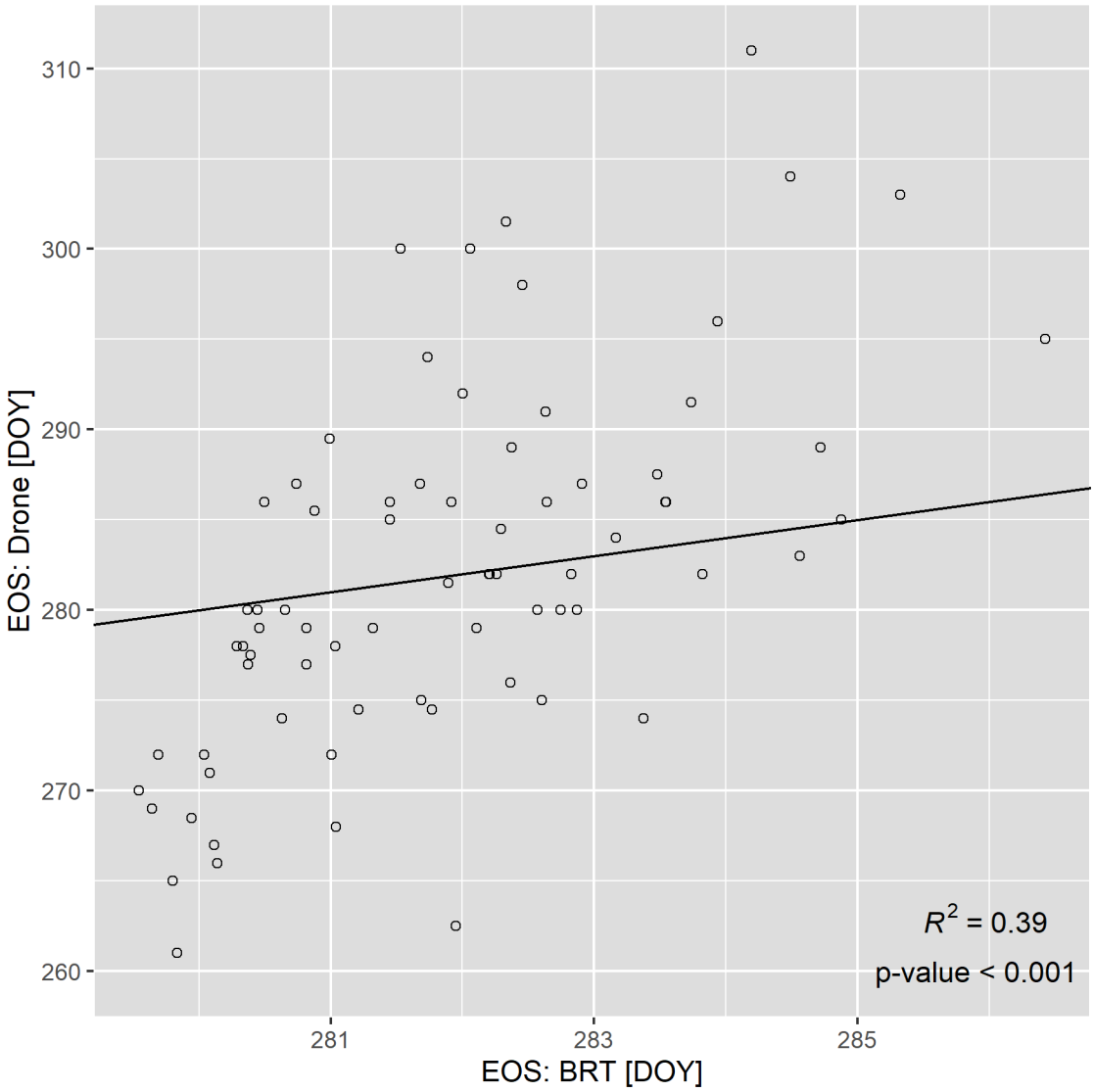

Figure S5: Scatterplot of the predicted (BRT) and observed (drone-derived) EOS values. The coefficient of determination and the p-value of the linear regression model of both data sets are shown at the bottom right. The black line represents the 1:1 line.

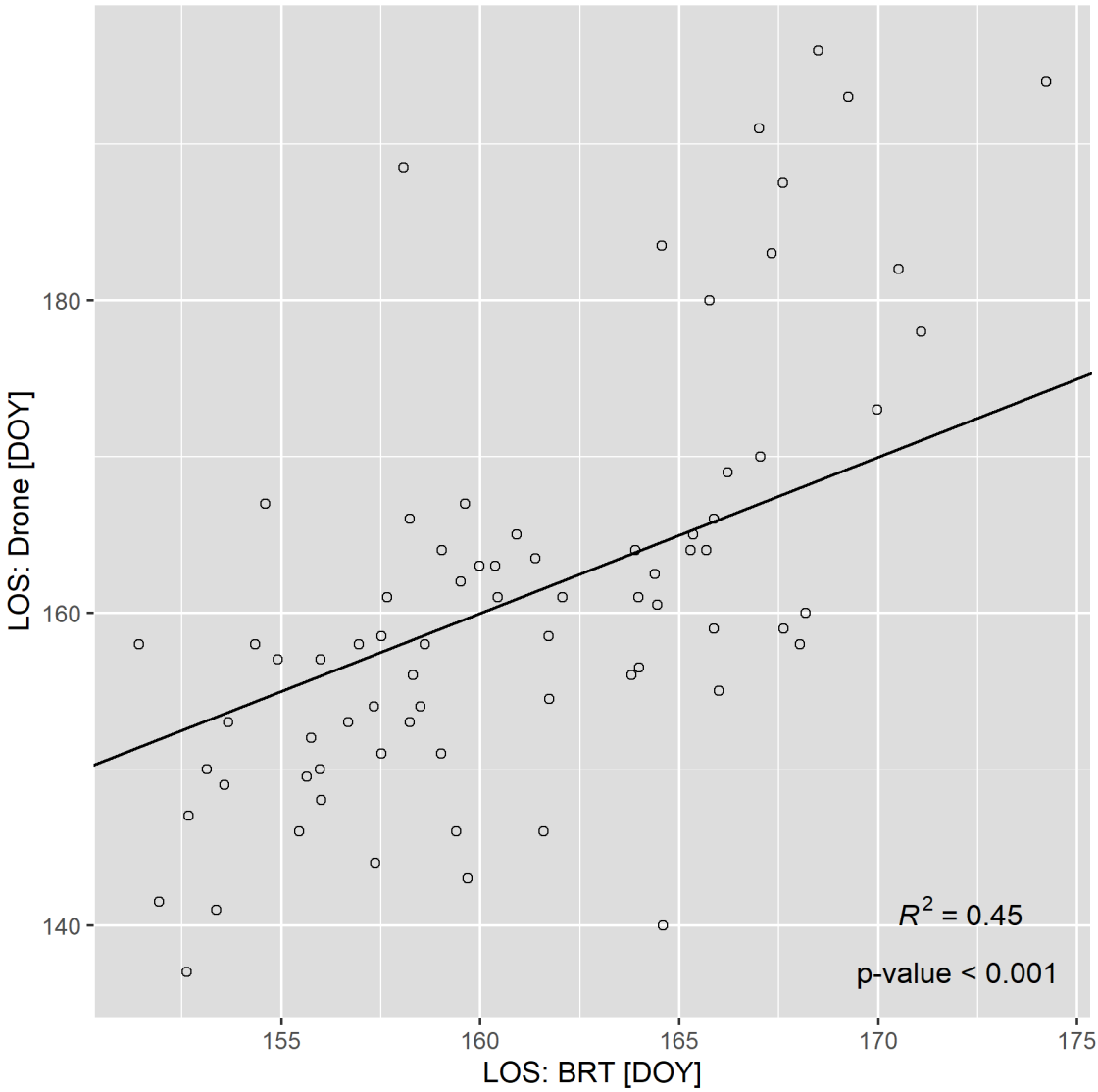

Figure S6: Scatterplot of the predicted (BRT) and observed (drone-derived) LOS values. The coefficient of determination and the p-value of the linear regression model of both data sets are shown at the bottom right. The black line represents the 1:1 line.

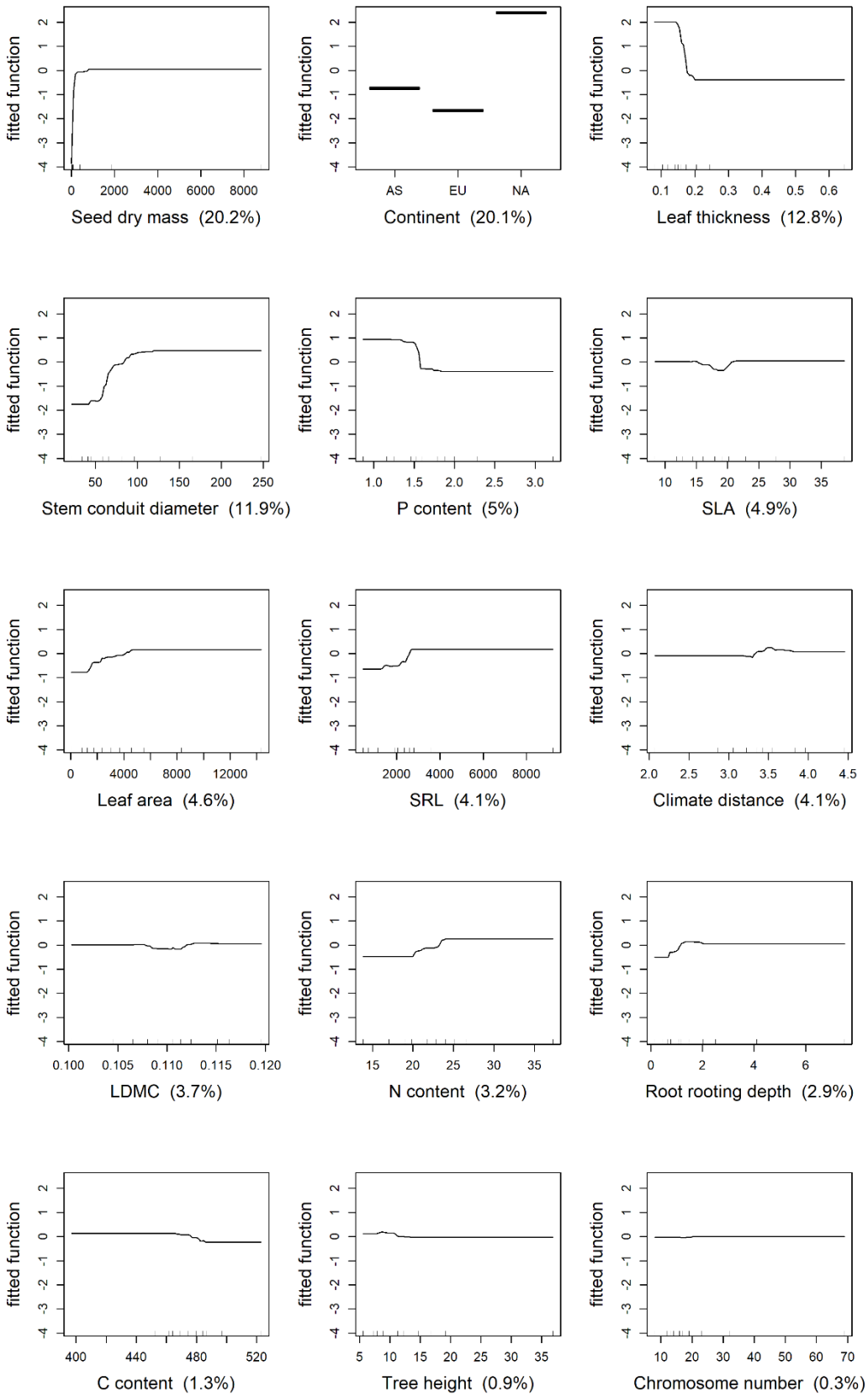

Figure S7: Partial dependency plots of the BRT between the individual functional traits or the climate distance and the SOS (cv correlation = 0.63). The relative importance of Figure 7a is shown below each plot.

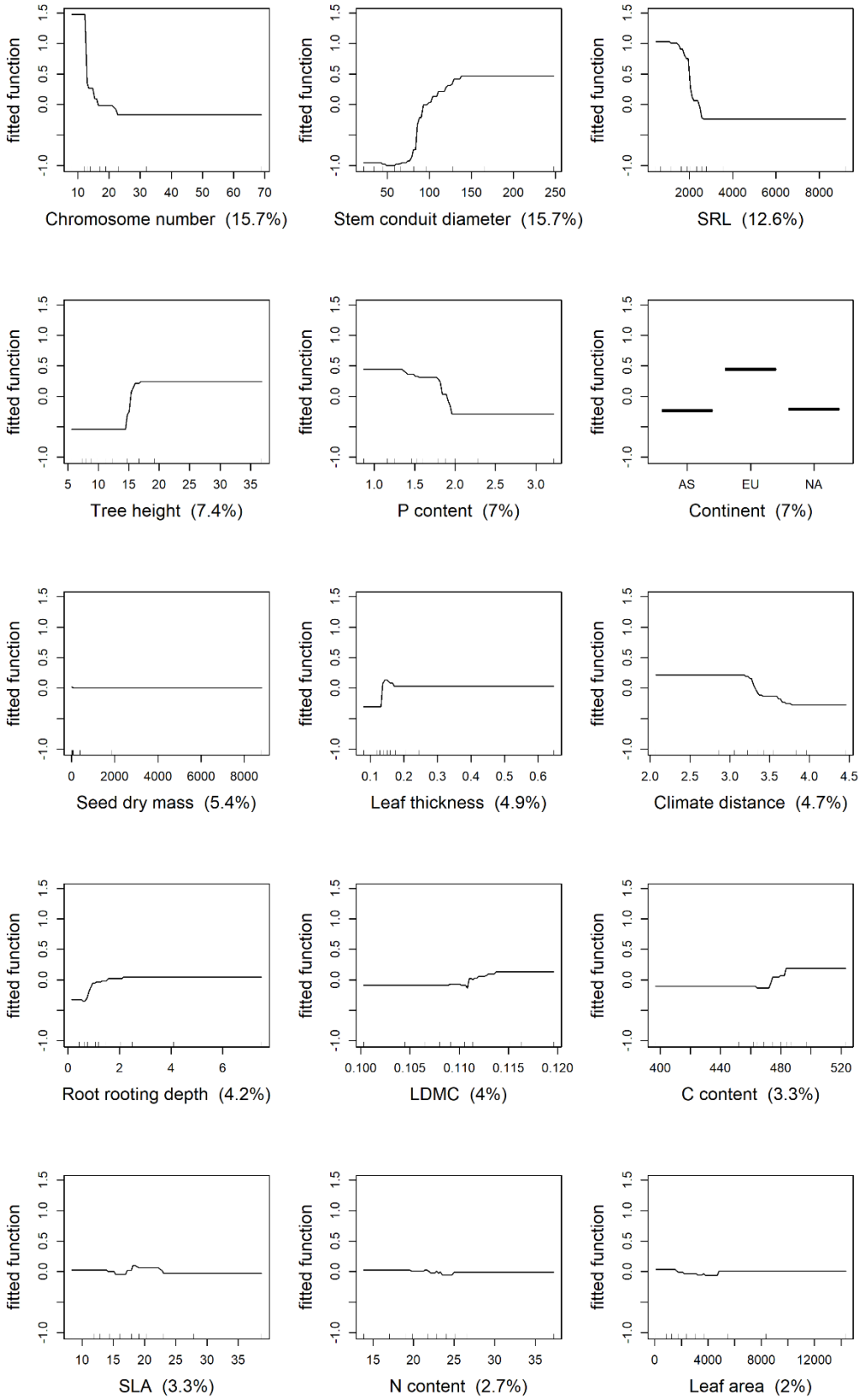

Figure S8: Partial dependency plots of the BRT between the individual functional traits or the climate distance and the EOS (cv correlation = 0.20). The relative importance of Figure 7b is shown below each plot.

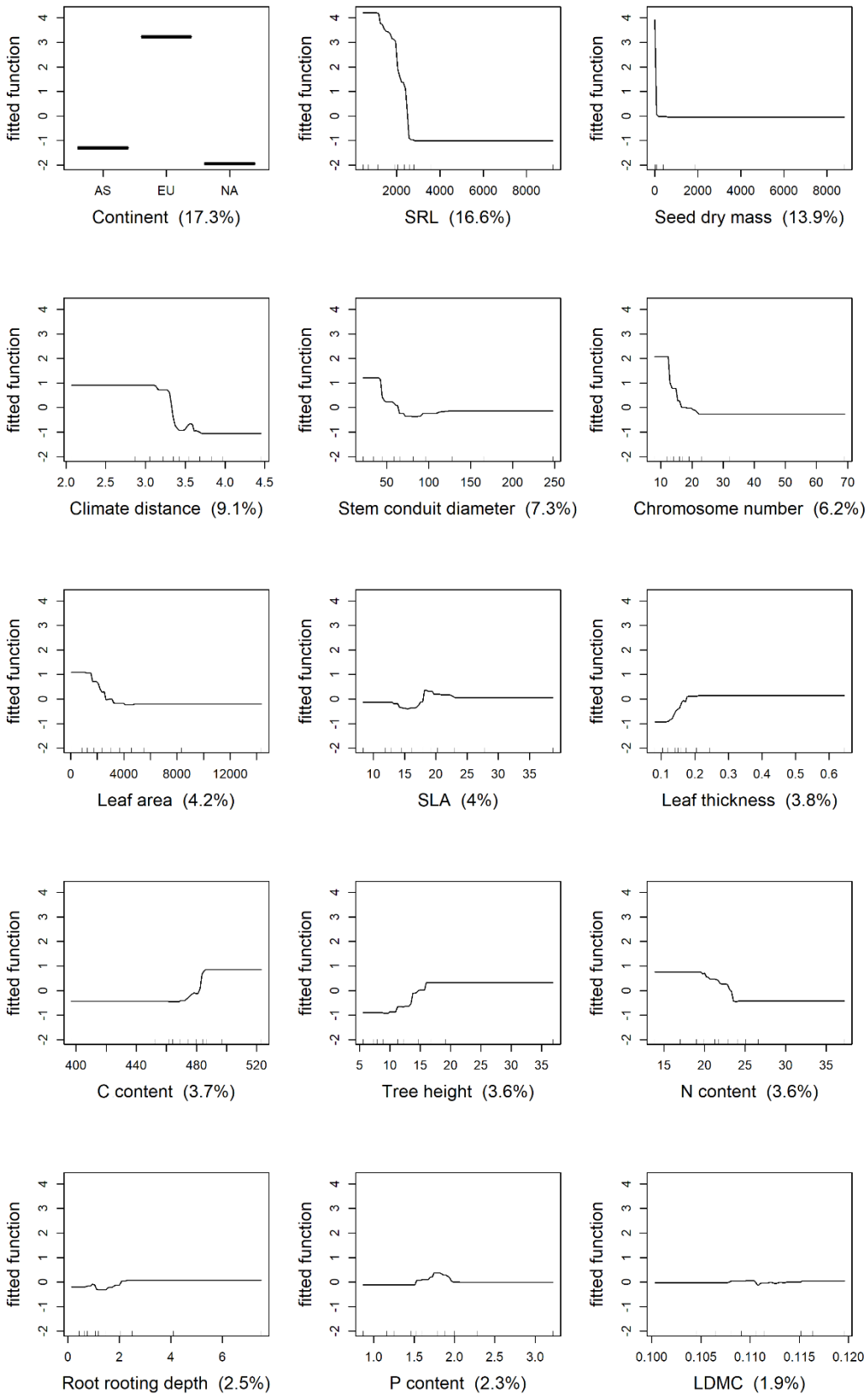

Figure S9: Partial dependency plots of the BRT between the individual functional traits or the climate distance and the LOS (cv correlation = 0.37). The relative importance of Figure 7c is shown below each plot.

References

Bavarian State Forestry, 2022. (C) Geodata. https://services1.arcgis.com/dzpA3ZtAF0zx03DV/arcgis/rest/services/Weltwald_Update_05_2022/FeatureServer (accessed 10 January 2024).

Bavarian Surveying Administration, 2024. Digitales Geländemodell 1m (DGM). https://geodaten.bayern.de/opengeodata/OpenDataDetail.html?pn=dgm1 (accessed 11 April 2024).

Rudolf, H., 2023. Weltwald Freising. https://www.weltwald.de/fileadmin/user_upload/14-weltwald/pdfs/Weltwald_Freising_2023.pdf (accessed 27 September 2023).